

LOAN COPY: RETURN TO  
AFWL TECHNICAL LIBRARY  
KIRTLAND AFB, N.M.

NASA  
TP  
1651  
c.1

NASA Technical Paper 1651



# Ice Crystal Growth in a Dynamic Thermal Diffusion Chamber

Vernon W. Keller

MAY 1980

**NASA**



NASA Technical Paper 1651

# Ice Crystal Growth in a Dynamic Thermal Diffusion Chamber

Vernon W. Keller

*George C. Marshall Space Flight Center*

*Marshall Space Flight Center, Alabama*



National Aeronautics  
and Space Administration

**Scientific and Technical  
Information Office**

1980

## ACKNOWLEDGMENTS

It is with sincere gratitude that the author expresses appreciation to the many persons who lent assistance during the duration of this project. The advice and encouragement of Dr. John Hallett of the University of Nevada were invaluable, and Professors Vern Frazier, Rodney Harrington, Bruce Johnson, Richard Schneider, William Scott, and Vern Smiley offered assistance and helpful suggestions. Mrs. Patricia Harris and Mr. James Heidker of Water Resources, Desert Research Institute, made available and instructed me in the operation and use of a gas-liquid chromatograph. Drs. Jeffrey Anderson and Robert Smith of the Marshall Space Flight Center, NASA, made available the use of an automated 16 mm cine film analyzer for measurement of crystal lengths.

This research was supported by the National Science Foundation under research grant numbers ATM75-10935 (formerly DES75-10935) and ATM77-07995 and was the basis of a dissertation for the degree of Doctor of Philosophy in Physics, University of Nevada, December 1977. This report was completed at the Marshall Space Flight Center, NASA.

## ABSTRACT

Ice crystals were grown in a supersaturated environment produced by a dynamic thermal diffusion chamber, which employed two horizontal plates separated by a distance of 2.5 cm. Air was circulated between and along the 1.2 m length of the plates past ice crystals which nucleated and grew from a fiber suspended vertically between the two plates. Using a zoom stereo microscope with a magnification which ranged from 3X to 80X and utilizing both 35 mm still photographs and 16 mm time lapse cine films taken through the microscope, the variation of the shape and linear growth rate of ice crystals was examined as a function of the ambient temperature, the ambient supersaturation and the forced ventilation velocity. The ambient growth conditions were varied over the range of temperature  $0^{\circ}\text{C}$  to  $-40^{\circ}\text{C}$ , over the range of supersaturation 4% to 50% with respect to ice, i.e., over vapor density excesses ranging from  $0.07\text{ g m}^{-3}$  to  $0.7\text{ g m}^{-3}$ , and over the range of forced ventilation velocities  $0\text{ cm s}^{-1}$  to  $20\text{ cm s}^{-1}$ .

It is shown that the introduction of a ventilation velocity is roughly equivalent to increasing the ambient supersaturation. For a fixed ambient temperature and ambient supersaturation, the linear 'a'-axis growth rate is directly proportional to the square root of the ventilation velocity, as theory predicts, provided the crystal shape does not change significantly. The transitions plate  $\rightarrow$  dendrite and column  $\rightarrow$  needle occur at a lower ambient supersaturation as the ventilation velocity increases. A definite time constant, which is a function of the ambient temperature, the ambient supersaturation and the magnitude of the change in the ventilation velocity, exists for



the transition of both crystal shape and linear growth rate following a change in the ventilation velocity. For increasing ventilation velocities at a fixed ambient supersaturation the maximum in the linear growth rate near  $-15^{\circ}\text{C}$  apparently occurs at successively colder temperatures. Over the temperature range  $-4^{\circ}\text{C}$  to  $-6^{\circ}\text{C}$  growth occurs along a direction up to  $25^{\circ}$  from the 'c'-axis as the local supersaturation is increased. Thus, under the proper temperature conditions a change in the local supersaturation can induce a change, not only in the absolute growth rates, but also in the relative growth rates along the 'a' and 'c'-axes.

In the presence of  $10\text{ }\mu\text{m}$  mean diameter droplets with concentrations of  $10^3$  to  $10^5\text{ cm}^{-3}$  droplet accretion accounted for over 90% of the growth of both ice crystal columns and dendrites at ventilation velocities of  $15\text{ cm s}^{-1}$ . However, even at higher velocities the most extensively rimed crystals still retained the original orientation of their crystalline axes. At velocities less than  $1.0\text{ cm s}^{-1}$  droplets of  $10\text{ }\mu\text{m}$  diameter or smaller evaporated as they approached a growing ice crystal and crystal growth was entirely by vapor diffusion.

The first vapor grown discoid ice crystals were observed. They grew in the temperature regime  $-5^{\circ}\text{C}$  to  $-7^{\circ}\text{C}$  at low local supersaturations, i.e., in the regime formerly believed to only support nearly equiaxed columns.

Results from these experiments are interpreted in terms of diffusion through a local boundary layer, whose thickness is a function of ventilation velocity, the diffusivity of water vapor and heat through air, and the crystal shape; and interaction with different nucleation and growth kinetics on different surfaces. Two-dimensional nucleation

and layer growth from corners or edges is believed to occur at ambient supersaturations significantly lower than present theories would predict. At low supersaturation and temperature the crystal habit and growth may be controlled by the presence of defects sometimes giving rise to crystals of habit opposite to that normally observed.

## TABLE OF CONTENTS

	Page
ACKNOWLEDGEMENTS.....	ii
ABSTRACT.....	iii
LIST OF TABLES.....	viii
LIST OF FIGURES.....	ix
I. INTRODUCTION.....	1
II. REVIEW OF PREVIOUS WORK.....	5
A. Ice Crystal Terminology and Ice Crystal Habit.....	6
B. Ice Crystal Growth in a Static Environment.....	13
C. Ice Crystal Growth in a Ventilated Environment.....	21
D. Some Other Parameters Affecting Ice Crystal Growth and Habit.....	25
1) Reduced and Increased Ambient Pressure and Variation of the Molecular Weight of the Carrier Gas.....	25
2) Contaminants in the Carrier Gas.....	30
3) Effect of an Applied Electric Field.....	32
4) Crystal Dislocations.....	35
III. ICE CRYSTAL GROWTH RATE—THEORY AND EXPERIMENT.....	37
A. Molecular Diffusion.....	37
B. Convective Diffusion.....	44
IV. EXPERIMENTAL APPARATUS AND PROCEDURE.....	59
A. Apparatus.....	59
B. Calibrations and Procedure.....	74
V. RESULTS AND CONCLUSIONS.....	109
A. Crystal Growth in a Droplet Free Environment.....	109
1) Predominant Growth Along the 'a'-Axis.....	109
2) Predominant Growth Along the 'c'-Axis.....	142
B. Crystal Growth in an Environment with Droplets.....	150
C. Growth of Discoid Crystals from the Vapor.....	154
D. Growth of Crystals at Intermediate to Low Ambient Super- saturation.....	158
E. Growth of 'Peculiar' or Prism-Faced Crystals.....	162
VI. APPLICATION OF RESULTS AND SUGGESTIONS FOR FUTURE STUDY.....	168
A. Application to the Atmosphere.....	168

	Page
B. Application to Crystal Growth.....	171
C. Suggestions for Future Study.....	174
APPENDIX A AIR DRIVE MEASUREMENTS.....	176
APPENDIX B WATER VAPOR TABLES.....	179
APPENDIX C CALCULATION OF AMBIENT CONDITIONS.....	185
APPENDIX D RELATIVE MAGNITUDES OF HEAT TRANSFER.....	189
BIBLIOGRAPHY.....	195

# LIST OF TABLES

<u>TABLE</u>		<u>PAGE</u>
I	Experimental temperature pairs at which water saturation occurs.....	95
II	Effect of temperature variation of the top or bottom plate on the maximum supersaturation, case (a).....	96
III	Effect of temperature variation of the top or bottom plate on the maximum supersaturation, case (b).....	97
IV	Habit of ice crystals growing at $-30^{\circ}\text{C}$ .....	160
B-I	Saturation vapor pressure over ice.....	180
B-II	Saturation vapor pressure over water.....	181
B-III	Density of pure water vapor at saturation over ice.....	182
B-IV	Density of pure water vapor at saturation over water...	183
B-V	Percent supersaturation with respect to ice at which water saturation occurs.....	184
C-I	Specimen calculations of the ambient chamber conditions.	187

## LIST OF FIGURES

<u>FIGURE</u>	<u>PAGE</u>
2.1 Schematic representation of possible ice crystal growth forms.....	7
2.2 The unit cell for the hexagonal ice structure.....	8
2.3 Observed basic ice crystal forms.....	9
2.4 Ice crystal habit as a function of temperature and supersaturation relative to ice.....	10
2.5 Ice crystal habit as a function of temperature and vapor density excess over that of ice.....	11
2.6 Pictorial diagram showing the dependence of ice crystal type upon both temperature and supersaturation relative to ice.....	11
2.7 The static diffusion cloud chamber used by Hallett and Mason for growing ice crystals at various temperatures and supersaturations.....	15
2.8 Distinction between dendritic, sector, and doric crystals.....	17
2.9 The temperature variation of the rate of growth of a layer 250 Å thick. Excess vapor density $0.25 \text{ gm}^{-3}$ .....	20
2.10 Schematic diagram of the habit and the growth feature of small ice crystals with respect to the vapor diffusivity and the thermal conductivity.....	28
2.11 The effect of iso-butyl alcohol on ice crystal habit....	31
3.1 Vapor density of water and ice and vapor density difference between water and ice versus temperature.....	39
3.2 Surfaces of constant vapor density and temperature surrounding a growing plate-like ice crystal.....	41
3.3 Comparison of moisture and heat terms from the mass growth rate equation as a function of temperature.....	45
3.4 Growth rates as a function of temperature of an ice crystal with $C=1/4\pi$ in a water-saturated cloud at two pressures. The temperature for maximum rate of growth is indicated on each curve.....	50

<u>FIGURE</u>		<u>PAGE</u>
3.5	Relative rate of mass increase of crystals growing at water saturation in a static environment.....	51
3.6	Mass of ice crystals versus temperature for various times after seeding a supercooled water cloud.....	51
3.7	Variation of estimated crystal axial growth rates with temperature.....	52
3.8	Falling velocity versus dimension of plane type crystals.	53
3.9	Experimental measurements of the linear growth rates of the basal and prism faces of ice as a function of temperature.....	55
3.10	The growth rate is determined by mass transfer and by interfacial incorporation kinetics, which must take place sequentially and at the same rate.....	57
4.1	Parallel conducting plates with associated equilibrium temperature and vapor density profiles.....	59
4.2	Ice crystals grow from a fiber suspended vertically between two horizontal parallel plates.....	63
4.3	Diagram of the dynamic thermal diffusion chamber (top view).....	66
4.4	View of the dynamic thermal diffusion chamber from above, beyond the end.....	67
4.5	A horizontal temperature profile taken 1.00 cm above the bottom plate in the dynamic thermal diffusion chamber ( $T_t = -10.0^\circ\text{C}$ ; $T_b = -12.2^\circ\text{C}$ ).....	76
4.6	A vertical temperature profile taken at the horizontal center of the dynamic thermal diffusion chamber ( $T_t = -10.0^\circ\text{C}$ ; $T_b = -10.3^\circ\text{C}$ ).....	78
4.7	A vertical temperature profile taken at the horizontal center of the dynamic thermal diffusion chamber ( $T_t = -7.9^\circ\text{C}$ ; $T_b = -20.7^\circ\text{C}$ ).....	78
4.8	Variation of temperature with ventilation velocity at a fixed height and distance from the entrance of the working section.....	80
4.9	Vertical velocity profiles taken at the horizontal center of the dynamic thermal diffusion chamber.....	82

<u>FIGURE</u>		<u>PAGE</u>
4.10	Horizontal velocity profiles taken 1.36 cm above the bottom plate in the dynamic thermal diffusion chamber...	83
4.11	Velocity response when the fan is turned on and off.....	84
4.12	Vertical supersaturation profile in a thermal diffusion chamber ( $T_t=-8.1^{\circ}\text{C}$ ; $T_b=-20.6^{\circ}\text{C}$ ). Calculated assuming a linear vapor density with height.....	89
4.13	Vertical supersaturation profile in a thermal diffusion chamber ( $T_t=-1.5^{\circ}\text{C}$ ; $T_b=-20.5^{\circ}\text{C}$ ). Calculated assuming a linear vapor density with height.....	89
4.14	The form and extent of the toroidal circulation is a function of the forced ventilation velocity.....	93
4.15	Temperature—vapor density conditions at the surface (point B) and in the environment (point A) of a growing crystal.....	98
4.16	Calculated profile of maximum and "true" vapor density excess for a static environment ( $T_t=-8.9^{\circ}\text{C}$ ; $T_b=-22.1^{\circ}\text{C}$ ).	100
4.17	Ice crystal columns growing against a blue background. (Color photograph).....	108
4.18	Ice crystal dendrites growing against a red background. (Color photograph).....	108
5.1	A forced ventilation velocity enhances ice crystal growth into the airstream. ( $T_t=-4.5^{\circ}\text{C}$ ; $T_b=-20.2^{\circ}\text{C}$ ).....	110
5.2	Ice crystal length as a function of time for successive ventilation velocities of 3.0, 0 and 7.0 $\text{cm s}^{-1}$ , under constant ambient conditions of temperature, $-15.8^{\circ}\text{C}$ , and vapor density excess, $0.279 \text{ g m}^{-3}$ , at the height of the crystal base, 0.70 cm above the bottom plate. Angle of crystal from horizontal was $+18^{\circ}$ . ( $T_t=-4.5^{\circ}\text{C}$ ; $T_b=-20.2^{\circ}\text{C}$ ).....	112
5.3	A forced ventilation velocity affects both ice crystal shape and linear growth rate.....	113
5.4	A forced ventilation velocity enhances the growth of a crystal particularly near its leading edges.....	117
5.5	Length of the crystal in Figs. 5.3 and 5.4 as a function of time for successive ventilation velocities of 0 and 7.0 $\text{cm s}^{-1}$ , under constant ambient conditions of temperature, $-13.9^{\circ}\text{C}$ , and vapor density excess, $0.385 \text{ g m}^{-3}$ , at the height of the crystal base, 0.78 cm above the bottom plate. Angle of crystal from horizontal was $+3^{\circ}$ . ( $T_t=-2.3^{\circ}\text{C}$ ; $T_b=-19.1^{\circ}\text{C}$ ).....	119



<u>FIGURE</u>		<u>PAGE</u>
5.6	The crystal shape and linear growth rate are functions of the ambient temperature, the ambient supersaturation, and the forced ventilation velocity.....	120
5.7	The linear growth response of an ice crystal under ambient conditions of temperature, $-13.7^{\circ}\text{C}$ , and vapor density excess, $0.352\text{ g m}^{-3}$ , when the ventilation velocity, $v$ , was suddenly decreased from $v = 7.0$ to $v = 0\text{ cm s}^{-1}$ at time $t = 0$ . ( $T_t = -4.5^{\circ}\text{C}$ ; $T_b = -20.2^{\circ}\text{C}$ ).....	121
5.8	The crystal shape and linear growth rate response to a change in the forced ventilation velocity is a function of the ambient temperature, the ambient supersaturation and the magnitude of the change in the forced ventilation velocity.....	123
5.9	The linear growth response of an ice crystal under ambient conditions of temperature, $-14.0^{\circ}\text{C}$ , and vapor density excess, $0.243\text{ g m}^{-3}$ , when the ventilation velocity, $v$ , was suddenly increased from $v = 0$ to $v = 5.0\text{ cm s}^{-1}$ at time $t = 0$ . ( $T_t = -7.8^{\circ}\text{C}$ ; $T_b = -21.5^{\circ}\text{C}$ ).....	124
5.10	Isopleths of linear 'a'-axis growth rates ( $\mu\text{m s}^{-1}$ ) for a ventilation velocity = $0\text{ cm s}^{-1}$ .....	127
5.11	Isopleths of linear 'a'-axis growth rates ( $\mu\text{m s}^{-1}$ ) for a ventilation velocity = $3.0\text{ cm s}^{-1}$ .....	128
5.12	Isopleths of linear 'a'-axis growth rates ( $\mu\text{m s}^{-1}$ ) for a ventilation velocity = $7.0\text{ cm s}^{-1}$ .....	129
5.13	Isopleths of forced ventilation velocity ( $\text{cm s}^{-1}$ ) for an ambient temperature = $-14.5^{\circ}\text{C}$ .....	132
5.14	Isopleths of ambient vapor density excess ( $\text{g m}^{-3}$ ) for an ambient temperature = $-14.0^{\circ}\text{C}$ .....	135
5.15	The vapor field and flow of water molecules over a growing ice surface with steps propagating from left to right.....	136
5.16	A model of layer by layer growth on the prism faces.....	139
5.17	A dendrite viewed edge-on shows the base is thicker than the tip.....	141
5.18	Macroscopic steps propagating across the basal face of a hollow column.....	143

<u>FIGURE</u>		<u>PAGE</u>
5.19	Ice crystals immediately assume a columnar habit when transferred from a plate-like to a column-like temperature regime despite the presence of a forced ventilation velocity along the 'a'-axis.....	145
5.20	Ice crystal columns introduced to a forced ventilation velocity may assume preferred linear growth along a direction other than the 'c'-axis.....	147
5.21	At higher ambient supersaturations preferred linear growth may occur along a direction other than the 'c'-axis, even in the absence of a forced ventilation velocity.....	149
5.22	Rimed ice crystal columns.....	151
5.23	Rimed ice crystal dendrites.....	153
5.24	Ice platelets and columns both growing at $-5^{\circ}\text{C}$ under different local ambient conditions of supersaturation.....	155
5.25	Simultaneous growth of columns and plates sometimes occurs at low supersaturation.....	159
5.26	Two stages in the growth of a prism-faced or "peculiar" ice crystal. The direction of the 'c'-axis is indicated with an arrow.....	164
5.27	A prism-faced ice crystal responds to the introduction of a forced ventilation velocity.....	165
5.28	'Peculiar' ice crystals may assume a variety of unusual shapes.....	167
A-1	The air drive motor shaft speed is directly proportional to the d.c. current which is supplied to the servo motor...	177
A-2	The ventilation velocity in the working section of the chamber is directly proportional to the d.c. current which is supplied to the servo motor.....	178
C-1	Calculated ambient crystal growth conditions at the chamber center for a given pair of chamber top and bottom plate temperatures.....	188

## I.

## INTRODUCTION

The growth of ice crystals is of practical interest in meteorology because of the major role which they play in precipitation processes. In fact, nearly all precipitation which falls from clouds over large land masses, whether in winter or summer, is at one time during the precipitation process composed of the ice phase. On the other hand, the growth of ice crystals is also important in providing information about crystal growth processes. The fact that ice is inexpensive, has a wide range of well-defined forms or habits and can be grown without the use of expensive furnaces normally associated with crystal growth, makes it an ideal choice for intensive basic crystal growth studies.

Ice can be formed by either of two processes: solidification from the liquid phase or condensation from the vapor phase. If solidification takes place in a 'pure' substance it is called growth from the 'melt'. Otherwise it is called growth from 'solution'. Crystals grown by condensation from the vapor phase are called vapor grown crystals. In either case, crystals will only grow if the solution or vapor in contact with them is supersaturated or, in the case of a melt, undercooled.

The actual form, or habit, of ice crystals may vary widely, these differences being dependent on the conditions under which the growth has taken place. In fact, the growth of ice crystals and their resultant habits is determined by a myriad of variables. Nonetheless, these variables may be divided into two rather broad and sometimes

overlapping categories: those which primarily influence the flux of water molecules to, and the transport of heat from, the crystal surface; and those which primarily govern the distribution of the molecules on the crystal surface and their subsequent incorporation into the crystal lattice. The former category might be termed "environmental or ambient kinetic effects" and the latter "surface kinetic effects". The resultant crystal habit will be determined by an integration over both time and space of the relative magnitudes of these two terms. Of course, it should be realized that the relative magnitudes of these terms may vary significantly from one crystallographic face to another on the same crystal.

In this work emphasis is placed primarily on vapor grown ice crystals. Of particular interest is their habit and growth rates over the range of ambient conditions of temperature, pressure, supersaturation and ventilation velocity existing in the earth's atmosphere. This is important because the habit of the ice crystals not only affects their linear growth rates and riming, i.e., accretional growth characteristics, but may also be important in determining secondary crystal production. These characteristics, in turn, determine the rate at which precipitation can form in a cloud.

In the atmosphere, the ambient variables which determine the crystal habit and growth rate may fluctuate with both space and time in some complicated manner. Therefore, it is profitable to perform experiments in the laboratory under as well controlled conditions as possible. These laboratory experiments provide insights into the fundamental growth characteristics of the crystals; they help verify, modify or disprove existing theories; and they complement both surface

and airborne field investigations. The extent to which these laboratory studies can be directly applied to the atmosphere depends upon the effectiveness with which the laboratory design simulates the atmospheric process. In practice, experimentally simulating the variations which each of the ambient parameters undergoes in a cloud and at the same time providing a method for close observation of the growing ice crystal is a virtually impossible task. Thus, in any experiment designed to study the growth of ice crystals one must first determine which parameters he wishes to study; then design and build a system in which these parameters are controlled and the remaining parameters are held constant at some appropriate value.

In the past, experiments have been performed in the laboratory with temperature, pressure and supersaturation as controlled variables but with ventilation dependent upon free convection. Other experiments have been performed in which ice crystals fell through a supercooled water cloud with temperature as the controlled variable and ventilation dependent upon the terminal velocity of the particles. In this case growth occurs at, or near, ambient conditions of water saturation and an ice supersaturation which depends only on temperature. Still other experiments have been performed in which an ice crystal was grown on a substrate where temperature, air pressure and supersaturation were controlled. However, in this case the substrate dominates the heat flow and ventilation is small and uncontrolled.

The advantage of the chamber used in this study is that it has the capability of independently simulating the ambient temperature, pressure, supersaturation and ventilation velocity, all under controlled conditions. To date, no other laboratory instrument has had this capability.

The purpose of this particular study was to attempt, through the use of a controlled environment, to answer some of the questions associated with the growth of ice crystals. I was most interested in determining how ice crystal growth varies as a function of ambient temperature, supersaturation and, particularly, ventilation velocity, i.e., the fall velocity of the crystal; and how the transition from plates to dendrites and from columns to needles is dependent upon the ambient supersaturation and the ventilation velocity. I am also interested in the growth of ventilated ice crystals in an environment with droplets, and in the habit of ice crystals at low supersaturation.

## II.

### REVIEW OF PREVIOUS WORK

A history of early observations and sketches of ice crystals, as detailed by Hellman (1893), is reported in the books of both Nakaya (1954) and Hobbs (1974). According to this history, observations and sketches of ice crystals were made as early as 1550. Intricate crystal structure, however, was first observed following the discovery of the microscope in the latter half of the seventeenth century. Even so, not until the discovery of photography could the crystal structure be accurately and quickly recorded. Following the arrival and widespread use of photography, Bentley (1931), using photomicroscopy, produced over 6000 spectacular photographs showing the broad variation of forms that exist in natural ice crystals.

Despite these early studies, only recently, with knowledge of molecular processes and crystal aspects, has an attempt been made to reach a comprehensive understanding of ice crystal growth mechanisms and the role which they play in the determination of precipitation. Ukichiro Nakaya and his fellow workers of Japan were the first to undertake such a project in the laboratory, beginning in 1932. Nakaya devised an experiment in which he grew snow crystals in his laboratory under controlled temperature and supersaturation conditions. From these studies he was able to produce for the first time artificial snow crystals which closely resembled those found in the atmosphere. His books and various papers contain hundreds of photomicrographs, not only of these snow crystals, but also of natural crystals. Nakaya made a distinction between a snow crystal and an ice crystal. He

defined the ice crystal as the crystal of ice formed in the air by condensation of water vapor. This ice crystal then represents what he called the 'germ' for the snow crystal. He also called the crystals formed from supercooled water droplets by seeding, ice crystals. He believed that the form and structure of the snow crystal that is grown from this germ of ice or ice crystal are determined by the meteorological conditions met after this germ is formed. Although he realized that it is not possible with this designation to draw a distinct line between snow and ice crystals, he believed that since it was possible to grow a snow crystal under different meteorological conditions from those under which it was nucleated that this designation would be useful in eliminating possible confusion between the two processes. This distinction is still made by many from the 'Japanese school'; however, the 'European school', for the most part, have made no differentiation between the two terms and often use them interchangeably. In this study no distinction will be made between the two terms.

Paralleling the early studies of snow crystals by Nakaya and his fellow workers were atmospheric observations and both laboratory and theoretical studies in various other parts of the world. These observations and studies have continued to the present time. The list of those participating and their contributions over the years is prodigious. However, detailed histories and summaries of these contributions may be found in Mason (1971), Lamb (1970) and Hobbs (1974).

#### A. Ice Crystal Terminology and Ice Crystal Habit

The external shape of an ice crystal is determined by the relative rates of growth of the different crystallographic faces. That is, those crystallographic faces or planes having the fastest rate of



growth also disappear most readily. This fact results in the observed most prevalent ice crystal growth form under normal temperature and pressure conditions being a prism bounded on the two ends by the slowly growing  $\{0001\}$  "basal" faces and on the six sides by the slowly growing  $\{10\bar{1}0\}$  "prism" faces. The crystallographic faces are designated here by their Miller-Bravais indices. Figure 2.1(a) and (b) illustrate this most prevalent growth form. Crystallographic directions

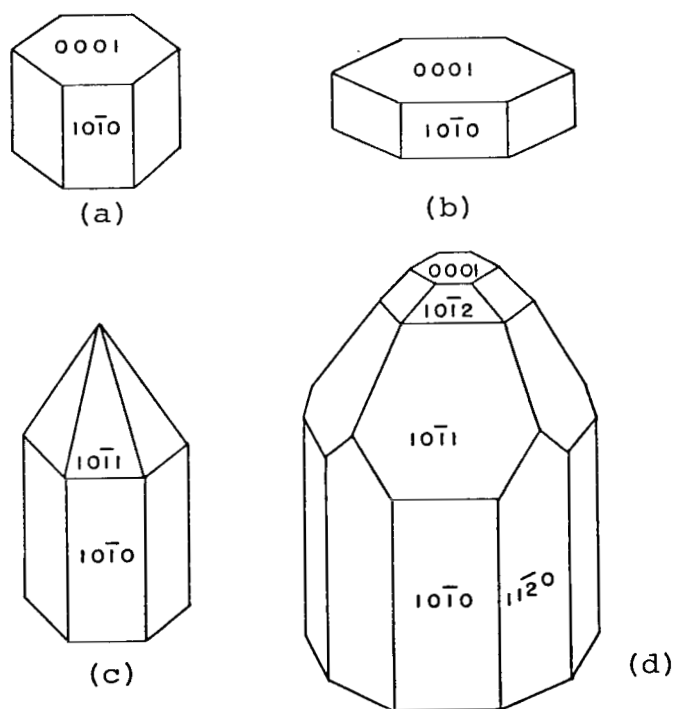


Fig. 2.1 Schematic representation of possible ice crystal growth forms. Wolff (1955)

are indicated by enclosing the Miller-Bravais indices in square brackets. For the hexagonal symmetry of ice the crystallographic direction  $[0001]$  indicates a direction perpendicular to the basal face  $(0001)$  and is called the 'c'-axis. The basal face contains three

'a'-axes oriented  $120^\circ$  from each other. That is, the crystallographic direction  $[11\bar{2}0]$ , for example, which is perpendicular to the crystallographic face  $(11\bar{2}0)$  in Fig. 2.1(d), indicates the direction of one of these 'a'-axes. Furthermore, due to symmetry considerations the 'a'-axes are indistinguishable so growth along any of the 'a'-axes can be said to be along the  $\langle 11\bar{2}0 \rangle$  crystallographic direction. Figure 2.2 shows the unit cell for the hexagonal ice structure. The basic crystal

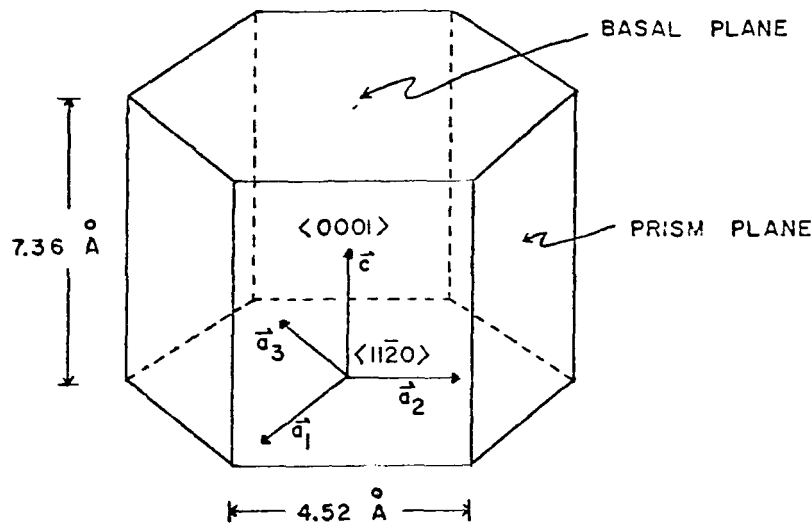


Fig. 2.2 The unit cell for the hexagonal ice structure. Gamara (1972)

habit is determined by the ratio of the lengths along the 'c' and 'a'-axes. If the ratio  $c/a$  is large the crystal is prismatic, Fig. 2.1(a). Whereas, if the ratio  $c/a$  is small the crystal is plate-like, Fig. 2.1(b). Ice crystals are commonly classified into one of five basic crystal habits: hexagonal solid prisms, hexagonal hollow prisms, needles, hexagonal plates and dendrites. Figure 2.3 illustrates these five basic habits.

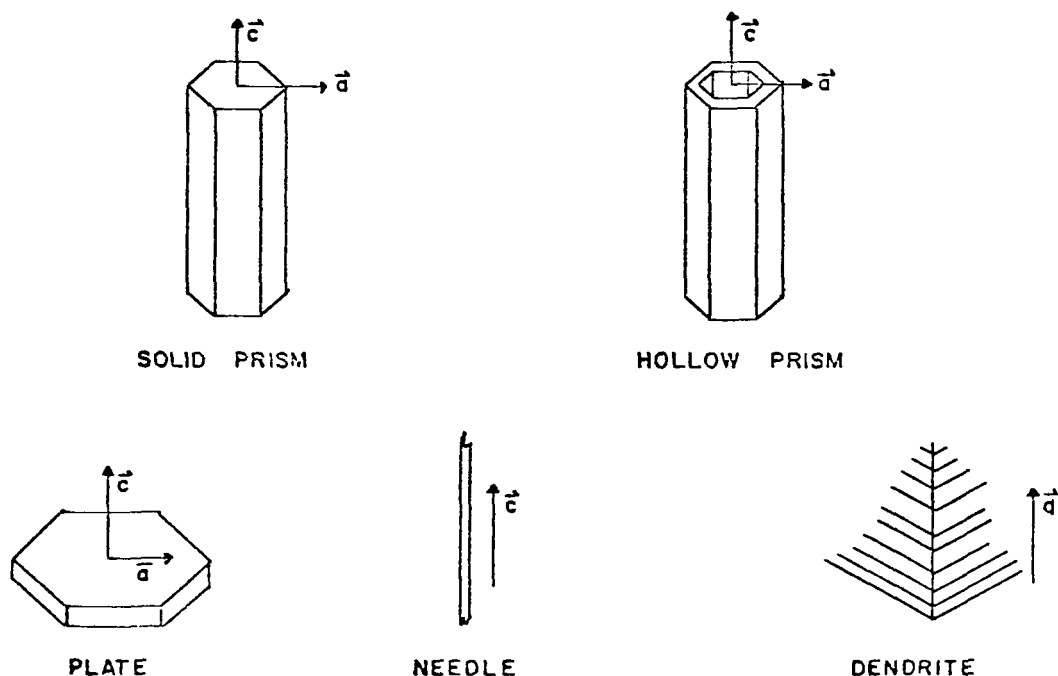


Fig. 2.3 Observed basic ice crystal forms. Gamara (1972)

Much effort has been expended in delineating the ice crystal habit as a function of the ambient atmospheric conditions. It is now generally conceded that temperature is of primary importance and ambient supersaturation is of secondary importance in determining the ice crystal habit. These findings are the culmination of several laboratory experiments and a multitude of atmospheric observations.

One of the first attempts to display the habit of ice crystals as a function of both the ambient temperature and supersaturation, or vapor density excess, was made by Nakaya. These diagrams are often referred to as 'Nakaya diagrams'. Figure 2.4 is such a diagram and shows the effect of both temperature and supersaturation on ice crystal habit. This diagram is based largely on the laboratory work of Hallett and Mason (1958a). If instead of graphing percent supersaturation relative to ice, one graphs vapor density excess over ice, one obtains

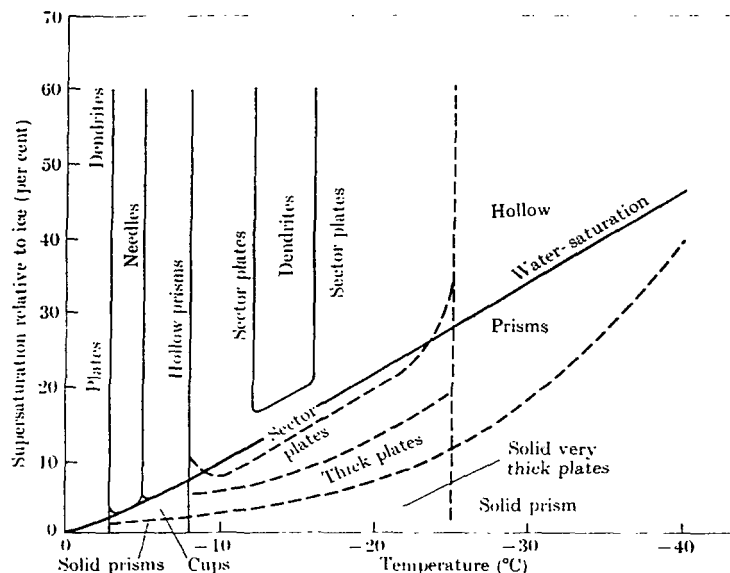


Fig. 2.4 Ice crystal habit as a function of temperature and supersaturation relative to ice. From Mason (1971)

a diagram like Fig. 2.5 which shows the results obtained by Kobayashi (1958) in his laboratory experiments. Likewise, Magono and Lee (1966) have presented this same type 'Nakaya diagram' more pictorially, as illustrated in Fig. 2.6, for natural crystals occurring in the atmosphere. One of the most striking characteristics common to all three of these 'Nakaya diagrams' is the fact that near water saturation the basic crystal habit makes three transitions between  $0^{\circ}\text{C}$  and  $-30^{\circ}\text{C}$ . That is, the basic crystal habit is plates from  $0^{\circ}\text{C}$  to  $-3^{\circ}\text{C}$ , prisms from  $-3^{\circ}\text{C}$  to  $-8^{\circ}\text{C}$ , plates from  $-8^{\circ}\text{C}$  to  $-25^{\circ}\text{C}$  and prisms again for temperatures colder than  $-25^{\circ}\text{C}$ . There is some disagreement about the absolute value of the temperatures, for example within  $1^{\circ}\text{C}$  or  $2^{\circ}\text{C}$ , at which these transition boundaries occur, but their existence is well established. The transition boundaries at  $-3^{\circ}\text{C}$  and  $-8^{\circ}\text{C}$  are sharp, whereas the transition boundary near  $-25^{\circ}\text{C}$  is more gradual.

The effect of ambient supersaturation is to exaggerate the

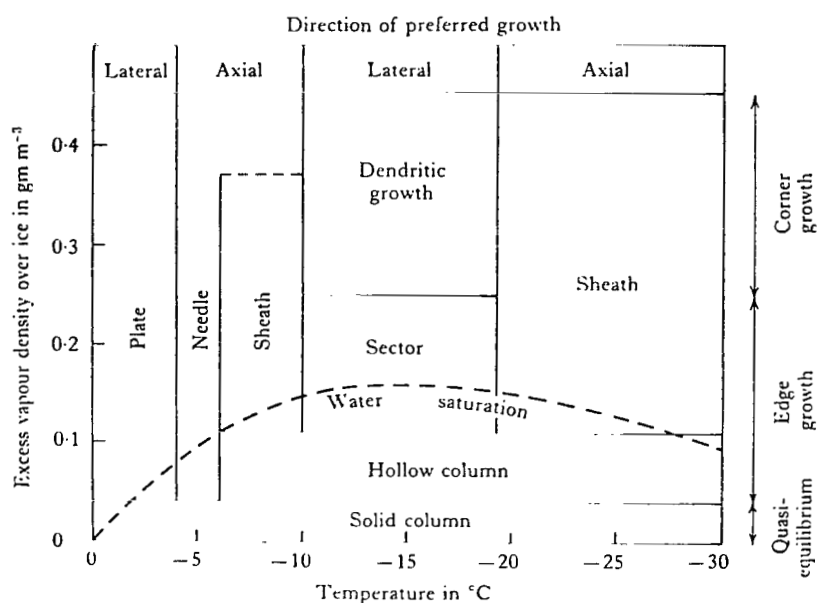


Fig. 2.5 Ice crystal habit as a function of temperature and vapor density excess over that of ice. Kobayashi (1958)

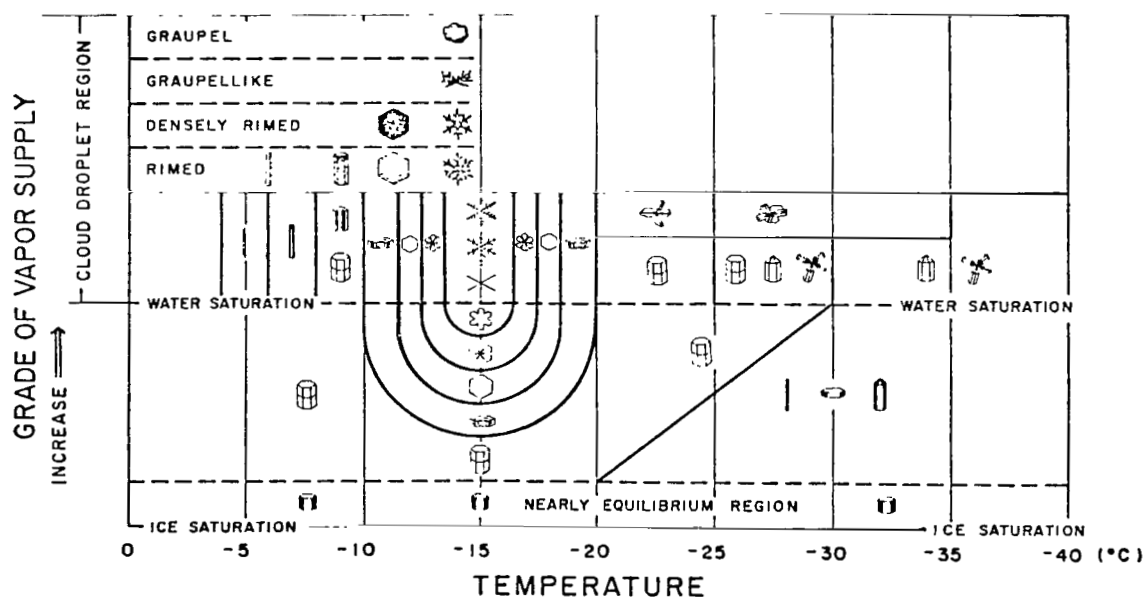


Fig. 2.6 Pictorial diagram showing the dependence of ice crystal type upon both temperature and supersaturation relative to ice. Magono and Lee (1966)

extremes in habit. In fact, over the temperature region  $0^{\circ}\text{C}$  to  $-30^{\circ}\text{C}$  and at large values of ambient supersaturation, the ratio of crystal axes,  $c/a$ , may vary over such a wide range of values as .01 for large thin plates to approximately 50 for long narrow needles.

A comprehensive understanding of ice crystal growth must include an explanation of why, near water saturation, and within specific temperature ranges, the growth should take place preferentially along the 'a'-axis and, at other temperatures, along the 'c'-axis. In any attempt to fully explain these different relative growth rates it is necessary to consider the growth mechanisms by which the crystal faces are propagated. Hence, an account must be made not only of the crystal structure of ice and its equilibrium forms, but also of the surface kinetic possibilities of adsorption and diffusion of molecules across the surface of the individual growing crystal faces, of the accommodation of these molecules into the crystal lattice, and of the temperature and vapor diffusion fields which surround the crystal.

In the past, several experiments have been devised and performed in an attempt to gain an insight into how the surface kinetics of the crystal and other relevant parameters interact under different ambient conditions to produce the observed crystal habits. The recurring difficulty in these experiments has been in accurately determining the actual conditions in which the ice crystal growth took place.

In general, the fewer the parameters involved in the experiment, the simpler it is to separate the effects due to one individual parameter. However, the fewer the parameters involved the less the experiment simulates actual crystal growth conditions in a cloud. I have chosen to separate my discussion of previous experiments into two

classes: those experiments utilizing a static environment, that is, the carrier fluid flow is a minimum and those experiments utilizing a ventilated environment.

#### B. Ice Crystal Growth in a Static Environment

The first experiments dealing with ice crystal growth in a semi-static environment were conducted by Nakaya (1954) in a convection chamber. He grew the crystals on a fine rabbit's hair suspended in a cylindrical cold-chamber. A beaker of water, the temperature of which could be controlled and maintained as warm as desired, was located at the base of the chamber and served as the moisture source. A fog, produced over the warm water, rose due to natural convection, becoming supercooled before reaching the ice crystals suspended in its path. Therefore, the ice crystals grew in an ambient environment which was near water saturation but which also contained small water droplets. The ventilation velocity or carrier fluid velocity, although probably less than  $5 \text{ cm s}^{-1}$ , was not insignificant. The presence of the water droplets and the ventilation velocity made calculation of the "true" supersaturation of the environment impossible. So the results were not only difficult to interpret, but, because the precise effect of neither the ventilation velocity nor the presence of the water droplets was known, it was also difficult to compare these results with those of other experiments where no droplets were present and the convection velocities were much smaller. Even though it was difficult, in these experiments, to separate the independent effects of the ambient supersaturation, the ventilation velocity and the presence of the water droplets on the crystal habit, Nakaya was able to extract enough information to compose the first 'Nakaya diagram'.

Later laboratory experiments by Kobayashi (1957), Hallett and Mason (1958a), Hallett (1965), and Rottner and Vali (1974) employing static thermal diffusion chambers have helped to better establish the relationship of ice crystal habit to ambient temperature and supersaturation.

The basic operating principle of the static thermal diffusion chamber is the same as that for the dynamic thermal diffusion chamber used in this study. The static thermal diffusion chamber consists of a sealed chamber with two horizontal plates separated by a vertical distance of 1 to 20 cm. The temperature of the plates is controlled independently with the top plate being maintained at a warmer temperature than the bottom plate to suppress convection due to thermal instability. If the warmer top plate is coated with ice or water, it acts as a water vapor source and the bottom plate as a vapor sink. The density of the water vapor at the two ice plate surfaces is equal to the equilibrium vapor density of ice at that respective temperature. Both the density of the water vapor and the ambient air temperature vary almost linearly with height between the two surfaces. However, the equilibrium vapor density, at any height, is an exponential function of temperature and thus the air between the two plates is supersaturated with respect to ice. (For a more detailed account of this operating principle see Chapter IV). The maximum supersaturation occurs near the center of the chamber and may be changed by varying the temperature difference between the top and bottom plates, larger temperature differences corresponding to higher supersaturations. Therefore, if liquid water is used as the vapor source at the top plate, instead of ice, larger temperature differences can be sustained



and much larger supersaturations may be obtained in the chamber. At supersaturations much greater than water saturation, any aerosols or particles present in the chamber nucleate and form water droplets which grow and then settle to the chamber floor due to gravity. When such nuclei have all settled out, very high supersaturations, several hundred percent with respect to ice, can be achieved such that even the ions produced along paths of cosmic rays nucleate water droplets. Ice crystals are grown on a fine fiber of glass, nylon or hair suspended vertically in the center of the chamber. A diagram of the modified static thermal diffusion chamber used by Hallett and Mason (1958a) is presented in Fig. 2.7.

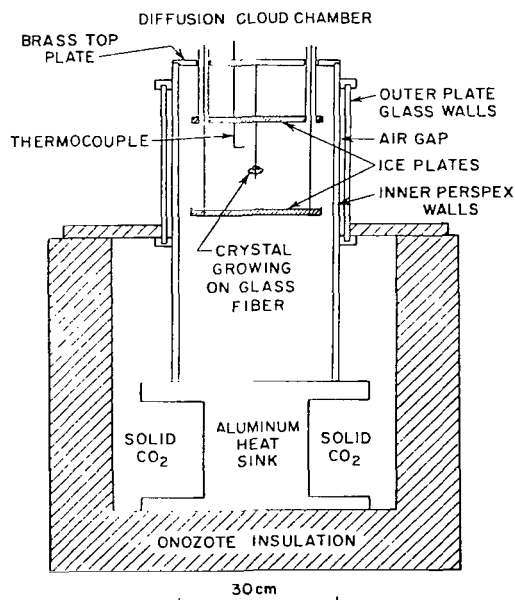


Fig. 2.7 The static diffusion cloud chamber used by Hallett and Mason for growing ice crystals at various temperatures and supersaturations. Mason (1963)

One of the chief advantages of both the convection chamber and

the thermal diffusion chamber over many of the other artificial or natural environments in which ice crystal growth has been studied is the fact that ice crystals can be grown and observed in them over long periods of time. The ambient growth conditions can either be maintained relatively constant or they can be altered during the period of crystal growth.

Nakaya (1954), and later Kobayashi (1957), changed the ambient conditions of supersaturation and temperature in their convection chambers during the period of crystal growth. Likewise, Hallett and Mason (1958a), by varying the vertical distance between the horizontal plates of their modified diffusion chamber, Fig. 2.7, were able to change the ambient supersaturation without changing the temperature in the very center. A primary dependence of the crystal habit on temperature with a secondary dependence on supersaturation was found by all. Further, they all found that when a growing crystal was introduced to a different ambient environment the new growth immediately assumed the habit characteristic of that new environment. This strongly suggested that the ice crystal habit is a product of the ambient environment and of the crystal growth processes but not of the nucleation of the seed crystal. The secondary dependence of the habit on supersaturation was dramatically illustrated by the fact that at a constant temperature, near  $-14^{\circ}\text{C}$ , dendritic growth was only observed when the air was significantly supersaturated with respect to water. At somewhat lower supersaturations, but still greater than water saturation, crystals which Hallett and Mason (1958a) called "dorites", i.e., spear-like, grew. At progressively lower supersaturations sector plates, then plates, and finally, nearly equiaxed crystals grew.

It should be noted that words such as dendrites, dorites and sectors, as applied to ice crystals, are descriptive terms and not quantitative assessments of either the crystal habit or linear growth rate. In fact, these terms may have quite dissimilar meanings to different individuals. Nakaya (1954) separated the crystals which were arbitrarily called dendrites into two classes: "dendritic" and "sector" crystals. He attempted to classify the crystals according to the branch tip, that is, according to the final ambient conditions encountered in its formation. If the branch tip was a straight-line structure he called the crystals sector. Figure 2.8(a) and (b) illustrate these designations, whereas Fig. 2.8(c) illustrates the widest form of the crystal which Hallett called a dorite. Although these

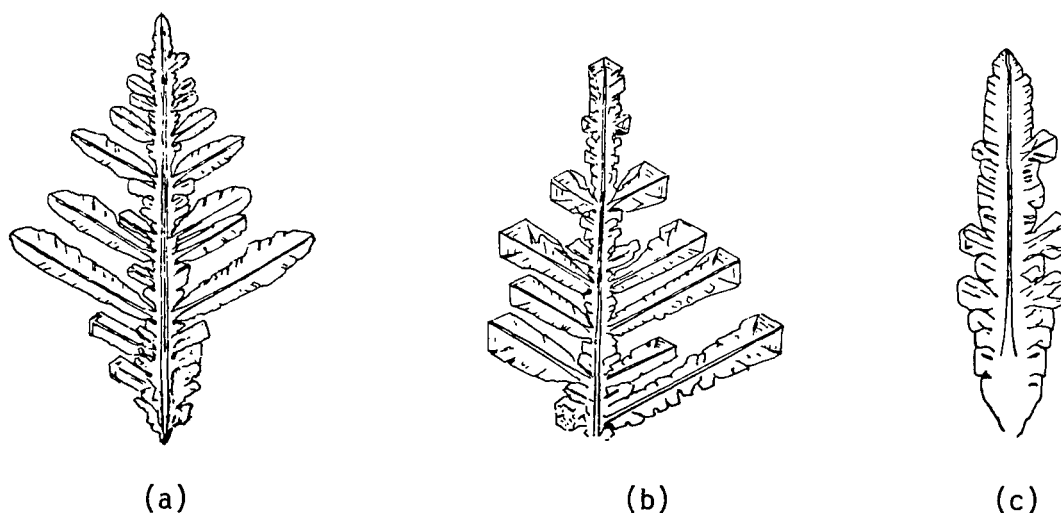


Fig. 2.8 Distinction between dendritic, sector and doritic crystals.  
Nakaya (1954)  
(a) 'true' dendritic crystal  
(b) dendritic crystal with sector-like structure  
(c) 'dorite' crystal

definitions are useful, they are somewhat ambiguous. It is sometimes helpful, although awkward, to include another adjective in the

descriptive term and thus describe the crystals as "sector plates", "sector dendrites", and so forth.

Still other experiments have been performed in a static environment in which ice crystals were grown on a substrate. The experiments of Shaw and Mason (1955); Bryant, Hallett and Mason (1959); Hallett (1961); Mason, Bryant and Van den Heuvel (1963); Kobayashi (1965); Lamb (1970); and Anderson (1974) are representative of this type of study.

In the experiments of Shaw and Mason (1955) and of Lamb (1970) the ice crystals grew on a smooth metal surface, whereas in the experiments of Bryant, Hallett and Mason (1959); Hallett (1961); Mason, Bryant and Van den Heuvel (1963); Kobayashi (1965); and Anderson (1974) the ice crystals grew on the face of a crystal of dissimilar material. In such special growth, where crystals of one material grow in a definite orientation on a crystal face of another material they are said to exhibit "oriented overgrowth" or "epitaxy". Thus, epitaxial growth of ice crystals is said to occur when the direction of the 'c'-axis of the growing ice crystal bears a simple relationship to the crystallographic orientation of the substrate. Bryant, Hallett and Mason (1959) studied the epitaxial growth of ice crystals on such varied materials as AgI, CuS, CdI<sub>2</sub>, PbI<sub>2</sub>, V<sub>2</sub>O<sub>5</sub>, brucite, calcite, muscovite, orthorhombic HgI<sub>2</sub> and orthorhombic iodine. However, the crystals most commonly used for ice crystal epitaxial growth have been AgI, PbI<sub>2</sub> and CuS (covellite).

Bryant, Hallett and Mason (1959) were the first to observe that very thin ice crystal plates growing epitaxially on fresh {0001} covellite cleavage surfaces exhibited interference colors in reflected

white light. These interference colors can be calibrated and hence the thickness of the growing ice crystals can be determined. Other epitaxial substrates also exhibit this interference phenomena.

It has been found that at low and moderate supersaturations, these epitaxial ice crystal plates will often grow laterally for long periods of time without thickening, that is, without a detectable change in interference color. However, if the growing crystal comes in contact with either another crystal or an obstacle, then successive new layers of growth spread from the point of contact. Likewise, if the ambient supersaturation is suddenly increased or a large electric field is introduced, the crystal begins to thicken but, in these cases, much more uniformly. This thickening process has been interpreted as the propagation of steps across the crystal surface. Below a critical supersaturation these steps are formed by a process of heterogeneous nucleation. At high supersaturations, however, the thickening process has been interpreted as successive two-dimensional nucleation followed by lateral growth.

Hallett (1961), and later others, found that the speed of propagation of these steps, a few hundred angstroms in height, is inversely proportional to the step height for a given temperature and ambient supersaturation. This result is interpreted as meaning that water molecules impinging on the exposed ice crystal surface are not incorporated immediately into the crystal lattice but may be adsorbed and migrate short distances, i.e., a few  $\mu\text{m}$ , over the crystal surface before being either incorporated into the steps or evaporating, i.e., being desorbed, from the surface. For a constant ambient vapor density excess and a given step height, Hallett (1961) found a remarkable

temperature variation, shown in Fig. 2.9, in the speed of propagation

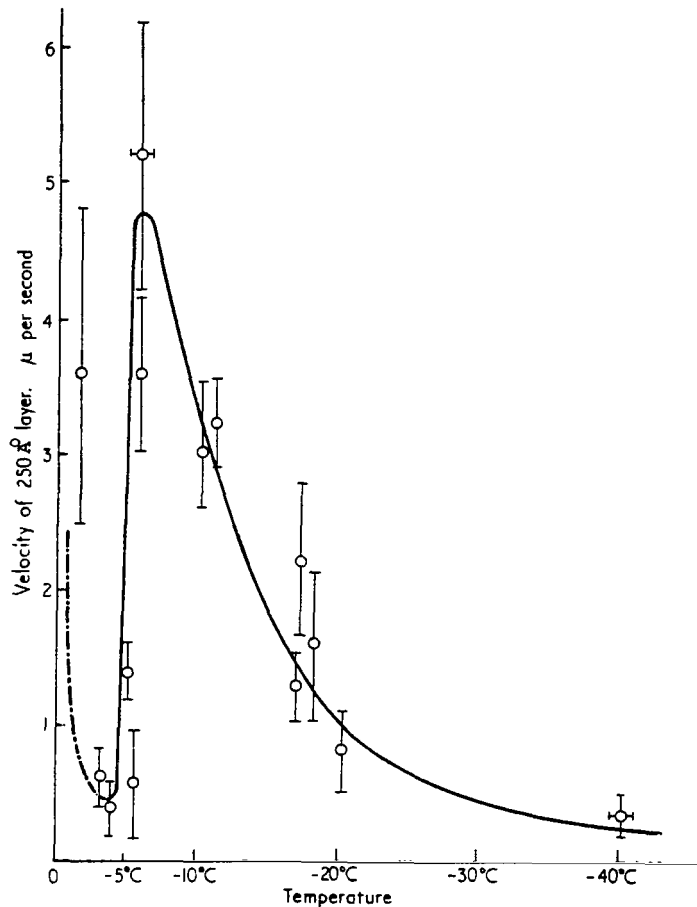


Fig. 2.9 The temperature variation of the rate of growth of a layer 250 Å thick. Excess vapor density  $0.25 \text{ g m}^{-3}$ . Hallett (1961)

of these steps. Later experiments by Mason, Bryant and Van den Heuvel (1963) and Kobayashi (1965) confirmed the general shape of the curve found by Hallett (1961) but suggested it should be shifted to colder temperatures by about  $4^{\circ}\text{C}$ . However, Ryan and Macklin (1969) pointed out that essentially the same equipment was used in all these experiments and although Hallett (1961) adjusted his experimental data with an empirical temperature correction of  $4^{\circ}\text{C}$ , which was apparently neces-

sary, the other experimenters did not. Hence, the discrepancy in the results is probably not real.

There are problems, as with other experiments, associated with ice crystal growth on a substrate. The substrate dominates the heat flow and the ventilation is uncontrolled. Furthermore, when thin ice crystals grow on a substrate the local atomic fitting between the ice crystal and the substrate is the primary factor initiating the deposit orientation. As the ice crystals grow laterally, the degree of lattice misfit must affect the stress and stability of the growing ice crystal and possibly induces dislocations which could significantly affect the growth. Anderson (1974) and Anderson and Hallett (1977), for example, interpreted some of their results, particularly for thin crystals, as being induced by the presence of this crystal strain. Hence, growth on a substrate does not fairly simulate the conditions encountered by an ice crystal growing in the free air.

### C. Ice Crystal Growth in a Ventilated Environment

Marshall and Gunn (1955) were among the first to postulate that the carrier fluid velocity or ventilation velocity could play a significant role in determining the 'effective' vapor density excess over the crystal and thus its growth. Later, Hallett (1965) suggested that a ventilation velocity would cause the supersaturation dependent habit transitions, for example, plates to dendrites, and prisms to needles, to occur at a lower ambient supersaturation than found in the static case. However, the only experiments, prior to studies with the dynamic thermal diffusion chamber, designed to study the effect of ventilation on ice crystal growth from the vapor have involved ice crystals falling through a supercooled water cloud. Representative

of this type experiment are the studies of Aufm Kampe, Weickmann and Kelley (1951); Reynolds (1952); Mason (1953); Isono, Komabayasi, Yamanaka and Fujita (1956); Fukuta (1969); and Ryan, Wishart and Shaw (1976). This type of experiment is generally carried out in a cold chamber in which a cloud of supercooled water droplets is "seeded" by some mechanism to produce ice crystals which then grow and fall out. As the crystals grow, they deplete the vapor supply and thus lower the ambient supersaturation. Therefore, droplets must be added to maintain an ambient environment near water saturation. Also, as the crystals grow their terminal fall velocity and hence their ventilation velocity increases. Furthermore, the presence of the droplets and ice crystals makes the 'effective' supersaturation near the crystals difficult to determine but even more difficult to control. So, although these studies closely simulate the crystal growth conditions encountered in a cloud, they do not allow close observations of the growing crystals, very long growth times (maximum of about 200 seconds), constant environmental growth conditions, or a separation of the related but distinct effects of droplets and the ventilation velocity. Nonetheless, these experiments have proven very valuable in providing further evidence that ice crystal habit is a primary function of temperature with a secondary dependence on supersaturation. Moreover, these experiments have not only shown the manner in which ice crystal mass growth rate varies as a function of the ambient temperature, but, in addition, have provided valuable data which has been used in predicting mass growth rates from empirical models.

Experiments not directly related to ice crystal growth from the vapor, but which show, at least qualitatively, the effect of ventila-



tion velocity on crystal growth have been performed in both melts and solutions.

Several investigations, Kumai and Itagaki (1953); Lindenmeyer (1959); Hallett (1960); Knight (1962); Hallett (1964); Camp (1965); Macklin and Ryan (1965); Knight (1966); Lindenmeyer and Chalmers (1966) and Pruppacher (1967), to name a few, have been made of ice crystal growth from the melt and the solution under static conditions, both growing freely in the fluid and on a substrate.

Other experiments, Fernandez (1967); Fernandez and Barduhn (1967); Poisot (1968); Miksch (1969); Vlahakis (1972) and Vlahakis and Barduhn (1974), have been performed in which ice crystals grew in a flowing supercooled liquid.

The results of these experiments relevant to this study may be briefly summarized. It was found that the growth rate of the ice crystals, as expected, increased with increasing supercooling and increasing velocity of flow.

In the static case, for crystals growing freely in the fluid, the general relation for growth along the 'a'-axis, valid for supercoolings less than 20°C, is given by

$$da/dt = C_1 (\Delta T)^n \quad \text{in cm s}^{-1}.$$

$\Delta T$  is the supercooling in °C;  $C_1$  is a function of the properties of the liquid, being equal to about 0.1 for pure water and decreasing with increasing solute concentration; and  $n$  is a constant equal to about 2.0. The growth rate along the 'c'-axis is about 100 times less than growth along the 'a'-axis for supercoolings of about 3°C and becomes even less at smaller supercoolings. However, at large supercoolings

of about 15°C the growth rates along both axes are comparable. Hallett (1964) suggested that this marked change in growth along the 'c'-axis with supercooling might be due to a transition from a growth process controlled by concentration of imperfections to one controlled by surface nucleation.

In the ventilated case there is enhanced growth in the upstream direction and suppressed growth in the downstream direction. This is the result of latent heat being carried downstream from the crystal tip and subsequently reducing the supercooling and hence the growth rate in the downstream region. Thus in the ventilated case, at velocities as low as 0.042 cm s<sup>-1</sup> and as high as 46 cm s<sup>-1</sup>, the growth rate along the 'a'-axis in cm s<sup>-1</sup> is given by

$$da/dt = \frac{A}{1+B} V^{1/2} \Delta T^{3/2}$$

where A is a function of the known properties of pure water and ice and B is a function of the solution, V is the ventilation velocity in cm s<sup>-1</sup> and ΔT is the supercooling in °C. There is, however, an anomaly. That is, the growth rate versus solute concentration has a maximum rather than simply decreasing as the solute concentration increases. This anomaly is located in the dilute concentration range and the effect is not solute specific, but occurs with both electrolytes and nonelectrolytes. Furthermore, the maximum growth rate is more pronounced with increased supercooling. This anomaly remains to be explained.

Some observations of Hallett (1964) of growth in static super-cooled water are also interesting. He found that with increased supercooling both the separation and width of the secondary dendrite arms

decreased. He also observed that the angle of the growth front of an individual dendrite, determined by the relative rates of growth along primary and secondary  $\langle 11\bar{2}0 \rangle$  branches, increased with decreasing temperature from an angle of about  $60^\circ$  at  $-1^\circ\text{C}$  to a maximum of  $120^\circ$  at  $-8^\circ\text{C}$ , so that the limiting shape of the growth front became hexagonal. This limiting form occurred when the growth rates of the primary and secondary branches became equal and the secondary branches were nucleated very near the tip of the primary branch.

#### D. Some Other Parameters Affecting Ice Crystal Growth and Habit

Several experiments in the past have been performed in an attempt to determine the variation in crystal growth due, not only to the temperature, ambient supersaturation and ventilation velocity, but also to such varied parameters as reduced or increased ambient pressure, the molecular weight and thus the thermal and vapor diffusivity of the carrier gas, contaminants in the carrier gas, an applied electric field and even dislocations in the crystals themselves. The observed variation of crystal habit associated with each of these parameters gives information which is vital not only in distinguishing ambient from surface kinetic effects but also in delineating the relative magnitudes of their importance under various growth conditions.

#### Reduced and Increased Ambient Pressure and Variation of the Molecular Weight of the Carrier Gas

Isono, Komabayasi and Ono (1957) and Isono (1958) studied the growth and habit of ice crystals produced by seeding a supercooled cloud of water droplets with silver iodide, in a cold chamber containing different atmospheres. When crystals were grown in either hydrogen at a pressure of one atmosphere or in air at low pressure, 20 to 80 mm Hg, they observed nearly isometric growth,  $c/a = 1$ , over the

entire temperature range  $-7^{\circ}\text{C}$  to  $-16^{\circ}\text{C}$ . However, at a pressure of one atmosphere the growth habits observed in carbon dioxide, nitrogen and oxygen were similar to those formed in air at normal pressure.

Kobayashi (1958) using a convection chamber also investigated the effect of reduced air pressure on ice crystal habit and found comparable results. However, when Van den Heuvel and Mason (1959) performed experiments in a static thermal diffusion chamber using reduced pressures as low as 20 mm of Hg or using gases with differing molecular weights, they found variations in the rate of growth in accord with the thermal conductivity and the vapor diffusivity of the carrier gas, but they observed no real changes in the habits of the ice crystals. They suggested that traces of contaminants may have been present in the apparatuses of the Japanese workers. Later, it was suggested by Lamb (1970) that errors in the determination of the ambient supersaturation may have been the real source of conflict giving these differing experimental results. As Kobayashi acknowledged, it is very difficult to control the ambient supersaturation in an environmental gas through which water molecules readily diffuse.

In an attempt to elucidate the contributions of the vapor diffusivity and the thermal conductivity of the carrier gas to the overall ice crystal habit, Gonda and Komabayasi (1970), Gonda and Komabayasi (1971), Gonda (1976) and Gonda (1977) performed a series of experiments in which they grew small ice crystals, 20 to 50  $\mu\text{m}$  diameter, in various atmospheres by seeding, with silver iodide smoke, a supercooled water droplet cloud contained in a small cold chamber. The atmospheres consisted of varying mixing ratios of helium and argon gases at both reduced and increased ambient pressures. By

changing the mixing ratios of these two inert gases and their total pressure it was possible to vary both the diffusion coefficient of water vapor and the thermal conductivity of the ambient atmosphere independently over a wide range of values. From early experiments they drew the following conclusions:

- 1) The absolute growth rate of ice crystals increased with a decrease in the mean molecular weight of the carrier gas.
- 2) The size of the central featureless portion of hexagonal plate crystals increased with a decrease in the mean molecular weight of the carrier gas.
- 3) Hexagonal plates which exceeded a certain critical size developed branches at their six corners. This critical size increased as the mean molecular weight of the carrier gas decreased.

Gonda's later experiments were conducted to study specifically the individual effects of the vapor diffusivity and the thermal conductivity. Figure 2.10 shows diagrammatically the relative effect as determined by Gonda (1976) of the vapor diffusivity and the thermal conductivity on the habit of small ice crystals at temperatures of  $-7^{\circ}\text{C}$  and  $-15^{\circ}\text{C}$  respectively. From these results and the results of other experiments they concluded the following:

- 1) Under conditions of constant vapor diffusivity ( $D = 0.77 \text{ cm}^2 \text{ s}^{-1}$ ), skeletal structures and dendritic structures developed more readily as the thermal conductivity of the atmosphere was increased.
- 2) Under conditions of constant thermal conductivity ( $K = 34.4 \times 10^{-5} \text{ cal cm}^{-1} \text{ s}^{-1} \text{ }^{\circ}\text{C}^{-1}$ ), skeletal structures and

dendritic structures developed less readily as the vapor diffusivity was increased.

- 3) The dependence of the habit of small ice crystals on temperature was most pronounced at high ambient pressures, but had a tendency to vanish at low ambient pressures.

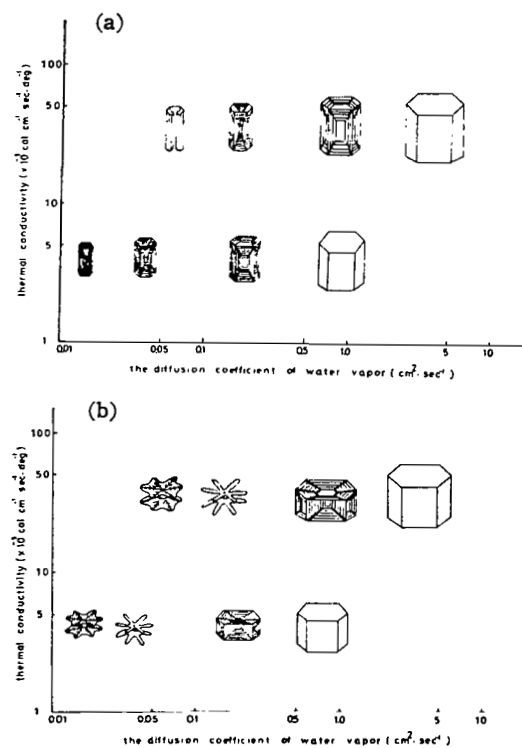


Fig. 2.10 Schematic diagram of the habit and the growth feature of small ice crystals with respect to the vapor diffusivity and the thermal conductivity. (a) at  $-70^{\circ}\text{C}$ ; (b) at  $-150^{\circ}\text{C}$ . Gonda (1976)

They also suggested that the habit and growth features of ice crystals under identical ambient conditions are dependent upon the size of the crystals. Komabayasi (1970) performed a theoretical calculation and found that the effect of the diffusion coefficient on the shape of ice crystals is much larger when the crystal is small than when it is

large. Therefore, he reasoned that considerable discretion should be exercised in comparing the habit and growth features of crystals larger than about 1 mm diameter, for example, those of Van den Heuvel and Mason (1959), with those of crystals less than 50  $\mu\text{m}$  diameter.

The experiments of Lamb (1970), which utilized a stainless steel substrate in an environment of pure water vapor over the temperature range  $0^{\circ}\text{C}$  to  $-20^{\circ}\text{C}$ , were particularly valuable in providing information concerning surface kinetic effects. Since no vapor diffusion field existed over the crystals grown in an environment of pure water vapor and since the natural flow of heat was reversed by growing the ice crystals on a substrate of high thermal conductivity, surface kinetic effects were much more important than normal in controlling the crystal growth. Lamb found that in pure water vapor, at low pressure, ice crystals were generally regular hexagonal crystals when initially formed. However, as they increased in size both the sharp edges and the well defined crystallographic features disappeared. On the other hand, when significant amounts of either air or some other gas were present, the crystal edges and corners remained sharp even when the crystals grew quite large. Whether the gas present, at these low pressures, was air or helium made no visually detectable difference. In either case, the surface structure of the crystals grown under these conditions was more complicated than that of crystals grown in pure water vapor. Under conditions of crystal growth in pure water vapor, Lamb ascribed the sharp crystal features, that is, distinct crystallographic faces to 'inherent' surface kinetic effects controlling the growth mechanism. As these crystals grew larger and thicker, heat transfer to the substrate through the poorly heat conducting ice

crystal was diminished, so the ice crystal surface farthest from the substrate warmed up due to continued release of latent heat and hence its growth rate decreased to compensate for this reduced heat transfer. The thin lateral edges of the crystal, however, maintained good thermal contact with the substrate and growth in the lateral directions continued at an unreduced rate giving crystals a characteristic two-dimensional appearance. Lamb attributed the differences in crystal features when a carrier gas was present to the introduction of a vapor diffusion field rather than to the interactions of the carrier gas with the surface kinetics of the crystal. That is, when air was present the resistance to mass transfer controlled the growth rate, whereas in pure vapor the resistance to heat transfer was the limiting factor.

#### Contaminants in the Carrier Gas

Several experiments have shown that the normal ice crystal habits can be profoundly modified by the presence of certain organic vapors. Vonnegut (1948) observed that the addition of butyl alcohol of about  $10^{-2}$  mb partial pressure changed the ice crystals growing in a supercooled cloud of droplets at  $-20^{\circ}\text{C}$  from hexagonal plates to hexagonal columns. Schaefer (1949) found several vapors such as acetone, acetic acid, nitric acid, silicones and alcohols effective in modifying the crystal growth and habit. Hallett and Mason (1958a) and (1958b) using a static thermal diffusion chamber observed that small amounts of camphor vapor affected the crystal growth such that needle-like crystals appeared at all temperatures between  $0^{\circ}\text{C}$  and  $-40^{\circ}\text{C}$ . They also investigated in some detail the effect of iso-butyl alcohol on the ice crystal habit. Figure 2.11 from Hallett (1968) shows this effect as



a function of iso-butyl alcohol concentration over a wide range of ambient temperatures. As can be noted from the figure, at high concentrations of iso-butyl alcohol the habit at  $-15^{\circ}\text{C}$  reverts to a

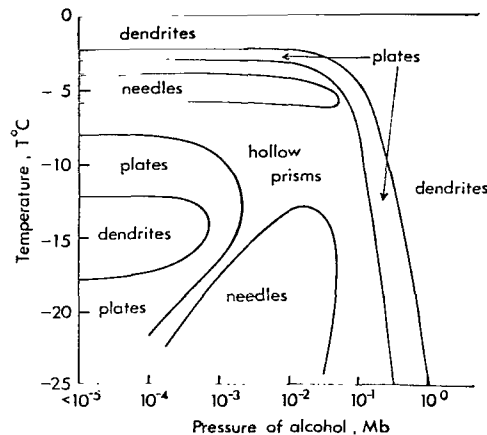


Fig. 2.11 The effect of iso-butyl alcohol on ice crystal habit.  
Hallett (1968)

malformed type of dendritic growth. Anderson, Sutkoff and Hallett (1969) showed how the presence of vapors of methyl 2-cyanacrylate resin suppressed dendritic growth along the 'a'-axis and induced fine fibers a few micrometers in diameter to grow along the 'c'-axis.

It would appear that since foreign vapor concentrations, too small to affect the macroscopic mass and heat transfer processes are, nonetheless, effective in upsetting the normal crystal habits that they must somehow interfere with the surface kinetics. Furthermore, from these and other experiments, it appears that chemicals which are somewhat polar are most effective in modifying ice crystal habits. Indeed, if surface kinetic processes are, in fact, a growth limiting mechanism and the ice crystal surface is polar as it is believed to be, then these experimental results are reasonable, although by no

means completely understood.

### Effect of an Applied Electric Field

Just as with variations of other macroscopic parameters, observations of changes in ice crystal growth as a consequence of the application of an external electric field can be used to infer properties of the normal ice crystal growth processes.

Although several studies, each producing essentially similar results, have been made of the influence of applied electric fields on ice crystals growing in supercooled water clouds, the investigation of Evans (1973) was probably the most thorough. Other experiments, such as those by Bartlett, Van den Heuvel and Mason (1963) and Crowther (1972), have been performed in a static thermal diffusion chamber where the presence of cloud droplets was not necessary to sustain ice crystal growth conditions. In all three of the experiments cited, individual ice crystals were secured on a fiber in the presence of an electric field and could be observed throughout the growth process. Maybank and Barthakur (1967) employing a small cold cell also grew stationary ice crystals both with and without an applied electric field. They used, as the vapor source, a single water drop 1-2 mm in diameter suspended near the growing crystal. In each case the electric field was produced by one of two methods. In the first method the electric field resulted from charging, to a high voltage potential, either positive or negative, the metal fiber on which the crystals grew. In the second method the crystals grew from an insulated fiber placed in a uniform electric field. In this case the electric field resulted from oppositely charging two parallel plates.

In the various experiments employing a supercooled water cloud,

it was observed that at applied voltages to the metal fiber of less than or equal to  $\pm 3000$  V, electro-riming occurred. That is, long chains of crystals following the electric lines of force outwards from the electrodes grew very rapidly. These chains were largely composed of conglomerates of small crystals and very little could be deduced about the effects of the electric field on the individual ice crystal habits. However, at applied voltages exceeding  $\pm 6000$  V a silent discharge occurred creating a space charge in the vicinity of the electrode. Most of the cloud droplets entering this region acquired a charge of the same sign as the electrode and were consequently repelled, leaving a virtually droplet-free space around the wire. Subsequent growth of ice crystals on the wire electrode was from the vapor only. The crystals tended to grow as slender "needles" oriented in the direction of the field. The tendency for these "needles" to develop fragile branches was a strong function of the rate of growth which, in turn, was governed by the local vapor density. In fact, a critical local vapor density was necessary for the formation of branched "needles" at all.

The experiments conducted in the absence of cloud droplets, for example, in the static thermal diffusion chamber, demonstrated that below a critical threshold value of the external electric field near  $450 \text{ volt cm}^{-1}$ , neither electro-riming nor rapid vapor growth called 'electric growth' occurred. At field strengths somewhat larger than this threshold value, a time-lag existed between the application of the applied field and commencement of rapid growth. This time-lag decreased with increasing electric field strength. This time-lag was ascribed to the dependence of the magnitude of the local electric field

at the tip of the ice crystal on the shape of the growing tip. This local field, being larger the sharper the tip, varied from crystal to crystal and even with time for the same crystal. 'Electric growth' in large uniform external fields of about  $500 \text{ volt cm}^{-1}$  or larger always took the form of "needles" with few if any side branches. When the field was removed side branches developed in the usual way. Near  $-4^{\circ}\text{C}$  and  $-12^{\circ}\text{C}$  the growth was generally along the ordinary  $\langle 0001 \rangle$  and  $\langle 11\bar{2}0 \rangle$  directions respectively. Sometimes, however, with proper orientation of the crystal to the external field, growth occurred along the  $\langle 10\bar{1}0 \rangle$  direction over this whole temperature range. Normal growth has never been observed along this direction. The linear rate of 'electric growth' was observed to be from 10 to 100 times faster at the same ambient temperatures and supersaturations than the linear rate of ordinary needles or dendrites. Although ice crystals grew equally well whether the metal fiber on which they were situated was of either polarity, 'electric growth' did not occur at all in a  $50 \text{ cycle s}^{-1}$  alternating field even at peak voltages five times greater than those needed to initiate 'electric growth' in a steady potential. Another interesting observation was the fact that the 'electric' crystals fractured spontaneously with the expelled fragments being highly charged. New growth then resumed on the remaining crystal remnant. Sometimes, rather than fragmenting, the growing crystal ejected a vortex ring from its tip which was interpreted as consisting of small clouds of ions made visible by their subsequent condensation of water vapor.

It is an understatement to say that the observations of ice crystal growth in an electric field are poorly understood. Although

the increased growth rate may be exclusively attributable to either ambient kinetics, as suggested by Evans (1973), or to surface kinetics, it is also possible that 'electric growth' is somehow a complex function of both.

### Crystal Dislocations

The importance of dislocations in facilitating ice, or for that matter, any other crystal growth, particularly at low ambient supersaturations where two-dimensional nucleation is ineffective, has long been recognized. Since it was known that surface irregularities or steps on the growing crystal faces make accommodation of free molecules easier than on a smooth face, a mechanism for the repeated initiation of these steps on each new crystal growth layer was needed to explain observed growth at low ambient supersaturations. F. C. Frank (1949) proposed the existence of internal spiral or screw dislocations. Wherever a screw dislocation emerged on a crystal face a step would be initiated and propagated to each new growth layer. In general, this particular type of dislocation is only one of several which might be present in a given crystal. Depending on both the ambient conditions and the history of the crystal, the actual concentration of each type of dislocation present may vary over wide ranges. Until quite recently, studies of these dislocations have been limited to such indirect methods as etching or observing growth after scratching the surface or performing some other such mechanical or thermal disturbance. However, with the advent and widespread use of x-ray topographic technology in recent years these observations are becoming more direct and quantitative.

In summary, it is evident that although our knowledge of ice crystal growth processes is still lacking, much has been learned in a relatively short period of time.

## III.

## ICE CRYSTAL GROWTH RATE - THEORY AND EXPERIMENT

It has already been stated that the growth of an ice crystal is determined by a large number of variables. This is understandable since a water molecule must pass through several steps in going from a state of free movement in the carrier gas to a fixed position in the crystal. That is, it must be transported to the crystal where it is adsorbed on the crystal surface. In the process of adsorption it must release a portion of its latent heat. It must migrate across the crystal surface to a growth site, generally a step or a kink in a step. Finally, the remainder of the latent heat must be liberated at the growth site as the water molecule becomes incorporated into the crystal lattice. It should be noted that all these steps in the crystal growth process are reversible and if the reverse processes take place sublimation is said to occur.

From a macroscopic viewpoint the growth from the vapor of an ice crystal in air primarily consists of the simultaneous transfer of mass and heat. Transfer of mass involves the diffusion of water vapor through the air to the crystal. Transfer of heat involves both the diffusion of heat from the crystal and a radiation balance between the crystal and its surroundings. Since both diffusion processes will be enhanced by forced and natural convection, the total diffusion process is a combination of molecular and convective diffusion.

A. Molecular Diffusion

The non-steady state flux equation for molecular diffusion of water molecules through air is given by

$$D\nabla^2 C_w = \partial C_w / \partial t,$$

where  $C_w$  is the concentration of the water molecules and  $D$  is the diffusion coefficient which is a function of the composition of the carrier gas and varies inversely with the carrier gas pressure. The term  $\partial C_w / \partial t$  gives the variation in concentration of the water molecules with time. For the steady state  $\partial C_w / \partial t = 0$ , and a determination of the diffusive flux of water molecules reduces to the solution of Laplace's equation. Unfortunately, the number concentration of water molecules is difficult to measure directly. However, the equilibrium partial pressure of the water vapor can be measured directly as a function of temperature and expressed, by means of the ideal gas law, as the vapor density,  $\rho$ , in  $\text{g m}^{-3}$ . Figure 3.1 shows the vapor densities at saturation over plane ice and water surfaces respectively as a function of temperature. The difference in these two saturated vapor densities is also plotted against the scale on the right hand side. Since  $\rho$  is directly proportional to the concentration of the water molecules, it is possible to write

$$D\nabla^2 \rho = \partial \rho / \partial t.$$

If an ice crystal is introduced to a new environment, then after the diffusion field surrounding it has attained a steady state,  $\partial \rho / \partial t = 0$ . In which case,  $\nabla^2 \rho = 0$ , or the vapor density at any point in space is given by the Laplacian equation, subject to  $\rho$  satisfying the boundary conditions at the surface of the crystal and at infinity. Thus, an analogy, for equivalent boundary conditions, can be made between the vapor field around a crystal and the electrostatic potential field



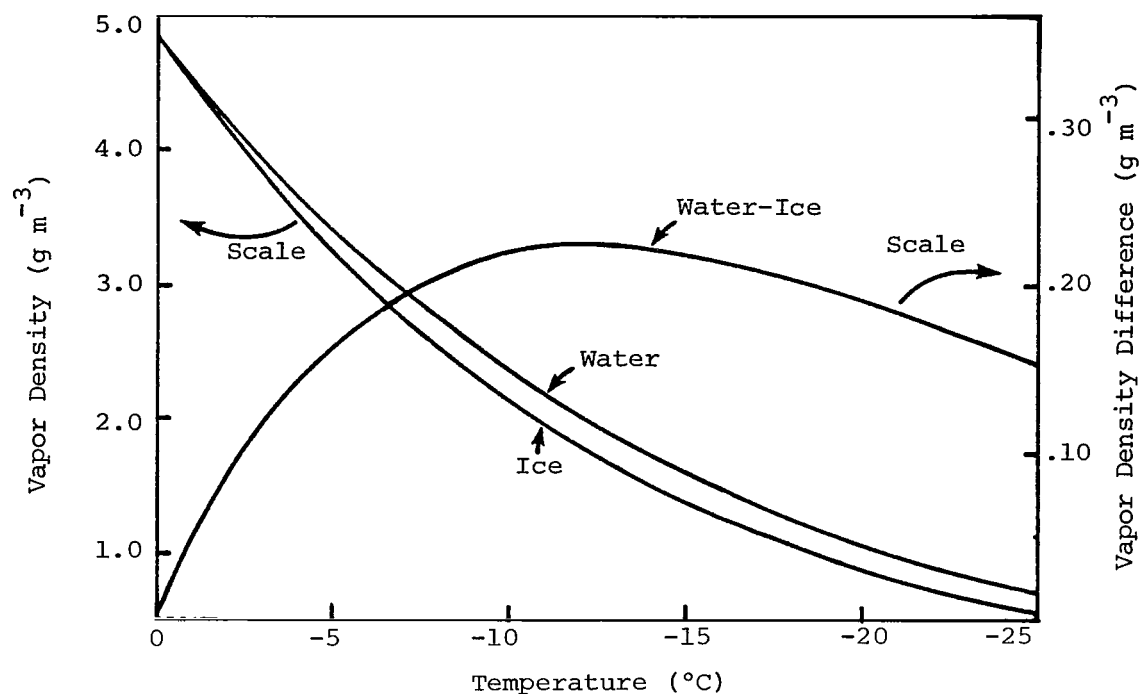


Fig. 3.1 Vapor density of water and ice and vapor density difference between water and ice versus temperature.

around a charged conductor with the same shape and size as the crystal. As the crystal grows, latent heat is released at the crystal surface in an amount directly proportional to the mass of vapor deposited. The flux of heat from the surface by conduction is given by

$$\Phi_{\text{HEAT}} = -K \vec{\nabla} T$$

where  $K$  is the thermal conductivity of the substance through which the heat is conducted and  $\vec{\nabla} T$  is the gradient of temperature surrounding the crystal. The quantity which determines the rate of diffusion of temperature is called the thermometric conductivity or simply the thermal diffusivity and is defined as

$$k = \frac{K}{\rho_0 c_p}$$

where  $K$  is the thermal conductivity,  $\rho_0$  is the density of the substance through which the heat is conducted and  $C_p$  is the specific heat at constant pressure of the heat conducting substance. Hence, the thermal diffusivity determines the rate of cooling due to a given temperature distribution according to the equation

$$k\nabla^2 T = \partial T / \partial t,$$

which implicitly assumes the thermal conductivity is not a function of temperature. For a steady state to exist, the latent heat must be dissipated at the same rate at which it is released. Otherwise, the crystal surface will warm up and the vapor density over the crystal surface will increase. In the steady state  $\partial T / \partial t = 0$ , in which case  $\nabla^2 T = 0$ , or the temperature at any point in space is given by the Laplacian equation, subject to  $T$  satisfying the boundary conditions at the surface of the crystal and at infinity. Figure 3.2 demonstrates the resulting vapor density and temperature fields surrounding a stationary growing crystal. No attempt has been made to illustrate the effect of the crystal corners on either the temperature or the vapor density field.

Using the analogy between the vapor field around a crystal and the electrostatic potential field around a charged conductor with the same shape and size as the crystal and employing the proper boundary conditions, i.e.,  $V = V_c$  at the charged conductor surface and  $V = V_\infty$  at infinity for the electrostatic potential field and equivalently for the vapor field around a growing crystal  $\rho = \rho_{ice}(T_c)$  at the crystal surface and  $\rho = \rho_\infty(T_\infty)$  at infinity, the rate of increase in the mass,  $m$ , of a crystal with electrostatic capacity,  $C$ , is shown by Mason (1971)

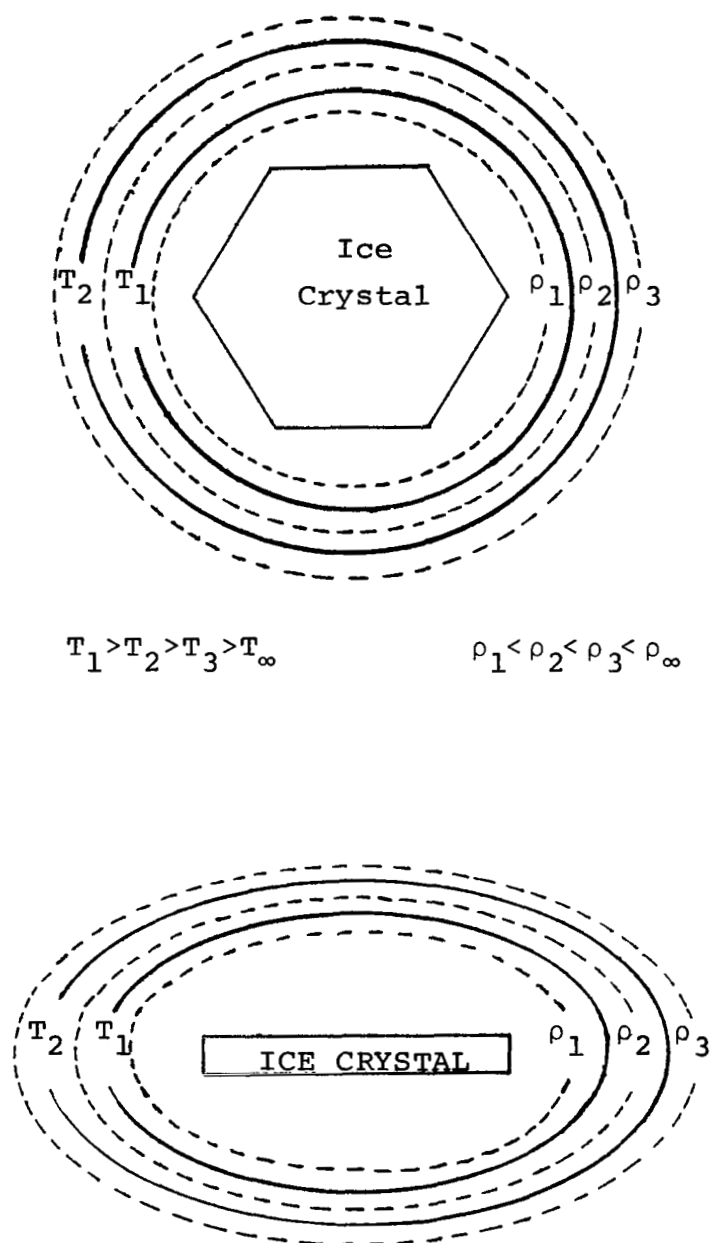


Fig. 3.2 Surfaces of constant vapor density and temperature surrounding a growing plate-like ice crystal. Adapted from Van den Heuvel (1960)

to be

$$dm/dt = 4\pi C D (\rho_{\infty}(T_{\infty}) - \rho_{ice}(T_C))$$

where  $D$  is the diffusion coefficient of water vapor in air,  $\rho_{\infty}(T_{\infty})$  the vapor density at a large distance from the ice crystal, and  $\rho_{ice}(T_C)$  the vapor density at the surface of the growing crystal. Since the latent heat released by the molecules deposited on the surface warms the crystal surface a few tenths of a degree Celsius above its surroundings, the vapor density,  $\rho_{ice}(T_C)$ , at the surface of a growing crystal is larger than the vapor density,  $\rho_{ice}(T_{\infty})$ , at the surface of a non-growing crystal. Hence, the "true" vapor density excess  $\Delta\rho_{true}$ , environmental minus the crystal surface vapor density, with respect to the growing ice surface is less than would occur if the crystal surface did not warm up.

The basic equation for diffusional growth of ice in a spherically symmetric vapor density field can be written as

$$dm/dt = A D d\rho/dr. \quad (3.1)$$

The latent heat released at the surface of a crystal which is growing at a rate  $dm/dt$  is

$$dQ/dt = L dm/dt \quad (3.2)$$

where  $L$  is the latent heat. For steady state growth the left side of eq. (3.2) must be balanced by the rate of heat removal by conduction, i.e., radiation is assumed negligible. The thermal conduction equation for spherical symmetry can be written

$$dQ/dt = -A K dT/dr. \quad (3.3)$$

By combining eqs. (3.1), (3.2), and (3.3), the equilibrium relationship between  $\rho$  and  $T$  can be given in the form of the differential equation

$$d\rho/dT = - \frac{K}{DL} \quad (3.4)$$

where, in general,  $K$ ,  $D$  and  $L$  are functions of  $T$ . This differential equation defines the variations of  $\rho$  with  $T$  between ambient conditions and the boundary conditions at the surface of the growing crystal. That is, it defines the relative spacings between the surfaces of constant vapor density and the surfaces of constant temperature in Fig. 3.2.

Utilizing the vapor diffusion—thermal conduction equilibrium of a growing crystal and using the vapor diffusion and thermal conduction equations in conjunction with the latent heat, the ideal gas law, and water vapor density relations, one can compute a theoretical crystal mass growth rate equation in terms of experimentally measurable quantities. This has been done and is given by Mason (1971) to be

$$dm/dt = \frac{4\pi C\sigma}{A+B} \quad (3.5)$$

where  $\sigma = [\rho/\rho_s(T)-1]$  is the supersaturation of the environment relative to ice,  $C$  is the electrostatic capacity of the crystal and  $A$  and  $B$  are given as

$$A = \frac{L}{KT} \left[ \frac{LM}{RT} - 1 \right]$$

$$B = \frac{RT}{DMP_s(T)}.$$

$L$  is the latent heat of sublimation,  $M$  is the molecular weight of ice,  $K$  is the thermal conductivity of air,  $R$  is the universal gas constant,  $T$  is the ambient temperature in  $^{\circ}\text{K}$ ,  $D$  is the diffusion coefficient of water vapor in air, and  $P_s(T)$  is the saturation vapor pressure over a plane ice surface at the ambient temperature  $T$ . At constant air pressure the terms  $A$  and  $B$  are functions of temperature only. The  $A$  term is the heat term and denotes the conduction of heat from the growing crystal. The  $B$  term is the moisture term and gives the relation for the transfer of mass to the crystal surface. Figure 3.3 is a plot of the magnitude of these two terms as a function of temperature at an ambient pressure of 1000 mb. At other pressures the  $B$  term would be given by  $P_a/1000$  of its value where  $P_a$  is given in mb. Figure 3.3 indicates that at cold ambient temperatures and high ambient pressures the transfer of mass and not the transfer of heat is the primary ambient kinetic effect controlling the ice crystal growth.

#### B. Convective Diffusion

If convection is taken into account then both the vapor density and temperature fields surrounding the crystal will be altered. That is, the gradients  $d\rho/dr$  and  $dT/dr$  will be steeper in the direction into the flow. A rough model, adapted from Mason (1953), which shows the effect of a ventilation velocity on the crystal mass growth rate is presented below.

The solution of the non-steady state equation

$$D\nabla^2\rho = \partial\rho/\partial t$$

for a sphere of radius  $r_0$  with the boundary conditions  $\rho = \rho_{\infty}(T_{\infty})$  everywhere when  $t = 0$  and the vapor density  $\rho_{ice}(T_c')$  at the crystal

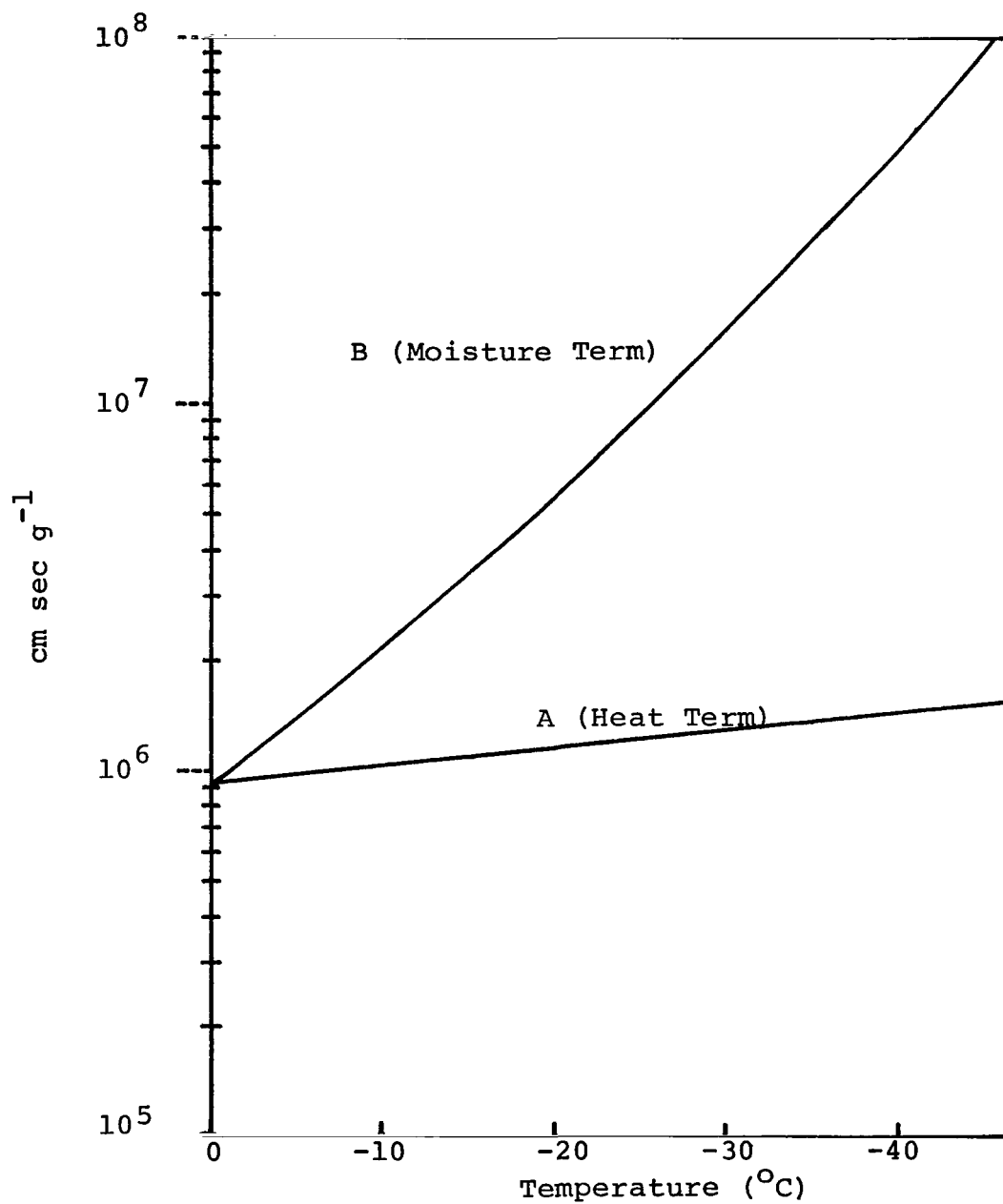


Fig. 3.3 Comparison of moisture and heat terms from the mass growth rate equation as a function of temperature. Uses values of  $K$ ,  $D$  and  $L$  at  $-10^{\circ}\text{C}$ , and at a pressure of 1000 mb.

surface is constant for all values of  $t$  is given by

$$\frac{\rho_{\infty}(T_{\infty}) - \rho(r)}{\rho_{\infty}(T_{\infty}) - \rho_{ice}(T_c')} = \frac{r_0}{r} \left[ 1 - \operatorname{erf} \left( \frac{r-r_0}{2(Dt)^{1/2}} \right) \right]$$

where  $T_c'$  is the crystal surface temperature in a static environment.

So

$$(\partial \rho / \partial r)_{r=r_0} = (\rho_{\infty}(T_{\infty}) - \rho_{ice}(T_c')) \left[ \frac{1}{r_0} + \frac{1}{(\pi D t)^{1/2}} \right]$$

Thus, eq. (3.1) becomes

$$dm/dt = AD \, d\rho/dr = 4\pi CD (\rho_{\infty}(T_{\infty}) - \rho_{ice}(T_c')) \left[ 1 + \left( \frac{r_0^2}{\pi D t} \right)^{1/2} \right]$$

where the capacitance for the sphere is  $r_0$ . Thus,

$$(dm/dt)_{\text{ventilated}} = (dm/dt)_{\text{static}} \left[ 1 + \left( \frac{r_0^2}{\pi D t} \right)^{1/2} \right]$$

where the second term in the square brackets is a measure of the increase in mass due to ventilation. This term will be large only if  $(\pi D t)^{1/2} \ll r_0$ . The quantity  $(\pi D t)^{1/2}$  may be defined as the thickness of the diffusion boundary layer and has the dimensions of a length. For a spherical ice particle of radius  $r_0$  within a velocity flow  $v$ , the time  $t$  for which any given parcel of air will remain in contact with it before being replaced by fresh air will be given approximately by  $t = 2r_0/v$ . Hence, the diffusion field will have approximately this time in which to spread out from the crystal surface. Therefore, the mass growth rate of a ventilated ice sphere will be increased by a ventilation factor

$$f = 1 + \left( \frac{v r_0}{2\pi D} \right)^{1/2}.$$



The condition for the concentration gradient near the crystal to be considerably augmented due to the presence of the ventilation velocity is

$$2\pi Dr_0/v \ll r_0^2$$

or

$$vr_0 \gg 2\pi D.$$

Hence, from strictly a mass growth rate standpoint a ventilated crystal can be regarded as growing at rest in a steady-state field and eq.

(3.5) can be applied to the mass growth rate without appreciable error provided  $vr_0/D < 2\pi$ . However, even in this case, the ventilation velocity may affect the way in which the acquired mass is distributed over the crystal surface and hence the detailed crystal shape. Since the Reynolds number  $Re$  is given by  $Re = \frac{2r_0v}{\nu}$  and the Schmidt number  $Sc$  is given by  $Sc = \nu/D$  where  $\nu$  is the kinematic viscosity of the air, their product is given by

$$Sc \cdot Re = \frac{2r_0v}{D}$$

so the ventilation factor is

$$f = 1 + \frac{1}{2\sqrt{\pi}} Sc^{\frac{1}{2}} Re^{\frac{1}{2}}.$$

At  $0^\circ\text{C}$  the Schmidt number is given numerically by  $Sc = .1346/.226 = .60$  so the ventilation factor becomes

$$f = 1 + 0.23 Re^{\frac{1}{2}}.$$

An analogous result is obtained if the temperature field rather than the vapor density field is considered. However, in that case, the change with time of heat, rather than mass, is considered and one

obtains

$$(dQ/dt)_{\text{ventilated}} = (dQ/dt)_{\text{static}} \left[ 1 + \left( \frac{r_o^2}{\pi k t} \right)^{\frac{1}{2}} \right]$$

where the thermal diffusivity  $k$  has replaced the analogous vapor diffusivity coefficient  $D$ . Furthermore, since the Prandtl number  $Pr$  is given by  $Pr = \nu/k$ , the product of the Prandtl and Reynolds numbers is

$$Pr \cdot Re = \frac{2r_o \nu}{k}$$

and the heat ventilation factor is then given by

$$f_H = 1 + \frac{1}{2\sqrt{\pi}} Pr^{\frac{1}{2}} Re^{\frac{1}{2}}$$

where to a first approximation,  $f = f_H$ .

Since the ventilation factor  $f$  was only "derived" for a sphere its application to other shapes is questionable. In particular, one might expect the coefficient of the Reynolds number to vary with the shape of the crystal and also with the location at which the flow separates from the crystal. Nonetheless, no other acceptable theoretical method of determining the effect of ventilation is available so with the inclusion of the ventilation factor, eq. (3.5) becomes

$$dm/dt = \frac{4\pi C \sigma f}{A+B} . \quad (3.6)$$

Equation (3.6) can only be used to predict the mass growth rate if the electrostatic capacity  $C$  of the crystal is known. Houghton (1950) suggested that shapes of conductors of known capacity be used to approximate the shapes of actual crystals. McDonald (1963) by experimentally measuring the electrostatic capacities of brass models of various ice

crystal shapes found that complicated shapes gave only small deviations from theoretical values of capacitance for symmetrical shapes with a similar appearance.

The capacitance for a circular disk is given by  $C = 2r/\pi$  and the mass of such a disk is given by  $m = \rho_d \pi r^2 h$  where  $r$  is the disk radius,  $\rho_d$  is the bulk density of the disk substance and  $h$  is the thickness of the disk. In this case eq. (3.6) reduces to

$$dm/dt = 2\pi r h \rho_d dr/dt = \frac{4\pi(2r/\pi)\sigma f}{A+B}$$

or

$$dr/dt = \left(\frac{4}{\rho_d \pi h}\right) \frac{\sigma f}{A+B} \quad (3.7)$$

which predicts the linear growth rate for a circular disk of constant thickness  $h$ . Likewise, for other simple shapes of known capacitance one can obtain a theoretical prediction of the linear growth rate.

Applying eq. (3.5) with  $C = 1/4\pi$  to an ice crystal in an ambient environment at water saturation gives the calculated mass growth rate in  $g\ s^{-1}$  as a function of temperature. The result of such calculations for two different ambient pressures are shown in Fig. 3.4. To obtain the true growth for any other  $C$ , the values need only be multiplied by  $4\pi C$ . Note that a maximum occurs at  $-14.25^\circ\text{C}$  at 1000 mb and at  $-16.75^\circ\text{C}$  at 500 mb. The maxima are primarily due to the fact that the difference between the saturated vapor densities over water and ice, Fig. 3.1, is a maximum near these temperatures. However, the pressure effect on the two curves, that is both the increase in absolute growth rate and the shift in the maximum growth rate to lower temperature as the pressure is decreased, is brought about by the increase in the diffusivity of water vapor with decreasing pressure.

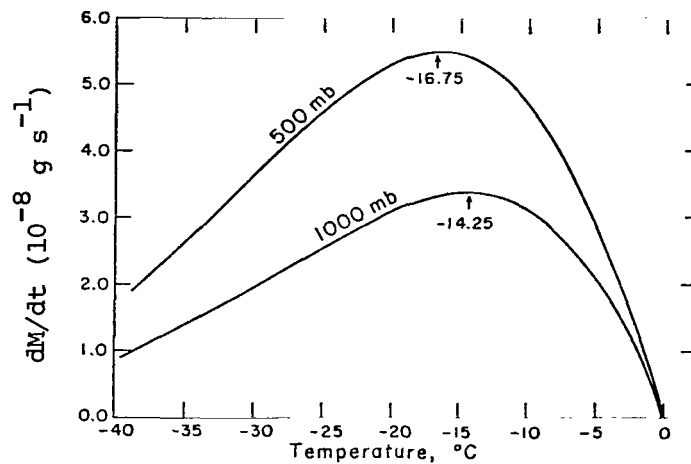


Fig. 3.4 Growth rates as a function of temperature of an ice crystal with  $C = 1/4\pi$  in a water-saturated cloud at two pressures. The temperature for maximum rate of growth is indicated on each curve. Byers (1965)

If surface kinetic effects were unimportant, one would expect to experimentally observe a relationship between mass growth rate and temperature similar to the theoretical prediction depicted in Fig. 3.4. However, such a simple relationship has not been observed. Hallett (1965) found, by growing ice crystals in a static thermal diffusion chamber at water saturation, two maxima to exist in the growth rate; one at  $-4^{\circ}\text{C}$  and the other at  $-15^{\circ}\text{C}$  with a minimum growth rate at  $-8^{\circ}\text{C}$ . These are illustrated in Fig. 3.5. Fukuta (1969) grew ice crystals in a cloud of supercooled water droplets and also found a dual maxima in the growth rate, Fig. 3.6. However, he observed the maxima to occur at slightly colder temperatures than found by Hallett. Ryan, Wishart and Shaw (1976) also grew ice crystals in a cloud of supercooled water droplets and found a dual maxima; one at  $-6^{\circ}\text{C}$  and the other at  $-15^{\circ}\text{C}$ . They also presented a diagram, Fig. 3.7, showing the individual linear crystal axial growth rates along both the 'a' and 'c'-axes. Note that the magnitude of the growth rate along the 'a'-axis

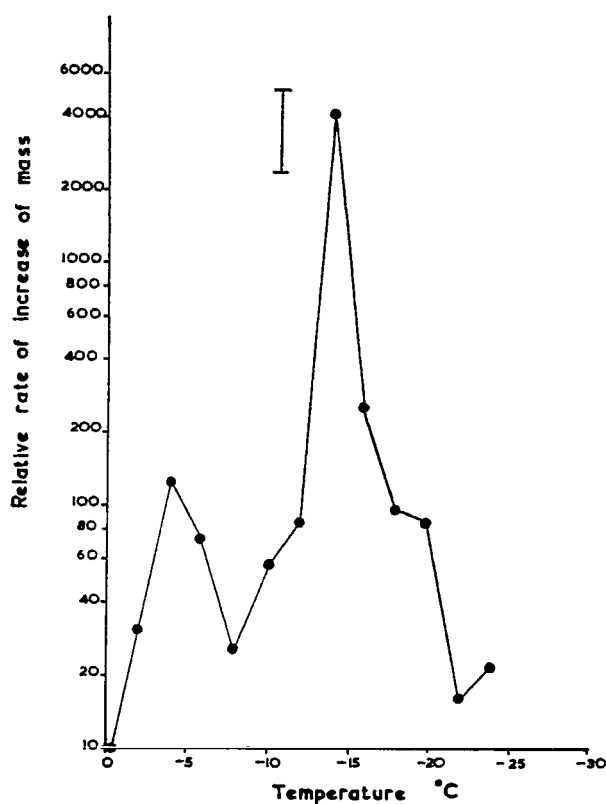


Fig. 3.5 Relative rate of mass increase of crystals growing at water saturation in a static environment. Hallett (1965)

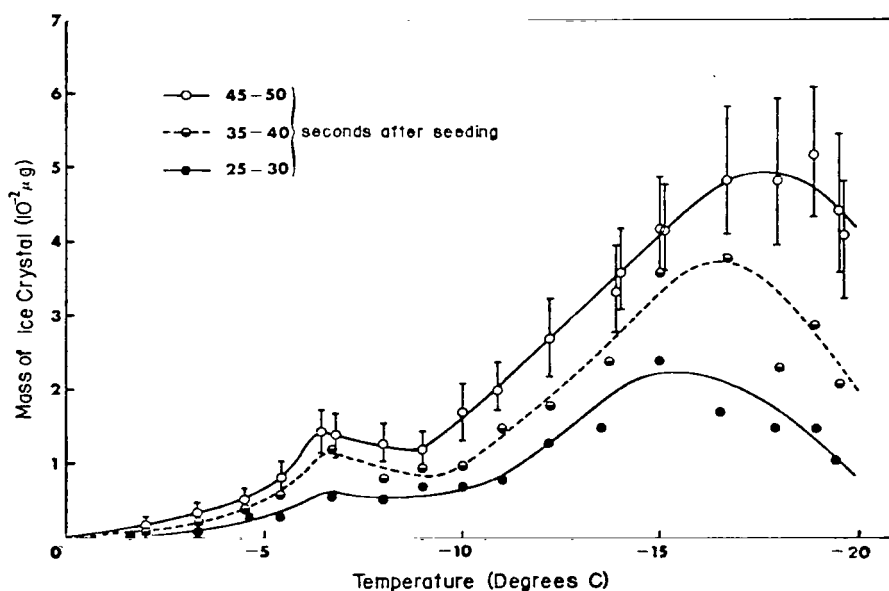


Fig. 3.6 Mass of ice crystals versus temperature for various times after seeding a supercooled water cloud. Fukuta (1969)

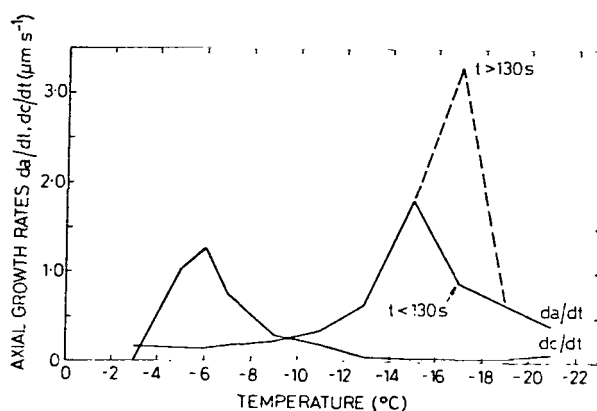


Fig. 3.7 Variation of estimated crystal axial growth rates with temperature. Ryan, Wishart and Shaw (1976)

at temperatures near  $-15^{\circ}\text{C}$  for small crystals, growth time less than 130 seconds, and for large crystals, growth time greater than 130 seconds, is quite different. This can be explained by inclusion of the ventilation factor. That is, the larger crystals fall faster than the smaller ones in accordance with the experimental results of Kajikawa (1972), for plane type crystals, Fig. 3.8. Terminal fall speeds of crystals of larger dimension are given by Nakaya and Terada, Jr. (1935).

Thorpe and Mason (1966) tested the validity of eq. (3.6) for Reynolds numbers ranging from 10 to 200 and ambient temperatures from  $0^{\circ}\text{C}$  to  $-20^{\circ}\text{C}$  by measuring the rates of evaporation of ice spheres. They found good agreement with the theory if they used  $(0.94 + 0.29 \text{Re}^{1/2})$  as the ventilation factor. Reynolds (1952) and Mason (1953) both made experimental measurements of mass growth rates for small crystals less than  $100 \mu\text{m}$  diameter grown in supercooled clouds in small cold chambers. Their results agreed within experimental error with the mass growth rates predicted by theory for a static environment, eq. (3.5).

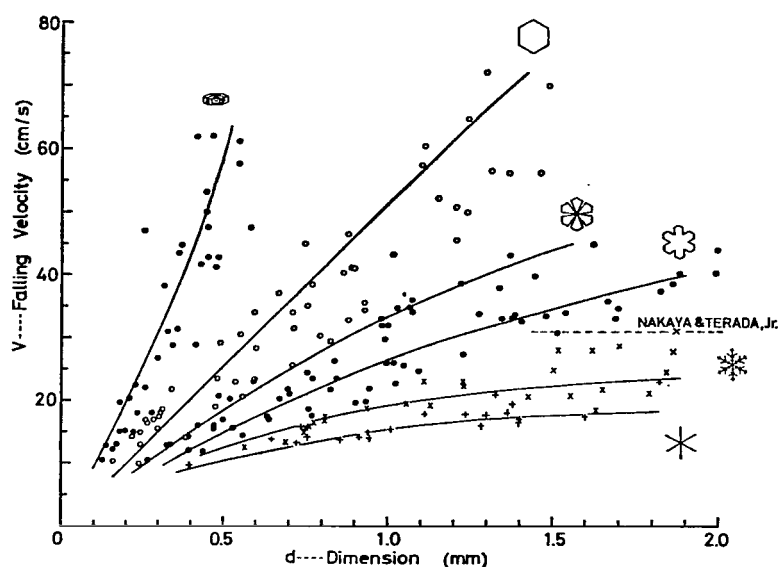


Fig. 3.8 Falling velocity versus dimension of plane type crystals. Kajikawa (1972)

Isono et al. (1956), who seeded a supercooled fog outdoors, found mass growth rates at temperatures near  $-4^{\circ}\text{C}$  which were nearly twice those predicted by theory for a static environment. The crystals grown in the outdoor experiment had longer available time for sustained growth than those in the cold chambers and were therefore larger being typically 300 to 400  $\mu\text{m}$  in length and hence had significant ventilation velocities. This would suggest that ventilation, as expected, may play a significant role in increasing the crystal growth rate.

Several numerical empirical models have been developed to predict the mass or linear growth rate of ice crystals within a cloud. Two basic approaches have been used. The first approach fits empirical equations to experimental data on the axial growth rates. It assumes that the crystal grows only along two axes and different relative

growth rates along the two axes result in different crystal habits. The models of Todd (1964), Hindman (1968) and Hindman and Johnson (1972) are examples of this approach. The other approach uses eq. (3.6) with the incorporation of parameters determined from field measurements and has been formulated by Jayaweera (1971) and Koenig (1971).

It is important to recognize that although eqs. (3.5) and (3.6) give a theoretical prediction of the mass growth rate of crystals in a static or ventilated environment, respectively, they do not predict the way in which the acquired mass is distributed over the crystal surface and hence the detailed crystal shape. They do not explain why, within specific temperature ranges, the growth should take place preferentially along the 'a'-axis and, at other temperatures, along the 'c'-axis. A complete understanding of ice crystal growth requires not only a knowledge of the rate of mass increase but also the way in which the accumulated mass is distributed over the crystal surface. Thus, it is necessary to have an understanding of the growth mechanisms by which the crystal faces are propagated.

From a molecular standpoint, the macroscopic growth equation represented by eqs. (3.5) and (3.6) has some glaring deficiencies. Foremost is the fact that it does not consider surface kinetics. That is, it assumes that all molecules arriving at the surface are incorporated directly into the crystal lattice. It also assumes a constant vapor density or molecular concentration over the entire crystal surface. This would imply no surface migration of molecules.

Sometime ago, Marshall and Langleben (1954) hypothesized that vapor density excess was the primary growth mechanism controlling the



crystal habit. This would be true if it were not for surface kinetic effects. However, surface kinetic effects are very important and their relative magnitude of importance is a function of temperature for each crystallographic face. The experiments of Lamb (1970) in which ice crystals were grown in an environment of pure water vapor clearly demonstrated this fact. His results, presented in Fig. 3.9, show the

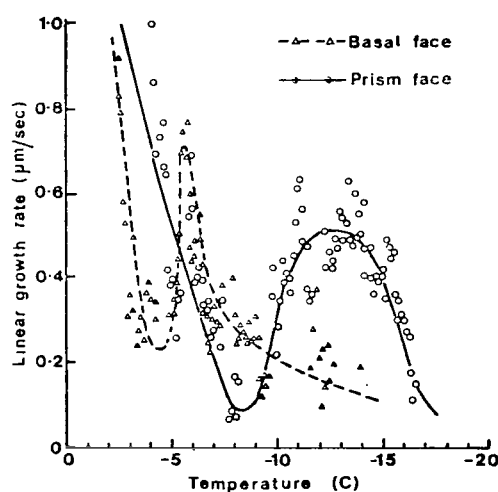


Fig. 3.9 Experimental measurements of the linear growth rates of the basal and prism faces of ice as a function of temperature. The ice crystals were situated in an environment of pure water vapor and the excess vapor pressure was constant at 10  $\mu$ m of mercury. Lamb and Hobbs (1971)

linear growth rate of both the basal and prism face as a function of temperature for a constant vapor density excess. These are called 'inherent' growth rates since they are governed by surface kinetic effects and not by the diffusion of water molecules to the crystal surface. The exact nature of the surface kinetic effects responsible for the shape of the curves in Fig. 3.9 is not known. Bernal (1958) speculated that the remarkable variation of ice crystal habit with temperature might be dependent on a variation with temperature of the

relative surface free energies of the individual crystallographic faces leading to different relative rates of nucleation and growth on the basal and prism faces as a function of temperature. Mason et al. (1963) suggested that the surface kinetic effects may be primarily due to the temperature dependence of the effective collection distance  $\lambda_c$  associated with each step. Fletcher (1968) and later Lacmann and Stranski (1972) have proposed a quasi-liquid film of varying thickness over the crystal surface to account for the temperature dependence of the surface kinetic effects.

The experimental evidence for surface migration is based on the finding of Hallett and others that the speed of propagation of small steps on a crystal surface is inversely proportional to the step height. Direct experimental evidence for a quasi-liquid film on ice is sparse. However, recent nuclear magnetic resonance (NMR) experiments on ice by Kvlividze, Kiselev and Ushakova (1970) and Kvlividze, Kiselev, Kurzaev and Ushakova (1974) may indicate such a film. In any case, although the precise mechanisms responsible for the surface kinetic effects are not fully understood, their effect can be observed under the proper ambient conditions as Lamb (1970) demonstrated.

In general, the crystal growth rate may be limited by insufficient transfer of heat, insufficient availability of water molecules, i.e., mass transfer, or by surface kinetic effects. Figure 3.3 showed that heat transfer is often not the limiting mechanism, at least at high pressures and low temperatures. However, if good heat transfer does exist, such as for growth on a substrate, the surface temperature of the growing crystal is reduced and the true vapor density excess over the crystal surface is increased. Hence, a reduction in the crystal

surface temperature is roughly equivalent to increasing the ambient vapor density. In most cases, the growth rate is limited by both mass transfer and surface kinetic effects. Figure 3.10 demonstrates how the effective vapor density is determined by the necessity of equality between the rates of transfer and deposition. In this figure,  $\rho_\infty$  is the ambient vapor density,  $\rho_c$  is the vapor density at the crystal surface and  $\rho_e$  is an effective vapor density such that  $(\rho_e - \rho_c)$  is the true vapor density excess over the crystal surface. Complete surface kinetics control corresponds to a nearly vertical mass transfer curve and/or a nearly horizontal surface kinetics curve. Conversely, mass transfer control corresponds to a nearly horizontal mass transfer curve and/or a nearly vertical surface kinetics curve. The introduction of a ventilation velocity corresponds to making the mass transfer curve more vertical and thus bringing the effective vapor density  $\rho_e$  closer to the ambient value  $\rho_\infty$ .

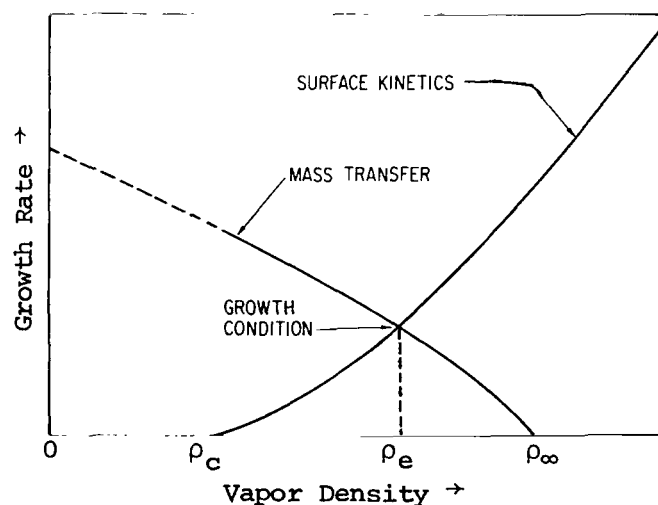


Fig. 3.10 The growth rate is determined by mass transfer and by interfacial incorporation kinetics, which must take place sequentially and at the same rate. Adapted from Wilcox (1971)

In summary although much is known about the general aspects of ice crystal growth under various ambient conditions, it is evident that a complete understanding of ice crystal growth has not yet been attained even under controlled conditions in the laboratory.

## IV.

## EXPERIMENTAL APPARATUS AND PROCEDURE

A. Apparatus

The dynamic thermal diffusion chamber is based on the same operating principle as that of the static thermal diffusion chamber. Two parallel, horizontal thermally conducting flat plates are separated by a small distance,  $d$ , as in Fig. 4.1. The top and bottom plate temperatures are controlled independently and are given by  $T_t$  and  $T_b$ , respectively. The top plate is maintained warmer than the bottom plate to make the system convectively stable. The equilibrium vapor density at the top and bottom plate ice surfaces is given by  $\rho_e(T_t)$

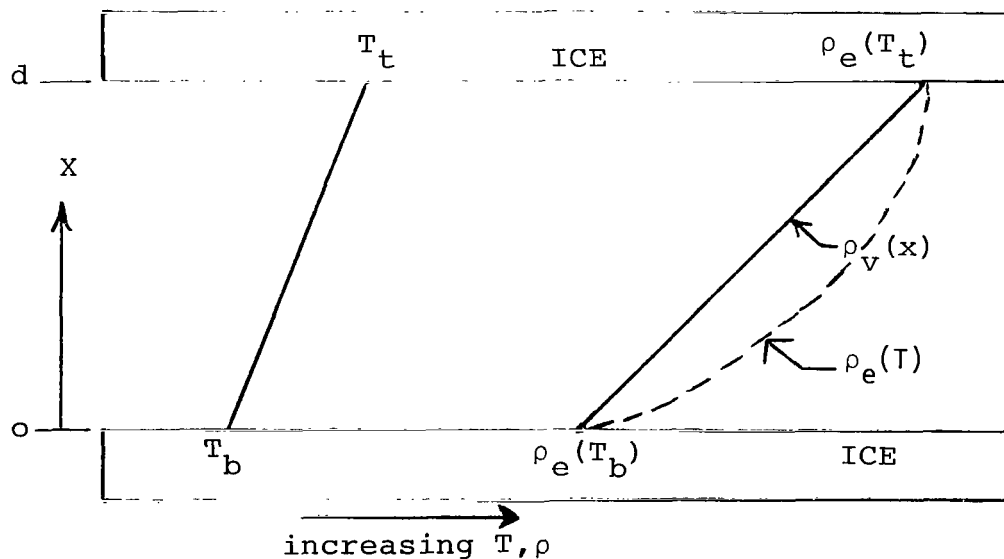


Fig. 4.1 Parallel conducting plates with associated equilibrium temperature and vapor density profiles. Adapted from Lamb (1970)

and  $\rho_e(T_b)$ . Both the temperature  $T$  and the density of water vapor

$\rho_v(x)$  vary almost linearly with height between the plates. However, since the equilibrium vapor density  $\rho_e(T)$  over either ice or water varies exponentially with temperature as was noted in Fig. 3.1, a supersaturation develops in the region between the plates. Unlike the static chambers, the dynamic chamber invokes a controlled airflow parallel to and along the length of the plates. In this case it is necessary to solve the non-steady state heat conduction and vapor transport equations

$$k\nabla^2 T = \partial T / \partial t \text{ and } D\nabla^2 \rho_v = \partial \rho_v / \partial t,$$

where  $k$  is strictly the thermal diffusivity of moist air but may be replaced by the thermal diffusivity of dry air since the mole fraction of water vapor within the chamber is only on the order of  $10^{-2}$ .  $T$  is the temperature,  $t$  is time,  $D$  is the diffusivity of water vapor in air and  $\rho_v$  is the density of water vapor. The boundary conditions for the heat transport equation are given by:

$$T = T_b \quad , \text{ for } x = 0, \text{ all } t$$

$$T = T_t \quad , \text{ for } x = d, \text{ all } t$$

$$T = T(x), \text{ for } t = 0, \text{ all } x.$$

Likewise, the boundary conditions for the vapor transport equation are given by:

$$\rho_v = \rho_{vb} \quad , \text{ for } x = 0, \text{ all } t$$

$$\rho_v = \rho_{vt} \quad , \text{ for } x = d, \text{ all } t$$

$$\rho_v = \rho_v(x), \text{ for } t = 0, \text{ all } x.$$

If the incoming sample of air at time  $t = 0$  is assumed to have a constant initial temperature distribution,  $T(x) = T_0$ , and contains water vapor saturated at the temperature  $T_0$  and having a density  $\rho_v(x) = \rho_{v0}$ , the solutions to the one-dimensional heat conduction and vapor transport equations are obtained by separation of variables to be:

$$T = \left( \frac{T_t - T_b}{d} \right) x + T_b + \sum_{n=1}^{\infty} \left[ \frac{-2(T_b - T_0)}{n\pi} + \frac{2(T_t - T_0)(-1)^n}{n\pi} \right] \left[ \sin \left( \frac{n\pi x}{d} \right) \exp \left( - \left( \frac{n\pi}{d} \right)^2 kt \right) \right] \quad (4.1)$$

and

$$\rho_v = \left( \frac{\rho_{vt} - \rho_{vb}}{d} \right) x + \rho_{vb} + \sum_{n=1}^{\infty} \left[ \frac{-2(\rho_{vb} - \rho_{v0})}{n\pi} + \frac{2(\rho_{vt} - \rho_{v0})(-1)^n}{n\pi} \right] \left[ \sin \left( \frac{n\pi x}{d} \right) \exp \left( - \left( \frac{n\pi}{d} \right)^2 Dt \right) \right] \quad (4.2)$$

The time dependent exponential response term in each of these equations gives their respective time constants (for  $n = 1$ )

$$\lambda_T = \frac{d^2}{\pi^2 k} \quad \text{and} \quad \lambda_{\rho_v} = \frac{d^2}{\pi^2 D}.$$

After a sufficiently long time, that is several time constants, the exponential terms in both these non-steady state solutions go to zero and the steady-state linear temperature and vapor profiles are given by

$$T = \left( \frac{T_t - T_b}{d} \right) x + T_b \quad \text{and} \quad \rho_v = \left( \frac{\rho_{vt} - \rho_{vb}}{d} \right) x + \rho_{vb}.$$

These are the same solutions obtained by solving directly the one-dimensional Laplacian equations

$$\partial^2 T / \partial x^2 = 0 \text{ and } \partial^2 \rho_v / \partial x^2 = 0.$$

The supersaturation at any height  $x$  above the bottom plate is given by

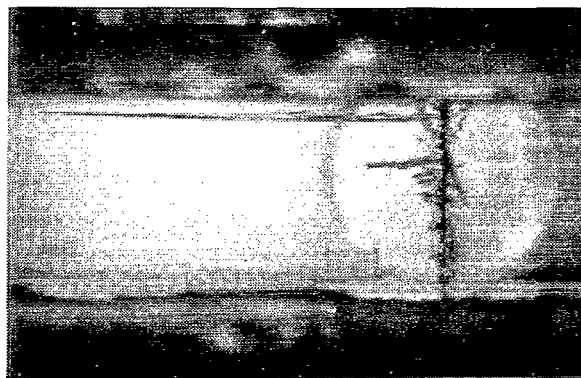
$$\sigma(x) = \frac{\rho_v(x) - \rho_e[T(x)]}{\rho_e[T(x)]}, \text{ where } \rho_v(x) = \frac{\rho_e[T(d)] - \rho_e[T(0)]}{d} x + \rho_e[T(0)].$$

The supersaturation may be expressed relative to either ice or water depending on which equilibrium vapor density is used. In either case the supersaturation is often multiplied by 100 and expressed in percent. For a given set of top and bottom plate temperatures the supersaturation relative to ice is always larger than that relative to water. In fact, the supersaturation relative to ice in the thermal diffusion chamber will never be negative in the steady-state unless heat enters the system through the sidewalls. On the other hand, it is not unusual for the supersaturation relative to water to be negative, that is, undersaturated with respect to water in which case water droplets evaporate. This means that ice crystals will grow in an ambient environment in which water droplets evaporate. The situation of undersaturation with respect to water but supersaturation with respect to ice is common in natural clouds and is called the Bergeron process.

The air flowing between the horizontal plates of the dynamic thermal diffusion chamber is required to approach vapor and thermal equilibrium with the steady-state moisture and temperature profiles before reaching the end of the chamber where the ice crystals grow from a thin glass fiber suspended vertically between the two plates as in Fig. 4.2. The time needed for the air to approach these equilibrium values to



within 98 percent is given by  $4\lambda$  seconds where  $\lambda$  is the time constant for the process under consideration. The minimum chamber length necessary is given by  $L = vt$  where  $v$  is the maximum air velocity and  $t = 4\lambda$ .



1.0 cm

Fig. 4.2 Ice crystals grow from a fiber suspended vertically between two horizontal parallel plates.

Thus, for vapor or thermal equilibrium to occur the chamber length must be given by

$$L = 4v\lambda_{\rho_V} = \frac{4vd^2}{\pi^2 D} \quad \text{for vapor equilibrium}$$

and

$$L = 4v\lambda_T = \frac{4vd^2}{\pi^2 k} \quad \text{for thermal equilibrium}$$

where  $d$  is the distance over which the diffusion must occur. The diffusivity of water vapor in air is a little larger than the thermal diffusivity of the air. This results in vapor equilibrium occurring before temperature equilibrium. Thus, as Fitzgerald (1970) has shown, the chamber will experience transient supersaturations higher than the steady-state values if the incoming air sample is saturated and

colder than the top plate temperature. This is of major importance if the chamber is employed in the measurement of nuclei spectra but is of little consequence in the present application.

The maximum distance over which the diffusion of moisture and heat must operate is the plate separation,  $d$ . For air,  $k \doteq D \doteq .2 \text{ cm}^2 \text{ s}^{-1}$  and the necessary chamber length is given in terms of the plate separation and flow velocity as

$$L = 2.03 \, v d^2. \quad (4.3)$$

Thus the length of the chamber necessary for air with a given velocity to reach equilibrium must increase as the square of the plate separation. If both the top and bottom plates are coated with ice, one would expect vapor diffusion from each plate and the actual diffusion distance to be somewhat less than the total plate separation. In this case the length calculated from eq. (4.3) would be an overestimate.

The Reynolds number  $Re$ , defined as the ratio of inertial to viscous forces, is given for flow within closed tubes as

$$Re = \frac{4r_H v}{\nu}$$

where  $r_H$  is the hydraulic radius, and  $\nu \doteq .125 \text{ cm}^2 \text{ s}^{-1}$  is the kinematic viscosity of air. The hydraulic radius is used for non-circular pipes and channels and is defined as the ratio of the cross-sectional flow area to the wetted perimeter. If the width of my rectangular dynamic chamber is denoted by  $w$  then the hydraulic radius is given by

$$r_H = \frac{wd}{2(w+d)}$$

and the Reynolds number becomes

$$Re = \frac{2v}{v} \frac{(wd)}{(w+d)} \quad (4.4)$$

If the Reynolds number is less than about 2000 the flow in a smooth pipe will generally be laminar, Kay (1963). However, if the Reynolds number exceeds 2000 or if the surface is very rough the flow will become turbulent.

My dynamic thermal diffusion chamber has a plate separation of 2.5 cm and a horizontal width of 9.0 cm. This gives a dimensionless Reynolds number

$$Re = 31.3 v$$

where  $v$  is the airflow in  $\text{cm s}^{-1}$ . For smooth tubes this implies laminar flow for velocities as large as  $60 \text{ cm s}^{-1}$ . These values of plate separation and horizontal width are both compromises. This large a separation is needed to insure that there is sufficient space for relatively large crystals, i.e., approximately 1 cm in length, to grow with a minimum of inhomogeneities in temperature, supersaturation and ventilation velocity. A greater width is preferred over the present value to minimize sidewall effects. However, if the width were any greater than the present value, the distance from the optical viewing window to the crystal would be greater than the focal length of our stereo microscope and would result in the sacrifice of a great deal of optical resolution.

Figure 4.3 is a cutaway diagram of my dynamic thermal diffusion chamber as viewed from above and Fig. 4.4 is a photograph of the chamber as viewed from above, beyond the end. The chamber was generally operated as a closed system with the air being continuously recirculated.

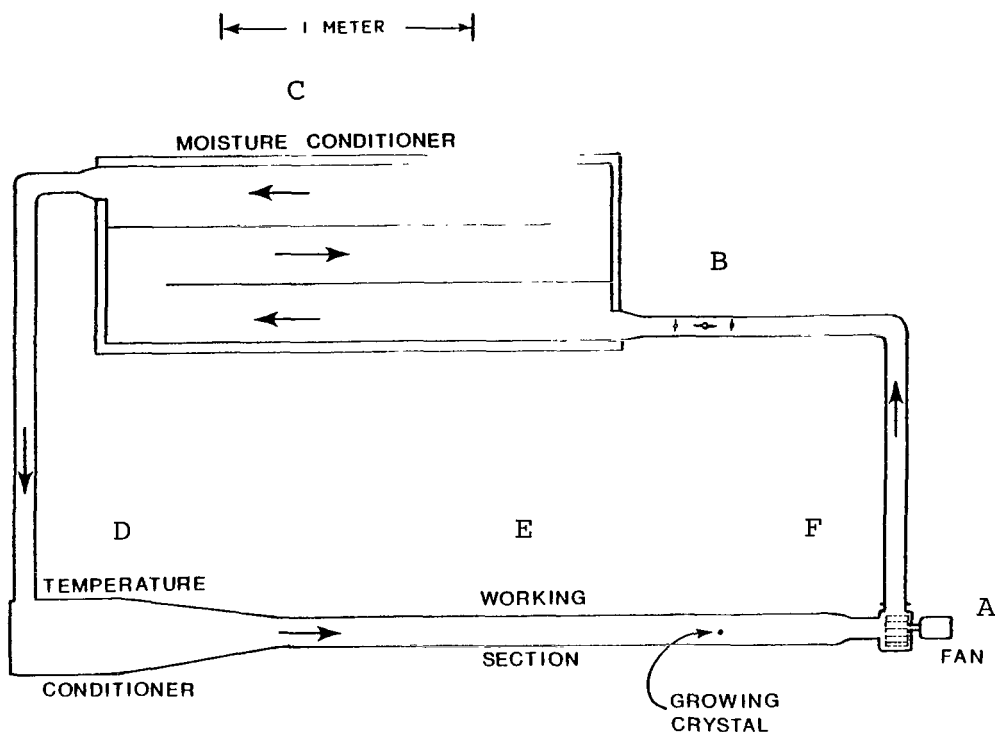


Fig. 4.3 Diagram of the dynamic thermal diffusion chamber. (Top View)

However, it has the capability of being readily separated at point F, Fig. 4.3, and used as an open system. The entire chamber lies in a nearly horizontal plane to suppress natural convection around the loop. The air drive indicated by point A, Fig. 4.3, consists of a Dayton No. 2C781 shaded pole blower fan driven directly by a servo motor. The 28 volt d.c. servo motor system is speed controlled with a 10 turn potentiometer and has a maximum speed of 2300 RPM. The regulated d.c. current to the servo motor is indicated in microamperes on a meter with a 2 3/4" diameter face marked off in 50 divisions. A switch varies the full scale deflection of the meter to any one of the values 50, 100, 150, 200, 500 or 1000 microamperes. Since the RPM of the

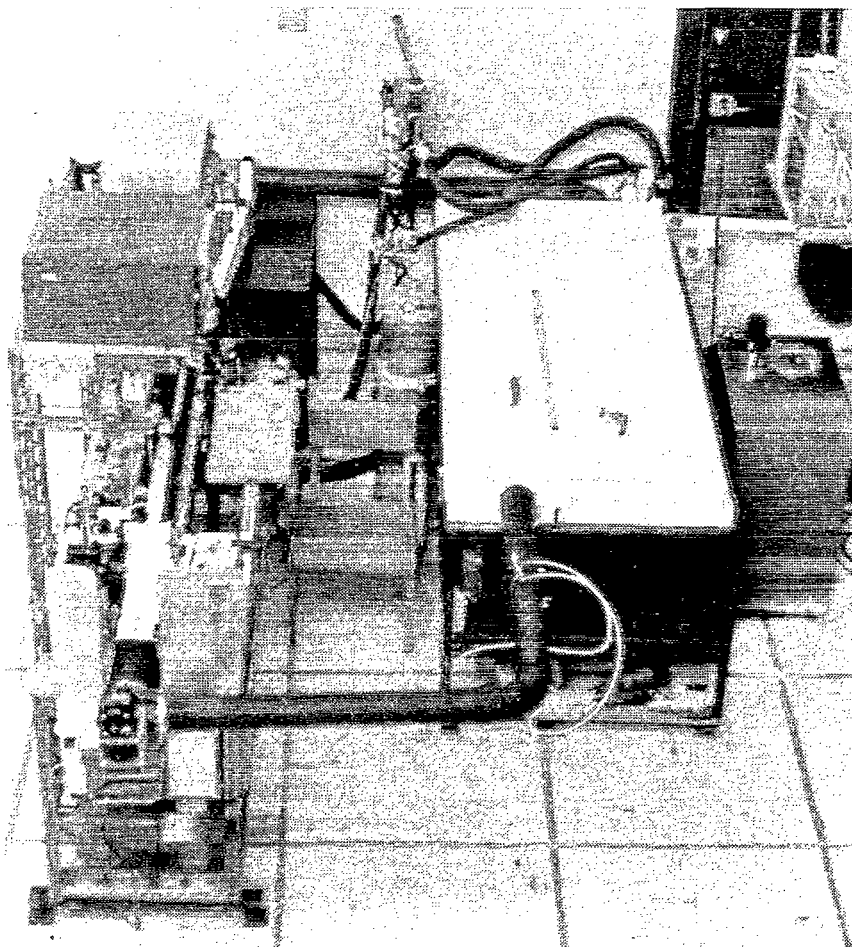


Fig. 4.4 View of the dynamic thermal diffusion chamber from above, beyond the end.

servo motor and, in turn, the airflow in the chamber is directly proportional to this regulated current, these meter readings are more than adequate to provide a reproducible velocity at each set point. For a given meter setting the servo motor system maintains a constant ventilation velocity in the working section of the chamber. Furthermore, the ventilation velocity resulting from this air drive system can be varied in infinitesimal increments over the entire range of interest,  $0.1 \text{ cm s}^{-1} \leq v \leq 1.0 \text{ m s}^{-1}$ . A 1/8 HP Bodine motor capable of 5000 RPM and equipped with a Minarik variable speed control is connected to the blower fan drive shaft via a V-belt and pulley. This motor, when employed, produces ventilation velocities of several  $\text{m s}^{-1}$  and is used in conjunction with a 2.5 m long scraper stick to blow the chamber clear of frost obstructions.

The components of the chamber between points A and B and points C and D, Fig. 4.3, are connected with 3" diameter stainless steel pipe jointed with aluminum couplings fitted with Viton O-rings.

Point B, Fig. 4.3, indicates a butterfly valve used to close off the normal flow through the circular pipe and force the chamber air through an air filter. The air filter system, which removes both the cloud condensation nuclei (CCN) and the Aitken nuclei, consists of a Dyna-Vac Viton diaphragm pump and a circular cannister 22 cm in diameter and 23 cm in length packed with sterile absorbent cotton. The diaphragm pump provides an almost constant volume airflow rate of  $6.4 \text{ liter min}^{-1}$  even across such large pressure drops as the 10.8 inches of water pressure drop across the circular cannister. At this flow rate the entire volume of air in the chamber is filtered every 6 or 7 minutes.

The moisture conditioner, indicated by point C, Fig. 4.3, is an ice labyrinth which preconditions the air before it enters the working section of the chamber. A large stainless steel tray 79 cm wide, 180 cm long and  $3\frac{1}{2}$  cm deep, containing cooling coils, has 30 liters of distilled water poured into it making the depth of water about 2.5 cm and covering all the cooling coils. Another rectangular stainless steel tray of just slightly smaller dimensions is inverted and fitted inside the first tray. Fins protrude from the top tray into the water nearly the length of the trays. When the water is frozen, an air tight ice labyrinth is formed with stainless steel sides and top and an ice bottom. The air path through the moisture conditioner is over 5.0 m in total length and approximately 22 cm wide by 1 cm high. This moisture conditioner was designed to precondition the air for a maximum ventilation velocity of  $50 \text{ cm s}^{-1}$  in the working section of the chamber. This corresponds to a volume flow rate of  $1.25 \text{ liter s}^{-1}$  or a linear velocity of  $95 \text{ cm s}^{-1}$  in the ice labyrinth when Poiseuille type flow, that is a maximum velocity  $3/2$  times the mean, is assumed. The time constant for molecular diffusion in this case is given by

$$\lambda_{\rho_v} = 0.5 \text{ seconds.}$$

The chosen labyrinth dimensions allow over five time constants for the air to approach the equilibrium vapor density of the ice surface even for ventilation velocities in the working section of  $50 \text{ cm s}^{-1}$ . Since the ventilation velocities employed in this study are less than half this value, the air remains in the ice labyrinth several time constants longer than necessary to approach 99% equilibrium. The necessary ice labyrinth area could have been reduced to about one-fourth the value

used if an ice surface had been employed on both the top and bottom. However, it would be very difficult to handle a top tray of the necessary dimensions if it were full of ice. Also since ice is employed only on the bottom, the top can always remain intact except for cleaning and the water can be added directly to the bottom tray and drained through a stop cock after each experiment. Likewise, if the separation between the ice surface and the top tray were much smaller than 1 cm the time constant for diffusion would be greatly reduced, but it would be critical how level the tray is, how much warping is present in the top tray, how much water is added for each experiment and how the water freezes.

A 36 gauge copper-constantan thermocouple was located just beneath the surface of the ice in the labyrinth. This double junction thermocouple was referenced to an ice-water bath mixture and the millivolt output was read on a Data Technology Corp. model 350 digital volt meter. Counterflow was used in the heat exchanging coils to minimize the temperature gradients in the ice both across the labyrinth and down its length. This resulted in maximum temperature gradients across the ice surface of about  $0.5^{\circ}\text{C}$ . For the present study the temperature of the ice in the moisture conditioner was not critical but was generally maintained intermediate between the top and bottom plate temperatures of the working section. If the ice labyrinth temperature were warmer than the top plate temperature of the working section, the air entering the working section would be moist and would condense on the chamber walls. If the temperature of the ice labyrinth were very cold, the air entering the working section would be drier than necessary and the time for vapor equilibrium to occur in the working section would be a maximum.



The temperature conditioner, indicated by point D, Fig. 4.3, is a radiator 25 cm long, 25 cm wide and 10 cm high. Since the airflow must make a change in direction of  $90^{\circ}$  when it enters the temperature conditioner, three metal sheets were curved from different points on the radiator to the circular pipe where they were spaced to collect equal volumes of air. It was necessary, however, to insert a honeycomb screen in the circular pipe just ahead of the collection point of the three sheets to create turbulence and ensure that the air is always divided in the same proportions even at higher velocities when the parabolic flow in the circular pipe becomes more marked. There is 0.47 cm distance between the vertical fins in the radiator and the fins are 0.03 cm thick. A honeycomb covers the exit of the radiator. The individual honeycombs are 0.67 cm across and the fins are 0.04 cm thick. The honeycomb material has a thickness of 1.4 cm. This arrangement gives a uniform flow at the exit of the temperature conditioner across its entire face independent of the air velocity.

The temperature of the radiator is controlled by regulating both the temperature and flow of the coolant passing through it. This temperature is monitored with a thermocouple. In this study the temperature of the radiator was not critical and often the radiator was not cooled at all. Nonetheless, its presence gives the chamber an additional versatility. It is important to note that the temperature conditioner should never be operated colder than the moisture conditioner or frost will be deposited on the radiator.

The effuser, constructed of stainless steel sheet material, is 25 cm in width and 10 cm in height where it is connected to the temperature conditioner. Being 61 cm in length, it contracts to a width

of 9 cm and a height of 2.5 cm where it joins the working section of the chamber. At these low velocities the need for an effuser is marginal, so the angle of contraction is not critical.

The working section consists of three portions: the pre-moisture section, the actual working section and the post-working section. Each of the three sections is 9 cm in width and 2.5 cm in height. Both the upper and lower horizontal plates are constructed of aluminum and the sides of the chamber are of plexiglass which is a poor thermal conductor. The pre-moisture section is 64 cm in length. Along this length the top and bottom plate temperatures are maintained independently of one another and at nearly the same temperature as that of the corresponding plate in the actual working section. The top plate of the pre-moisture section is not coated with ice. The purpose of this section is to allow additional time for the incoming air to come to thermal equilibrium with the nearly linear temperature profile between the two horizontal plates.

The actual working section is 122 cm long and has double walled plexiglass sidewalls with a double pane optical glass window opposite the growing crystals. The plexiglass sidewalls serve to insulate the top from the bottom and provide visible access to the entire section. The chamber sidewall not containing the optical glass window has nine 1/2" test holes milled along its length with accompanying plexiglass plugs machined to fit. Both temperature and velocity probes are inserted into the working section through holes drilled in the plugs. The probes can be moved with respect to the plugs and the plugs can be rotated so temperature and velocity profiles can be obtained over the entire horizontal and vertical expanse of the working section. A

1/8" thick by 1" wide neoprene gasket cemented around the bottom of the top plates' perimeter acts as a mold for the ice surface. The top plate has a thermocouple imbedded just beneath the ice surface. When the top plate is operated at temperatures above freezing, a 1/8" thick stainless steel substrate 3" in width with .012" thick stainless steel wicking material fused to its exposed surface is screwed to the top plate fitting snugly into the mold normally reserved for the ice surface. The wick coated substrate which serves as the water vapor source consists of two lengths which butt together and are gravity fed distilled water from each end of the working section. The top plate has an oval hole 1.3 cm in width by 3.5 cm in length which is located 15 cm from the exit of the working section. This hole is fitted with a plug which holds the glass fiber on which the ice crystals grow. The plug has an ice or water surface respectively to match the rest of the top plate except for the press fitted 0.4 mm diameter tube through which the glass fiber is inserted. This plug seals with an O-ring and can be easily removed to facilitate the recovery of the ice crystals grown on the glass fiber. The bottom plate has two thermocouples attached to its unexposed surface. One thermocouple is interfaced with the control of the cooling unit, whereas the output of the other, along with the output of the thermocouple fixed to the top plate, is continuously recorded on a three channel chart recorder to ensure that no possible variations in temperature, during the period of crystal growth, go undetected.

The post-working section is 38 cm in length and is not coated with ice. Its purpose is to insure that if any thermal gradient induced convection cells are present near the exit of the working

section they occur well downstream from the growing crystals.


The cooling for the top plate along the entire working section is provided by a Neslab LT-9 circulator which uses isopropyl alcohol as the coolant. This circulator maintains the temperature of the alcohol stable to within  $\pm 0.05^{\circ}\text{C}$  over the temperature range  $+10^{\circ}\text{C}$  to  $-30^{\circ}\text{C}$ . The cooling for the ice labyrinth, the temperature conditioner, and the bottom plate is provided by a built to order circulator from Cincinnati Sub-Zero. The coolant is also isopropyl alcohol with a temperature stability to within  $\pm 0.05^{\circ}\text{C}$ , this time with an adjustable temperature range from  $0^{\circ}\text{C}$  to  $-50^{\circ}\text{C}$ . A heat load consisting of a large radiator has been added to the system to increase the temperature stability.

#### B. Calibrations and Procedure

An ice surface is formed on the top plate of the actual working section by lifting the top assembly of this section, inverting it, resting it on a special plywood panel, filling the neoprene mold with distilled water, freezing it and smoothing it level with the gasket height by rolling a heated 4" diameter solid brass cylinder down its length. The assembly is then re-inverted, lowered into place and sealed by securing the sidewalls to it with a gasket and screws. Additional sealing requirements, particularly around the glass fiber and sidewall plugs, are met with Apiezon sealing compound, a special inert claylike substance with an extremely low vapor pressure. To minimize possible temperature gradients both across and along the length of the top and bottom plates, the cooling fluid enters alternate cooling pipes via a manifold arrangement at each end of the plates. For both the top and bottom assembly the cooling pipes which

are in contact with one another and the aluminum plate are all cemented together with a high thermal conductivity epoxy, providing excellent heat transfer between the pipes and the aluminum plates, thus inducing a more uniform temperature distribution over the exposed plate surfaces. The actual working section, salvaged from an earlier prototype dynamic thermal diffusion chamber, has been modified but is the same basic unit described in more detail by Gamara (1972).

The uniformity of temperature over both the top and bottom plate surfaces has been tested in a series of experiments. Gamara (1972) utilizing these same plates made several runs with thermistors imbedded in the ice surface on the top plate and found a uniform temperature (within  $\pm 0.05^{\circ}\text{C}$ ) both across and along the length of the plate. Employing thermocouples inserted through the plugs in the chamber side-walls, I have measured the temperature of the exposed surfaces of both the top and bottom plates to be uniform within  $\pm 0.1^{\circ}\text{C}$  except within 5 cm distance of either the entrance or exit of the working section where the temperature was  $0.3^{\circ}\text{C}$  to  $0.4^{\circ}\text{C}$  warmer. With such temperature uniformity over the two plates, a linear temperature distribution in the steady state should exist in the region between the upper and lower plates provided no flux of heat occurs through the sidewalls. To determine the validity of this postulate both horizontal and vertical temperature profiles were taken between the two plates for a variety of both top and bottom plate temperatures and ventilation velocities. Most of these profiles were taken through the test hole plug located 15 cm from the exit, i.e., at the position where crystal growth on the fiber occurs. The vertical temperature profiles were taken with a 36 gauge copper-constantan thermocouple shaped in the form of a crank,


, where it protruded through the sidewall plug. This shape facilitated temperature measurements over the entire vertical height and also provided a 4 cm length of thermocouple at the same height and temperature of the thermocouple tip thus reducing possible errors in the temperature measurement. Figure 4.5 shows a horizontal temperature profile taken 1.00 cm above the bottom plate with the top

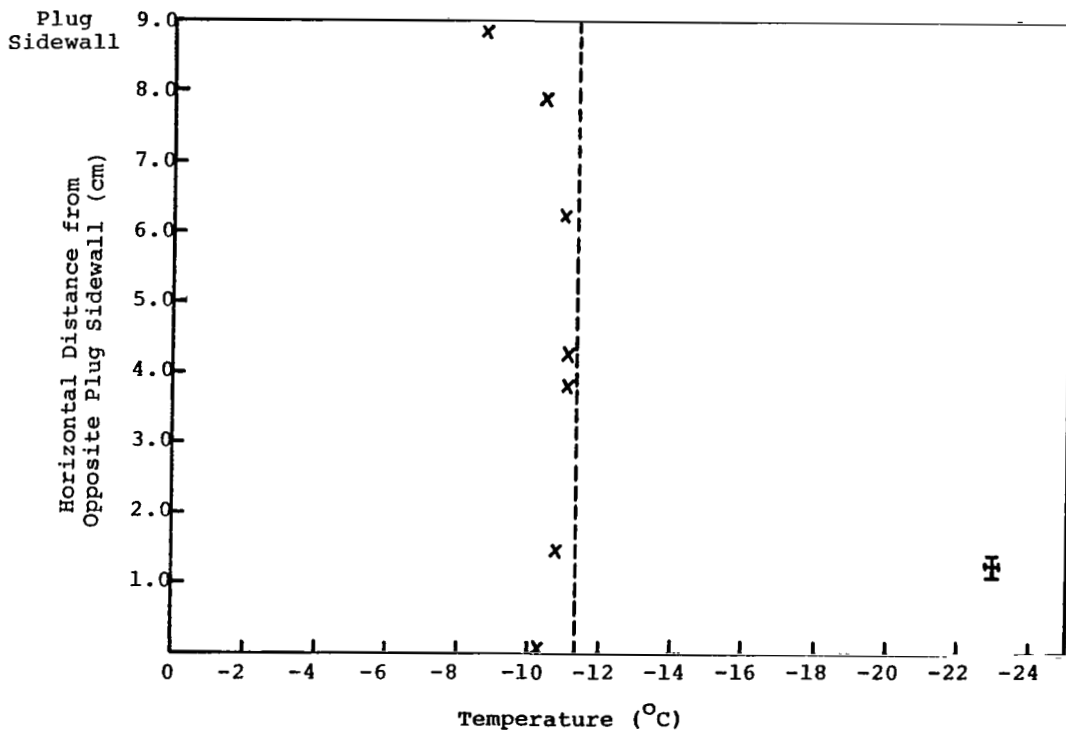


Fig. 4.5 A horizontal temperature profile taken 1.00 cm above the bottom plate in the dynamic thermal diffusion chamber ( $T_t = -10.0^\circ\text{C}$ ;  $T_b = -12.2^\circ\text{C}$ ).

plate temperature equal to  $-10.0^\circ\text{C}$ , the bottom plate temperature equal to  $-12.2^\circ\text{C}$ , and the ventilation velocity zero. The dashed line at  $-11.3^\circ\text{C}$  indicates the temperature at this height assuming a vertical linear temperature profile between the two plates. The deviation of

the actual temperature from this value near the chamber sidewall opposite the plug is real. However, the actual deviation near the plug sidewall is not really as large as indicated because nearly all but the very junction of the thermocouple was outside the chamber and at a warmer temperature resulting in a temperature measurement error. The general shape of this horizontal temperature profile and the fact that the temperature even at the horizontal center of the chamber was  $0.2^{\circ}\text{C}$  warmer than it should be indicates that some heat is entering the chamber through the sidewalls. Vertical temperature profiles taken at zero velocity such as Figs. 4.6 and 4.7 also show that at any given height the actual temperature is tenths of a degree Celsius warmer than the temperature at that height assuming a linear temperature profile. These two figures portray both the actual temperature profile, marked with X's, and the theoretical linear temperature profile, indicated by the solid line, in the region between the upper and lower plates. Figure 4.6 shows these vertical temperature profiles for a top plate temperature of  $-10.0^{\circ}\text{C}$  and a bottom plate temperature of  $-10.3^{\circ}\text{C}$ . Figure 4.7 gives the vertical temperature profiles for an upper plate temperature of  $-7.9^{\circ}\text{C}$  and a lower plate temperature of  $-20.7^{\circ}\text{C}$ . Note from these two figures that the larger deviations from the linear temperature profile occur near the middle and upper portions of the chamber.

The top plate temperature is defined as the temperature measured by the thermocouple imbedded just beneath the surface of the ice in the middle of the top plate and 70 cm from the entrance of the working section. The temperature measured by the thermocouple imbedded on the backside of the bottom plate and 15 cm from the exit of the working

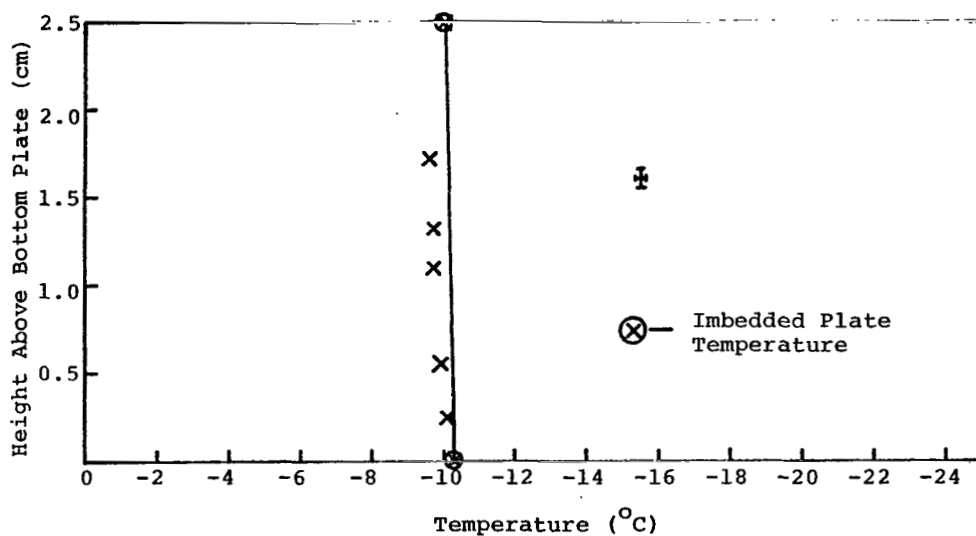


Fig. 4.6 A vertical temperature profile taken at the horizontal center of the dynamic thermal diffusion chamber ( $T_t = -10.0^\circ\text{C}$ ;  $T_b = -10.3^\circ\text{C}$ ).

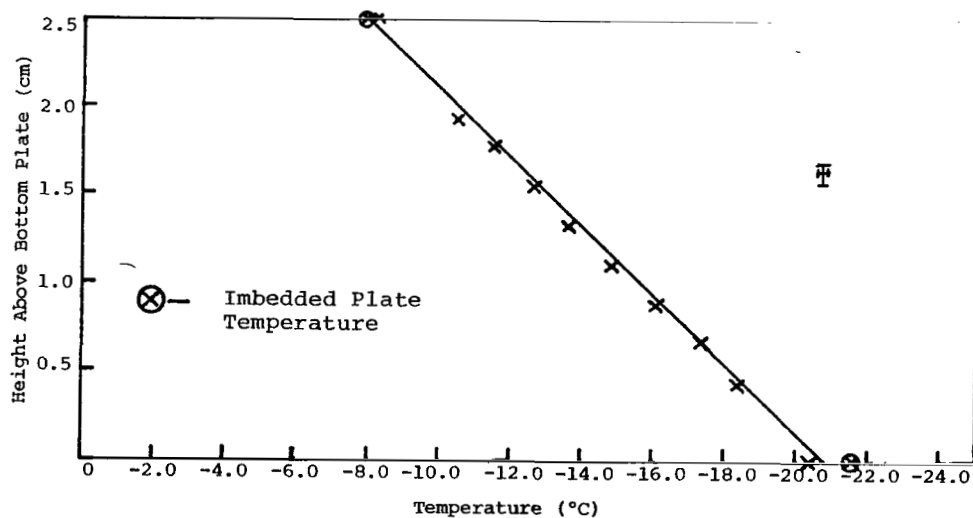


Fig. 4.7 A vertical temperature profile taken at the horizontal center of the dynamic thermal diffusion chamber ( $T_t = -7.9^\circ\text{C}$ ;  $T_b = -20.7^\circ\text{C}$ ).



section is always colder than the relevant bottom plate temperature. The temperature obtained by placing a thermocouple against the upper exposed surface of the bottom plate gives the relevant bottom plate temperature if no ice crystals grow there. However, at high ambient supersaturations, resulting from large temperature differences between the top and bottom plates, numerous crystals grow on the bottom plate making thermal contact between the thermocouple and the plate poor and also raising the local temperature tenths of a degree Celsius by the release of latent heat. Hence, under these conditions, as in Fig. 4.7, the relevant bottom plate temperature lies between the imbedded and surface contact temperatures and is obtained by fitting the best straight line to the points composing the measured vertical temperature profile.

Since the length of the chamber necessary for steady state transfer of heat between the upper and lower plates is a function of ventilation velocity and since heat does enter through the sidewalls, it is important to know how the temperature at any given vertical point in the chamber varies with the velocity. Figure 4.8 shows this variation of temperature with velocity at a height of 1.25 cm above the bottom plate and in the horizontal center of the chamber for two different distances from the entrance of the working section; 40 cm and 107 cm. The position 107 cm from the entrance of the working section is the location at which ice crystal growth on the glass fiber takes place. The experimental points in Fig. 4.8 were taken with the temperature conditioner at room temperature and the moisture conditioner at  $-4.5^{\circ}\text{C}$  for a top plate temperature of  $-10.1^{\circ}\text{C}$  and a bottom plate temperature of  $-10.1^{\circ}\text{C}$ . Note from Fig. 4.8 that the temperature at the position

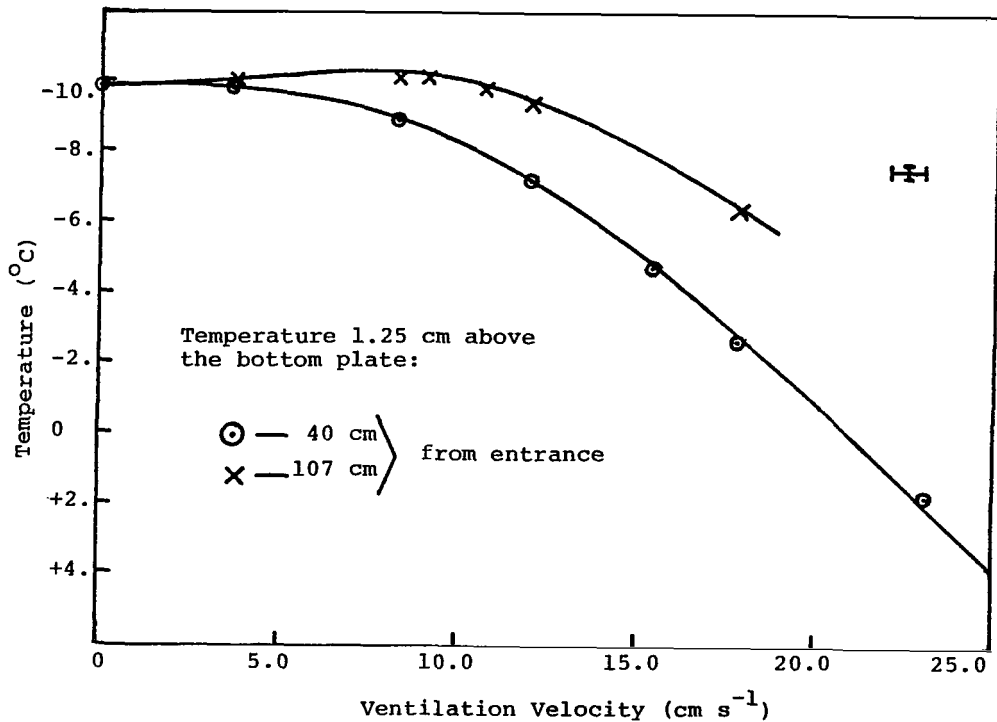


Fig. 4.8 Variation of temperature with ventilation velocity at a fixed height and distance from the entrance of the working section. ( $T_t = -10.1^\circ\text{C}$ ;  $T_b = -10.1^\circ\text{C}$ ).

of the glass fiber, indicated with X's, becomes colder by tenths of a degree Celsius as the velocity increases from zero to about 9 or 10  $\text{cm s}^{-1}$  and then warms quite rapidly at higher velocities. The lowering of the temperature at low velocities demonstrates the elimination of the wall effects in the horizontal center of the chamber when a flow is present. The rise in temperature at higher velocities indicates the maximum velocity for which diffusive equilibrium of heat occurs at that particular distance from the working section entrance. At the location of the glass fiber this maximum velocity is about 10  $\text{cm s}^{-1}$ , being slightly higher if either the temperature conditioner is operated near the top plate temperature or the moisture conditioner is

operated at a temperature intermediate between the top and bottom plate temperatures.

The ventilation velocities in my dynamic thermal diffusion chamber were in general determined with a Thermo-Systems, Inc. hot-wire anemometer system employing component models 1050, 1051-2 and 1057 with a model 1271-T1.5-6 tungsten hot wire probe. The probe is factory calibrated specifically for low velocities at an ambient temperature of  $-10^{\circ}\text{C}$  and a sensor temperature of  $100^{\circ}\text{C}$ . This sensor temperature is a compromise. Higher sensor temperatures require that a smaller temperature correction be applied to readings taken at ambient temperatures other than  $-10^{\circ}\text{C}$ . However, larger natural convection velocities at the hot wire, leading to bad measurements at low velocities, are associated with the higher sensor temperatures. For velocity measurements, the hot-wire anemometer probe was fixed in the chamber sidewall plug at the chamber position of the glass fiber. The hot wire, 1 mm in length, was always parallel to both the top and bottom plates of the chamber thus lying along an isotherm. The height of the hot wire above the bottom plate was adjustable and was determined with a stereo microscope equipped with a micrometer eyepiece. This same method was used in determining the position of the thermocouple for temperature measurements. Hence, the position of either the thermocouple or the hot wire probe could be determined in the vertical to within  $\pm 0.1$  mm and in the horizontal to within  $\pm 1.0$  mm.

Appendix A shows that the transition from laminar to turbulent flow occurred around  $40\text{ cm s}^{-1}$  with a turbulence level of  $\pm 2.5\text{ cm s}^{-1}$ . Since the turbulent regime occurred only at velocities much larger than those employed in this study, a consideration of laminar flow alone is

sufficient.

Figures 4.9 and 4.10 illustrate the vertical and horizontal velocity profiles respectively. The vertical profile was taken 4.5 cm

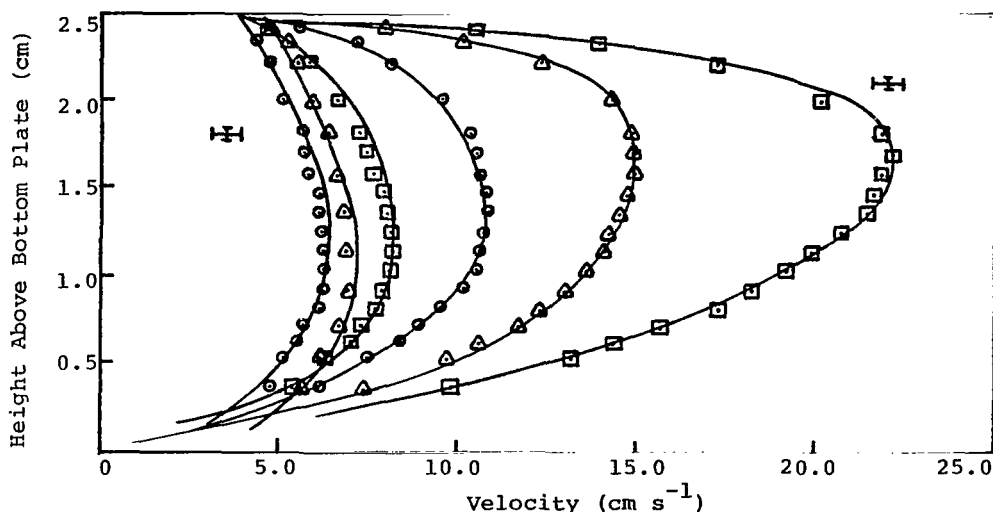


Fig. 4.9 Vertical velocity profiles taken at the horizontal center of the dynamic thermal diffusion chamber.

from the plug sidewall, that is, in the horizontal center of the chamber. The horizontal velocity profile was taken at a height of 1.36 cm above the bottom plate. Both profiles were taken with the top plate temperature at  $-10.2^{\circ}\text{C}$ , the bottom plate temperature at  $-10.5^{\circ}\text{C}$  and no ice on the bottom plate. As expected from the chamber dimensions, the horizontal flow did not become fully developed at as low velocities as flow in the vertical. For velocities greater than  $10\text{ cm s}^{-1}$  the maximum velocity occurred slightly above the vertical center of the chamber.

The ventilation velocity for a particular RPM of the fan was a marked function of the static pressure. The static pressure was in turn a function of how much water was placed in the moisture conditioner and how this water froze. This necessitated making a velocity calibra-

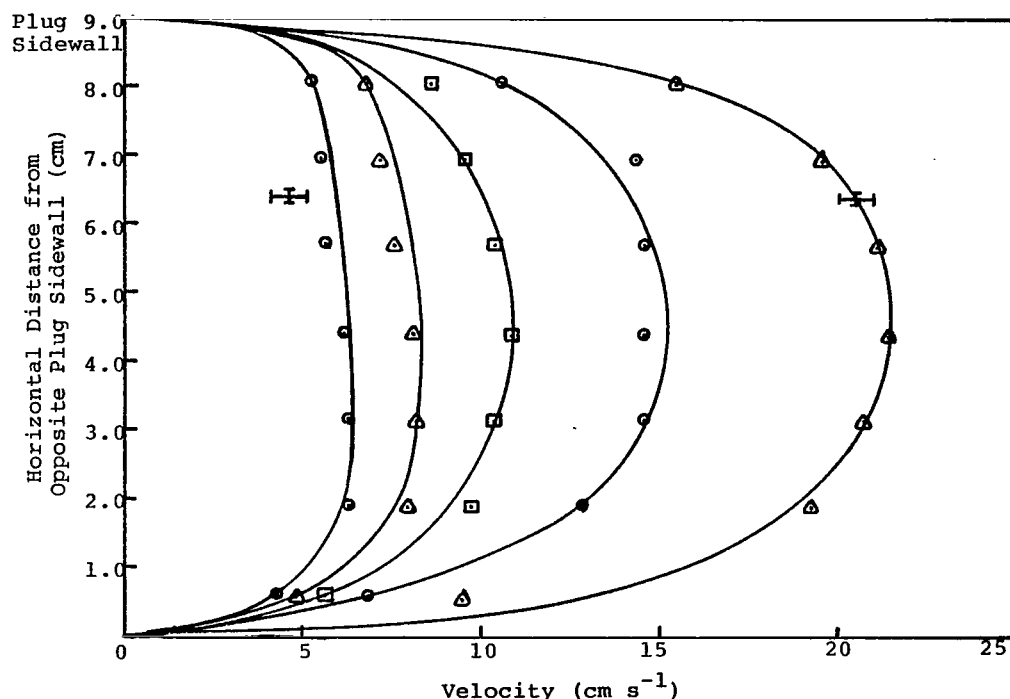


Fig. 4.10 Horizontal velocity profiles taken 1.36 cm above the bottom plate in the dynamic thermal diffusion chamber.

tion versus RPM of the fan, i.e., motor setting in microamperes, each time water was placed in the moisture conditioner and frozen.

The velocity response of the dynamic chamber, as measured by the hot-wire anemometer probe located 107 cm from the working section entrance, is presented in Fig. 4.11 as a function of time. Since time in Fig. 4.11 increases from right to left, the peak on the right shows the velocity overshoot due to a surge of air when the fan was switched on. The line with the series of undulations superimposed on it indicates the magnitude of the steady state velocity,  $23 \text{ cm s}^{-1}$ , for this motor setting or RPM and the magnitude of the undulations represent the turbulence level at this velocity. The dip on the left indicates

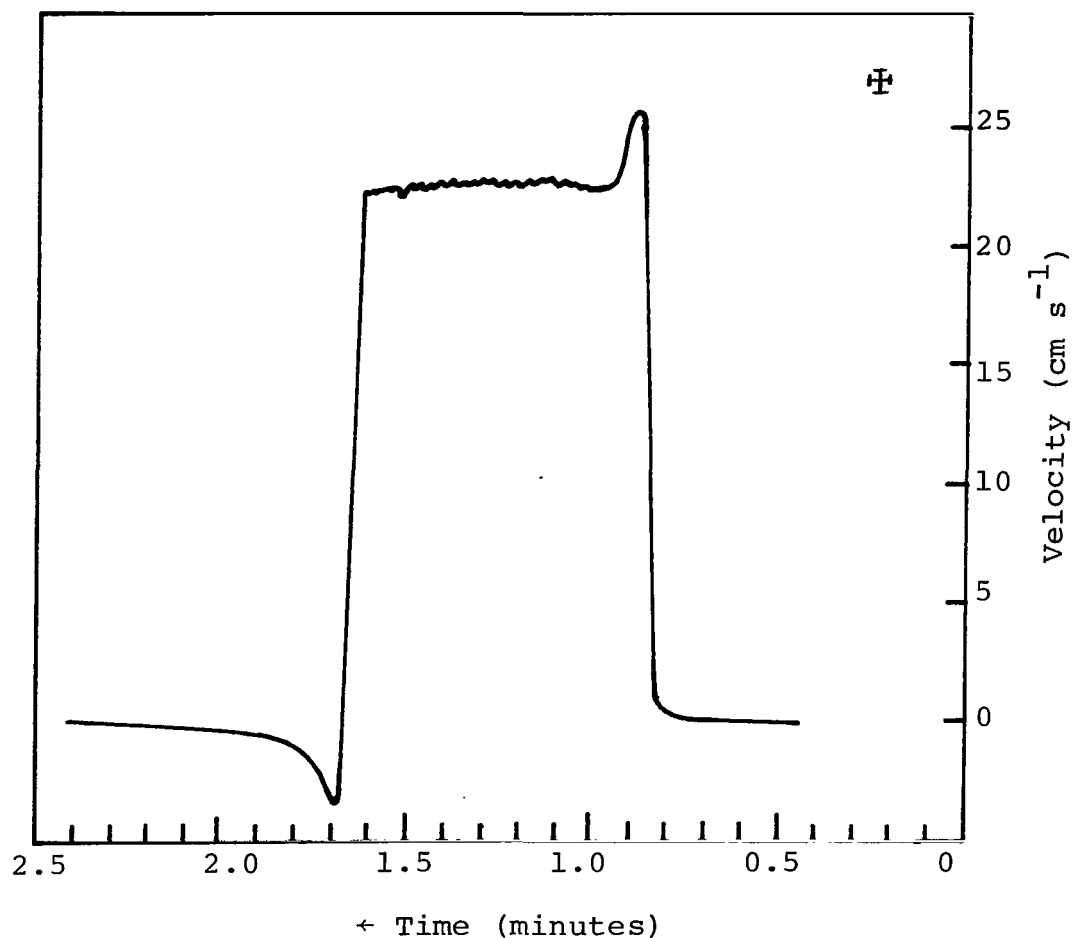


Fig. 4.11 Velocity response when the fan is turned on and off.

the response of the hot-wire anemometer when the fan was switched off but does not necessarily imply a momentary reverse flow in the chamber. In fact, such a reverse flow was never observed. Although the velocity response was almost immediate, the steady state velocity occurred about 10 seconds after the servo motor was switched on at this RPM with an overshoot magnitude approximately 10 percent of its steady state value. At lower RPM the velocity response was slightly slower but the overshoot magnitude was even a smaller percentage of its steady state value and the steady state velocity occurred sooner.

When an ice surface was present on the bottom plate, it was observed that for velocities greater than about  $15 \text{ cm s}^{-1}$  small ice particles approximately 5 to 10  $\mu\text{m}$  diameter were lifted from the bottom plate and carried with the air stream. When the fan motor was switched off and on there was a delay of from 15 to 20 seconds before the ice particles were observed. The presence of the ice particles makes high velocity measurements perilous to the hot wire probe. However, an even more serious consequence of their presence is the limitations they impose on high velocity applications of the dynamic chamber.

The accuracy of the hot-wire anemometer velocity measurements was verified by two different approaches. In the first approach, the shutter speeds of two 35 mm Pentax cameras were electronically calibrated. It was determined that for shutter speeds slower than or equal to 1/125 second the maximum variation in the shutter speed was less than two percent of the mean value of twelve experimental measurements at each shutter speed. For a given ventilation velocity or motor setting, photographs were made of small water droplets, approximately 10  $\mu\text{m}$  diameter, which followed the airstream and were illuminated with a high intensity mercury vapor lamp. The photographs showed the droplet paths for a given shutter speed as straight lines. The distance traversed by a droplet for a given film exposure time was determined from the length of this straight line and divided by the shutter speed giving the velocity of the droplet and thus the airstream in  $\text{cm s}^{-1}$ . The second approach involved using the Dyna-Vac diaphragm pump with its nearly constant volume output independent of static pressure as the air driving unit. In this case, the volume flow was measured with a factory calibrated airflow meter to be  $6.4 \pm .1 \text{ liter min}^{-1}$ . The horizontal

and vertical velocity profiles in the working section for this flow were taken with the hot-wire anemometer. An eighth order curve fit was applied to these velocity profile points to give the three dimensional velocity profile in the working section. This velocity profile was then integrated by applying the divergence theorem to give the volume flow. Finally, the calculated volume flow was compared with the experimentally determined volume flow. Both these approaches gave results consistent with the factory calibration of the hot-wire anemometer.

From all available data it was estimated that the hot-wire anemometer velocity measurements between  $3 \text{ cm s}^{-1}$  and  $25 \text{ cm s}^{-1}$  had an absolute accuracy of  $\pm .4 \text{ cm s}^{-1}$  and a relative accuracy of about  $\pm 3\%$ . The percent variation of absolute accuracy was much larger at low velocities than at high velocities due to the interaction of natural convection from the heated hot wire with the forced ventilation. The velocity set-point repeatability was within  $\pm 2\%$  over the entire range  $0 \text{ cm s}^{-1}$  to  $25 \text{ cm s}^{-1}$ .

In computing supersaturation profiles in a thermal diffusion chamber, it has generally been assumed that the partial density of the water vapor is linear with height between the two plates of the chamber. Second order diffusion effects such as the mass transfer due to the temperature gradient (Soret effect), the energy or heat transfer due to the concentration gradient (Dufour effect), and the temperature dependence of the diffusion coefficients have been ignored. Only recently, however, Katz and Mirabel (1975) have solved numerically the heat and mass flux equations for a two-component system in which only one component, i.e., water, was diffusing without assuming linear



temperature, linear partial pressure or linear partial density profiles between the plates. They included effects such as the temperature and composition dependence of the binary diffusion coefficient and of the mixture (air + water) thermal conductivity, the heat carried by the diffusing water molecules and both the Soret and Dufour effects. Using a top plate temperature of  $+20^{\circ}\text{C}$  for a chamber at a total pressure of 1 atm, they found that the "best" solution to the complete heat and mass flux equations including all effects differed from that obtained by assuming linear temperature and linear partial pressure profiles by only 1% over a range of temperature difference between the two plates of from  $0^{\circ}\text{C}$  to  $20^{\circ}\text{C}$ . They also found that assuming linear temperature and linear partial density profiles underestimated the value obtained from the "best" solution by about 12%. Hence, by fortuitous circumstances the use of a linear partial pressure profile between the plates gives a better representation of the ambient supersaturation in a thermal diffusion chamber with infinite parallel plates than does the use of a linear partial density profile. It will be shown that this is not necessarily true for a chamber with finite parallel plates.

I developed two separate computer programs to calculate the supersaturation profiles in a thermal diffusion chamber with a plate separation,  $d$ . One program assumed a linear partial pressure profile, the other assumed a linear partial density profile and both assumed a linear temperature with height between the two plates. I used the Goff-Gratch formulation to calculate the equilibrium partial pressure of water vapor over both a plane surface of water and a plane surface of ice as a function of temperature. The density of water

vapor at saturation over an ice surface was obtained from the saturation vapor pressure according to the equation

$$\rho_{ei}(T) = \frac{P_{ei}(T)}{C_v R_w T} \quad (4.5)$$

where  $\rho_{ei}(T)$  is the equilibrium vapor density in  $\text{g m}^{-3}$  over an ice surface at the temperature  $T$ ,  $P_{ei}(T)$  is the saturation vapor pressure in millibars over an ice surface at the temperature  $T$ ,  $C_v$  is the "compressibility factor" for water vapor, introduced to correct for the deviations of water from ideal gas laws,  $R_w$  is the gas constant for water vapor,  $4.6150 \times 10^6 \text{ erg g}^{-1} \text{ } ^\circ\text{K}^{-1}$  and  $T$  is the temperature of the vapor in  $^\circ\text{K}$ . In a similar manner, the density of pure water vapor at saturation over a plane surface of water,  $\rho_{ew}(T)$ , was found by substituting the saturation vapor pressure over a water surface,  $P_{ew}(T)$ , for the saturation vapor pressure over an ice surface in eq. (4.5). It should be noted that tables in the Smithsonian Meteorological Tables and elsewhere of saturation vapor pressure over either water or ice were obtained by computing the Goff-Gratch equations at  $0.5^\circ\text{C}$  temperature increments and interpolating to get the values at  $0.1^\circ\text{C}$  intervals. The use of a computer has greatly simplified these computations. Therefore, tables of both saturation vapor pressure and density of pure water vapor at saturation over both water and ice surfaces obtained by computing the Goff-Gratch equations at  $0.1^\circ\text{C}$  temperature increments are included in Appendix B. Also included in this appendix is the percent supersaturation with respect to ice at which water saturation occurs as a function of temperature.

Figures 4.12 and 4.13 illustrate the computer calculated super-

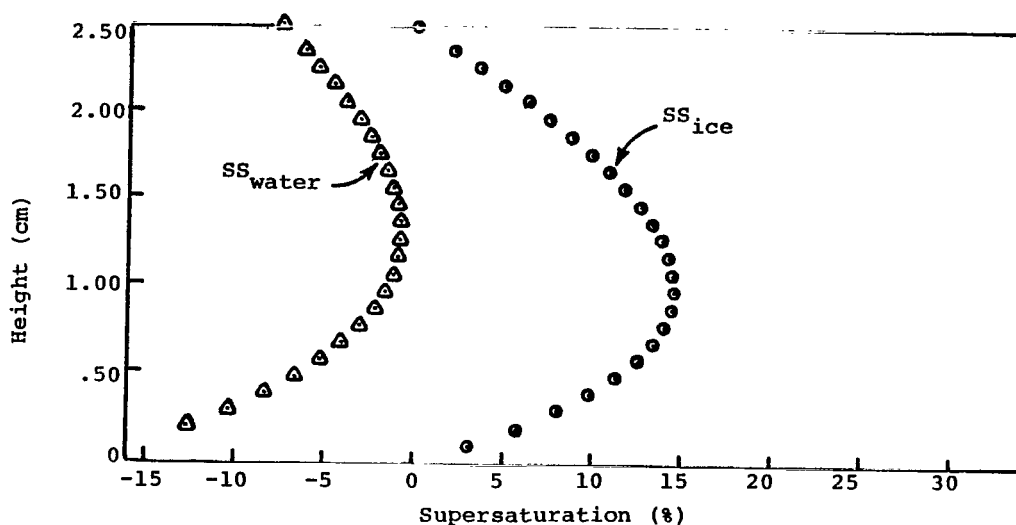


Fig. 4.12 Vertical supersaturation profile in a thermal diffusion chamber ( $T_t = -8.1^\circ\text{C}$ ;  $T_b = -20.6^\circ\text{C}$ ). Calculated assuming a linear vapor density with height.

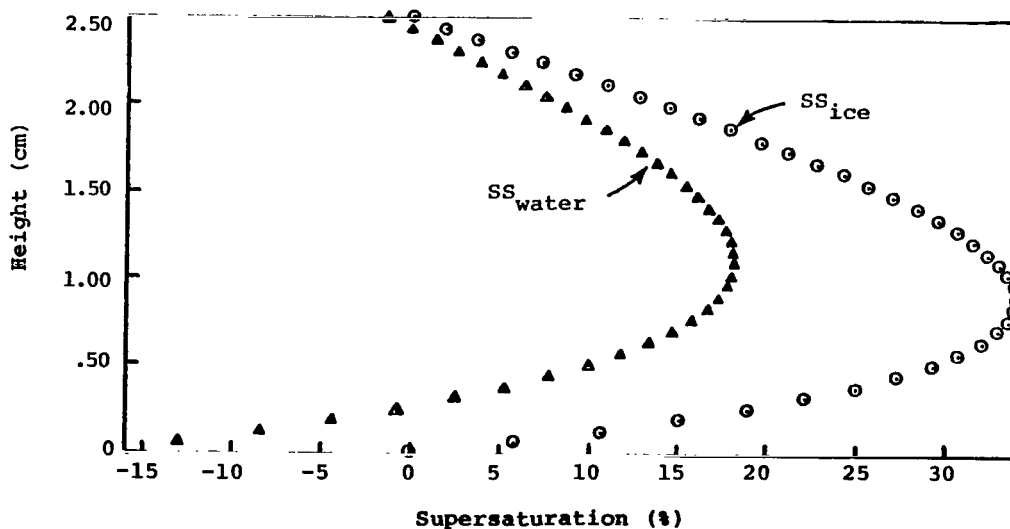


Fig. 4.13 Vertical supersaturation profile in a thermal diffusion chamber ( $T_t = -1.5^\circ\text{C}$ ;  $T_b = -20.5^\circ\text{C}$ ). Calculated assuming a linear vapor density with height.

saturation profiles with respect to both an ice and water surface for two different pairs of chamber plate temperatures. These supersaturation profiles were calculated assuming a linear partial density with height between the plates. Notice from these two figures that the maximum supersaturation with respect to ice is located below the vertical center of the chamber and is displaced even lower for larger temperature differences between the two plates. Also note that the maximum supersaturation with respect to water follows this same trend but occurs slightly higher in the chamber.

In most calculations of the supersaturation profile inside a thermal diffusion chamber it is assumed that diffusion of water vapor and heat takes place between two parallel infinite plates. It is therefore very important to know just what aspect ratio, i.e., ratio of chamber width to chamber height, is large enough to permit this assumption. Twomey (1961) showed that for a static chamber an aspect ratio of 4 was the minimum for a saturation ratio of 1.01 with respect to water before wall effects became significant. Elliott (1971) calculated that the aspect ratio should be no less than 5 and preferably 6 or 7 or even larger. He further calculated that for a static chamber with a 1 cm plate separation and an aspect ratio of 5 one could safely use about 2.5 mm on either side of the centerline. For this same chamber with an aspect ratio of 7.5 one could use about 1 cm on either side of the centerline. These calculations were performed in the interest of using a thermal diffusion chamber to estimate the population of cloud condensation nuclei (CCN). However, this type of analysis is applicable to my dynamic thermal diffusion chamber where ice crystal growth on a vertical support located in the center of the chamber is

the primary interest.

The most prominent wall effect is the introduction of heat through the sidewalls which manifests itself in raising the temperature and hence lowering the supersaturation. Furthermore, this introduction of heat through the sidewalls leads to the formation of a toroidal circulation with rising motion along the walls and sinking motion nearer the middle of the chamber. The introduction of heat through the sidewalls has its most pronounced effect on the ambient supersaturation at low values of supersaturation; that is, when the temperature difference,  $\Delta T$ , between the top and bottom plates is small. However, the effect becomes less significant as the forced ventilation velocity is increased from zero to the maximum velocity for which the incoming air continues to attain both thermal and vapor equilibrium.

I performed a series of experiments, in addition to the temperature measurements already described, to determine the extent of the toroidal circulation in my chamber. I made the chamber an open circuit by raising the motors and circulation fan. A 35 mm Pentax camera with an attached 200 mm lens and bellows was mounted on a tripod and positioned to view along an axis parallel and into the forced ventilation velocity. With a top plate temperature of  $-1.5^{\circ}\text{C}$  and a bottom plate temperature of  $-20.5^{\circ}\text{C}$ , giving a theoretical supersaturation greater than water saturation, i.e., Fig. 4.13, CCN nucleated to form water droplets thus maintaining a supersaturation greater than or equal to water saturation. There was, nonetheless, an insufficient density of droplets to effectively photograph the toroidal circulation as a function of velocity for velocities in excess of  $8.0 \text{ cm s}^{-1}$ . For higher ventilation velocities it was necessary to introduce droplets

generated by an Ultramist III nebulizer and having a  $10\text{ }\mu\text{m}$  mean diameter, into the chamber through the port hole located 5 cm from the entrance of the working section. For velocities less than  $17\text{ cm s}^{-1}$  the droplets were introduced through a  $3/8$ " diameter polyurethane tube 13 cm in length which was inserted horizontally into the port hole slightly above the vertical center of the chamber. Four holes in the tube, each approximately  $750\text{ }\mu\text{m}$  diameter and located at distances 2.5, 4.1, 6.4 and 8.3 cm respectively from the chamber sidewall opposite the port hole, allowed the droplets to be introduced parallel to the velocity. For ventilation velocities greater than  $17\text{ cm s}^{-1}$  the holes in the polyurethane tube became plugged with ice in a short time. Hence, for velocities greater than  $17\text{ cm s}^{-1}$  the droplets were introduced perpendicular to the ventilation velocity without the aid of the polyurethane tube. In both cases the droplets were introduced into the dynamic chamber airstream with the aid of a small controlled and measured flow of air from a commercially filled compressed air bottle. This was effective and good photographs were obtained for velocities from 0 to  $21\text{ cm s}^{-1}$ . For ventilation velocities greater than  $8\text{ cm s}^{-1}$  the introduction of the droplets created turbulence. This was particularly true for ventilation velocities greater than  $17\text{ cm s}^{-1}$  because the droplets were introduced perpendicular to the main airstream. Figure 4.14(a), (b), (c) and (d) are photographs showing the toroidal circulation for ventilation velocities of 0, 6.7,  $13.8 \pm .9$  and  $20.5 \pm 1.4\text{ cm s}^{-1}$  respectively.

Note from these photographs that a region apparently devoid of droplets existed in the upper portions of the chamber. This was a

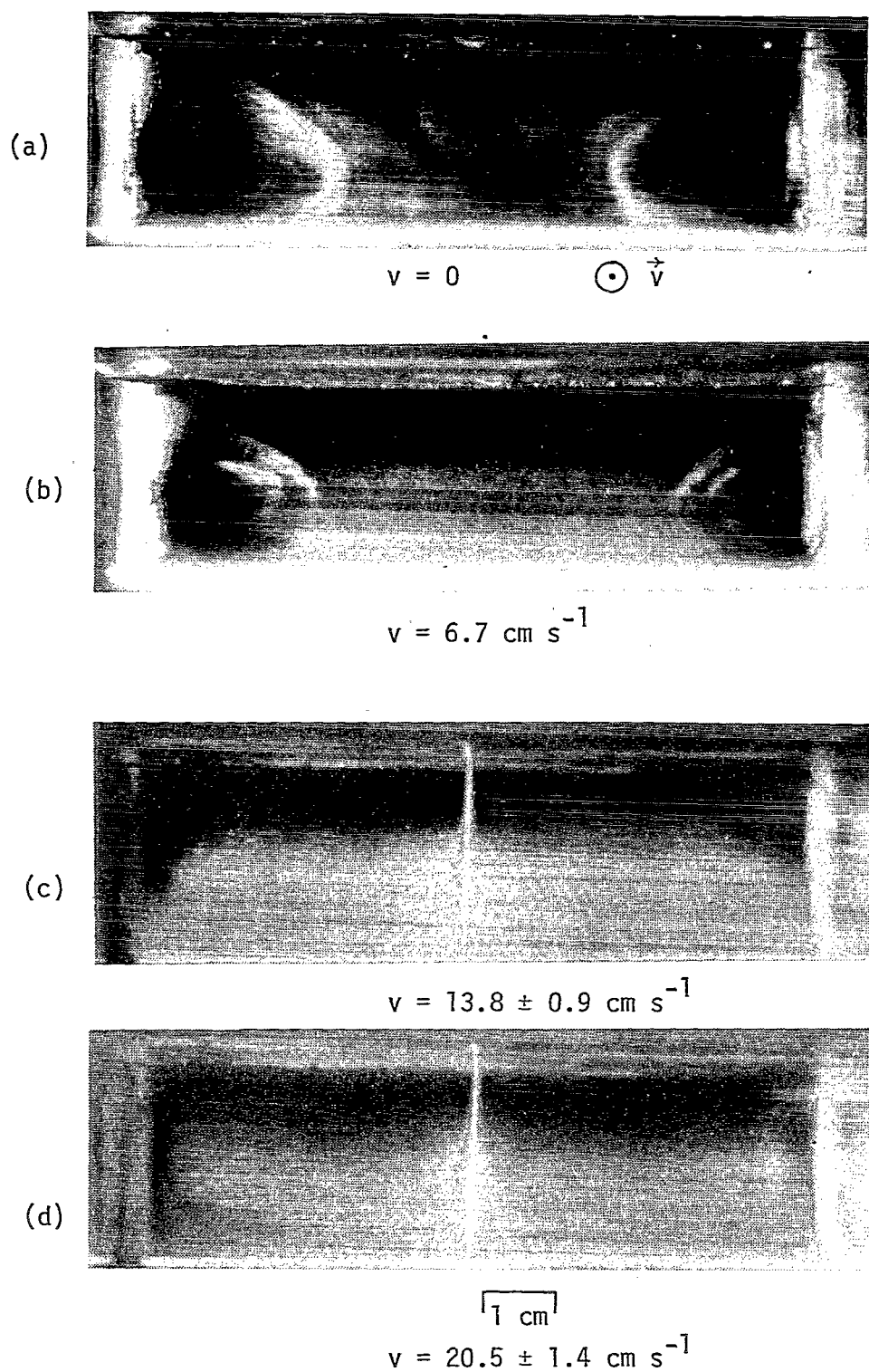


Fig. 4.14 The form and extent of the toroidal circulation is a function of the forced ventilation velocity.

consequence of both the maximum supersaturation occurring near the vertical center of the chamber and the finite growth times required for observable droplets. Also notice from these photographs that the introduction of a ventilation velocity forced the toroidal circulation closer to the chamber sidewall and away from the centerline of the chamber. This was the basis for the result obtained in Fig. 4.8 concerning temperature measurements. That is, at a given point near the centerline of the chamber the temperature lowered a couple tenths of a degree Celsius when a small velocity was introduced. The direction of the toroidal circulation also explains why larger deviations from the linear temperature profile occurred near the vertical middle and upper portions of the chamber as determined from Figs. 4.6 and 4.7.

I determined experimentally that for appropriate top and bottom plate temperature pairs giving a band of maximum supersaturation slightly above water saturation near the vertical center of the chamber, CCN nucleated near the upper portions of this band and formed droplets which then settled slowly toward the bottom plate. As the droplets fell below this band of maximum supersaturation and into a region undersaturated with respect to water they evaporated and completely disappeared before reaching the bottom plate. Due to the finite time required for either the growth or evaporation process to occur, the band of observable droplets was displaced slightly below the band of maximum supersaturation. The vertical width of this band was established by the temperature difference between the top and bottom plates, larger temperature differences corresponding to higher supersaturations and therefore wider bands of droplets. In an experimental attempt to



determine how well the computed supersaturation profiles for a thermal diffusion chamber with infinite horizontal plates matched the moisture profiles in my chamber with an aspect ratio of 3.6, I alternatively set the top or bottom plate temperature at a fixed value and incremented the temperature of the other plate by intervals of less than  $0.1^{\circ}\text{C}$  so that the band of droplets became successively narrower until freely floating water droplets, i.e., less than  $5\text{ }\mu\text{m}$  diameter, no longer were visible either with the naked eye and the aid of a laser or through our stereo microscope. I made the assumption that these pairs of top and bottom plate temperatures gave a maximum supersaturation in the chamber equal to water saturation. This assumption depends on the postulate that only a small number of nuclei activated at relative humidities less than water saturation grow to an observable size, i.e.,  $5\text{ }\mu\text{m}$  diameter. Table I is a tabulation of such experimentally determined temperature pairs. Using these temperature pairs and assuming a linear

Table I Experimental Temperature Pairs  
at Which Water Saturation Occurs.

T. top( $^{\circ}\text{C}$ )	T bottom( $^{\circ}\text{C}$ )	Assumes Linear Vapor Pressure		Assumes Linear Vapor Density	
		Maximum % SS <sub>wrt</sub> Water	Maximum % SS <sub>wrt</sub> Ice	Maximum % SS <sub>wrt</sub> Water	Maximum % SS <sub>wrt</sub> Ice
-2.6	-11.6	+0.14	7.2	-0.38	6.5
-5.9	-17.3	+0.23	12.6	-0.68	11.4
-9.0	-22.0	+0.51	17.7	-0.78	16.1
-10.9	-24.4	+0.11	20.0	-1.31	18.1

vapor pressure exists between the top and bottom plates, one calculates a maximum supersaturation in the chamber greater than water saturation by about 0.11 to 0.51 percent with respect to water as the top plate

temperature varies over the range  $-2.5^{\circ}\text{C}$  to  $-11.0^{\circ}\text{C}$  and the corresponding bottom plate temperature varies over the range  $-11.5^{\circ}\text{C}$  to  $-24.5^{\circ}\text{C}$ . Again using these temperature pairs and assuming a linear vapor density exists between the top and bottom plates, one calculates a maximum supersaturation in the chamber less than water saturation by about 0.4 to 1.3 percent with respect to water over the same top and bottom plate temperature ranges as above. Hence, at least near water saturation, assuming a linear vapor pressure in calculating the supersaturation profile in my dynamic thermal diffusion chamber overestimates the actual supersaturation. On the other hand, assuming a linear vapor density in calculating the supersaturation profile underestimates the actual supersaturation. Therefore, near water saturation the ambient supersaturation at any height in my chamber can be calculated and specified with both an upper and lower limit.

The effect of a temperature variation of  $\pm 0.1^{\circ}\text{C}$  at either the top or bottom plate on the maximum supersaturation is shown in Tables II and III for two quite different temperature pairs. Both the maximum

Table II Effect of Temperature Variation of the Top or Bottom Plate on the Maximum Supersaturation, case (a).

T bottom ( $^{\circ}\text{C}$ ) T top ( $^{\circ}\text{C}$ )	-11.5		-11.6		-11.7	
-2.5	+0.23 (-0.30)	7.2 (6.5)	+0.33 (-0.21)	7.3 (6.6)	+0.42 (-0.13)	7.5 (6.8)
-2.6	+0.05 (-0.46)	7.0 (6.3)	+0.14 (-0.38)	7.2 (6.5)	+0.24 (-0.30)	7.3 (6.6)
-2.7	-0.13 (-0.63)	6.8 (6.2)	-0.04 (-0.55)	7.0 (6.4)	+0.05 (-0.47)	7.2 (6.5)

Table III Effect of Temperature Variation of the Top or Bottom Plate on the Maximum Supersaturation, case (b).

T bottom (°C) T top (°C)	-24.3		-24.4		-24.5	
-10.8	+0.18 (-1.24)	19.9 (18.1)	+0.39 (-1.06)	20.3 (18.4)	+0.60 (-0.87)	20.6 (18.7)
-10.9	-0.09 (-1.49)	19.6 (17.8)	+0.11 (-1.31)	20.0 (18.1)	+0.32 (-1.13)	20.3 (18.4)
-11.0	-0.37 (-1.75)	19.3 (17.5)	-0.17 (-1.57)	19.7 (17.8)	+0.04 (-1.38)	20.0 (18.1)

supersaturation with respect to water, i.e., the left hand figures in each column, and the maximum supersaturation with respect to ice, i.e., the right hand figures in each column, are presented in these tables. The supersaturations in parenthesis were calculated by assuming a linear vapor density between the two plates and the unparenthesized supersaturations were calculated by assuming a linear vapor pressure. Notice that the effect on the supersaturation is more pronounced if a temperature variation occurs on the top plate than if a variation occurs on the bottom plate.

At very low supersaturations, resulting from small temperature differences between the top and bottom plates, the effect of the side-walls on both the temperature and the supersaturation is a maximum and in this case assuming either a linear vapor pressure or a linear vapor density between the plates probably leads to an overestimation of the ambient supersaturation in the chamber.

Since there is a difference in both the temperature and vapor density over an ice crystal which is growing as compared to one that is not growing due to the release of latent heat, the relevant growth

conditions are not the ambient or environmental conditions but the conditions which the crystal surface actually experiences. However, since these conditions are not readily determined, the ambient moisture, temperature and ventilation velocity conditions are generally specified. Nonetheless, by using conduction-diffusion equilibrium as discussed in Chapter III, eq. (3.4)

$$d\rho/dT = \frac{-K}{DL} \quad (4.6)$$

one can calculate a "true" vapor density excess for a crystal growing in a static environment. That is, in a plot of vapor density vs. temperature, eq. (4.6) corresponds to a curve such as that shown in Fig. 4.15 along with the saturation vapor density curve for ice. In Fig. 4.15 point B corresponds to conditions at the crystal surface. On the other hand, the ambient conditions correspond to some point A which is at a higher vapor density and lower temperature. In general, point A is defined by the experimental condition and it is necessary to find point B and thus the "true" vapor density excess  $\Delta\rho$  for growth in a static environment.

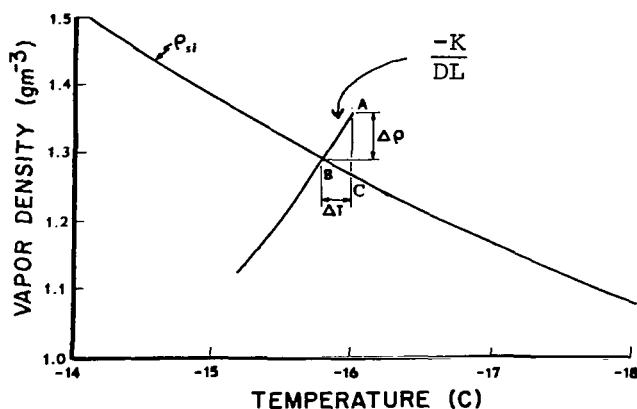


Fig. 4.15 Temperature-vapor density conditions at the surface (point B) and in the environment (point A) of a growing crystal. From Rottner (1971)

Marshall and Langleben (1954) using a finite difference form of equation (4.6) assumed  $K$ ,  $D$  and  $L$  were constant for the interval between points A and B. Since their treatment was equivalent to using a straight line between points A and B graphical determination of point B was simplified.

In the computer program which I developed to calculate the supersaturation profile in a thermal diffusion chamber assuming linear partial density and linear temperature with height between the two plates, I included a section to calculate the "true" vapor density excess for ice crystal growth in a static environment and also a calculation of the maximum vapor density excess, that is, the difference between the vapor densities at point A and point C in Fig. 4.15. In calculating the "true" vapor density excess in a static environment I included the temperature dependencies of both  $D$  and  $K$  but I used the value of the latent heat of sublimation at  $0^{\circ}\text{C}$  since it only varies 0.1% over the temperature range  $0^{\circ}\text{C}$  to  $-20^{\circ}\text{C}$ . I also used an environmental atmospheric pressure of 850 mb which is the average pressure for Reno, Nevada. Figure 4.16 illustrates the resulting computer calculated profiles of both "true" vapor density excess for a static environment and maximum vapor density excess for a top plate temperature of  $-8.9^{\circ}\text{C}$  and a bottom plate temperature of  $-22.1^{\circ}\text{C}$ . A sample of the actual computer output for this temperature pair is included in Appendix C. Also included in Appendix C is a diagram showing the calculated maximum vapor density excess which occurs in the vertical middle of the chamber as a function of the top plate and midpoint of the chamber temperatures.

Note that the profiles of vapor density excess in Fig. 4.16 have their maxima near the vertical center of the chamber. These maxima,

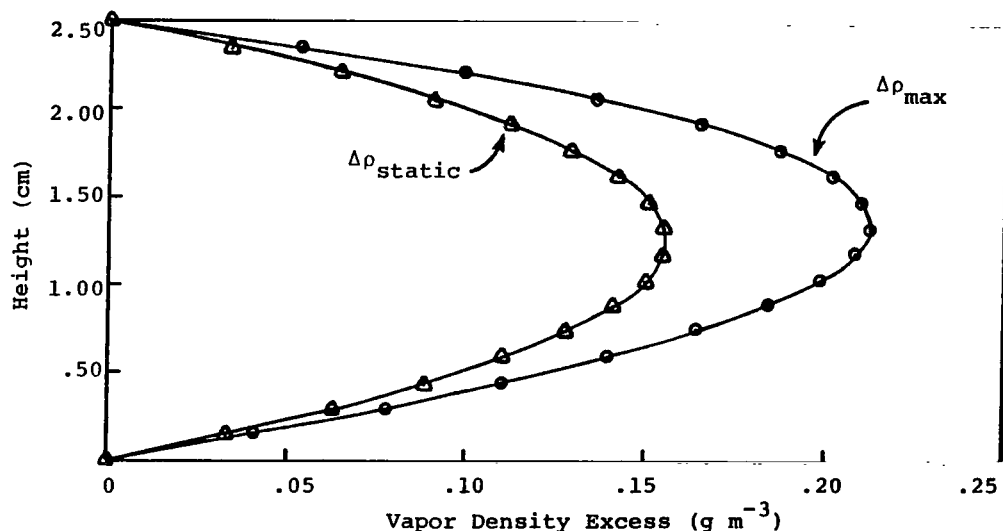


Fig. 4.16 Calculated profile of maximum and "true" vapor density excess for a static environment ( $T_t = -8.9^{\circ}\text{C}$ ;  $T_b = -22.1^{\circ}\text{C}$ ).

unlike the maxima in the supersaturation profiles, Figs. 4.12 and 4.13, occur even higher in the chamber for larger temperature differences between the top and bottom plates. Thus, for large temperature differences, i.e., greater than  $20^{\circ}\text{C}$ , between the plates the maxima for the vapor density excess, the supersaturation with respect to water, and the supersaturation with respect to ice all occur at somewhat different vertical positions in the chamber. The consequence of this is that when any one of these moisture designations is used to specify the ambient condition for growth occurring at various vertical positions in a thermal diffusion chamber with such large temperature differences between the plates, a simple relationship does not exist to determine the other two moisture designations accurately. This is not a serious problem in this study since temperature differences between the plates rarely exceeds  $20^{\circ}\text{C}$ . However, this can be a very serious problem in static thermal diffusion chambers where much larger temperature differences are often employed.

Two quite different definitions implicitly exist in the literature as to the vapor density excess for a given temperature at which water saturation occurs. One definition simply assumes, that for a given temperature, water saturation occurs at a vapor density excess equal to the difference in the saturation vapor density over a plane water surface and the saturation vapor density over a plane ice surface at that temperature. In this case, the vapor density excess for which water saturation occurs as a function of temperature is given by Fig. 3.1. This curve corresponds to the maximum vapor density excess as in Fig. 4.16. The other definition assumes a conduction-diffusion equilibrium as in eq. (4.6) and Fig. 4.15. Thus, this definition takes into account the rise in temperature of the crystal surface due to the release of latent heat. This was the definition employed by Kobayashi in Fig. 2.5. This definition of water saturation corresponds to the "true" vapor density excess over a growing crystal in a static environment as in Fig. 4.16. Thus, the first definition specifies water saturation in terms of the ambient environment and the second definition specifies water saturation in terms of the environment with respect to a growing unventilated crystal. The first definition is used in this study.

Since changing the temperature of the ice crystal surface alone corresponds to changing the "true" vapor density excess over the crystal surface, any process which changes the crystal surface temperature will affect its growth rate. In particular, if heat is conducted away from the crystal surface, through the crystal itself and into the substrate, i.e., the glass fiber, or carried away by a ventilation velocity, the crystal will grow faster. Contrariwise, if sufficient heat is supplied to the crystal surface from the substrate or through radiation from

either an illumination lamp or the top plate of the chamber, the crystal will grow more slowly. Since they are very important, the relative magnitudes of heat transfer from the crystal surface by conduction to the substrate, conduction to the air, convection to the air, and radiation were calculated and are presented in Appendix D. Their relative magnitudes listed in decreasing order of importance were found to be; convection to the air, conduction to the air, conduction to the glass fiber and radiation.

The temperature of the glass fiber was measured by placing a 36 gauge copper-constantan thermocouple against it. When a ventilation velocity was introduced, the temperature at a given height of both the air and the glass fiber decreased by about  $0.2^{\circ}\text{C}$  in conformity with the results found earlier, i.e., Fig. 4.8. Even so, no detectable temperature difference, i.e., less than  $\pm .05^{\circ}\text{C}$ , was observed between the air and the glass fiber at the same height in the chamber regardless of whether or not the glass fiber was in contact with the bottom plate or whether or not a ventilation velocity existed. However, when the glass fiber was in contact with the bottom plate and the plate temperatures were given by one of the temperature pairs in Table I, small water droplets condensed, after a long period of time, on the glass fiber near the vertical center of the chamber even though freely floating water droplets were not observed. This suggested that possibly the glass fiber was slightly colder, i.e., less than  $.05^{\circ}\text{C}$  colder, than the ambient air at a given height. When the glass fiber was replaced with a copper wire of comparable diameter and one end of the copper wire was terminated one centimeter above the bottom plate but the other end extended through the top plate into the room air, the temperature



of the copper wire at a given height was tenths of a degree Celsius warmer than the ambient air at that height. This temperature difference decreased in magnitude when a ventilation velocity was introduced. When good thermal contact was made between the copper wire and the bottom plate, that is, the copper wire was bent so 1.25 cm of copper wire lay along the bottom plate, no detectable temperature difference existed between the air and the copper wire at the same height in the chamber either with or without the presence of a ventilation velocity. These results can be explained in terms of the difference in thermal conductivity between copper and glass; the thermal conductivity of copper being nearly 500 times that of glass. Therefore, when ice crystal growth took place from a glass fiber along a horizontal isotherm, that is at an angle of  $90^0$  to the vertical fiber, an insignificant amount of heat, for all but short crystals at very low ambient supersaturations, was conducted from the crystal surface to the fiber. However, when growth took place at an angle from the horizontal, the crystal traversed a temperature gradient and a small amount of heat was conducted along the crystal. If the crystal angled upward, toward the top plate, the base of the crystal was colder than the crystal tip and heat was conducted away from the crystal tip to the glass fiber enhancing the crystal growth rate. On the other hand, if the crystal angled downward, toward the bottom plate, the base of the crystal was warmer than the ambient air at the crystal tip but, due to the release of latent heat, not necessarily warmer than the crystal tip. In this case, heat conduction along the crystal was less than for the case when the crystal angled upward but its direction was vague.

The proximity of the ice crystals to one another on the glass

fiber sometimes resulted in an overlap of their individual vapor fields and a consequent reduction in their growth rates. This competition between the growing crystals for the available water vapor was most pronounced in a static environment at low ambient supersaturation. In this case, the vapor density field surrounding a crystal may extend several crystal diameters from the crystal. However, at high ambient supersaturations the vapor fields typically extended one or two crystal diameters from the crystal and even this distance was reduced when a ventilation velocity was employed.

The observed consequence of the superposition of these effects was that when two crystals with different base heights, the lower crystal growing upward and the higher crystal growing downward, approached one another, under conditions of low ambient supersaturation, the lower crystal with the colder base temperature grew at the expense of the upper crystal.

Since certain organic vapors affect normal ice crystal habits, every precaution was taken in this study to exclude from the system possible sources of such foreign vapors. As an added precaution, a contamination check was made of both the laboratory air and the air from the working section of the dynamic chamber. This was accomplished by using a Dyna-Vac diaphragm pump to draw an air sample through a cold trap comprised of a special glass tube immersed in solid  $\text{CO}_2$  (dry ice). The cold trap effectively condensed from the air the water vapor and any other gases present having a condensation temperature warmer than  $-78.5^\circ\text{C}$ , the sublimation temperature of solid  $\text{CO}_2$ . The resulting solid sample from the cold trap was melted, well mixed and then injected into a Varian Aerograph model 1740 gas-liquid chromatograph. The chromatograph column

used was a Porapak Q, 7' long by 1/8" O.D. stainless steel column with a 150/200 mesh. The carrier gas was nitrogen and a flame ionization detector was utilized. With this system the detectable limit was about one part unknown per million parts of the water sample. However, knowing the mixing ratio of the sampled air enabled this figure to be expressed in terms of the air sample, giving a detectable limit of about ten parts per billion of the unknown to the air sample. Using this contamination check system only one foreign vapor was detected in either the laboratory or the dynamic chamber air. The one detectable vapor was identified as isopropyl alcohol, the coolant of the two circulators. However, even this vapor only had a concentration between 0.02 and 0.2 parts per million (ppm) in the air and the concentration was the same in both the laboratory and dynamic chamber air samples. Therefore, possible effects of foreign vapors on the ice crystal growth rates were dismissed in this study.

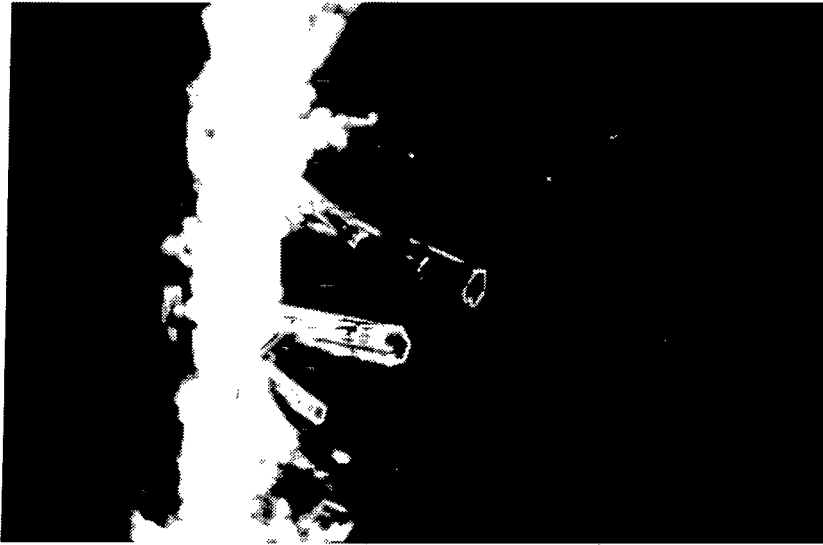
The normal procedure which was followed in operating the dynamic thermal diffusion chamber is given below. For each initial operation of the chamber, following a period of non-use, 30 liters of distilled water was placed in the moisture conditioner and frozen. Either an ice or water surface was employed on the chamber top plate depending on the range of ambient temperature and supersaturation desired. The top plate was secured in place with a gasket and screws. With both the top and bottom plate temperatures near  $-10^{\circ}\text{C}$  the air velocity was measured with the hot-wire anemometer as a function of the motor setting in microamperes. If the ice on the top plate was then replenished once or twice a week, depending on how rapidly it sublimated away, the chamber could be operated continuously for a period of two to three weeks without

a change in the velocity calibration. For day to day operation the chamber was made an open circuit by disassembling it at point F in Fig. 4.3 and raising the motors and circulation fan. Using the 2.5 m long scraper stick and employing the high speed Bodine motor, ice crystals growing on the bottom plate were removed from the chamber. The end of the chamber was re-assembled making it a closed system and the top and bottom plates were set at the desired temperatures. When temperature equilibrium was achieved for both plates, a vertical temperature profile was taken. For ambient supersaturations greater than water saturation the air was then passed through the nuclei filter for a period of from 30 minutes to 1 hour to insure that all the CCN were removed. If, following the filtration process, no droplets could be detected in the working section, a clean glass fiber was inserted into the chamber and the servo motor was set for the desired ventilation velocity. If droplets were detected, an air leak was indicated and steps were taken to eliminate it. Following the nucleation of ice crystals on the glass fiber, the fiber was rotated so the crystals to be observed and photographed grew directly into the airstream. A thermocouple, introduced through a small hole in the sidewall plug just opposite the growing crystals and sealed with Apiezon compound, could be retracted during the run so the thermocouple bead was flush with the chamber inner sidewall, thus preventing the growth of ice crystals on its tip, or it could be extended to measure the temperature near the ice crystals growing from the glass fiber. Hence, accurate ambient temperature measurements were obtained during the period of crystal growth.

Observations of the growing ice crystals were made using an M7-Wild Heerbrugg zoom stereo microscope. This microscope had a binocular

tube for viewing and a monocular tube for photomicroscopy. With the available choice of objectives: 1X or 0.5X, and eye pieces; 10X micrometer, 10X, 15X and 25X, this viewing system gave a wide range of magnification varying from about 3X to 80X. Ice crystal growth, as viewed through the stereo microscope, was recorded on film with either a 35 mm Pentax camera or a 16 mm Beaulieu cine-camera which was adapted to take time lapse photographs over the range one frame per fifteen minutes to 64 frames per second. This range was more than adequate for all the crystals grown. Both the time interval between successive frames and its variability were determined by taking time lapse photographs of a stop watch. Even at the lowest time lapse rate the variability of the time interval between successive frames was negligible.

In general, background lighting alone, supplied by an American Optical microscope lamp positioned on the opposite side of the chamber from the microscope, was used. The heat filtered background lighting was made uniform by passing it through a 1/8" thick frosted glass. This lighting arrangement eliminated possible radiational heating of the ice crystals due to the microscope lamp. When colored filters were placed between the frosted glass and the ice crystals and the ice crystals were illuminated directly with low intensity heat filtered light, spectacular photographs of the ice crystals against a colored background were obtained, as in Figs. 4.17 and 4.18. Simply changing the filter allowed any background color desired.



500  $\mu\text{m}$

Fig. 4.17 Ice crystal columns growing against a blue background.



Fig. 4.18 Ice crystal dendrites growing against a red background.

## V.

## RESULTS AND CONCLUSIONS

A. Crystal Growth in a Droplet Free Environment

Both the shape and the linear growth rate of ice crystals grown in the dynamic thermal diffusion chamber were found to be marked functions of the forced ventilation velocity. This was particularly evident for growth under ambient conditions such that the introduction of a forced ventilation velocity resulted in a supersaturation dependent secondary habit transition, i.e., plate→dendrite or column→needle.

Predominant Growth Along the 'a'-Axis

Figure 5.1 illustrates the difference in the shape of a crystal when grown along the 'a'-axis with and without a ventilation velocity. In both cases the crystal, indicated with the arrow, grew under ambient conditions of temperature near  $-15^{\circ}\text{C}$  and at an ambient supersaturation near 22.5% with respect to a plane ice surface. Photograph 5.1 (a) shows the shape and length of the various crystals 9.0 minutes after the glass fiber was inserted into the chamber. During this time a ventilation velocity,  $\vec{v}$ , flowed from left to right with a constant magnitude of  $3.0 \text{ cm s}^{-1}$ . The velocity was decreased from  $3.0 \text{ cm s}^{-1}$  to zero as shown in Fig. 5.1 (b) at time  $t = 21.0$  minutes after the fiber was inserted. Figure 5.1 (c) shows the shape which the crystals assumed in the absence of a velocity. The plates grew at a slightly warmer temperature and lower supersaturation than that encountered by the spear-like, dendrite crystal. The ventilation velocity was increased from 0 to  $7.0 \text{ cm s}^{-1}$  at time  $t = 53.0$  minutes, and 6.0 minutes later the crystals had resumed a dendritic shape as illustrated in Fig. 5.1 (d).

Glass fiber inserted at  $t = 0$  minutes with  $v = 3.0 \text{ cm s}^{-1}$

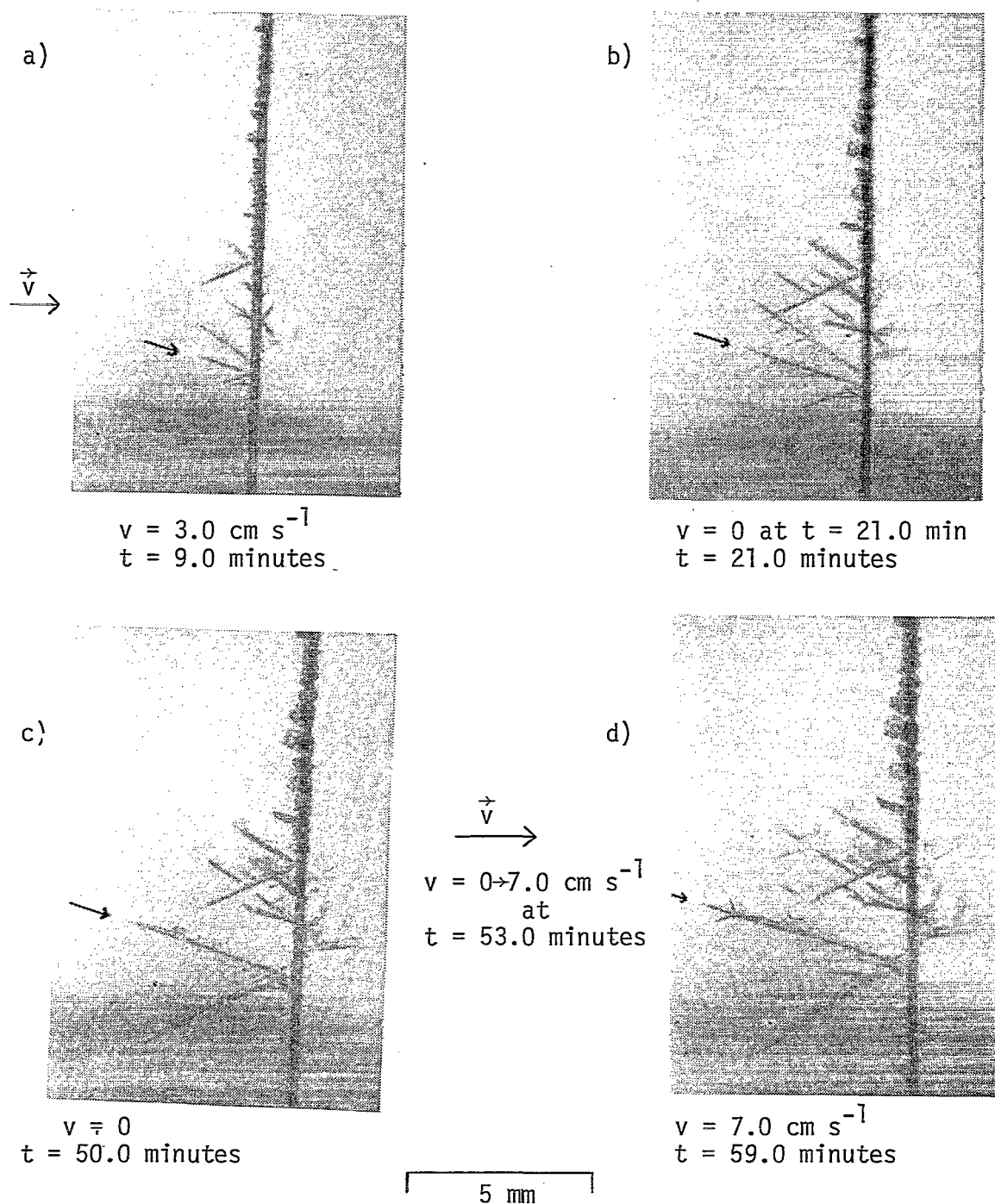


Fig. 5.1 A forced ventilation velocity enhances ice crystal growth into the airstream. ( $T_t = -4.5^\circ\text{C}$ ;  $T_b = -20.2^\circ\text{C}$ ).



These photographs show that a ventilation velocity enhances ice crystal growth into the airstream.

The length of the crystal, indicated with the arrow in Fig. 5.1, is plotted as a function of time in Fig. 5.2 for the successive ventilation velocities of 3.0, 0, and 7.0  $\text{cm s}^{-1}$ . For a given velocity, the crystal length along the 'a'-axis as a function of time can be represented with a straight line, whose slope gives the linear growth rate of the crystal. The linear 'a'-axis growth rate for this set of ambient temperature and supersaturation conditions was 2.2  $\mu\text{m s}^{-1}$  for a ventilation velocity of 3.0  $\text{cm s}^{-1}$ ; 0.72  $\mu\text{m s}^{-1}$  for the static case; and 2.8  $\mu\text{m s}^{-1}$  for a ventilation velocity of 7.0  $\text{cm s}^{-1}$ .

The supersaturation dependent secondary habit transition dendrite-dorite occurred when the ventilation velocity was reduced from 7.0 to 0  $\text{cm s}^{-1}$  at an ambient temperature near  $-14^{\circ}\text{C}$  and an ambient supersaturation of 25% with respect to ice, i.e., a vapor density excess equal to 0.39  $\text{g m}^{-3}$ . An example of this transition is given in Fig. 5.3 (a), (b), (c), and (d). Also note from Fig. 5.3 (e) that the crystal resumed a dendritic structure when the ventilation velocity was returned to its original magnitude, i.e., 7.0  $\text{cm s}^{-1}$ . Notice from these photographs that both the crystal shape and the linear growth rate were functions of the conditions of ambient temperature, ambient supersaturation, and forced ventilation velocity under which growth occurred. Secondary branches of dendrites, even though growing under the same ambient temperature conditions as a primary branch often grew broader or more plate-like because they "saw" a lower local supersaturation due to competition with other branches. This competition effect, however, was minimized when a forced ventilation velocity was applied.

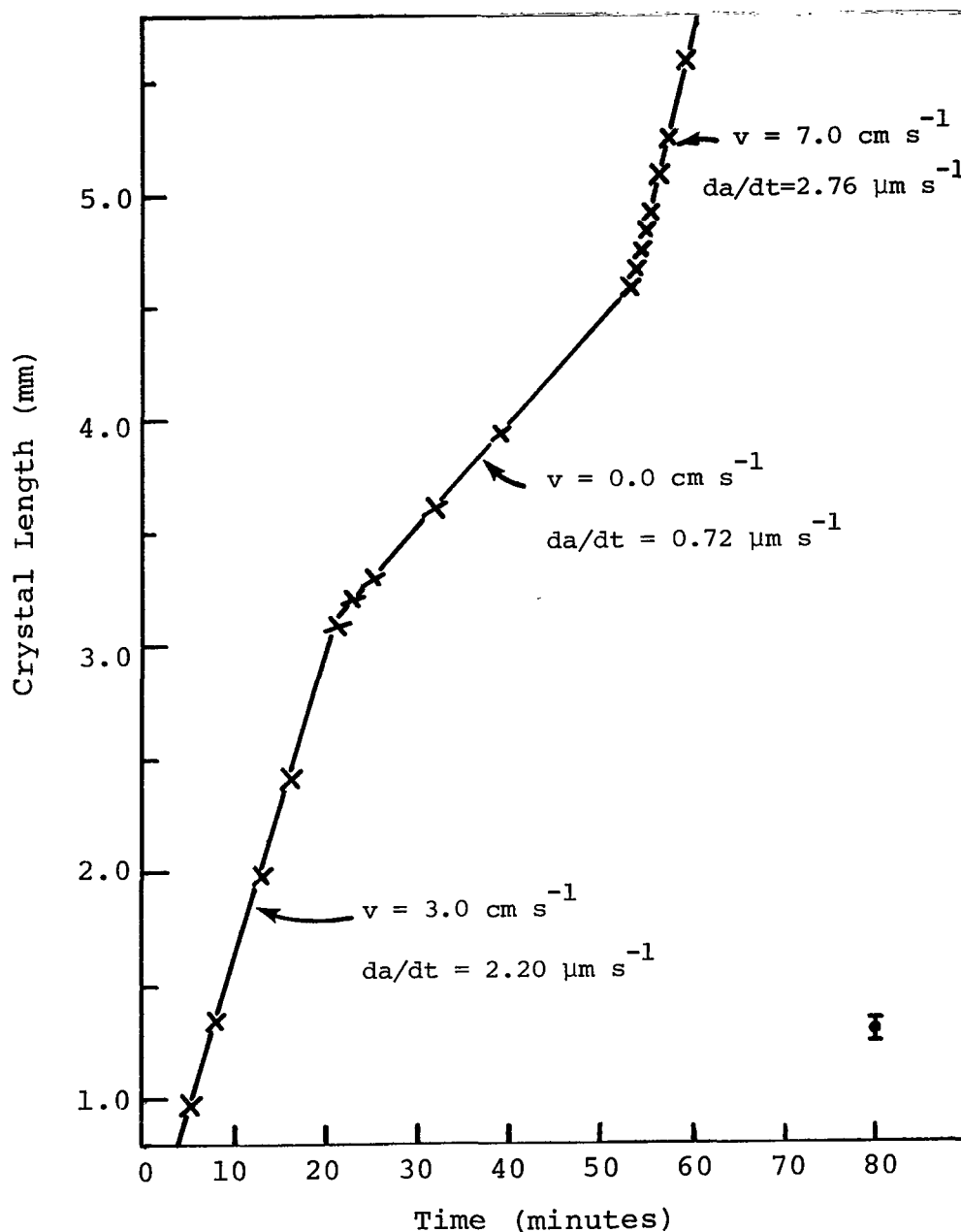


Fig. 5.2 Ice crystal length as a function of time for successive ventilation velocities of 3.0, 0 and 7.0 cm s<sup>-1</sup>, under constant ambient conditions of temperature, -15.8°C, and vapor density excess, 0.279 g m<sup>-3</sup>, at the height of the crystal base, 0.70 cm above the bottom plate. Angle of crystal from horizontal was +18°. ( $T_t = -4.5^\circ$ ;  $T_b = -20.2^\circ$ ).

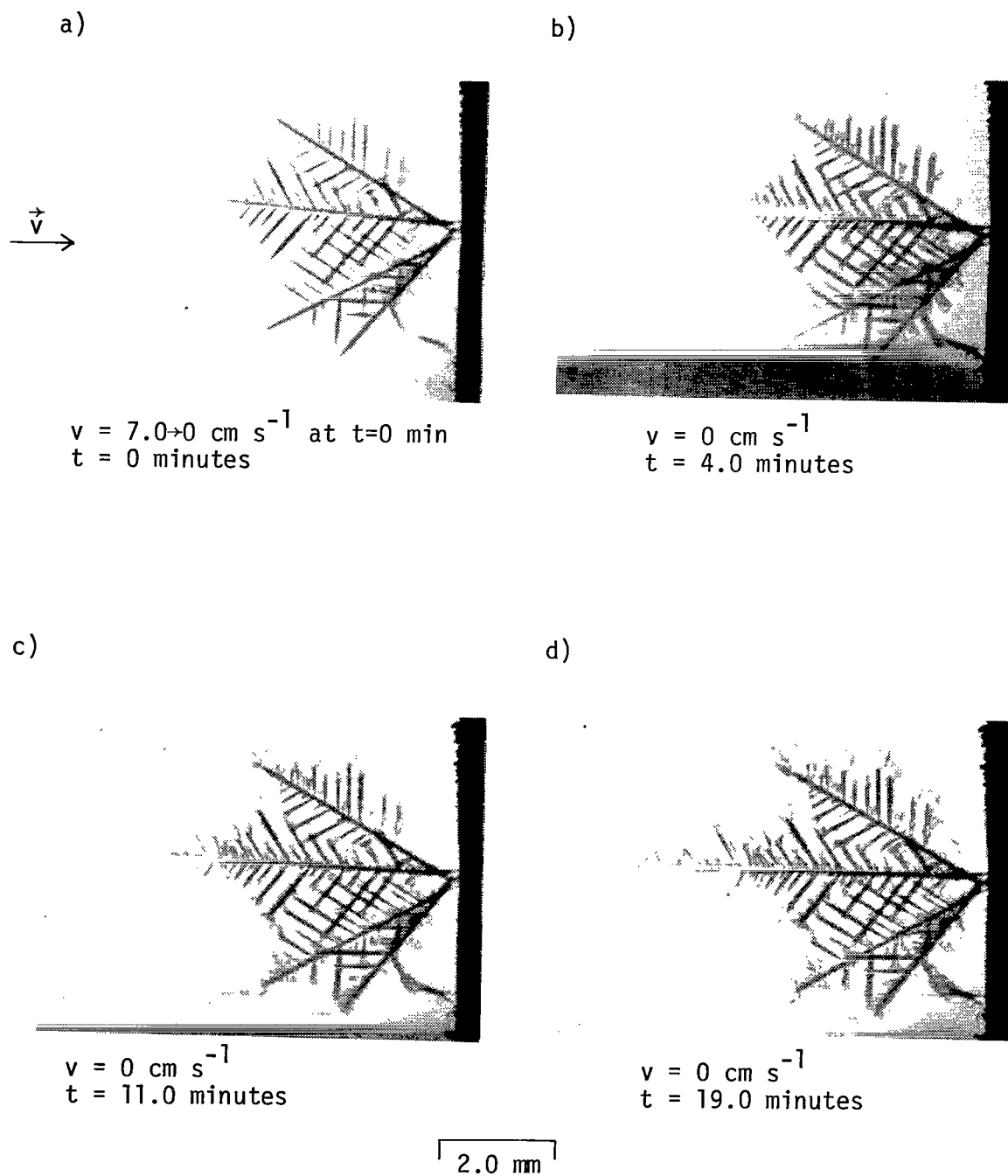
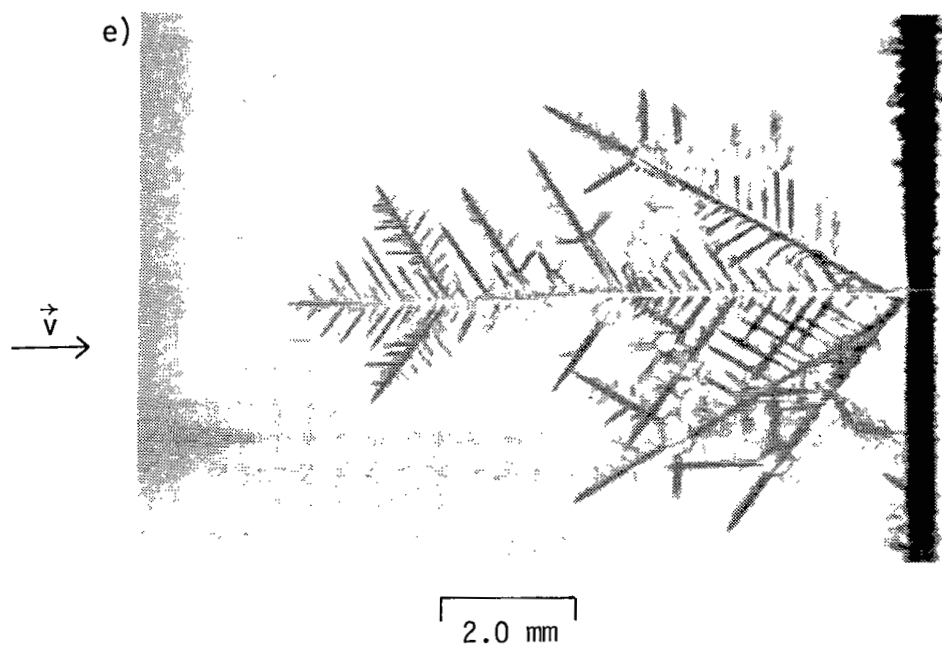


Fig. 5.3 A forced ventilation velocity affects both ice crystal shape and linear growth rate.

$v = 0 \rightarrow 7.0 \text{ cm s}^{-1}$  at  $t = 20.0$  minutes



$v = 7.0 \text{ cm s}^{-1}$

$t = 31.0$  minutes

Fig. 5.3 (Continued). A forced ventilation velocity affects both ice crystal shape and linear growth rate.

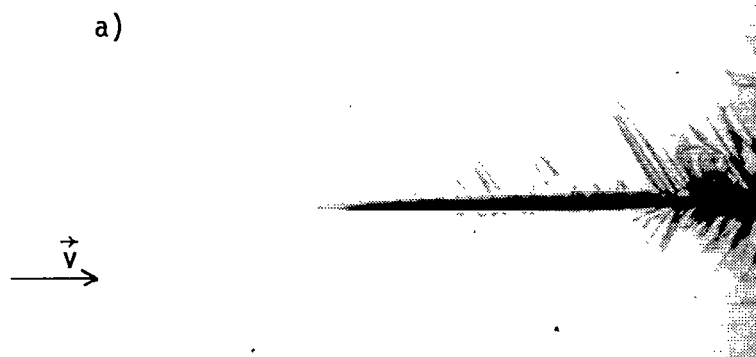
The task of separating the temperature and supersaturation effects at a fixed ventilation velocity was complicated by the fact that the crystals often nucleated and grew at an angle other than  $90^{\circ}$  to the glass fiber. At mid-chamber temperatures colder than or equal to about  $-10^{\circ}\text{C}$ , ice crystals nucleated on the solid glass fiber without external influence. At warmer temperatures nucleation was induced on the fiber by immersing it in liquid nitrogen before inserting it into the chamber. In both cases, it was found that employing a forced ventilation velocity immediately after the glass fiber was inserted into the chamber helped minimize the angle at which the dominant crystals grew from the horizontal, as well as inducing preferred growth in a direction parallel to the field of view and into the ventilation velocity. Once preferred growth occurred, further nucleation and growth of other crystals in the immediate neighborhood of a dominant crystal was suppressed due to competition for the available water vapor. Thus linear crystal growth rates were rarely assessed in this study if the crystal grew at an angle greater than  $\pm 20^{\circ}$  to the horizontal.

It was also important that the crystals grew parallel to the field of view of the microscope. If the crystals grew at an angle  $\phi$  from that field of view, then both the crystal length measurements and the subsequent linear crystal growth rates would be reduced by an amount  $(1 - \cos \phi)$ . For example, for an angle  $\phi = 20^{\circ}$  from this field of view the crystal growth rates would be reduced by as much as 6%. However, since at high magnification the depth of field of the stereo microscope was small, this could easily be detected and then corrected. That is, if at high magnification the crystal was partially out of focus, the glass fiber was rotated to ensure that the crystal grew

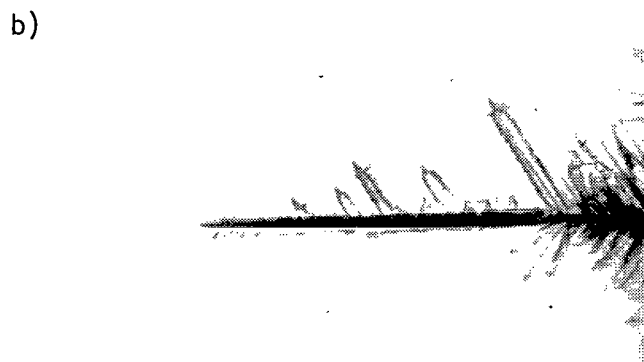
parallel to the field of view of the microscope and pointed directly into the ventilation velocity.

Fig. 5.3 illustrates a phenomena which was commonly observed during the growth of a dendrite under changing conditions of ventilation velocity. That is, when a velocity was removed, subsequent growth along the primary branch of the dendrite often assumed a slightly different orientation than before, as in Fig. 5.3 (d). However, when a velocity of the same magnitude as before was again employed, the primary branch of the dendrite resumed its former orientation, as in Fig. 5.3 (e). This may be explained in terms of the local vapor field surrounding the crystal being different in the two cases. The crystal in both cases attempted to grow along the maximum vapor field gradient. This is similar, although somewhat more pronounced due to the larger change in the local supersaturation induced by the introduction of a forced ventilation velocity, to an effect sometimes observed on the ribs of sector plates. That is, the ribs of sector plates also often grow curved in the direction of maximum water vapor. Frank (1974) termed this phenomena lacunary growth and Yamashita (1976) described it in more detail. In both the case of the dendrite and the sector plate, this curved growth is due to the fact that nucleation and growth occurs faster on one of the leading prism faces than it does on the adjacent one.

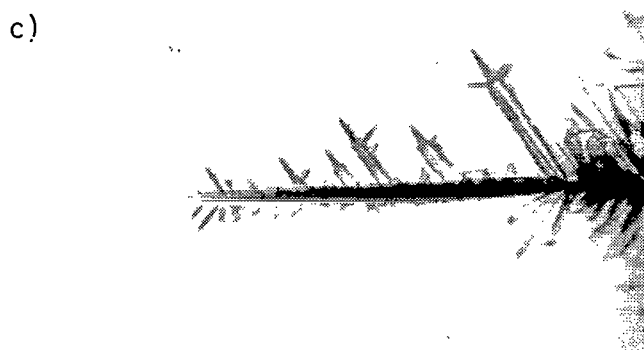
The photographs in Fig. 5.4 demonstrate how a ventilation velocity enhances growth along the leading edges of a crystal, resulting in this case in the transition *dorite*→*dendrite*. This set of photographs also shows in detail both the manner and time scale in which this transition proceeds. It fits into the time sequence of Fig. 5.3 between photographs



$v = 0 \rightarrow 7.0 \text{ cm s}^{-1}$  at  $t = 20.0 \text{ min}$   
 $t = 20.0 \text{ minutes}$



$v = 7.0 \text{ cm s}^{-1}$   
 $t = 21.0 \text{ minutes}$



$v = 7.0 \text{ cm s}^{-1}$   
 $t = 22.0 \text{ minutes}$

1.0 mm

Fig. 5.4 A forced ventilation velocity enhances the growth of a crystal particularly near its leading edges.

5.3 (d) and 5.3 (e).

The linear growth of the crystal portrayed in Figs. 5.3 and 5.4 is plotted in Fig. 5.5. Here, as in Fig. 5.2, the crystal length along the 'a'-axis as a function of time for a ventilation velocity of  $7.0 \text{ cm s}^{-1}$  is well represented by a straight line. However, for no forced ventilation velocity, that is, after the velocity was decreased from  $7.0 \text{ cm s}^{-1}$  to  $0 \text{ cm s}^{-1}$  at time  $t = 0$  minutes, the linear growth did not progress at a constant rate for about 6.0 minutes, i.e., until the doritic crystal tip had grown approximately 0.5 mm in length. The lower linear growth rate during this time period can be explained in terms of competition for the available water vapor between the primary doritic branch and the secondary branches. When the doritic branch had achieved a length of approximately 0.5 mm with no new branches this competition effect became much less significant and the doritic branch grew at a higher linear growth rate as indicated in Fig. 5.5.

An example of the supersaturation dependent transition dendrite→plate is shown in Fig. 5.6. Within 5.0 minutes after the velocity was reduced from  $7.0 \text{ cm s}^{-1}$  to  $0 \text{ cm s}^{-1}$  the growing dendrite tip had developed a rather substantial plate, as illustrated in Fig. 5.6 (d). This crystal later resumed a dendritic habit when a velocity of  $7.0 \text{ cm s}^{-1}$  was reintroduced. The linear growth response of this crystal to the removal of the ventilation velocity is given in Fig. 5.7. This graph shows that the linear growth rate did not immediately achieve a constant value upon removal of the forced ventilation velocity, but rather decreased with time, approaching a nearly constant rate after an elapsed time of 1.0 minute. Since the linear growth rate was higher for a period of 1.0 minute than the equilibrium rate under the imposed ambient growth



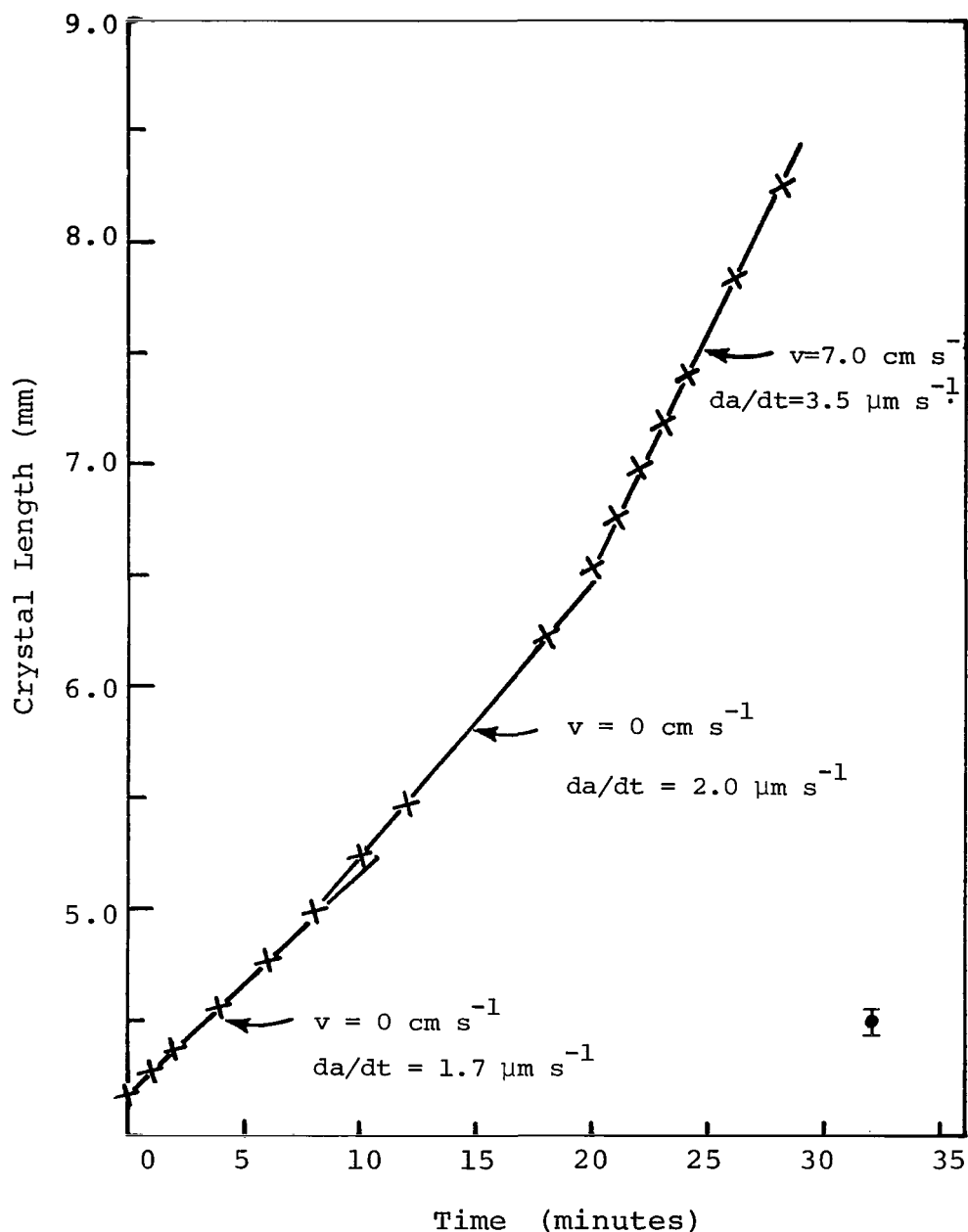


Fig. 5.5 Length of the crystal in Figs. 5.3 and 5.4 as a function of time for successive ventilation velocities of 0 and  $7.0 \text{ cm s}^{-1}$ , under constant ambient conditions of temperature,  $-13.9^\circ\text{C}$ , and vapor density excess,  $0.385 \text{ g m}^{-3}$ , at the height of the crystal base,  $0.78 \text{ cm}$  above the bottom plate. Angle of crystal from horizontal was  $+3^\circ$ . ( $T_t = -2.3^\circ\text{C}$ ;  $T_b = -19.1^\circ\text{C}$ ).

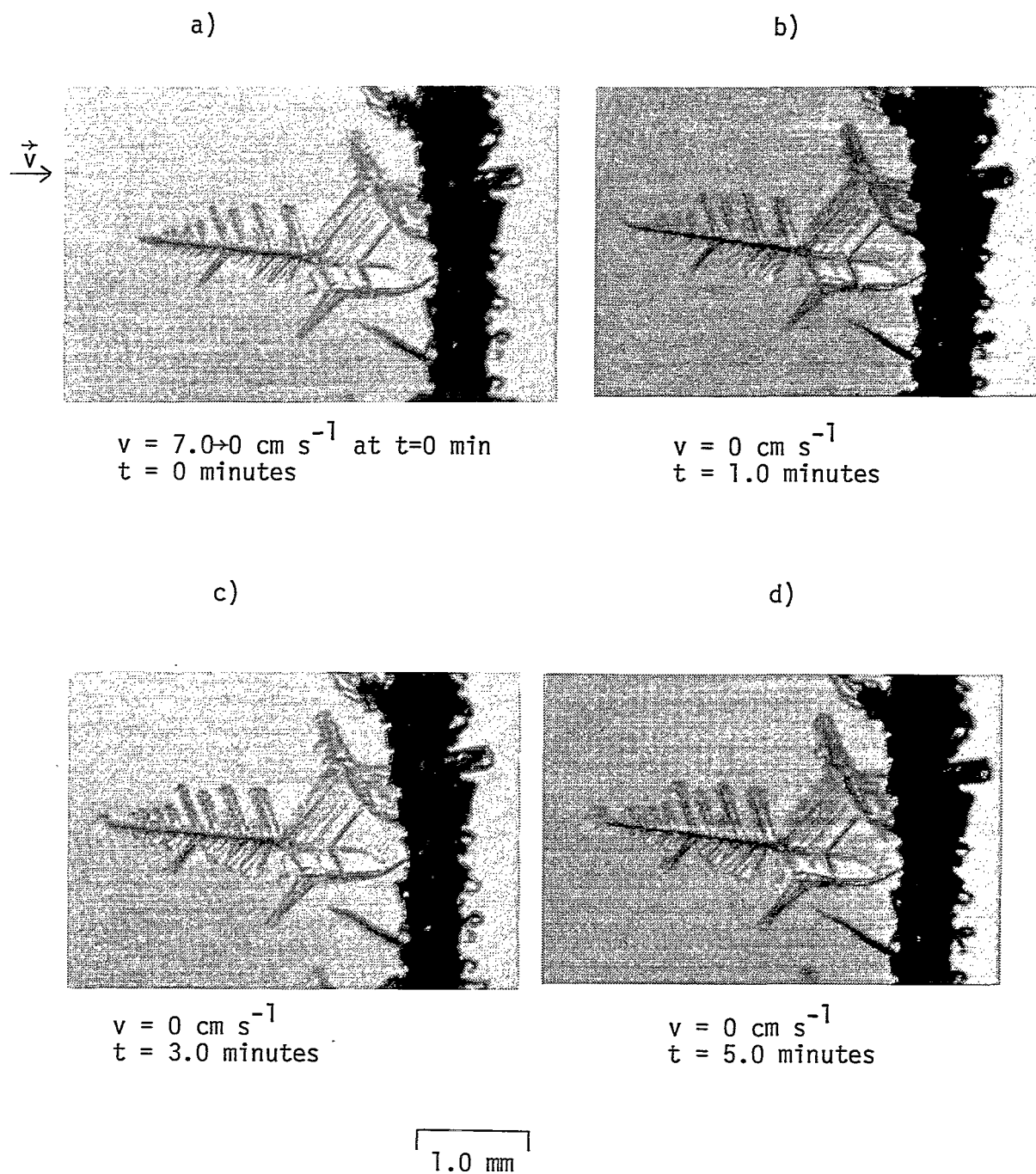


Fig. 5.6 The crystal shape and linear growth rate are functions of the ambient temperature, the ambient supersaturation and the forced ventilation velocity.

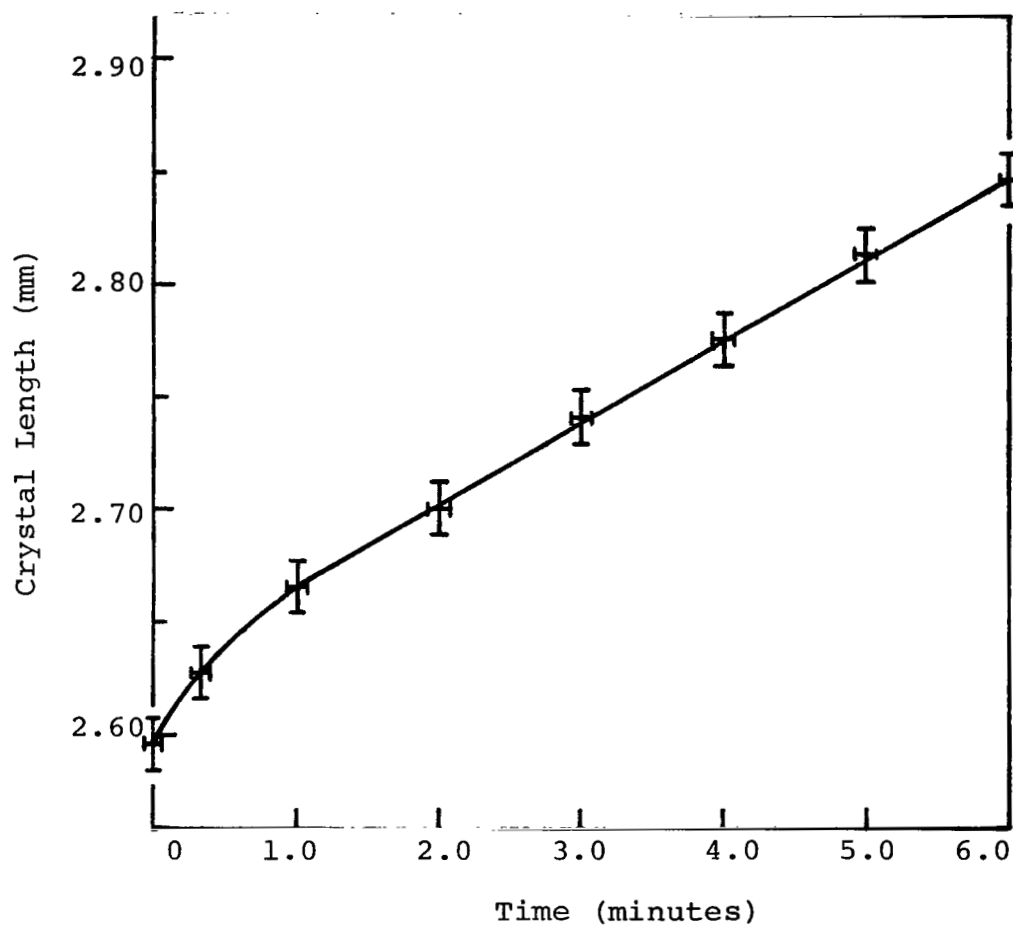


Fig. 5.7 The linear growth response of an ice crystal under ambient conditions of temperature,  $-13.7^{\circ}\text{C}$ , and vapor density excess,  $0.352\text{ g m}^{-3}$ , when the ventilation velocity,  $v$ , was suddenly decreased from  $v = 7.0$  to  $v = 0\text{ cm s}^{-1}$  at time  $t = 0$ . ( $T_t = -4.5^{\circ}\text{C}$ ;  $T_b = -20.2^{\circ}\text{C}$ ).

conditions, it can not be argued that there was a vapor competition effect. Furthermore, since the time required for the vapor field surrounding the crystal tip to come to equilibrium with the new growth conditions was approximately  $10^{-3}$  sec, an initial supply of water vapor near the crystal tip, in excess of the vapor demanded to sustain the new equilibrium linear growth rate of the crystal, can not explain this observation. Subsequent experiments revealed an explanation. For example, Fig. 5.8 illustrates the reverse transition plate→dorite brought about by increasing the forced ventilation velocity from 0 to  $5.0 \text{ cm s}^{-1}$  at time  $t = 0$  minutes. Figures 5.8 (b) and 5.8 (d) show this transition in detail and Fig. 5.8 (c) indicates the orientation of the crystal both to the glass fiber and to the ventilation velocity. This crystal grew at an angle of  $+30^{\circ}$  to the horizontal, somewhat larger than normally accepted. However, if the linear growth rates are used only over a small increment of length, for example 0.5 mm which is greater than necessary in the present case, then this crystal traverses a temperature gradient during this growth of less than  $0.2^{\circ}\text{C}$  and a moisture gradient of less than 0.3% supersaturation with respect to ice. In this case, when the ventilation velocity was increased from 0 to  $5.0 \text{ cm s}^{-1}$  at time  $t = 0$  minutes, it took over 2.0 minutes, as can be seen in Fig. 5.9, for the crystal to resume a constant linear growth rate.

The constant linear growth rate along the 'a'-axis for no forced ventilation velocity was  $0.4 \text{ } \mu\text{m s}^{-1}$  and for  $5.0 \text{ cm s}^{-1}$  was  $1.5 \text{ } \mu\text{m s}^{-1}$ . In Fig. 5.9, the linear growth rate increased with time in response to the introduction of a ventilation velocity at time  $t = 0$  minutes in much the same way that the linear growth rate decreased with time in

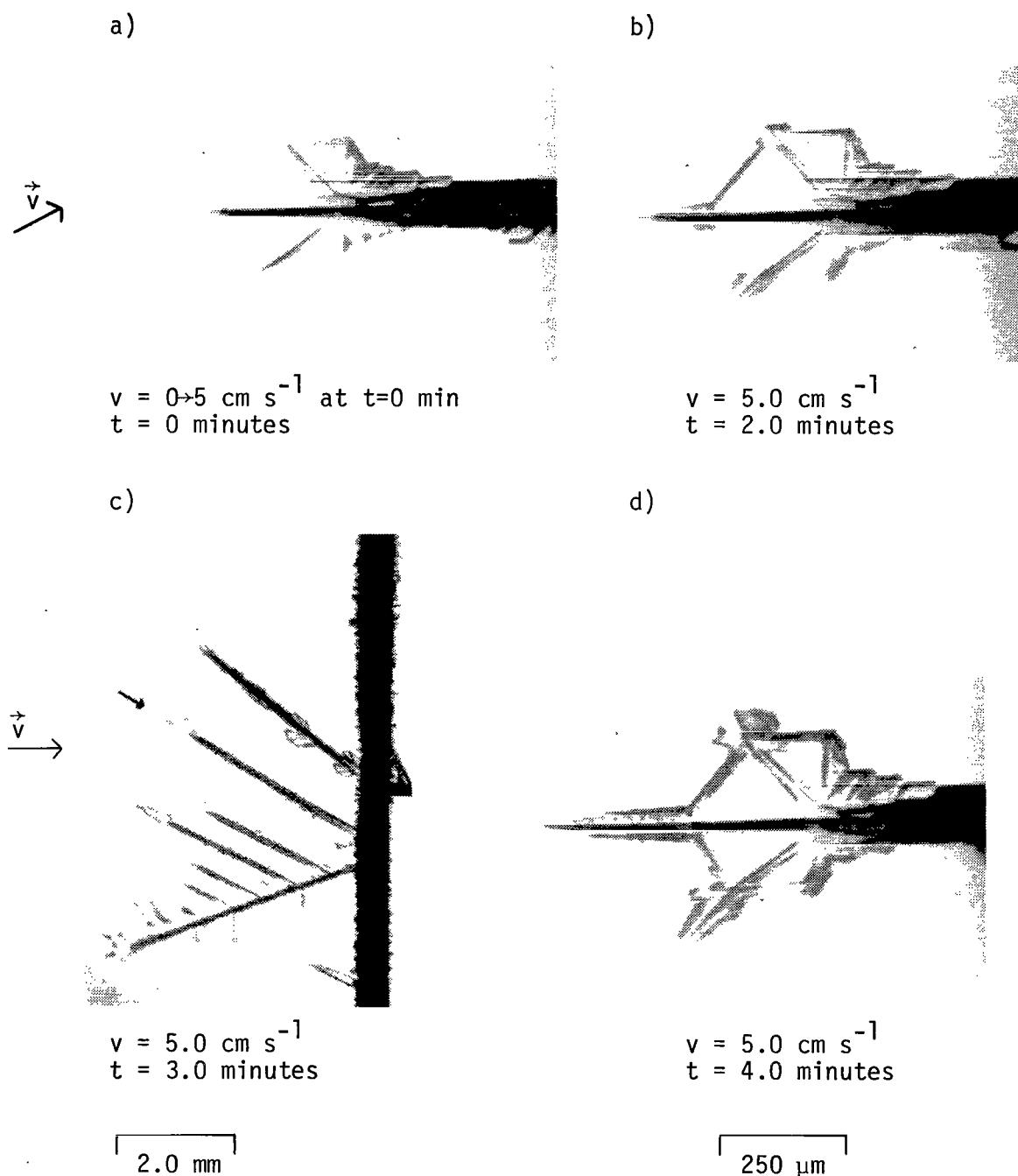


Fig. 5.8 The crystal shape and linear growth rate response to a change in the forced ventilation velocity is a function of the ambient temperature, the ambient supersaturation and the magnitude of the change in the forced ventilation velocity.

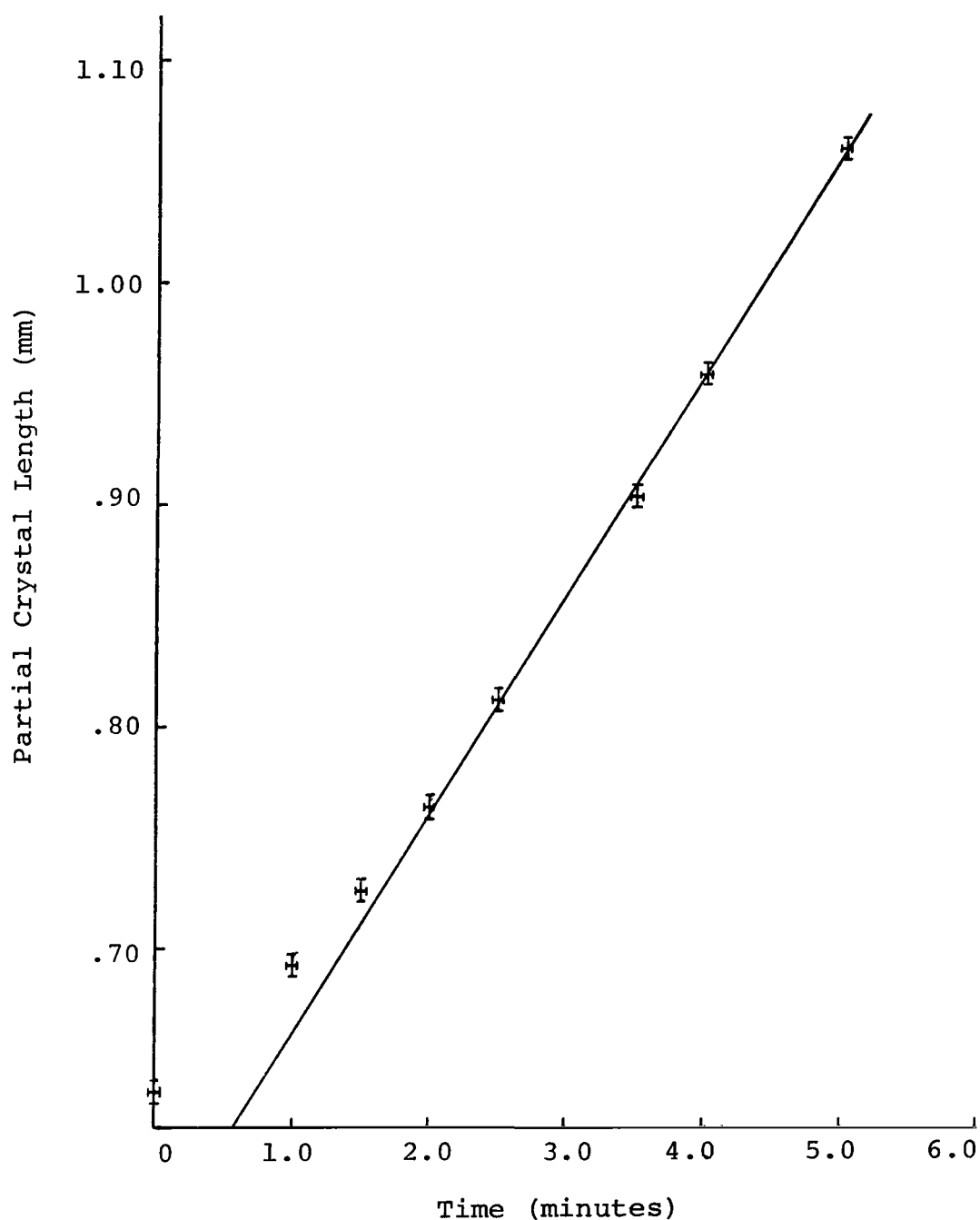


Fig. 5.9 The linear growth response of an ice crystal under ambient conditions of temperature,  $-14.0^{\circ}\text{C}$ , and vapor density excess,  $0.243\text{ g m}^{-3}$ , when the ventilation velocity was suddenly increased from  $v = 0$  to  $5.0\text{ cm s}^{-1}$  at time  $t = 0$ . ( $T_t = -7.8^{\circ}\text{C}$ ;  $T_b = -21.5^{\circ}\text{C}$ ).

Fig. 5.7 when the ventilation velocity was removed. Further experiments, documented with both 16 mm time lapse movies and 35 mm time lapse photographs, bore out this same symmetrical relationship and showed that the crystal shape and linear growth rate response to a change in the forced ventilation velocity is a function of the ambient temperature, the ambient supersaturation, and the magnitude of the change in the forced ventilation velocity. Near  $-14^{\circ}\text{C}$  the time constant for the transition of shape and growth velocity change was a maximum for the transition plate $\rightarrow$ dendrite. For the most extreme transitions of medium thick plates ( $\sim 200\text{ }\mu\text{m}$  thick) to dendrites or of dendrites to medium thick plates this time constant was on the order of one or two minutes. For the less extreme transitions of dendrite $\rightarrow$ dendrite or dendrite $\rightarrow$ dendrite the time constant was very small; typically, on the order of seconds.

One of the original objectives of this study was to determine, in as much detail as possible, the effect of a forced ventilation velocity on the linear growth rate, as well as on the shape of an ice crystal. Although the entire range of ambient temperatures from  $0^{\circ}\text{C}$  to  $-40^{\circ}\text{C}$  was investigated, the most detailed studies were conducted over the temperature range  $-14^{\circ}\text{C} \pm 3^{\circ}\text{C}$ . Over this range of temperatures, crystals were grown under ambient moisture conditions ranging from 4% to 50% supersaturation with respect to ice, i.e., at vapor density excesses ranging from  $0.07\text{ g m}^{-3}$  to  $0.70\text{ g m}^{-3}$ , and velocities ranging from  $0\text{ cm s}^{-1}$  to  $10\text{ cm s}^{-1}$ . Plots of crystal length versus time, such as Fig. 5.2, were made for each crystal. At least five crystal length measurements at each velocity were employed to obtain the linear crystal growth rate under that particular set of ambient growth conditions.

The time period of crystal growth at each velocity was maintained long enough to insure that the crystal achieved linear growth rate equilibrium. When this condition was purposely not met, the linear crystal growth rate at any given ventilation velocity was determined, in part, by the preceding velocity.

The compilation of the linear crystal growth rates over this range of ambient temperatures and ambient supersaturations was achieved for velocities of 0, 3.0, and 7.0  $\text{cm s}^{-1}$ . Figures 5.10, 5.11, and 5.12, which were drawn in an attempt to make use of this compilation of individual crystal growth measurements, are plots of the linear 'a'-axis growth rates versus ambient temperature along the abscissa and ambient vapor density excess along the ordinate for velocities of 0, 3.0, and 7.0  $\text{cm s}^{-1}$  respectively. Utilizing these individual crystal growth measurements, isopleths of linear 'a'-axis growth rates in  $\mu\text{m s}^{-1}$  have been drawn where possible. Error bars for both the ambient temperature and the ambient supersaturation include the effect of crystal growth occurring along vertical temperature and moisture gradients due to the fact that the crystals sometimes grew at an angle other than  $0^\circ$  from the horizontal. The fact that the error bars are longer at higher ambient vapor density excesses is indicative of the larger vertical gradients of both temperature and supersaturation necessary to produce these ambient moisture conditions.

The most obvious effect which can be deduced from these three figures of the forced ventilation velocity on ice crystal linear growth rates is that the introduction of a velocity reduces the ambient supersaturation necessary to sustain the same linear growth rate. This result is predicted by theory. In fact, as shown in Chapter III, theory



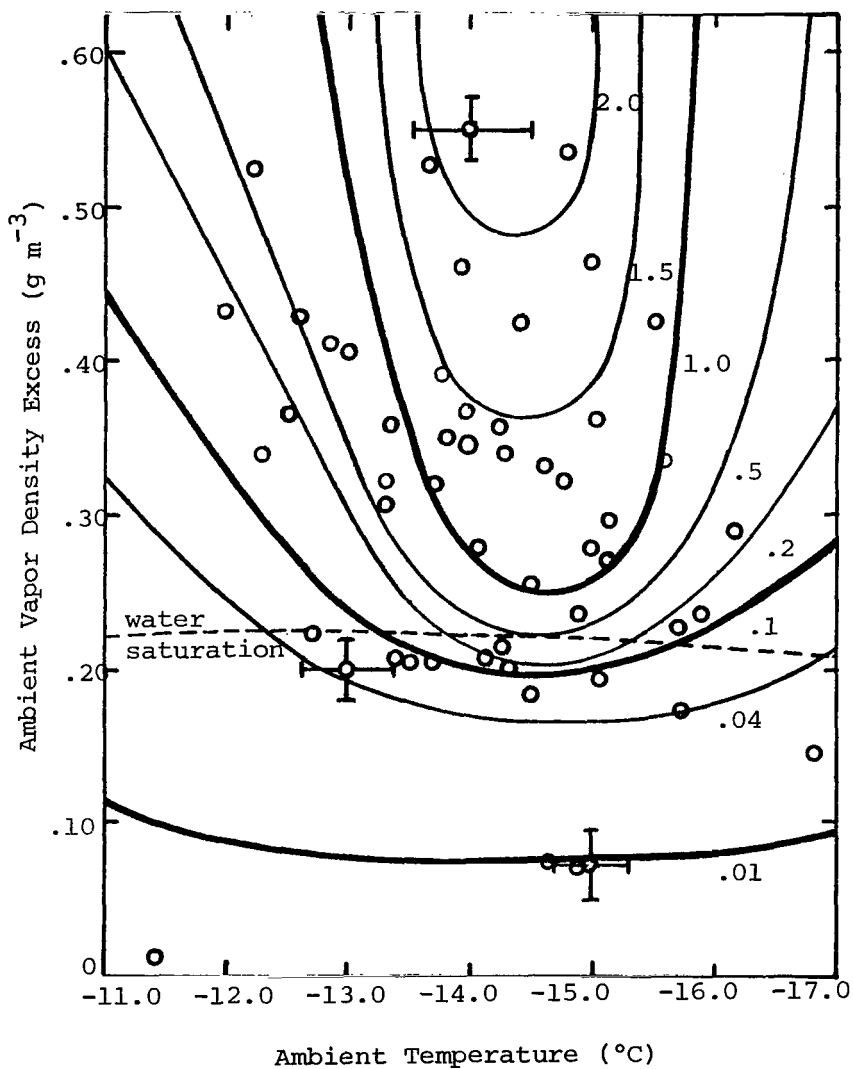


Fig. 5.10 Isopleths of linear 'a'-axis growth rates ( $\mu\text{m s}^{-1}$ ) for a ventilation velocity =  $0 \text{ cm s}^{-1}$ . Each circle denotes a set of individual crystal growth measurements.

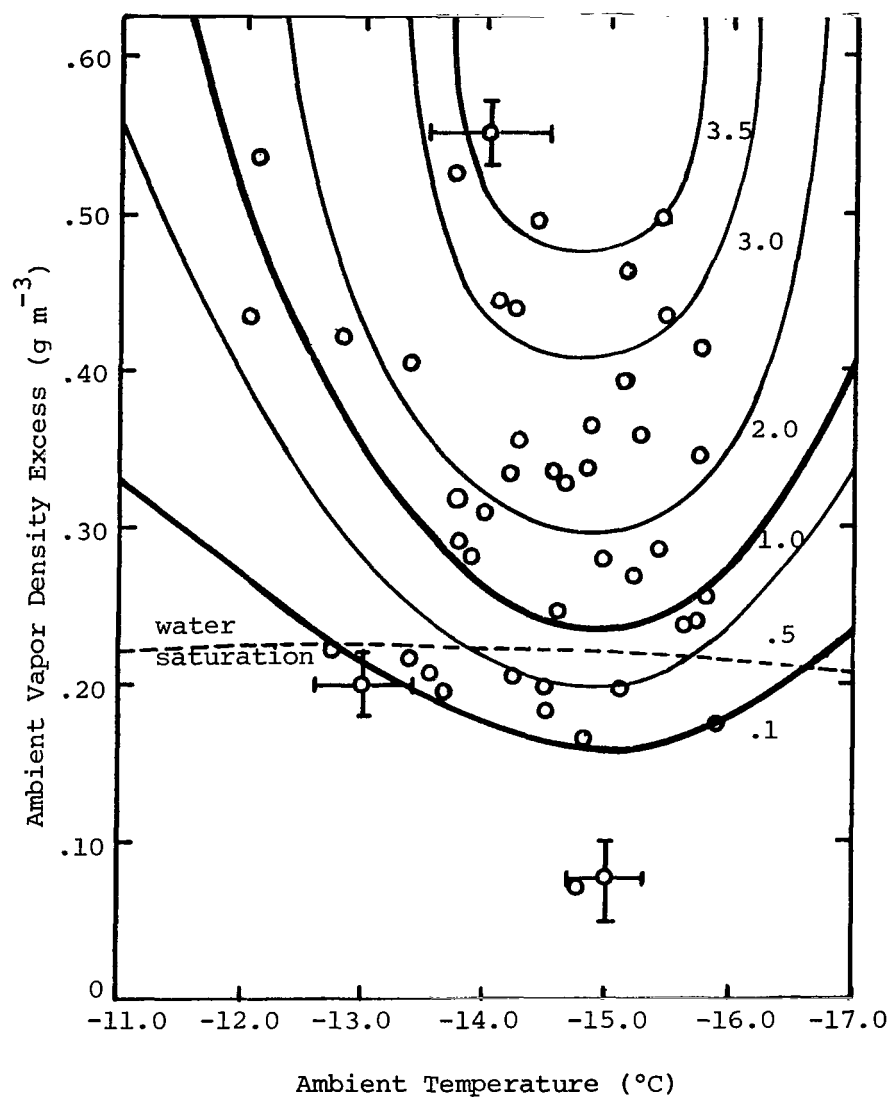


Fig. 5.11 Isopleths of linear 'a'-axis growth rates ( $\mu\text{m s}^{-1}$ ) for a ventilation velocity =  $3.0 \text{ cm s}^{-1}$ . Each circle denotes a set of individual crystal growth measurements.

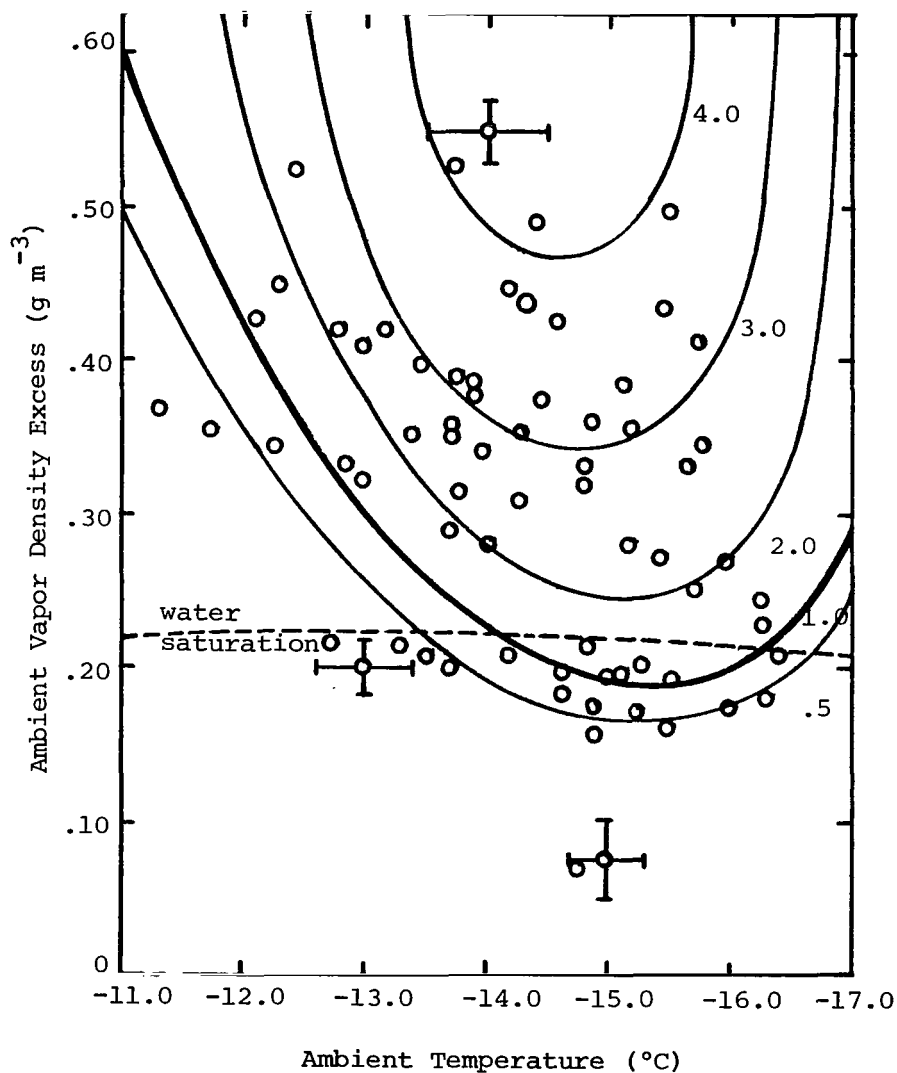


Fig. 5.12 Isopleths of linear 'a'-axis growth rates ( $\mu\text{m s}^{-1}$ ) for a ventilation velocity =  $7.0 \text{ cm s}^{-1}$ . Each circle denotes a set of individual crystal growth measurements.

predicts that the linear crystal growth rate for a given set of ambient temperature and supersaturation conditions is directly proportional to the square root of the forced ventilation velocity. On the other hand, theory does not predict that at higher ventilation velocities the maximum linear growth rate at a given ambient supersaturation occurs at successively colder temperatures. Although this result is not conclusive from these three figures, due to the relatively large error bars, it is interesting to compare this observation with the result of other experimenters. Although he did not address this point, the experimental results of Fukuta (1969), Fig. 3.6, indicate that the total mass of an ice crystal falling through a supercooled water cloud has a maximum near  $-15^{\circ}\text{C}$  at successively colder temperatures in direct proportion to the time after seeding. Of course, the longer the time after seeding, the larger the crystal and hence, the higher its terminal fall speed. If this observation is correct, it would explain why Fukuta, using ventilated freely falling crystals, observed the dual maxima in the mass growth rate versus temperature plot, Fig. 3.6, to occur at colder temperatures than found by Hallett (1965), Fig. 3.5, who obtained mass growth rates of crystals in a static environment. Further credence is given to this observation by the experimental results of Ryan, et. al., (1976), Fig. 3.7, even though they also did not address this point. They grew freely falling crystals in a supercooled water cloud and found that the maxima in the linear 'a'-axis growth rate, near  $-15^{\circ}\text{C}$ , occurred at an ambient temperature  $2^{\circ}\text{C}$  colder when the crystals were collected at times greater than 130 seconds after seeding than when they were collected at times less than 130 seconds after seeding.

If this result is real, as it appears to be, the explanation may be in terms of surface heating due to increased absolute mass growth rates when a ventilation velocity is introduced. Figure 5.13, which presents isopleths of forced ventilation velocity as a function of the ambient vapor density excess along the abscissa and linear 'a'-axis growth rate along the ordinate at an ambient temperature of  $-14.5^{\circ}\text{C}$ , was derived from Figs. 5.10, 5.11 and 5.12. This figure shows that the introduction of a ventilation velocity of only  $7.0 \text{ cm s}^{-1}$  at this ambient temperature is "roughly equivalent" to increasing the ambient vapor density excess in the static case by a considerable amount. In fact, for dendrites growing in a velocity field of only  $7.0 \text{ cm s}^{-1}$  this amount may be greater than  $0.3 \text{ g m}^{-3}$ . Conduction-diffusion equilibrium as discussed in Chapter IV shows that this would result in a crystal surface temperature rise of over  $1^{\circ}\text{C}$ . Larger ventilation velocities would correspond to even larger surface temperature rises. Thus, if a temperature dependent surface kinetic effect is responsible for the growth rate maxima near  $-15^{\circ}\text{C}$  in the static case, then since the introduction of a ventilation velocity may increase the absolute mass growth rate sufficiently to induce a rise in the surface temperature of the crystal, due to the increase in the release of latent heat, a colder ambient temperature is necessary for the surface kinetic effect to operate optimally at the same crystal surface temperature as in the static case.

It is interesting to note that reduced pressure, through an increase in the vapor diffusivity, also encourages the maximum mass growth rate to occur at colder temperatures, i.e., Fig. 3.4. Thus, freely falling ice crystals in high clouds, at low pressure, may have their

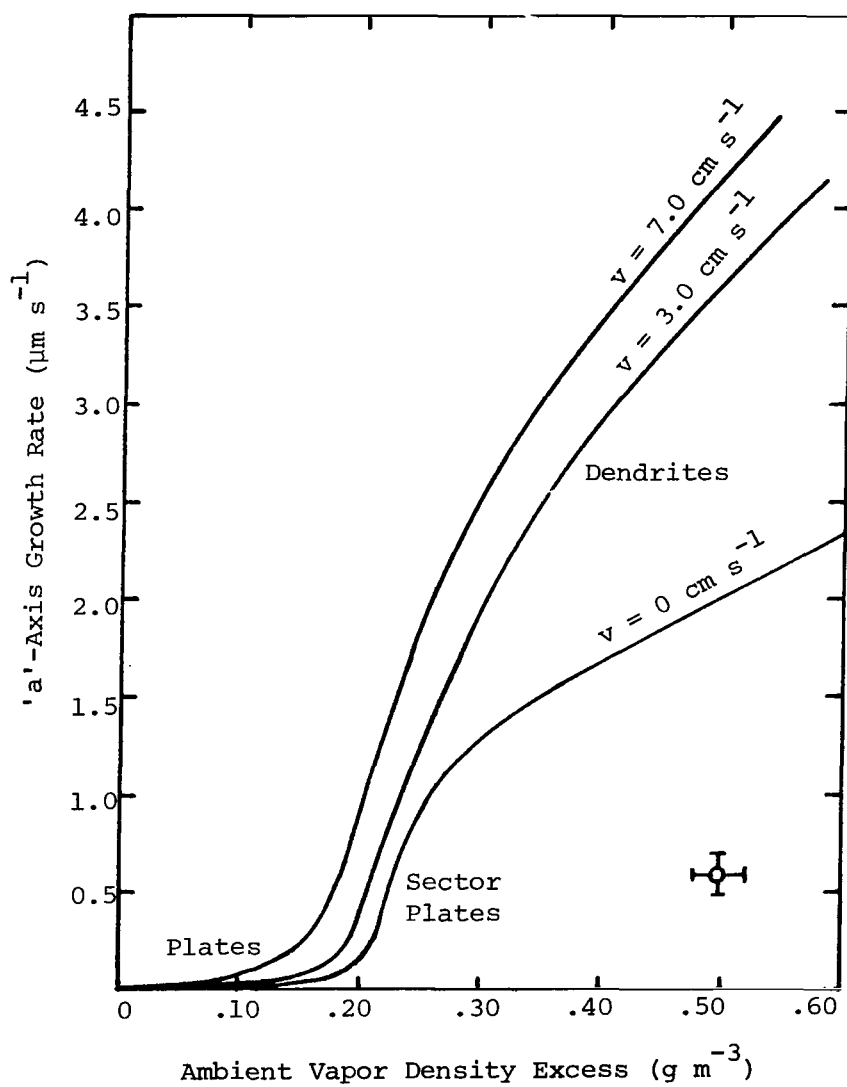


Fig. 5.13 Isopleths of forced ventilation velocity ( $\text{cm s}^{-1}$ ) for an ambient temperature =  $-14.5^\circ\text{C}$ .

growth rate maxima at an ambient temperature somewhat colder than  $-15^{\circ}\text{C}$ .

Figure 5.13 demonstrates quantitatively how the introduction of a forced ventilation velocity reduces the ambient supersaturation necessary to sustain the same linear growth rate. It illustrates the supersaturation regimes at this temperature in which plates, sector plates and dendrites occur. It shows how a small increase in local supersaturation, brought about either by an increase in the ambient supersaturation or by the introduction of a forced ventilation velocity, can have a dramatic effect on both the crystal shape and linear growth rate. For an ambient temperature of  $-14.5^{\circ}\text{C}$ , this effect is most pronounced at an ambient vapor density excess near  $0.20 \text{ g m}^{-3}$ , i.e., close to water saturation, where the transition plate→dendrite occurs.

Previous observations by Hallett (1965) indicated that in a static diffusion chamber, where crystals grew in an environment with the carrier gas velocity almost zero, the transition from ice crystal plates to dendrites took place somewhat above water saturation. However, observations of ice crystals in the atmosphere have indicated that this transition takes place at an ice supersaturation somewhat less than that equivalent to water saturation. Figures 5.10, 5.11, 5.12 and 5.13 show quantitatively how the transition plate→dendrite is a function of temperature, ambient supersaturation and carrier gas velocity. Furthermore, these figures demonstrate how it is possible to grow dendrites in the atmosphere at ice supersaturations less than that equivalent to water saturation. That is, the crystals fall at their terminal velocities, thus seeing a relative carrier gas velocity equal to their terminal fall speed which may typically be  $20 \text{ to } 30 \text{ cm s}^{-1}$ , i.e., Fig. 3.8. The effect of this relative carrier gas velocity is roughly

equivalent to increasing the ambient supersaturation.

Figure 5.14 shows the relationship of the linear 'a'-axis growth rate, at an ambient temperature of  $-14^{\circ}\text{C}$ , to the square root of the forced ventilation velocity. Each line is indicative of growth at one ambient supersaturation, expressed here in terms of the vapor density excess. In this figure (derived from Figs. 5.10, 5.11 and 5.12) the dashed lines are the extrapolation of the experimentally verified solid lines to higher forced ventilation velocities. Notice that the lines are quite straight where either plate growth or dendritic growth occurs, i.e., at either low or high ambient supersaturations. However, at intermediate supersaturations the crystal shape at this temperature changes significantly for small changes of either the supersaturation or the ventilation velocity. Thus, the linear 'a'-axis growth rate is directly proportional to the square root of the ventilation velocity, as theory predicts, if the crystal shape does not change significantly.

As shown in Chapter III, the present macroscopic theory of ice crystal growth rates is based on an electrostatic analogy, with the vapor density,  $\rho$ , being analogous to the electrostatic potential,  $v$ . A basic flaw of this theory, on the molecular scale, is that it assumes the crystal surface is at a constant potential or sees a uniform vapor density excess. In actuality, the vapor density excess is generally different from one crystal face to another on the same crystal, and a vapor density gradient often exists across an individual growing crystal face. In fact, analogous to the higher electric charge densities at the corners of a charged conductor, the crystal corners and edges generally have the highest local vapor density excess with lower local excess vapor densities near the center of a crystal face. In the



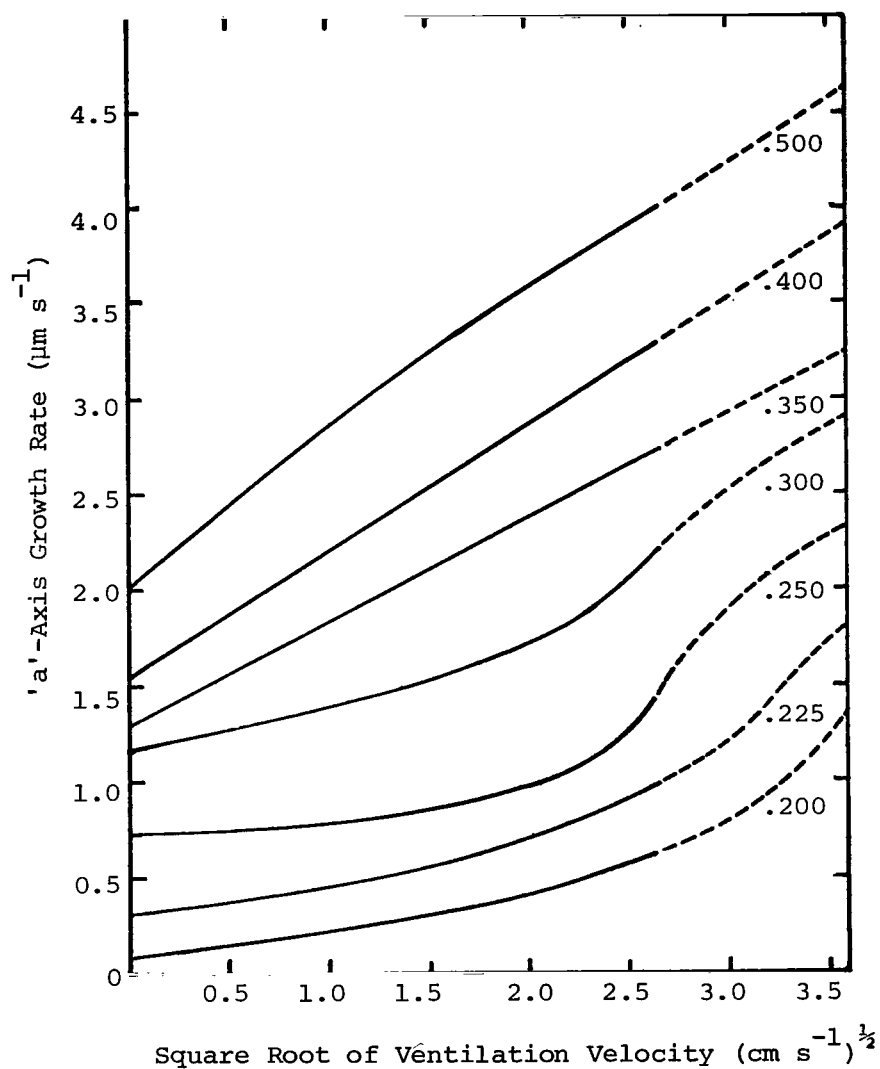


Fig. 5.14 Isopleths of ambient vapor density excess ( $\text{g m}^{-3}$ ) for an ambient temperature =  $-14\text{ }^{\circ}\text{C}$ .

case of two-dimensional nucleation and growth, steps on the crystal surface are nucleated at the crystal edge and propagate toward the center of that crystal face. As the steps propagate, the local vapor density field over the crystal surface must continually respond to the movement of these vapor sinks as illustrated in Fig. 5.15. In this figure the dashed lines denote isopleths of constant vapor density and the solid lines show the flow of the water molecules. Since the actual shape of the steps is not known, no attempt has been made in Fig. 5.15 to show their minutely exact effect on the vapor density field. Steps here are propagating from left to right. The impinging water molecules may be adsorbed between adjacent steps on the crystal surface and migrate short distances across the surface to a nearby step. As the steps move farther from the crystal edge toward the center of the crystal face the local vapor density excess decreases and the steps

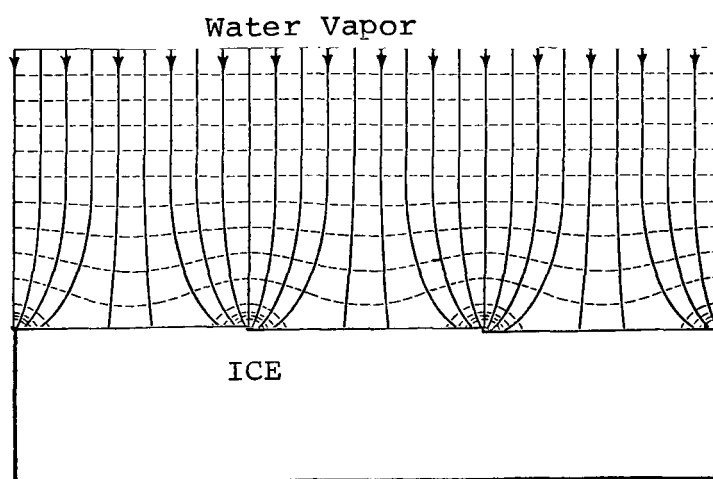


Fig. 5.15 The vapor field and flow of water molecules over a growing ice surface with steps propagating from left to right. Adapted from Scott (1977)

slow down. As the foremost advancing steps slow down, their collection

areas for surface diffused adsorbed molecules overlap and adjacent steps merge, further decreasing their advancement velocity. Both the rate at which the incoming water molecules can be incorporated into the crystal lattice at a given site and the velocity of propagation of the steps is a function of temperature and step height. These properties along with the magnitude of the flux of water molecules to a given site and hence the local vapor density excess are the basic controlling mechanisms for the linear crystal growth rates along both the 'a' and 'c' axes and hence of the crystal habit. By changing the relative magnitudes of these controlling mechanisms one can change the crystal habit. When a carrier gas velocity is introduced, the absolute and in most, if not all, cases even the relative magnitude of the flux of water molecules over various areas of a crystal face is increased. This is the result of vapor rich air flowing over the crystal surface and particularly enhancing the flux of water molecules to the crystal tip and leading edges. With the introduction of a ventilation velocity the "true" vapor density excess over the crystal lies between the curves in Fig. 4.16 and increases as the velocity increases. This results from the ventilation velocity contracting the ambient surfaces of constant vapor density and temperature as in Fig. 3.2 to very near the leading edge of the ice crystal. Diffusion of both water vapor to the growing crystal and heat from its surface then occurs through a boundary layer of approximate thickness

$$\delta \sim (\pi Dt)^{\frac{1}{2}},$$

as defined in Chapter III. Here D represents either the diffusivity of water vapor through air or the thermal diffusivity whichever is

appropriate for the boundary layer under consideration. For an ice crystal having a radius of curvature,  $r$ , at its leading tip, the diffusion boundary layer thickness there is a function of the velocity according to the relation

$$\delta \sim \left( \frac{\pi D r}{v} \right)^{1/2},$$

where  $D$  is the diffusivity of water vapor through air, and  $v$  is the magnitude of the velocity. For  $r = 10^{-2}$  cm,  $v = 10$  cm s<sup>-1</sup>, and  $D = 0.2$  cm<sup>2</sup> s<sup>-1</sup>,

$$\delta \sim 250 \text{ } \mu\text{m}.$$

Since the boundary layer thickness is inversely proportional to the square root of the ventilation velocity, it decreases with increasing velocity, thus allowing diffusion to occur more rapidly through the boundary layer. At high velocity this is equivalent to a nearly vertical mass transfer curve in Fig. 3.10. Following the introduction of a ventilation velocity the local vapor density field over the crystal surface is readjusted, almost immediately. However, increased local vapor density excesses at constant temperature imply increased nucleation rates and hence a greater number of steps. It is the propagation and redistribution of these steps on the crystal surface to new equilibrium values which leads to the observed time constants for the transition of crystal shape and growth velocity change when one or more of the ambient growth conditions, such as the forced ventilation velocity, is altered.

For example, the supersaturation dependent secondary habit transition plate→dendrite occurs near -14°C when a forced ventilation velocity

is introduced at a critical ambient supersaturation, because steps nucleated on the prism faces at the corners of the plate do not have time to propagate to the center of that face before a whole series of new steps are nucleated. Thus, if the steps nucleate at the corner of the prism face, preferential growth occurs at the corner of the plate leading to doric or dendritic growth. Figure 5.16 represents a situation in which the local vapor density excess and hence the nucleation rate of steps is higher at the corner  $BB'$  than at the other corners. For example, this could represent the case in which a ventilation

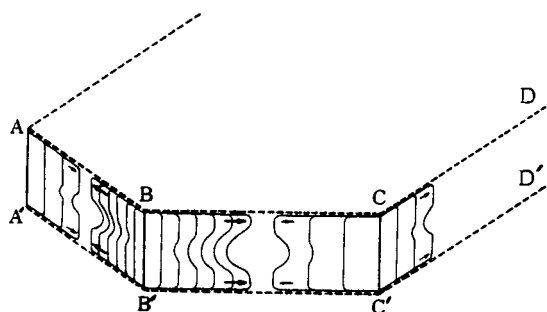


Fig. 5.16 A model of layer by layer growth on the prism faces.  
Adapted from Yamashita (1976)

velocity flows perpendicular to  $BB'$  and parallel to  $CD$ , i.e., the corner  $BB'$  grows into the wind. If the crystal continues to grow as a plate, even though the vapor density excess and hence the production rate of new layers is higher at the corner  $BB'$  than at the corners  $AA'$  or  $CC'$ , then the growth of the prism faces ( $ABB'A'$ ) and ( $BCC'B'$ ) is controlled by the layers which come from  $BB'$ . That is, the steps or layers nucleated at the corner  $BB'$  would in this case propagate beyond the center of the adjacent prism face, for example the prism face ( $BCC'B'$ ), and would merge with the steps or layers propagating

from the corner CC'. If, on the other hand, the crystal does not continue to grow as a plate but rather grows preferentially from one or more corners, at least two distinct possibilities exist. In the first case, nucleation of steps or layers at the corner BB' may occur at a slow enough rate such that the collection areas for surface diffused adsorbed molecules of these adjacent steps do not overlap until they have propagated some distance from the corner at which they were nucleated. In this case sector plates result. In the second case nucleation of steps or layers at the corner BB' may occur at a very high rate in which case the collection areas for surface diffused adsorbed molecules of adjacent steps overlap and the steps merge before they are able to propagate very far from the corner at which they nucleated. In this case dorites or dendrites result. It is important to realize that the vapor density excess and thus the nucleation rate of layers or steps at adjacent corners of the crystal may be quite different. Also it is important to understand that the vapor density excess controls the nucleation rate of the steps but the vapor density gradient controls the propagation of those steps. That is, if the vapor density gradient from a corner is large and negative and the nucleation rate is high, the steps repeatedly merge and hence travel a much shorter distance along the prism face than if the nucleation rate and the vapor density gradient were both much smaller. This was demonstrated by a crystal which grew as a dorite at one corner, where the vapor density excess was larger, but continued growing as a plate at the other corners. In a ventilation velocity field it is even possible for steps nucleated at a corner such as CC' in Fig. 5.16 to first move into a negative vapor density gradient just away from the corner CC' and slow down,

then move into a positive vapor density gradient and speed up as they propagate across the prism face (BCC'B') toward the corner BB'.

Depending on the ambient temperature and supersaturation, two-dimensional nucleation may occur on either the prism faces, the basal faces, or simultaneously on both. Figure 5.17 illustrates a dendrite viewed edge-on and shows that the base of the dendrite was thicker

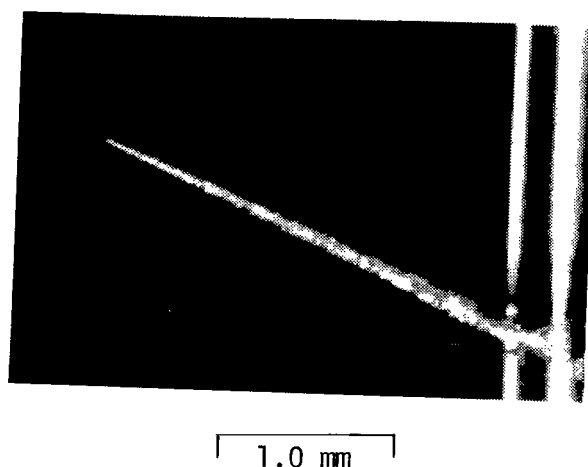


Fig. 5.17 A dendrite viewed edge-on shows the base is thicker than the tip.

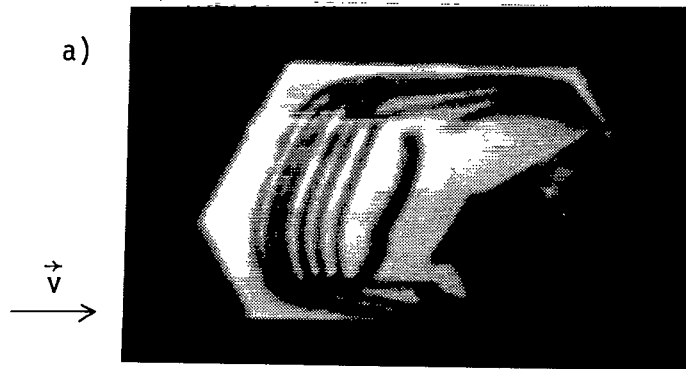
than the tip. When the forced ventilation velocity, or carrier gas velocity, was increased, the dendrite grew an even thinner crystal tip than before. On the other hand, when the velocity was removed, the linear crystal growth rate diminished and the crystal tip thickened to about the same thickness as away from the edge. These results were obtained despite the fact that the ambient supersaturation remained constant. This implies that any steps present on the basal face propagated from the crystal base toward the crystal tip. This must be true, because no matter how fast the tip might have grown relative to the

microscopic steps, if steps had nucleated on the basal face near the tip, the tip would have become thicker than the crystal base. When the ventilation velocity was turned off, the velocity of the thin steps propagating on the basal face from the crystal base to the crystal tip was faster than the linear growth rate of the thicker crystal tip. Hence, the thin steps reached the crystal tip sooner than before and produced a crystal of almost uniform thickness. The crystal base should always be a little thicker than the crystal tip at  $-14^{\circ}\text{C}$  unless all the steps were eliminated from the basal face and a 'step producer', i.e., the glass fiber, no longer existed near the crystal base. This implies that near  $-14^{\circ}\text{C}$  the prism faces are fairly good nucleation surfaces and the basal faces are very poor nucleation surfaces. In fact, near  $-14^{\circ}\text{C}$  two-dimensional nucleation probably occurs at the edge of the prism faces at ambient supersaturations, substantially below water saturation, but probably due to competition with the adjacent prism face, never occurs at the leading edge of the basal face, regardless of the ambient supersaturation.

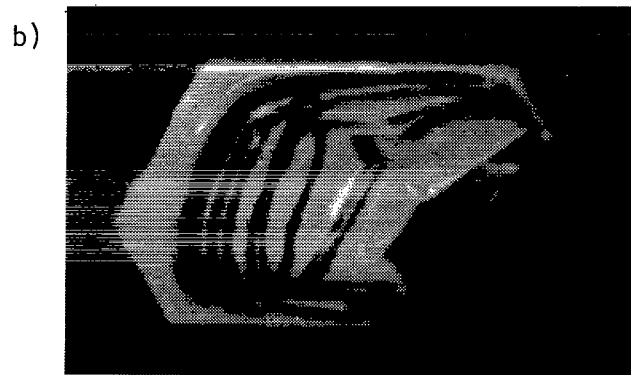
#### Predominant Growth Along the 'c'-Axis

Near  $-9^{\circ}\text{C}$  and a little above water saturation nucleation occurred at the edges of both the prism and basal faces but was slightly favored on the basal face. This resulted in the crystal habit being hollow columns, having a  $c/a$  ratio slightly greater than 1.0, with macroscopic stepped surfaces on both the basal and prism faces. Figure 5.18 illustrates macroscopic steps and their propagation on the basal face of such a crystal. These macroscopic steps were a few micrometers in height and propagated very slowly. In addition to nucleating and propagating steps or layers on the basal face and thus growing along

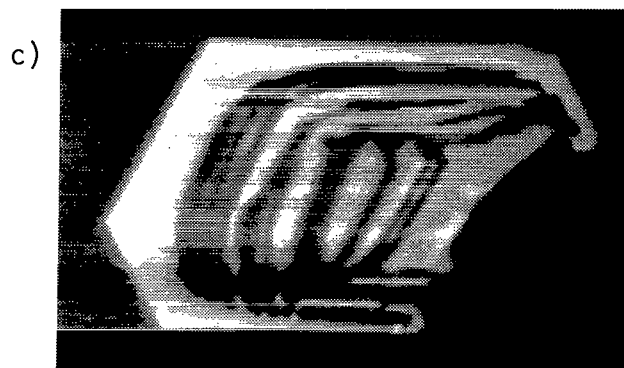




$v = 3.0 \text{ cm s}^{-1}$   
 $t = 0 \text{ minutes}$



$v = 3.0 \text{ cm s}^{-1}$   
 $t = 17.0 \text{ minutes}$



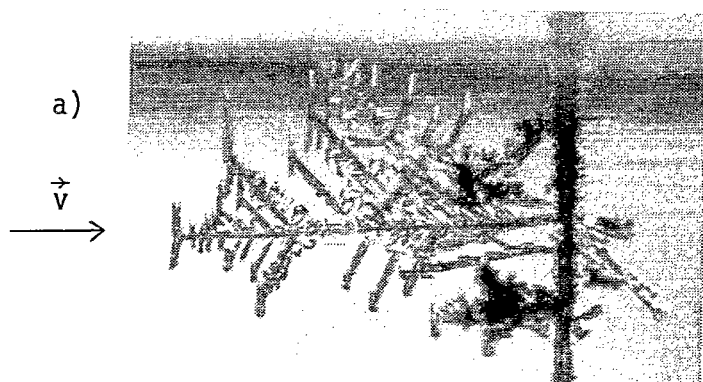
$v = 3.0 \text{ cm s}^{-1}$   
 $t = 63 \text{ minutes}$

250  $\mu\text{m}$

Fig. 5.18 Macroscopic steps propagating across the basal face of a hollow column.

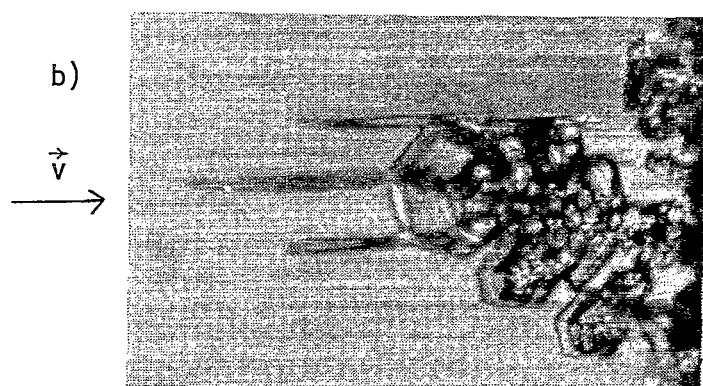
the 'c'-axis, this crystal grew laterally as well, i.e., by nucleation and growth on the prism faces. Thus, in the absence of any conflicting evidence, the growth of ice crystals at  $-9^{\circ}\text{C}$ , near water saturation, was interpreted to be by two-dimensional nucleation with subsequent propagation of microscopic steps which merged in the way discussed earlier to form the observed macroscopic steps.

The effect of temperature on the relative nucleation rates of the prism and basal faces was best illustrated by growing crystals at a temperature near  $-14^{\circ}\text{C}$  where nucleation is favored on the prism faces and then abruptly transferring the crystals to temperatures near  $-5^{\circ}\text{C}$  where nucleation is favored on the basal faces. Figure 5.19 illustrates the results of two such experiments. In the first experiment, Fig. 5.19 (a), the crystals grew as dendrites into a ventilation velocity of  $7.0 \text{ cm s}^{-1}$  at an ambient temperature near  $-14^{\circ}\text{C}$ . At time  $t = 0$  minutes the glass fiber, on which the crystals were growing, was raised in the chamber so that the crystals were transferred to a region with an ambient temperature near  $-5^{\circ}\text{C}$ . With the ventilation velocity maintained at  $7.0 \text{ cm s}^{-1}$  the crystals immediately began nucleating and growing on the basal faces. This resulted after a period of 22.0 minutes in columns growing with their 'c'-axes perpendicular to the ventilation velocity as in Fig. 5.19 (a). Hence, even though the prism faces at the leading edge of the crystal "saw" a larger local supersaturation or vapor density excess than the basal faces, due to the presence of the forced ventilation velocity, their growth rate was very small in comparison to growth along the 'c'-axis. In the second experiment, a crystal grew as a plate near  $-10^{\circ}\text{C}$ , but when transferred to a temperature near  $-4^{\circ}\text{C}$  at time  $t = 0$  minutes the crystal immediately



$$v = 7.0 \text{ cm s}^{-1}$$

2.0 mm



$$v = 3.0 \text{ cm s}^{-1}$$

1.0 mm

Fig. 5.19 Ice crystals immediately assume a columnar habit when transferred from a plate-like to a column-like temperature regime despite the presence of a forced ventilation velocity along the 'a'-axis.

sprouted needles from its corners, the regions of highest local vapor density excess, and at time  $t = 24.0$  minutes had assumed the shape shown in Fig. 5.19 (b). In this case the velocity was only  $3.0 \text{ cm s}^{-1}$ , and the plate was oriented at an angle from the direction into the airflow of about  $60^\circ$ . Since the needles grew perpendicular to the plates, they were oriented at an angle of about  $30^\circ$  from the direction into the airflow.

Although the relative rate of nucleation and growth on the basal and prism faces of an ice crystal is primarily a function of temperature, it is also a function of the local supersaturation or vapor density excess. Therefore, when a velocity is either introduced or removed, altering the local supersaturation over a crystal surface in a way already discussed, the resultant nucleation and growth of the crystal immediately responds on the microscopic scale to this new local supersaturation. However, the crystal does not achieve a new equilibrium growth rate and shape on the macroscopic scale until after a measurable time period. The modification of the relative rate of nucleation and growth on the basal and prism faces of an ice crystal induced by a change in the local supersaturation over the crystal was probably best demonstrated at an ambient temperature near  $-6^\circ\text{C}$  and an ambient supersaturation of 8.9% with respect to ice, i.e., a vapor density excess of  $0.26 \text{ g m}^{-3}$ . In the absence of a forced ventilation velocity the crystal grew as a column, at an angle of  $15^\circ$  from the horizontal, i.e., Fig. 5.20 (a), with a growth rate along the 'c'-axis of  $0.2 \text{ } \mu\text{m s}^{-1}$ . When a forced ventilation velocity of  $7.0 \text{ cm s}^{-1}$  was introduced at time  $t = 0$  minutes the crystal assumed a new preferred growth direction, as illustrated in Figs. 5.20 (b) and 5.20 (c), which was at an angle of  $8^\circ$  from

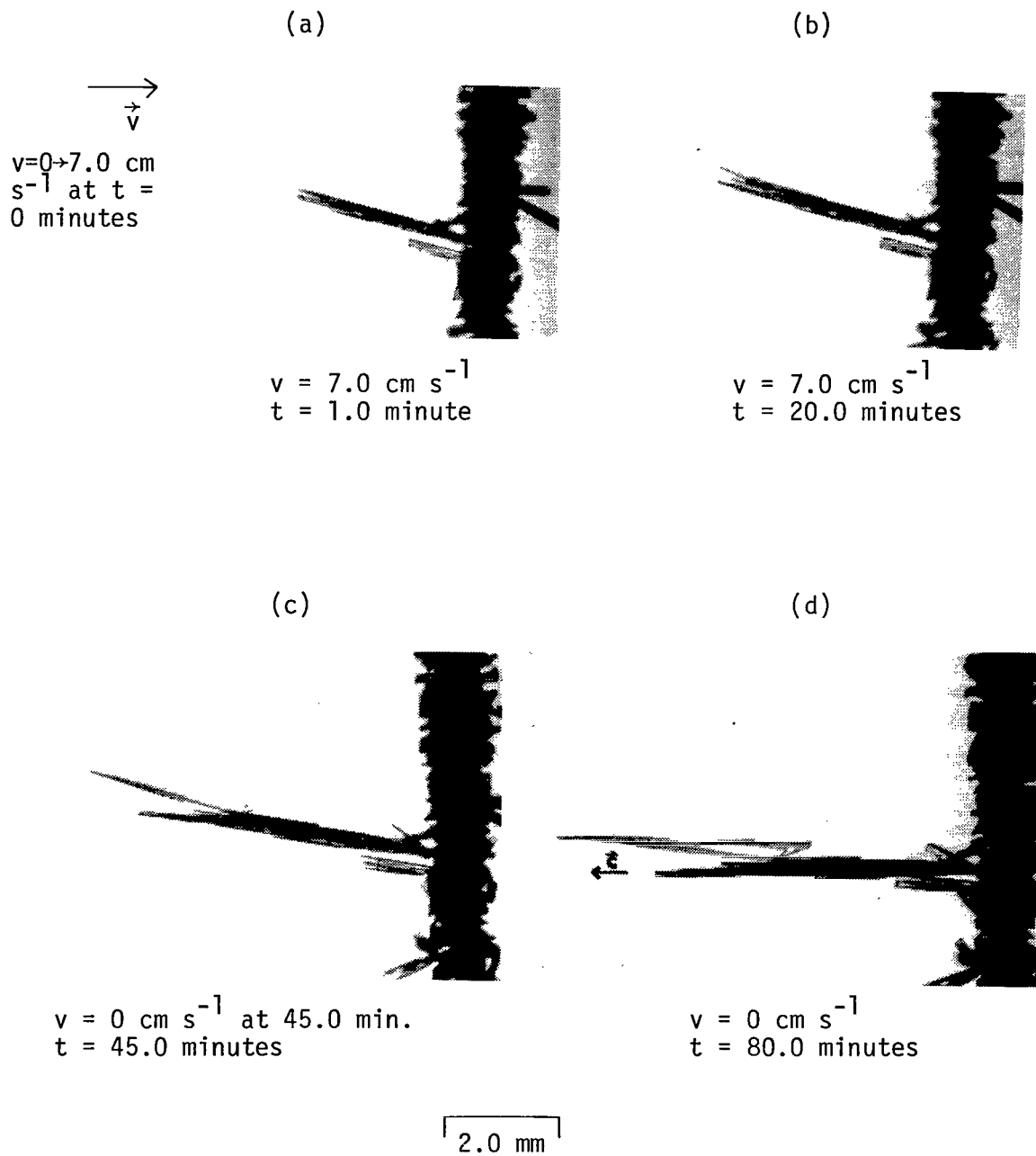


Fig. 5.20 Ice crystal columns introduced to a forced ventilation velocity may assume preferred linear growth along a direction other than the 'c'-axis.

the 'c'-axis. The linear growth rate along this new axis steadily increased, after the velocity was introduced, until it assumed an equilibrium rate of  $1.5 \mu\text{m s}^{-1}$ . This corresponded to a component of growth along the 'c'-axis equal to  $1.49 \mu\text{m s}^{-1}$  and a growth component along the 'a'-axis of only  $0.2 \mu\text{m s}^{-1}$ . When the velocity was removed at time  $t = 45.0$  minutes, the crystal resumed growth entirely along the 'c'-axis but at the higher rate of  $0.35 \mu\text{m s}^{-1}$ . This higher growth rate was presumably due to the column tip, Fig. 5.20 (d), being much narrower than before the velocity was introduced, Fig. 5.20 (a). When crystals were grown at a higher ambient supersaturation but still near  $-6^{\circ}\text{C}$ , they also assumed a preferred direction of linear growth other than along the 'c'-axis, even in the absence of a ventilation velocity. Figure 5.21 shows a crystal growing at an ambient temperature of  $-5.8^{\circ}\text{C}$  and an ambient supersaturation of 13.3% with respect to ice, i.e., a vapor density excess of  $0.41 \text{ g m}^{-3}$ . In this case, under conditions of no ventilation velocity, the preferred direction of growth was  $4^{\circ}$  to the 'c'-axis at a linear growth rate of  $1.5 \mu\text{m s}^{-1}$ . This corresponded to a component of growth along the 'a'-axis of only  $0.10 \mu\text{m s}^{-1}$  and a component of growth along the 'c'-axis of almost  $1.5 \mu\text{m s}^{-1}$ . At a velocity of  $7.0 \text{ cm s}^{-1}$ , the preferred direction of growth was  $7^{\circ}$  to the 'c'-axis at a linear growth rate of  $2.5 \mu\text{m s}^{-1}$ . In this case, the component of growth along the 'a'-axis was  $0.30 \mu\text{m s}^{-1}$  and the growth component along the 'c'-axis was  $2.48 \mu\text{m s}^{-1}$ . It can easily be seen from these examples that only a small relative change in the growth rates along the 'c' and 'a'-axes is necessary to induce growth in a new preferred direction.

Fiber inserted at  $t = 0$  minutes with  $v = 7.0 \text{ cm s}^{-1}$   
 $v = 0 \text{ cm s}^{-1}$  at  $t = 58.0$  minutes

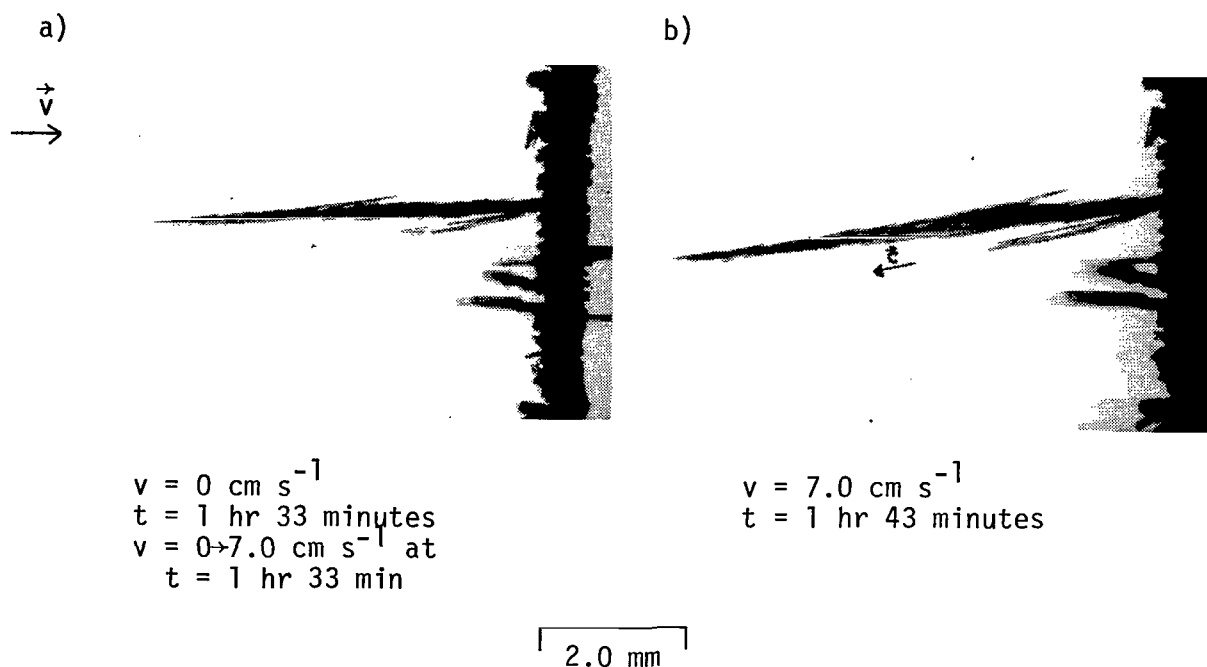


Fig. 5.21 At higher ambient supersaturations preferred linear growth may occur along a direction other than the 'c'-axis, even in the absence of a forced ventilation velocity.

Hallett (1965) grew crystals in a static vapor diffusion chamber, at temperatures near  $-4^{\circ}\text{C}$  and at an ambient supersaturation near 250% with respect to ice, which showed preferred growth along a direction  $25^{\circ} \pm 3^{\circ}$  to the 'c'-axis direction. These crystals grew hollow prisms behind their tips in shielded regions of lower supersaturation much as did the crystal in Fig. 5.21. Hallett confirmed the direction of the 'c'-axis by subsequently lowering the crystal to  $-15^{\circ}\text{C}$  and growing dendrites on the ends of the prisms. With the realization that the preferred growth direction did not lie in a simple crystallographic direction, he called these crystals "22 $^{\circ}$  needles". The observations

in this study indicate that there is nothing inherently special about the angle of  $22^\circ$  at  $-4^\circ\text{C}$ , but rather, growth along a preferred direction over the temperature range  $-4^\circ\text{C}$  to  $-6^\circ\text{C}$  is a function of the local supersaturation. That is, a change in the local supersaturation can induce a change, not only in the absolute growth rates, but also in the relative growth rates along the 'a' and 'c'-axes.

#### B. Crystal Growth in an Environment with Droplets

The riming efficiency of a crystal is determined by the crystal size, habit, and orientation, the relative carrier gas velocity, and the droplet size distribution and concentration. Since the crystal habit is itself a function of the carrier gas velocity and ambient supersaturation, riming of crystals in the atmosphere is a very complex process. In an attempt to gain an insight into the riming process and to demonstrate the versatility of the dynamic thermal diffusion chamber, a series of riming experiments were performed. Droplets of  $10\text{ }\mu\text{m}$  mean diameter were generated and introduced into the chamber as described in Chapter IV. The crystals to be rimed grew from a stationary solid glass fiber suspended vertically between the two horizontal chamber plates. Figure 5.22 is a sequence of photographs showing the extent of riming on columnar crystals, growing into the wind, for four different ventilation velocities. In this case, the top plate temperature of the chamber was  $-0.8^\circ\text{C}$  and the bottom plate temperature was  $-11.5^\circ\text{C}$ , giving a theoretical maximum ambient supersaturation in the chamber slightly greater than water saturation. Of course, the presence of high concentrations of water droplets ensured that the supersaturation was close to water saturation. On the other hand, at higher ventilation velocities, i.e., greater than  $15\text{ cm s}^{-1}$ , the incoming undersaturated

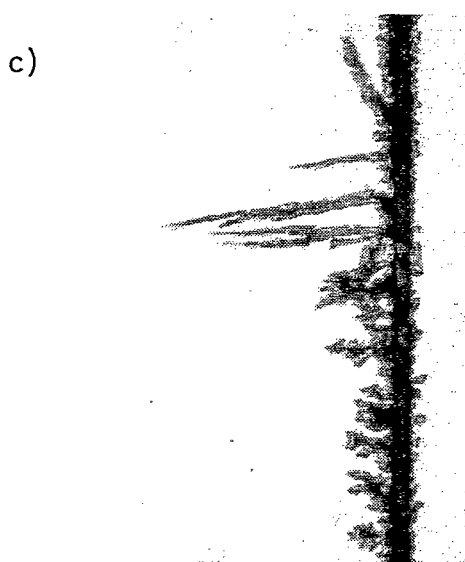




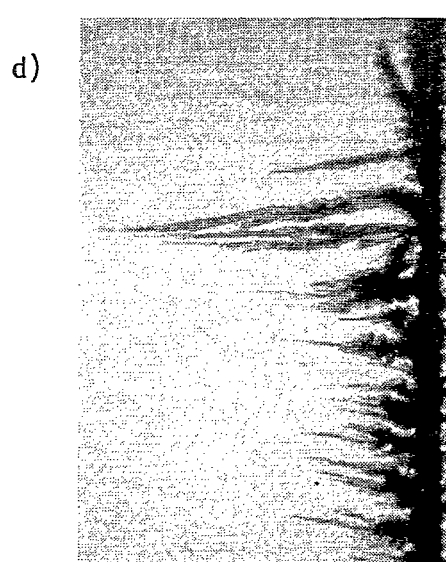
$v = 7.2 \text{ cm s}^{-1}$   
No droplets  
 $t = 91.0 \text{ minutes}$



$v = 8.4 \text{ cm s}^{-1}$   
with droplets  
 $t = 1 \text{ hr } 57 \text{ min.}$



$v = 15.7 \text{ cm s}^{-1}$   
with droplets  
 $t = 2 \text{ hr } 34 \text{ minutes}$



$v = 19.2 \text{ cm s}^{-1}$   
with droplets  
 $t = 2 \text{ hr } 53 \text{ minutes}$

2.0 mm

Fig. 5.22 Rimed ice crystal columns.

air no longer had sufficient time to approach equilibrium with either the linear temperature or vapor density profiles between the chamber plates, before it came into contact with the crystals. Hence, in the absence of droplets at higher velocities the crystals sublimated rather than grew. Figure 5.23 is a sequence of photographs showing the extent of riming on dendritic crystals for four different ventilation velocities. In this case, the chamber top plate temperature was  $-9.0^{\circ}\text{C}$  and the bottom plate temperature was  $-22.5^{\circ}\text{C}$ . This also resulted in a theoretical maximum ambient supersaturation in the chamber slightly greater than water saturation. Since, unfortunately, the droplet size distribution and concentration was a complicated function of the ambient supersaturation, the ventilation velocity and the horizontal and vertical position in the dynamic thermal diffusion chamber, it was impossible to obtain meaningful quantitative results from these riming experiments. However, some qualitative observations were made. As the ventilation velocity was increased from 0 to  $20\text{ cm s}^{-1}$ , in the presence of high droplet concentrations of mean diameter  $10\text{ }\mu\text{m}$ , the crystal growth was progressively controlled more by droplet accretion and less by vapor diffusion. In fact, in the presence of a ventilation velocity of  $15\text{ cm s}^{-1}$  droplet accretion accounted for over 90% of the crystal growth in both these experiments. This is a much lower velocity for the onset of riming than is typically observed in the atmosphere. However, the droplet concentrations in these experiments were very high, estimated to be typically several thousand per cubic centimeter, whereas, even in heavily polluted continental clouds, droplet concentrations with this mean diameter rarely exceed  $1000\text{ cm}^{-3}$ . The rimed columnar crystals in Fig. 5.22 appear much more delicate than do the rimed dendritic

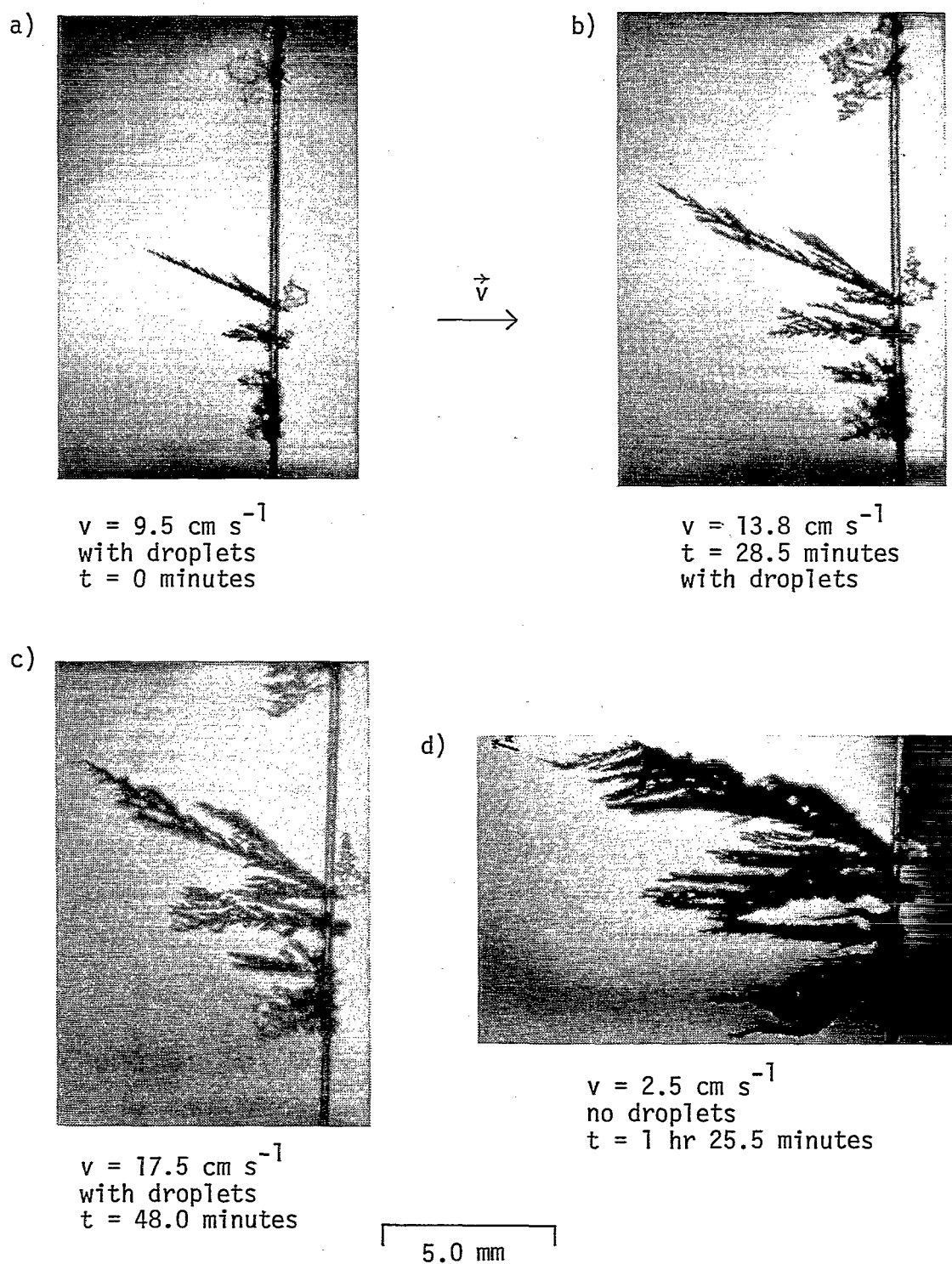


Fig. 5.23 Rimed ice crystal dendrites.

crystals in Fig. 5.23. Nonetheless, in both these experiments even the most extensively rimed crystals retained their original crystalline axes orientation. This was demonstrated by allowing vapor diffusional growth to take place on the rimed crystals as, for example, is shown in Fig. 5.23 (d).

For ventilation velocities less than  $1.0 \text{ cm s}^{-1}$ , it was observed through the stereo microscope that water droplets of  $10 \text{ }\mu\text{m}$  diameter or smaller evaporated and completely disappeared as they approached a growing ice crystal. The distance from the crystal at which the droplets disappeared was a function of the initial droplet size, the ventilation velocity and the crystal shape. For a given crystal shape this distance decreased with increasing droplet size or increasing velocity. At higher velocities the droplets flowed around the crystal unless they encountered a stagnation point, in which case the droplet would decelerate and impact upon the crystal surface. Following impaction the evaporating droplet would skitter along the surface until it completely evaporated, adhered to the surface and froze, or moved off the leeward side of the crystal.

### C. Growth of Discoid Crystals from the Vapor

While growing columnar crystals from the vapor at ambient temperatures over the range  $-5^{\circ}\text{C}$  to  $-7^{\circ}\text{C}$ , I observed that adjacent to the solid glass fiber, in regions of low local supersaturation resulting from competition between crystals, thin discoid crystals grew, as for example, on the leeward side of the fiber in Fig. 5.24. These were the first vapor grown discoid ice crystals ever to be observed. They had a thickness of only about 10 to  $20 \text{ }\mu\text{m}$  and grew at a linear rate of  $0.03 \text{ }\mu\text{m s}^{-1}$ . When they obtained a diameter of approximately  $300 \text{ }\mu\text{m}$  they

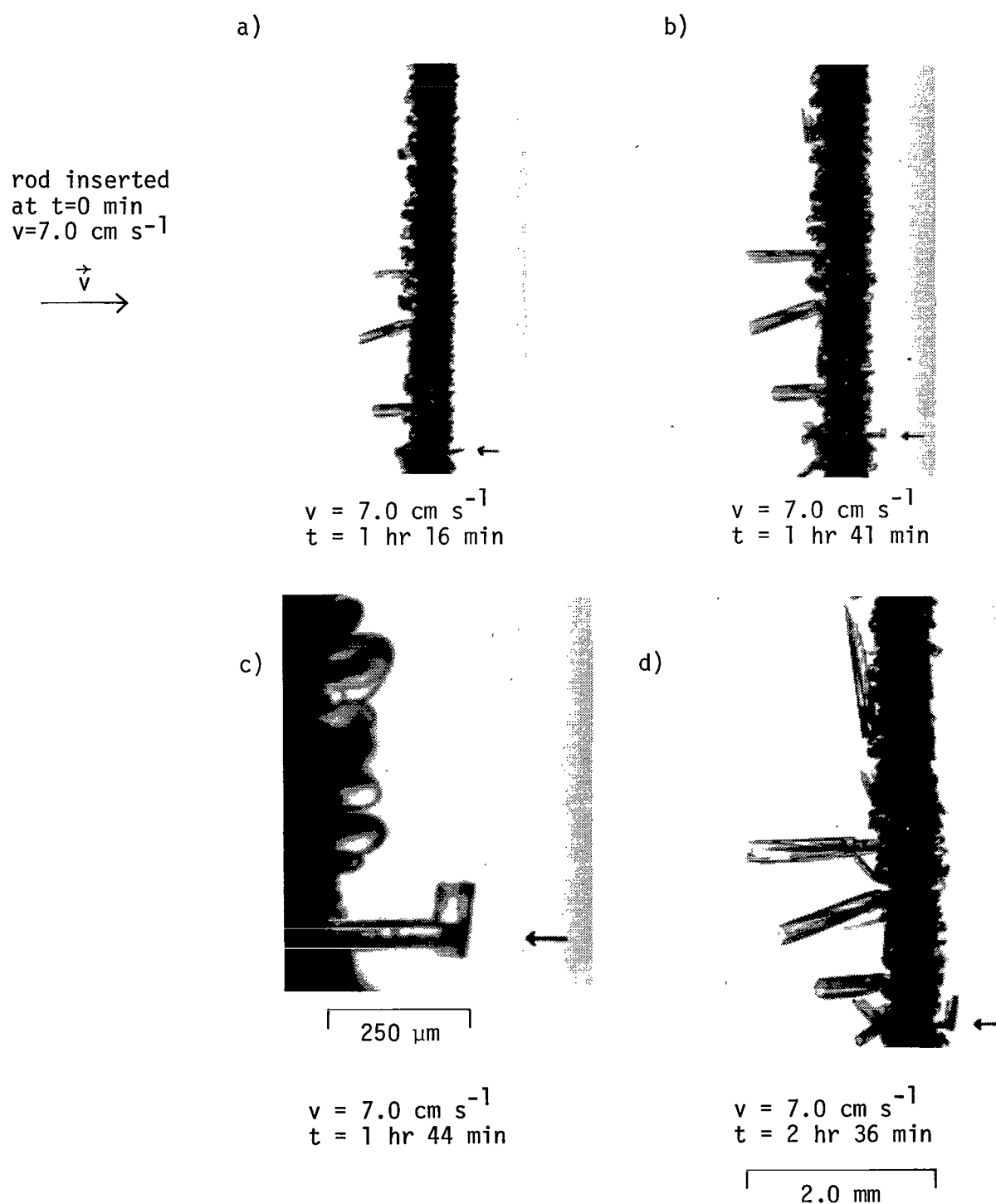


Fig. 5.24 Ice platelets and columns both growing at  $-5^{\circ}\text{C}$  under different local ambient conditions of supersaturation.

proceeded to nucleate and grow columns perpendicular to their tips as illustrated in Fig. 5.24 (c). Note that Fig. 5.24 (c) is an enlargement of the discoids and the crystal indicated with the arrow in Fig. 5.24 (a), (b), and (d). Thus, it was established that the discoids grew in the basal plane. This, in itself, was interesting since the  $c/a$  axial ratio for crystals grown in this temperature regime was formerly believed to never be smaller than 1.0, much less 0.03 as was the case for these discoids. When the liquid nitrogen cooled, 250  $\mu\text{m}$  diameter solid glass fiber was repeatedly inserted into the chamber at an ambient supersaturation equal to water saturation, that is, at an ice supersaturation of 6% or a vapor density excess of  $0.19 \text{ g m}^{-3}$ , the small crystals which nucleated and grew on the fiber were always columns when there was a large distance between them and always discoids when their population density was high. The time needed for these crystals to nucleate and grow to an observable size was of the order of minutes, i.e., much longer than the time needed for the liquid nitrogen cooled fiber to come to thermal equilibrium with the flowing airstream. Hence, the fact that the fiber was initially very cold did not determine the observable growth of the crystals. The repeated observations of either columns or discoids, depending on their population density is consistent with the argument that discoids grow in the temperature regime  $-5^{\circ}\text{C}$  to  $-7^{\circ}\text{C}$  at low local supersaturations. Since the tip of a discoid crystal was always thinner than its base, nucleation did not occur on the basal face near the tip. When, however, the local supersaturation was increased above a critical threshold value, by the introduction of a ventilation velocity, by reduced vapor competition between crystals, or by increasing the ambient supersaturation, nucleation occurred on

the basal face and the crystal habit became columnar. At still higher local supersaturations, the relative nucleation and rate of growth on the basal and prism faces, respectively, became even more pronounced and the columnar crystals became sheath or needle-like as did the upper column in Fig. 5.24 (d).

Following up these initial investigations, McKnight (to be published) has also grown both discoids and plates at an ambient temperature of  $-5^{\circ}\text{C}$  and an ambient supersaturation of 2.5% with respect to ice, i.e., a vapor density excess near  $0.1 \text{ g m}^{-3}$ . McKnight employed a sealed vertical ampoule about 5 cm in diameter near the base and 15 cm in length containing, as the vapor source, a sugar-water solution of known concentration and vapor pressure. The ampoule was immersed in a well-controlled temperature bath of glycol. The ice crystals grew from a solid glass fiber which was suspended vertically inside the ampoule and terminated about 1.0 cm above the sugar-water solution. The discoids grown in the ampoule had comparable thicknesses and growth rates to those grown in the dynamic thermal diffusion chamber. However, in this case, the local supersaturation was much nearer the ambient supersaturation and the only crystals which became columnar were those near the tip of the fiber directly over the sugar-water solution, and then, only when the fiber tip was positioned within a few millimeters of the solution surface. Even in the ampoule, the discoids rarely exceeded  $500 \text{ }\mu\text{m}$  in diameter before they grew scalloped edges and subsequently faceted prism faces. As the discoids grew in diameter they thickened from the base to the tip. When they became plates, typically,  $0.5 \text{ mm}$  in thickness and 2 to 3 mm in diameter their linear growth rates were reduced to about  $0.005 \text{ }\mu\text{m s}^{-1}$ .

Although neither the mechanism by which the vapor grown discoids grow, nor the reason why they grow scalloped edges and then faceted faces when they reach a critical diameter; is as yet understood, these experimental observations should contribute significantly to our total understanding of ice crystal growth.

D. Growth of Crystals at Intermediate to Low Ambient Supersaturation

Another area of experimental study which is very interesting and also provides much needed information about basic crystal growth processes, but plays only a minor role under atmospheric conditions, is the growth of ice crystals at intermediate to low ambient supersaturation. Current ideas of crystal growth mechanisms differentiate between growth by continuous surface or two-dimensional nucleation on a molecularly smooth surface, and growth which takes place by propagation of discrete steps on an otherwise molecularly smooth surface. The discrete steps may originate from surface accidents - particulate or molecular impurity, from regions elsewhere at higher supersaturation where surface nucleation has already taken place, such as from corners as illustrated in Fig. 5.16, or from dislocations. If the crystal dislocations are screw-type, the steps perpetuate from growth layer to growth layer. Continuous two-dimensional nucleation over the crystal surface is believed to be limited to higher ambient supersaturations, being under these conditions the dominant growth mechanism. Under very low ambient supersaturation growth conditions, dislocation initiated steps are believed to be the dominant growth mechanism. At intermediate to low ambient supersaturations, there has been considerable question as to what growth mechanism prevails.

McKnight (to be published) using vapor grown ice crystals from my



dynamic thermal diffusion chamber, vapor grown ice crystals from an isothermal chamber containing a little supercooled water or supersaturated sugar solution as the vapor source, natural frost crystals, and ice crystals grown from a slightly super-cooled melt, has studied ice crystal dislocation densities under various ambient conditions. One of his observations, Anderson, Keller, McKnight and Hallett (1976) is that crystals sometimes grow, apparently dislocation free, at ambient supersaturations significantly lower than present theories would allow.

At an ambient temperature near  $-30^{\circ}\text{C}$  and at ambient supersaturations near 20% with respect to ice, i.e., at a vapor density excess near  $0.07 \text{ g m}^{-3}$ , simultaneous growth of ice crystal plates and columns under identical ambient conditions occurred in my dynamic thermal diffusion chamber as illustrated both in Fig. 5.25 and in the paper by Anderson, et al. (1976). At much lower ambient supersaturations the

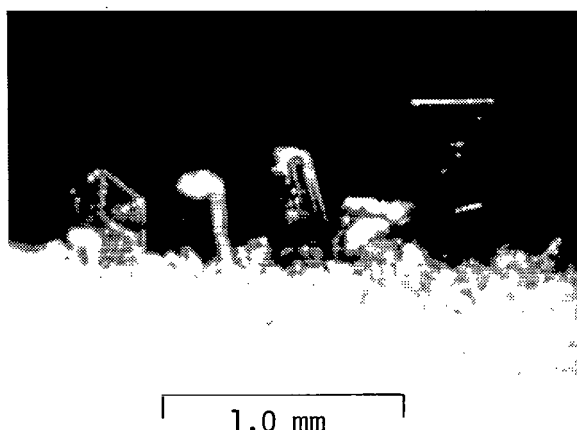


Fig. 5.25 Simultaneous growth of columns and plates sometimes occurs at low supersaturation.

crystals grew more or less equiaxed and at much higher ambient supersaturations the crystals grew as hollow columns. Table IV delineates

the habit of the ice crystals grown near  $-30^{\circ}\text{C}$  as a function of the "effective" ice supersaturation.

TABLE IV Habit of ice crystals growing at  $-30^{\circ}\text{C}$ .

<u>"Effective" ice supersaturation</u>	<u>Habit</u>	<u>c/a</u>
0		
5	equiaxed	1.0
10	simultaneous	1.0
15	solid columns and plates hollow	to
20		0.3
25		5
30 water saturation ←(zero velocity)		to
		10
>35	columns	>20

Anderson (1974) and Anderson, et. al. (1976) observed that ice crystals growing epitaxially on either covellite or silver iodide sometimes have basal faces which do not grow at all in the presence of a supersaturation between water and ice but can be induced to grow by increasing the ambient supersaturation to a critical value which is variable from crystal to crystal due, at least in part, to strain originating between the crystal and substrate.

The three independent observations of McKnight, Keller, and Anderson are consistent with the following hypotheses for growth within the range of conditions covered by these experiments:

(a) growth at and somewhat below water saturation is initiated in the absence of defects by a two-dimensional surface nucleation process.

(b) some crystal surfaces fail to grow at all at small ice super-

saturation; finite growth requires the presence of defects.

(c) growth habit under low supersaturation will be determined by the presence of defects; presence of defects in only the 'a' or 'c' direction will lead to growth only on that face and could give rise to crystals of habit opposite to that usually observed for a crystal with defects in both directions.

(d) habit at higher supersaturation and the details of the skeletal growth will be controlled by two-dimensional nucleation processes at the crystal corners and edges where the crystal protrudes into higher supersaturation regions.

For crystal growth habit under atmospheric conditions, the controlling factor will almost always be the surface nucleation process since most cloud processes take place at or a little below water saturation. In those situations in the atmosphere for which small ice supersaturations do exist, probably confined to regions of slow cooling by radiation or slow ascent situations with an abundant concentration of ice crystals, the habit, which is likely controlled by the initial defect distribution being retained during growth, may be opposite to that usually observed.

The surface nucleation process at the crystal corners and edges and subsequent propagation of steps to regions of lower local supersaturation, as described earlier, was the controlling factor for the majority of the crystals grown in the dynamic thermal diffusion chamber. In fact, all the crystals taken from my chamber and subsequently x-ray topographed were apparently dislocation free. However, topographs of crystals grown in my chamber at low supersaturation remain to be taken.

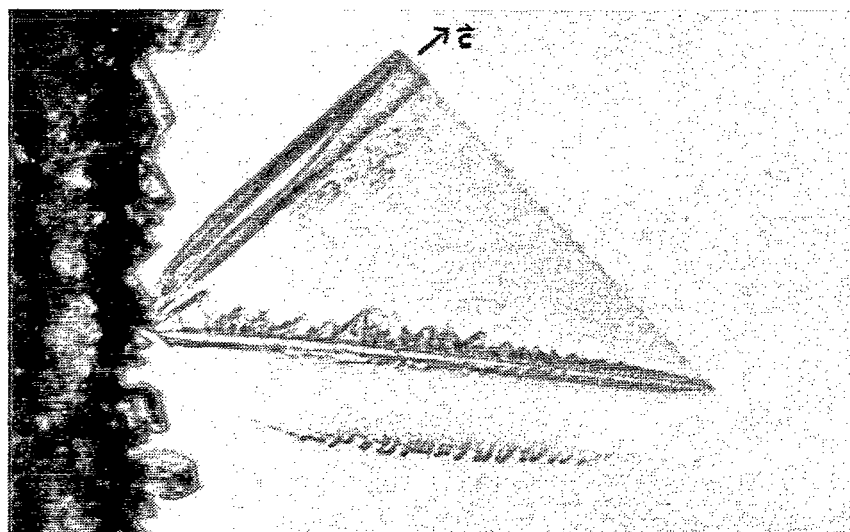
### E. Growth of 'Peculiar' or Prism-Faced Crystals

At temperatures near  $-30^{\circ}\text{C}$ , some of the crystals which grew from the solid glass fiber in the dynamic thermal diffusion chamber had very peculiar shapes. Several of these crystals were similar to the 'peculiar' natural crystals reported by Nakaya (1954, pg. 65), Kikuchi (1970), and Kikuchi (1971) and also to the artificially grown crystals reported by Yamashita (1971). Kikuchi observed this type of crystal in both Antarctica and Japan and noted that it was frequently mixed with a combination of bullets, columns and crossed plates, comprising, in general, less than 1% of the total number of crystals falling from clouds at temperatures colder than  $-25^{\circ}\text{C}$  but warmer than  $-35^{\circ}\text{C}$ . The actual conditions of growth, however, were difficult to ascertain since the crystals grew in natural clouds but were normally collected at the ground. Yamashita, on the other hand, observed this type of crystal when he seeded a supercooled water cloud near  $-25^{\circ}\text{C}$  with a metal rod previously immersed in either dry ice or liquid nitrogen. Yamashita believed the temperature of the seed rod might be an important factor in the subsequent formation of these peculiar crystals. Kobayashi (1976) suggested that some of these peculiar-shaped crystals may be explained as twins and he proposed a possible mechanism for their formation employing a generalized Coincidence-Site Lattice (CSL) concept. Kobayashi suggested that the twinned seed may originate in the atmosphere from the freezing of water droplets to form polycrystals and, in particular, to form twins at temperatures lower than  $-20^{\circ}\text{C}$ . He emphasized that although these crystals seem to have a peculiar shape, far from the normal hexagonal symmetry as a whole, they are indeed hexagonal and do not form a new classification of crystals.

Figure 5.26 shows two stages in the growth of a prism-faced or a particular 'peculiar' ice crystal which grew in the dynamic thermal diffusion chamber. This crystal grew at an ambient temperature of  $-28.6^{\circ}\text{C}$  and an ambient supersaturation of 15.5% with respect to ice, i.e., a vapor density excess of  $0.06 \text{ g m}^{-3}$ . At all stages of growth of this crystal there was no forced ventilation velocity. However, in the latter stages of growth, illustrated by Fig. 5.26 (b), the local supersaturation was lower due to competition with other crystals and this crystal grew a column on the tip of the rib, parallel to the column already growing at the opposite end of the crystal. The direction of the 'c'-axis is indicated in the figure. The surface structure of this crystal was investigated using several different lighting arrangements, i.e., background lighting, direct illumination, and specular reflection, and was found to be very complex. This crystal, particularly in the stage of growth shown in Fig. 5.26 (b), was stepped from its center to its outer edges. The upper edge of the crystal containing the exposed basal faces of the two columns was much thicker than the lower edge. The basal face of the small column was by no means smooth. In fact, with the exception of the lower left-hand corner, this crystal had few smooth surfaces of significant area. Notice in Fig. 5.26 (a) that the rib grew at an angle of about  $50^{\circ}$  from the 'c'-axis and extended into the vapor field slightly beyond the rest of the crystal thus providing a possible nucleation site for continued growth.

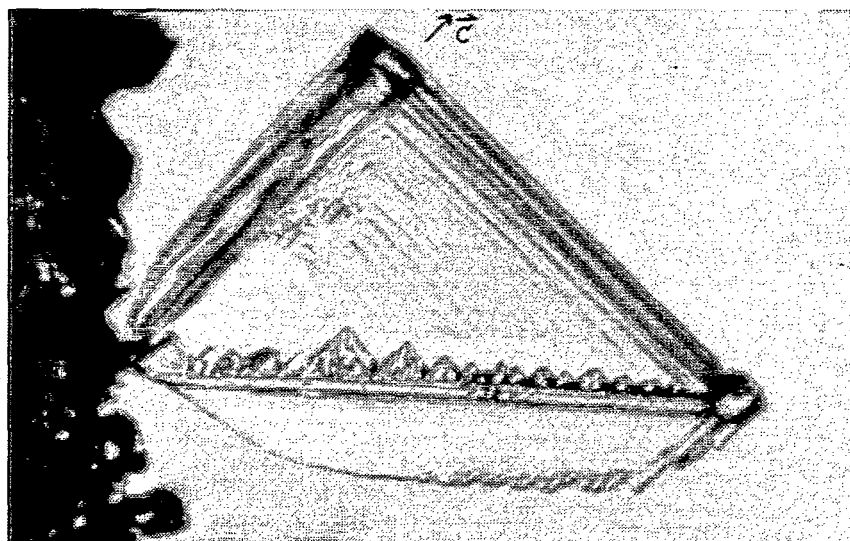
The effect of a forced ventilation velocity on the growth of this type of crystal is demonstrated in Fig. 5.27. This crystal grew at an ambient temperature of  $-33.7^{\circ}\text{C}$  and an ambient supersaturation of 57.7% with respect to ice, i.e., a vapor density excess of  $0.135 \text{ g m}^{-3}$ . When

a)



$v = 0$   
 $t = 15$  hours 10 minutes

b)



$v = 0$   
 $t = 21$  hours 40 minutes

500  $\mu\text{m}$

Fig. 5.26 Two stages in the growth of a prism-faced or 'peculiar' ice crystal. The direction of the 'c'-axis is indicated with an arrow.

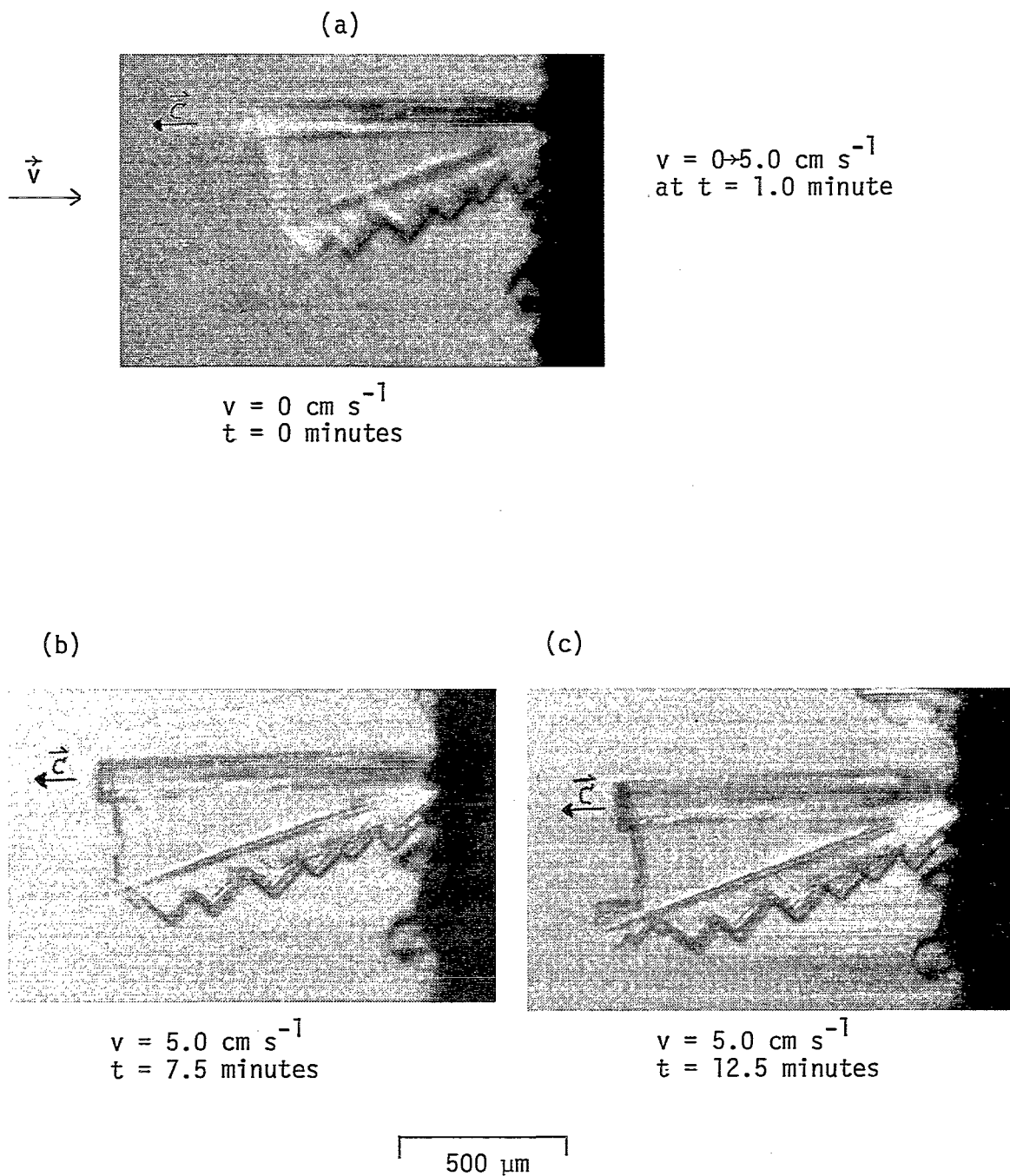


Fig. 5.27 A prism-faced ice crystal responds to the introduction of a forced ventilation velocity.

a ventilation velocity was introduced, it was only a few minutes before it was obvious that nucleation and growth was predominant at the tip of the rib as illustrated in Fig. 5.27 (b) and (c). Since the prism plane of this crystal did not lie quite perpendicular to the viewing field, it is difficult to accurately determine the angle between the rib and the 'c'-axis. However, this angle would certainly appear much smaller than the angle of  $50^{\circ}$  measured for the crystal in Fig. 5.26.

The variety of unusual shapes which the 'peculiar' ice crystals may assume is demonstrated in Fig. 5.28. The number of 'peculiar' crystals grown was insufficient to accurately assess how the shape of these crystals is a function of both the ambient temperature and supersaturation, or if, in fact, an initial "twinned seed" nucleation process contributes significantly to later stages of growth of the crystal. However, enough crystals were grown to provide the following qualitative observations. The crystals responded to an increase in the local supersaturation, i.e., through the introduction of a ventilation velocity, in much the same way as crystals at other temperatures. Nucleation and growth of 'peculiar' crystals occurred on the solid glass fiber even though the fiber was not cooled to either liquid nitrogen or dry ice temperatures, but, rather, was inserted into the chamber at room temperature. Nucleation and growth of 'peculiar' crystals occurred on the solid glass fiber even when the ambient supersaturation was maintained below water saturation. Over this range of ambient temperature and supersaturation the number of 'peculiar' crystals comprised a large percentage of the total number of crystals which grew. The angle between the rib and the 'c'-axis varied significantly from crystal to crystal.



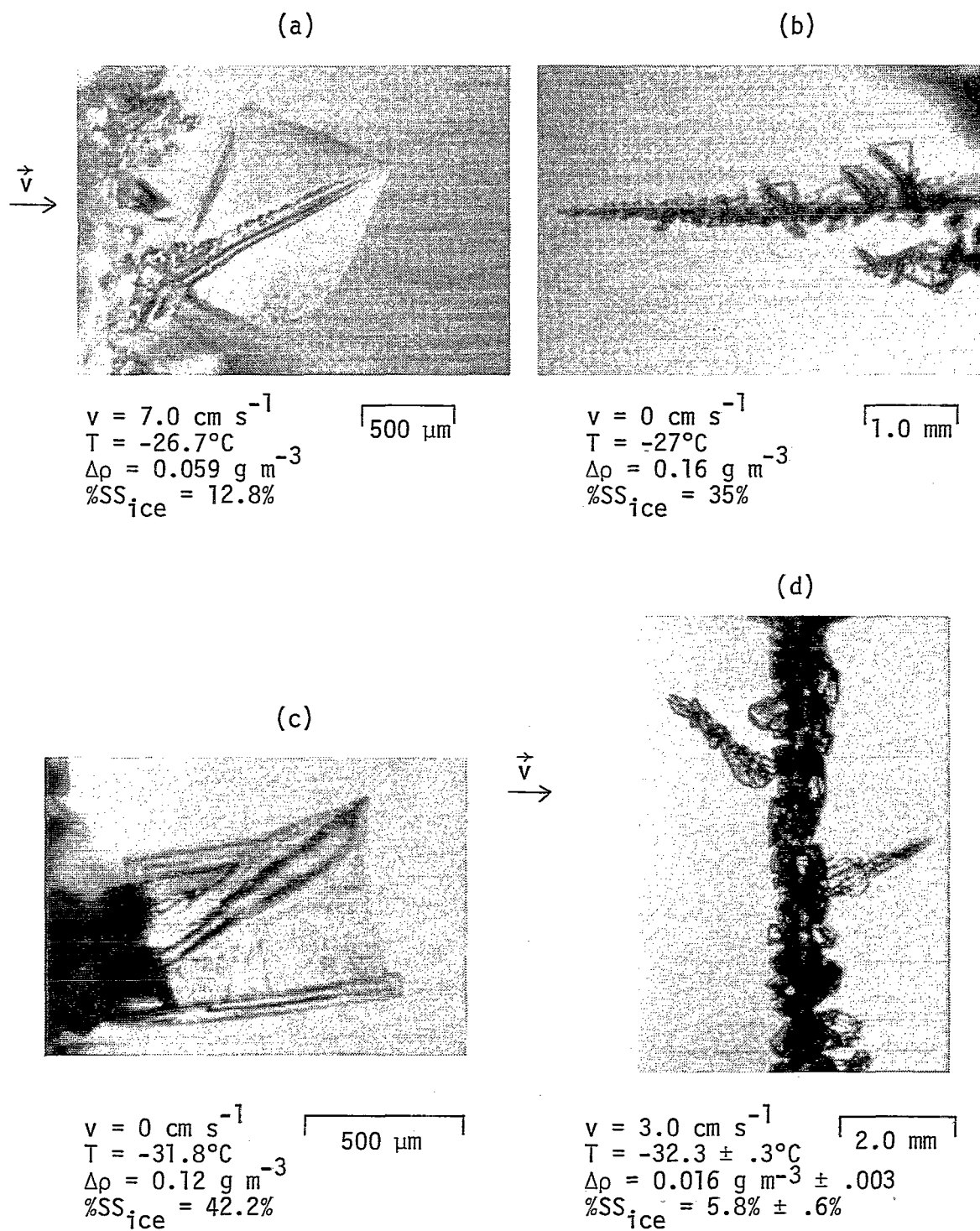


Fig. 5.28 'Peculiar' ice crystals may assume a variety of unusual shapes.

## VI.

APPLICATION OF RESULTS AND SUGGESTIONS  
FOR FUTURE STUDYA. Application to the Atmosphere

Caution should be exercised in applying either the quantitative linear growth rates or the onset of riming criteria obtained from these experiments directly to the atmosphere. Since ice crystals in these experiments grew from a stationary support their orientation in the moving airstream was fixed. On the other hand, the flow pattern of air around the freely floating ice crystals in the atmosphere may be quite variable. In the atmosphere, ice crystal plates, for example, often fall in an oscillatory manner with their basal plane perpendicular to the air flow. In these experiments, the basal plane of plates was usually oriented parallel to the air flow, resulting in preferential growth of the crystal corner oriented into the airstream. The ventilation velocities employed in this study in the absence of water droplets were less than or equal to  $10 \text{ cm s}^{-1}$ . This corresponds to terminal fall speeds of only very small crystals, typically less than 0.5 mm diameter. The presence of water droplets in the atmosphere both complicates the computation of the local supersaturation surrounding a growing ice crystal and introduces the possibility of ice crystal growth occurring by a combination of vapor growth and riming, both these growth characteristics being functions of the droplet size distribution and the droplet concentration. Considering these differences in growth conditions, the rates of growth determined in these experiments when employing a ventilation velocity of  $7.0 \text{ cm s}^{-1}$ , i.e., Fig. 5.12, compare favorably with the linear growth rates determined by Ryan, et. al.

(1976), i.e., Fig. 3.7, for small crystals 100  $\mu\text{m}$  to 300  $\mu\text{m}$  in diameter falling at velocities between 5  $\text{cm s}^{-1}$  and 10  $\text{cm s}^{-1}$  through an environment containing a cloud of water droplets at or near water saturation.

It should be noted in comparing linear crystal growth rates obtained in the present experiments with those of Kobayashi (1958), i.e., Fig. 2.5, Kobayashi (1961), Rottner (1971), or Rottner and Vali (1974) that they used a different definition of vapor density excess than normally employed in this study. They implicitly defined the vapor density excess over a growing crystal to be

$$\Delta\rho = \rho_{\infty}(T_{\infty}) - \rho_{\text{ice}}(T_c), \quad (6.1)$$

where  $\rho_{\infty}(T_{\infty})$  is the ambient vapor density and  $\rho_{\text{ice}}(T_c)$  is the saturated vapor density over a plane ice surface at the temperature of that growing crystal surface. They calculated the ice crystal surface temperature,  $T_c$ , from a conduction-diffusion equilibrium for a static environment in the way described in Chapter IV, i.e., Fig. 4.15. That is, in their experiments  $T_c$  was always given by  $T_c'$ , i.e., the ice crystal surface temperature in a static environment. Their definition of the vapor density excess was defined as  $\Delta\rho_{\text{static}}$  in Fig. 4.16. In actuality, eq. (6.1) gives the definition of the "true" vapor density excess for either a static or ventilated crystal and it could be used successfully if the crystal surface temperature,  $T_c$ , were known. However, since the surface temperature of a growing ice crystal is a function of the crystal shape, the ambient supersaturation and the ventilation velocity its accurate determination is immensely difficult. Hence, in this study the environmental vapor density excess was employed. This quantity is defined to be

$$\Delta\rho = \rho_{\infty}(T_{\infty}) - \rho_{ice}(T_{\infty}), \quad (6.2)$$

where  $\rho_{ice}(T_{\infty})$  is the saturated vapor density over a plane ice surface at the ambient temperature. That is, this definition gives the vapor density excess over a non-growing crystal. This definition of the vapor density excess was defined as  $\Delta\rho_{max}$  in Fig. 4.16 and is more nearly equivalent to the normal definition of ambient supersaturation as used in the 'Nakaya diagrams' of Hallett and Mason (1958a) and Mason (1971), i.e., Fig. 2.4.

Exercising the aforementioned cautions, the significance of these experimental results as applied to the atmosphere may be briefly summarized. I have demonstrated how it is possible to grow dendrites and needles in the atmosphere at ice supersaturations less than that equivalent to water saturation. That is, as the crystals fall they "see" a relative carrier gas velocity equal to their terminal fall speed. The effect of this carrier gas velocity is roughly equivalent to increasing the ambient supersaturation. This is an important result since accretion of droplets is a function of the crystal habit, with skeletal or dendritic structures offering larger surface areas and having better riming characteristics. A very important process in the atmosphere may be the initial growth of a small ice crystal plate, for example, near water saturation and at low terminal fall speed. As the crystal grows and reaches a higher terminal velocity its linear growth rate may increase substantially. As a result of the increased relative carrier gas velocity the crystal may go through the transition to a dendrite which offers a much larger collection area for both water droplets and pollutants. Hence, both the initiation of precipitation

and scavenging of pollutants may occur faster in these cases than has previously been predicted. Since the crystal growth rate is a function of temperature, having maxima near  $-6^{\circ}\text{C}$  and  $-15^{\circ}\text{C}$  which are a function of the crystal fall speed, optimum injection of ice nuclei in cloud seeding experiments utilizing dynamic cloud growth is a function of the temperature at the level of injection and the stage of cloud maturity.

Finally, I have shown that when an ice crystal undergoes a plate to dendrite or vice-versa transition there is a time constant for a new equilibrium linear crystal growth rate to be established. This means that the history of a crystal having fallen through changing ambient conditions of temperature, supersaturation and ventilation velocity cannot be uniquely specified.

#### B. Application to Crystal Growth

Diffusion of both mass and heat takes place through the boundary layer surrounding a growing crystal. To facilitate good transfer, this layer should be as thin as possible. Since the boundary layer thickness is inversely proportional to the square root of the ventilation velocity, as shown in Chapter V, an increase in the velocity decreases the boundary layer thickness. (In practice the boundary layer thickness is slightly different for the two processes). A decrease in the boundary layer thickness increases the flux of water vapor to and heat from a growing ice crystal and also induces partial pressure gradients of water vapor from the leading edge across the crystal surface. Hence, enhanced growth in a preferred direction results, and needles or dendrites, for example, grow depending on the ambient temperature.

The introduction of a ventilation velocity is not equivalent to

increasing the diffusion coefficient of water vapor through air, as a comparison of the results from these experiments with those shown in Fig. 2.10 demonstrates. That is, Fig. 2.10 shows that at a constant thermal conductivity of the air an increase in the diffusion coefficient leads to increased growth rates but to a decrease in the development of skeletal or dendritic structures. The experiments described in this study show that the introduction of a ventilation velocity leads to increased growth rates and to an increase in the development of skeletal or dendritic structures. This is consistent with the fact that an increase in the diffusion coefficient not only increases the flux of water molecules to a growing ice crystal but also increases the boundary layer thickness in direct proportion to the square root of the diffusion coefficient as shown in Chapter V. This results in enhanced growth, but since sustained partial pressure gradients of water vapor across the crystal surface are in this case smaller, the growth is also more uniform. This is also consistent with the observations of Lamb (1970), as described in Chapter II, that the surface structure of ice crystals grown in the presence of either air or helium at low pressure was more complicated than that of crystals grown in pure water vapor.

Figure 2.10 shows that under conditions of constant vapor diffusivity skeletal and dendritic structures developed more readily as the thermal conductivity of the atmosphere was increased. This is not unreasonable, since an increase in the thermal conductivity of the air or any other process which lowers the growing crystal surface temperature corresponds to increasing the "true" vapor density excess, i.e., supersaturation, over the crystal surface as described in Chapter IV. Thus, an increase in the thermal conductivity is nearly equivalent to

increasing the ambient supersaturation.

It is important to appreciate the fact that a ventilation velocity is not equivalent to increasing the diffusion coefficient. On the other hand, the ventilation velocity does not enhance growth by just lowering the crystal surface temperature. Rather, in addition to lowering the crystal surface temperature by conducting heat away, the ventilation velocity decreases the thickness of the boundary layer preferentially over the crystal surface. This increases the flux of water vapor to the crystal while maintaining partial pressure gradients of water vapor across the crystal surface.

In many crystal growth applications, such as in industry, it is desirable to grow uniform crystals in the least possible time. For these applications, the results obtained for ice crystals indicate that at a fixed supersaturation a large thermal conductivity of the carrier fluid is desired to promote higher growth rates, while maintaining a large ratio of the diffusion coefficient to the thermal conductivity to induce uniform growth. It is also important in these applications to maintain as uniform fields of temperature and vapor surrounding the crystal as possible.

In practice it is very difficult to maintain uniform fields of either vapor or temperature around a growing crystal. In addition to 'inherent' inhomogeneities in the vapor and temperature fields, the release of latent heat at the growing crystal surface often leads to natural convection. In the experiments described in this study the natural convection resulting from a growing dendrite was estimated to be  $1 \text{ mm s}^{-1}$ . This measurement was obtained by observing, with a stereo microscope equipped with a micrometer eyepiece, entrained water droplets,

approximately 5  $\mu\text{m}$  in diameter, convecting upward from growing dendrites whose basal plane was parallel to the horizontal. Smaller values of natural convection result from more slowly growing crystals.

Natural convection can be greatly reduced in 'Zero Gravity' experiments conducted in space, resulting in more uniform fields of both vapor and temperature. Consequently, crystal growth under these conditions should be more uniform.

### C. Suggestions for Future Study

Several ideas for possible future studies exist which employ the dynamic thermal diffusion chamber. If the working section of the chamber were doubled or tripled in length to obtain equilibrium ventilation velocities of 20 to 30  $\text{cm s}^{-1}$ , while retaining the nearly linear vertical profiles of both temperature and vapor density, the present experimental results could be extended to crystal fall speeds approaching those encountered in the atmosphere. If the working section of the chamber were modified, consideration should be given to increasing the chamber aspect ratio. A greater number of quantitative growth rates of columns and needles as a function of temperature, supersaturation and ventilation velocity are needed to enlarge upon the present results. Quantitative growth rates should be obtained for crystals at various orientations to the air stream to better assess the direct applicability of the present results to growing ice crystals falling freely in the atmosphere. Both the study of discoid crystal growth at low supersaturation and the study of prism-faced or 'peculiar' crystals at low temperature should be continued in conjunction with x-ray topographic studies of these crystals. An intensive study involving the growth of



scalloped plates near  $0^{\circ}\text{C}$  would be interesting. A comparison might be made between their growth and the growth of scalloped plates from discoids near  $-6^{\circ}\text{C}$ . It would be interesting and beneficial to study the simultaneous effect, on the growth rate and shape of ice crystals, of a direct current electric field and a ventilation velocity, particularly if they were applied perpendicularly to one another. Perhaps such a study would answer conclusively the question of whether or not the application of a d.c. electric field is equivalent to the introduction of a ventilation velocity.

## APPENDIX A

### AIR DRIVE MEASUREMENTS

Figure A-1 is a plot of the motor setting in microamperes, i.e., a measure of the regulated d.c. current to the servo motor which drives the shaded pole blower fan, versus the shaft speed of the motor, i.e., motor speed in RPM. The shaft speed of the motor was determined with a General Radio type 1538-A Strobotac electronic stroboscope. At low RPM the stroboscope calibration was not very accurate so there was some scatter in the experimental points at low motor settings.

Figure A-2 is a diagram showing the ventilation velocity in the working section of the chamber as a function of the motor setting in microamperes for one particular freezing of the water in the moisture conditioner, i.e., one static pressure. The bars on the experimental points in Fig. A-2 are not error bars. Rather, they denote the variability of the measured ventilation velocity, i.e., the magnitude of the turbulence, for that particular motor setting. Figure A-2 shows that the transition from laminar to turbulent flow occurred around  $40 \text{ cm s}^{-1}$  with a turbulence level of  $\pm 2.5 \text{ cm s}^{-1}$ .

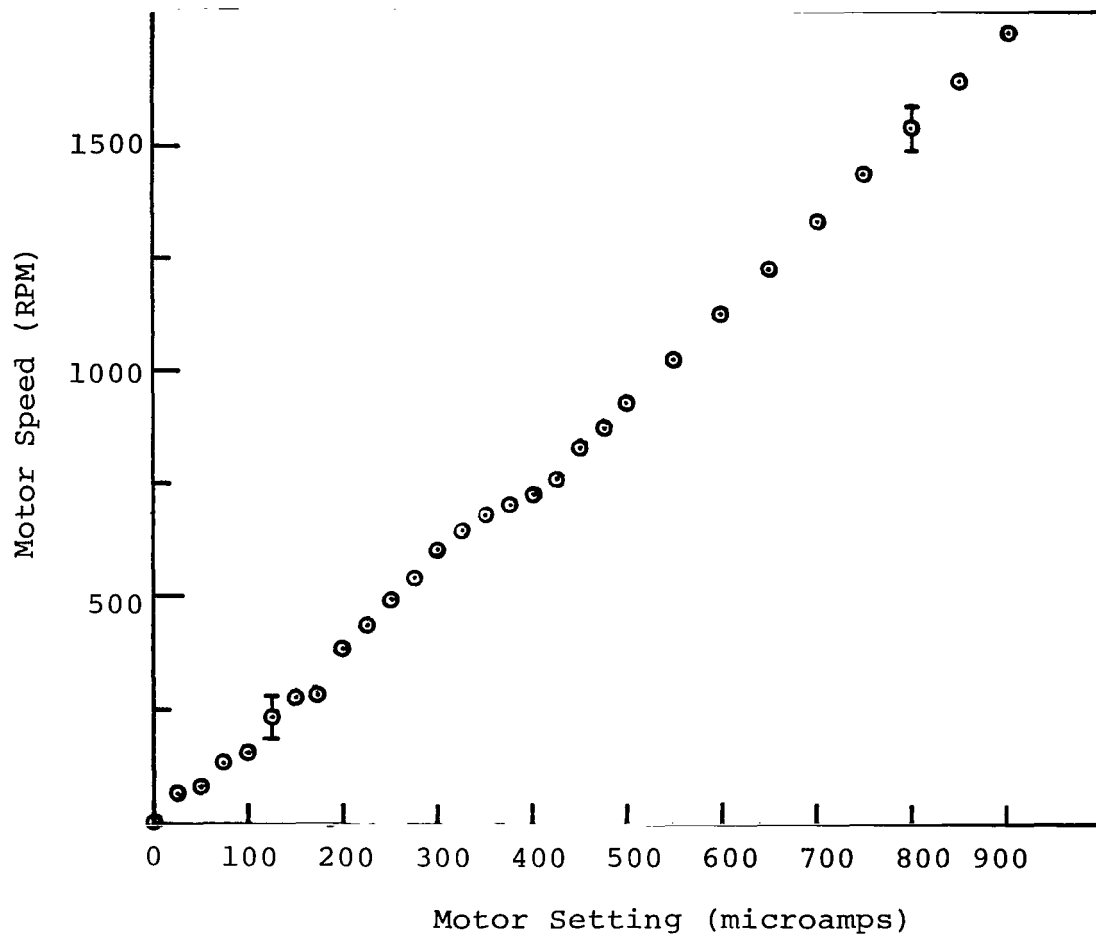


Fig. A-1 The air drive motor shaft speed is directly proportional to the d.c. current which is supplied to the servo motor.

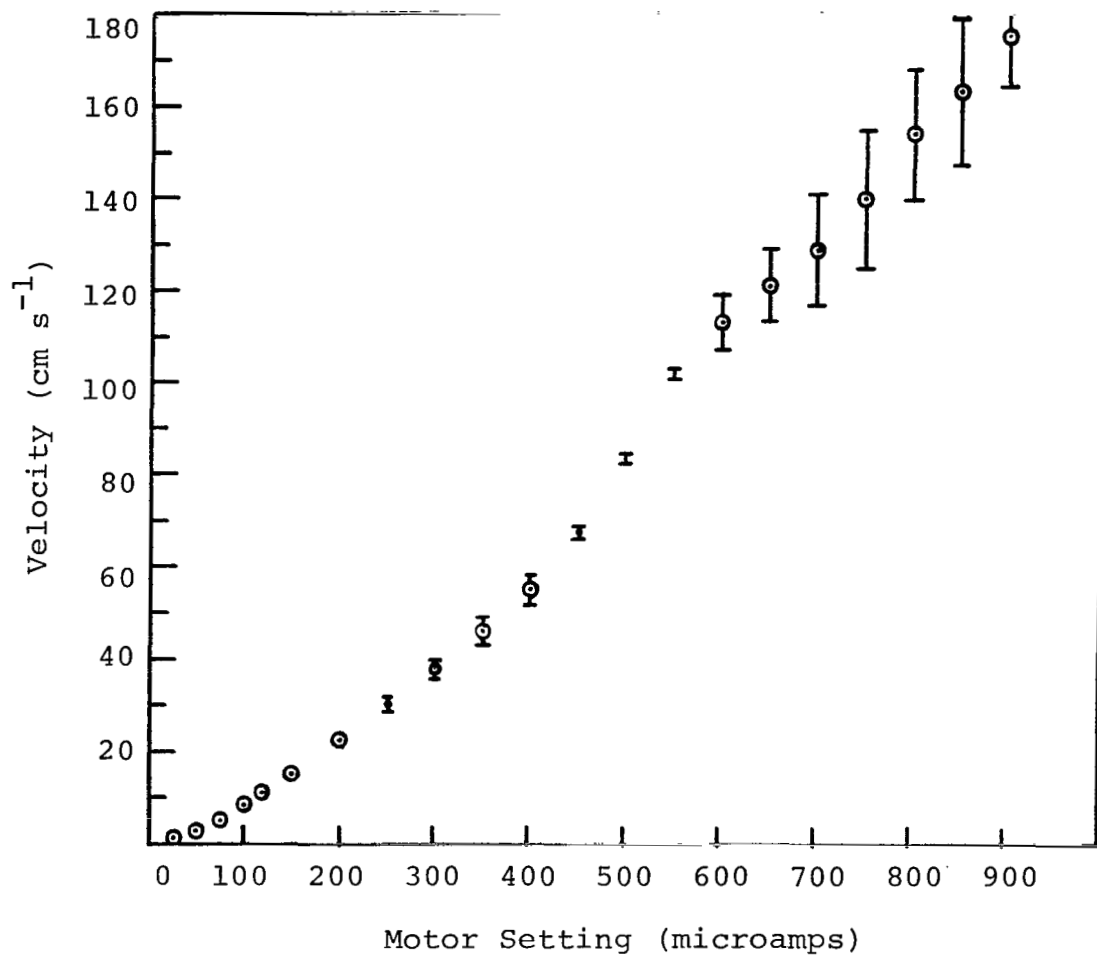


Fig. A-2 The ventilation velocity in the working section of the chamber is directly proportional to the d.c. current which is supplied to the servo motor.

## APPENDIX B

### WATER VAPOR TABLES

Tables B-I and B-II give, respectively, the saturated vapor pressure in millibars over plane ice and water surfaces as a function of temperature in degrees Celsius. Tables B-III and B-IV give, respectively, the saturated vapor density in  $\text{g m}^{-3}$  over plane ice and water surfaces as a function of temperature in degrees Celsius. The values in these four tables were obtained by evaluating the Goff-Gratch equations at  $0.1^{\circ}\text{C}$  temperature increments, taking into account through a compressibility factor the deviation of water vapor from the ideal gas law. The value in making computations at  $0.1^{\circ}\text{C}$  temperature increments, rather than at  $0.5^{\circ}\text{C}$  increments and interpolating, lies mainly in internal consistency resulting in smoother calculated supersaturation curves, i.e., Figs. 4.12 and 4.13.

No completely satisfactory formula exists for the vapor pressure over liquid water at temperatures below  $0^{\circ}\text{C}$ . However, direct extrapolation of the Goff-Gratch formulation gives values of the saturated vapor pressure with respect to water in the middle of the range suggested by other experimental investigators. Therefore, this formulation was adopted in Resolution 164 of the Twelfth Conference of Directors of the International Meteorological Organization (Washington, 1947) for the range  $0^{\circ}\text{C}$  to  $-50^{\circ}\text{C}$  pending further research.

Table B-V gives the percent supersaturation with respect to a plane ice surface at which water saturation occurs as a function of temperature in degrees Celsius.

Table B-I

## SATURATION VAPOR PRESSURE OVER ICE

TEMP(C)	.0	.1	.2	.3	.4	.5	.6	.7	.8	.9
UNIT	MM	MM	MM	MM	MM	MM	MM	MM	MM	MM
-0.0	6.107	6.057	6.007	5.954	5.909	5.860	5.812	5.764	5.717	5.664
-1.0	5.623	5.576	5.530	5.484	5.439	5.394	5.349	5.305	5.261	5.217
-2.0	5.173	5.130	5.089	5.045	5.003	4.961	4.920	4.879	4.839	4.797
-3.0	4.757	4.717	4.678	4.638	4.599	4.561	4.522	4.484	4.446	4.409
-4.0	4.372	4.335	4.298	4.262	4.225	4.190	4.154	4.119	4.084	4.049
-5.0	4.015	3.980	3.947	3.913	3.879	3.846	3.813	3.781	3.749	3.716
-6.0	3.695	3.653	3.622	3.590	3.560	3.529	3.499	3.468	3.439	3.409
-7.0	3.379	3.350	3.321	3.292	3.264	3.236	3.208	3.180	3.152	3.125
-8.0	3.097	3.070	3.044	3.017	2.991	2.965	2.939	2.913	2.888	2.862
-9.0	2.837	2.812	2.788	2.763	2.739	2.715	2.691	2.667	2.644	2.620
-10.0	2.597	2.574	2.551	2.529	2.506	2.484	2.462	2.440	2.418	2.397
-11.0	2.376	2.354	2.333	2.313	2.292	2.271	2.251	2.231	2.211	2.191
-12.0	2.172	2.152	2.133	2.114	2.094	2.076	2.057	2.038	2.020	2.002
-13.0	1.944	1.966	1.938	1.930	1.913	1.895	1.878	1.861	1.844	1.827
-14.0	1.811	1.794	1.778	1.762	1.745	1.730	1.714	1.698	1.682	1.667
-15.0	1.652	1.636	1.621	1.607	1.592	1.577	1.563	1.548	1.534	1.520
-16.0	1.506	1.492	1.478	1.464	1.450	1.437	1.424	1.410	1.397	1.384
-17.0	1.371	1.359	1.346	1.333	1.321	1.308	1.296	1.284	1.272	1.260
-18.0	1.248	1.236	1.225	1.213	1.202	1.190	1.179	1.168	1.157	1.146
-19.0	1.135	1.124	1.114	1.103	1.093	1.082	1.072	1.062	1.052	1.042
-20.0	1.0317	1.0219	1.0121	1.0024	.9928	.9833	.9739	.9645	.9552	.9461
-21.0	.9379	.9279	.9190	.9101	.9013	.8926	.8840	.8754	.8670	.8586
-22.0	.8502	.8420	.8338	.8257	.8177	.8097	.8018	.7943	.7862	.7785
-23.0	.7709	.7634	.7559	.7485	.7412	.7339	.7267	.7195	.7124	.7054
-24.0	.6995	.6936	.6878	.6820	.6763	.6705	.6646	.6581	.6515	.6451
-25.0	.6323	.6266	.6210	.6153	.6095	.6035	.5975	.5915	.5856	.5797
-26.0	.5720	.5663	.5606	.5549	.5494	.5438	.5384	.5329	.5276	.5223
-27.0	.5170	.5118	.5066	.5015	.4964	.4913	.4864	.4814	.4765	.4717
-28.0	.4669	.4621	.4574	.4527	.4481	.4435	.4390	.4345	.4301	.4256
-29.0	.4213	.4169	.4127	.4084	.4042	.4000	.3959	.3918	.3878	.3839
-30.0	.3794	.3759	.3720	.3681	.3643	.3605	.3568	.3531	.3494	.3457
-31.0	.3421	.3386	.3350	.3315	.3280	.3246	.3212	.3178	.3145	.3112
-32.0	.3079	.3047	.3015	.2983	.2951	.2920	.2889	.2859	.2829	.2799
-33.0	.2763	.2739	.2710	.2682	.2653	.2625	.2597	.2569	.2542	.2515
-34.0	.2488	.2461	.2435	.2409	.2383	.2357	.2332	.2307	.2282	.2257
-35.0	.2233	.2209	.2185	.2161	.2138	.2115	.2092	.2069	.2047	.2025
-36.0	.2002	.1981	.1959	.1938	.1917	.1896	.1875	.1854	.1834	.1814
-37.0	.1794	.1774	.1755	.1736	.1717	.1698	.1679	.1660	.1642	.1624
-38.0	.1606	.1588	.1571	.1553	.1536	.1519	.1502	.1485	.1469	.1452
-39.0	.1436	.1420	.1404	.1389	.1373	.1358	.1343	.1327	.1313	.1299
-40.0	.1293	.1279	.1265	.1254	.1240	.1226	.1212	.1199	.1185	.1172
-41.0	.1145	.1132	.1120	.1107	.1094	.1082	.1069	.1057	.1045	.1033
-42.0	.10213	.10096	.09981	.09866	.09753	.09641	.09530	.09420	.09312	.09204
-43.0	.09098	.08993	.08889	.08786	.08685	.08584	.08484	.08386	.08288	.08192
-44.0	.08097	.08002	.07909	.07817	.07725	.07635	.07546	.07457	.07370	.07284
-45.0	.07198	.07113	.07030	.06947	.06865	.06784	.06704	.06625	.06547	.06469
-46.0	.06393	.06317	.06242	.06168	.06094	.06022	.05950	.05879	.05809	.05740
-47.0	.05671	.05603	.05536	.05470	.05405	.05340	.05276	.05212	.05149	.05087
-48.0	.045026	.04435	.04368	.04302	.04237	.04173	.04109	.04046	.03983	.03920
-49.0	.04449	.04386	.04323	.04260	.04197	.04134	.04071	.04008	.03945	.03884
-50.0	.03935	.03874	.03813	.03751	.03690	.03629	.03568	.03507	.03446	.03386
-51.0	.03476	.03417	.03358	.03299	.03240	.03181	.03122	.03063	.03004	.02945
-52.0	.03067	.03009	.02951	.02893	.02835	.02777	.02719	.02661	.02603	.02545
-53.0	.02703	.02646	.02589	.02531	.02474	.02417	.02360	.02303	.02246	.02189
-54.0	.02340	.02284	.02228	.02171	.02115	.02059	.02003	.01947	.01891	.01835
-55.0	.01879	.01824	.01769	.01714	.01659	.01604	.01549	.01494	.01439	.01384
-56.0	.01429	.01375	.01320	.01265	.01210	.01155	.01100	.01045	.00990	.00935
-57.0	.011612	.01107	.01053	.01000	.00946	.00892	.00838	.00784	.00730	.00676
-58.0	.011413	.01088	.01035	.00982	.00929	.00876	.00823	.00770	.00717	.00664
-59.0	.011236	.01071	.01019	.00966	.00914	.00861	.00809	.00756	.00704	.00651

Table B-II

## SATURATION VAPOR PRESSURE OVER WATER

TEMP(C)	.0	.1	.2	.3	.4	.5	.6	.7	.8	.9
UNIT	MM	MM	MM	MM	MM	MM	MM	MM	MM	MM
-0.0	6.1178	6.0636	6.0196	5.9759	5.9325	5.8894	5.8466	5.8040	5.7618	5.7198
-1.0	5.6780	5.6366	5.5954	5.5544	5.5138	5.4734	5.4332	5.3934	5.3537	5.3144
-2.0	5.2753	5.2364	5.1979	5.1595	5.1214	5.0835	5.0460	5.0087	4.9716	4.9347
-3.0	4.8981	4.8617	4.8256	4.7897	4.7541	4.7187	4.6835	4.6485	4.6138	4.5793
-4.0	4.5451	4.5111	4.4773	4.4437	4.4103	4.3772	4.3443	4.3116	4.2791	4.2467
-5.0	4.2144	4.1830	4.1514	4.1200	4.0888	4.0579	4.0271	3.9966	3.9662	3.9351
-6.0	3.9061	3.8764	3.8469	3.8175	3.7884	3.7594	3.7307	3.7022	3.6733	3.6447
-7.0	3.6177	3.5899	3.5623	3.5349	3.5077	3.4807	3.4539	3.4272	3.4008	3.3745
-8.0	3.3484	3.3224	3.2967	3.2711	3.2457	3.2205	3.1955	3.1706	3.1459	3.1214
-9.0	3.0371	3.0129	3.0049	3.00250	3.0013	2.9774	2.9545	2.9313	2.9083	2.8854
-10.0	2.8627	2.8402	2.8178	2.7955	2.7735	2.7516	2.7298	2.7082	2.6867	2.6654
-11.0	2.6443	2.6233	2.6024	2.5817	2.5612	2.5408	2.5205	2.5004	2.4804	2.4606
-12.0	2.4409	2.4213	2.4019	2.3826	2.3635	2.3445	2.3256	2.3069	2.2883	2.2699
-13.0	2.2515	2.2334	2.2153	2.1974	2.1796	2.1619	2.1444	2.1269	2.1097	2.0925
-14.0	2.0755	2.0585	2.0417	2.0251	2.0085	1.9921	1.9758	1.9596	1.9436	1.9276
-15.0	1.9118	1.8961	1.8805	1.8650	1.8496	1.8343	1.8192	1.8042	1.7893	1.7744
-16.0	1.7597	1.7451	1.7307	1.7163	1.7020	1.6879	1.6738	1.6599	1.6460	1.6323
-17.0	1.6186	1.6051	1.5916	1.5783	1.5651	1.5519	1.5389	1.5260	1.5131	1.5004
-18.0	1.4777	1.4652	1.4527	1.4403	1.4281	1.4159	1.4038	1.3919	1.3799	1.3671
-19.0	1.3664	1.3549	1.3437	1.3318	1.3204	1.3091	1.2979	1.2868	1.2758	1.2649
-20.0	1.2540	1.2432	1.2326	1.2219	1.2114	1.2010	1.1906	1.1803	1.1701	1.1600
-21.0	1.1500	1.1400	1.1301	1.1203	1.1106	1.1009	1.0914	1.0819	1.0724	1.0631
-22.0	1.0534	1.0446	1.0354	1.0264	1.0174	1.0084	.9996	.9908	.9821	.9734
-23.0	.9649	.9564	.9479	.9395	.9312	.9230	.9148	.9067	.8986	.8907
-24.0	.8827	.8749	.8671	.8594	.8517	.8441	.8365	.8291	.8216	.8143
-25.0	.8070	.7997	.7925	.7854	.7783	.7713	.7644	.7575	.7506	.7438
-26.0	.7371	.7304	.7238	.7172	.7107	.7042	.6978	.6915	.6852	.6789
-27.0	.6727	.6666	.6605	.6544	.6484	.6425	.6366	.6307	.6249	.6191
-28.0	.6134	.6078	.6022	.5966	.5911	.5856	.5802	.5748	.5695	.5642
-29.0	.5589	.5537	.5485	.5434	.5384	.5333	.5283	.5234	.5185	.5136
-30.0	.5094	.5040	.4993	.4946	.4899	.4853	.4807	.4762	.4717	.4672
-31.0	.4628	.4584	.4540	.4497	.4454	.4412	.4370	.4328	.4287	.4246
-32.0	.4205	.4165	.4125	.4086	.4046	.4007	.3969	.3931	.3893	.3855
-33.0	.3818	.3781	.3745	.3709	.3672	.3637	.3602	.3567	.3532	.3497
-34.0	.3463	.3430	.3396	.3363	.3330	.3297	.3265	.3233	.3201	.3170
-35.0	.3139	.3108	.3077	.3047	.3017	.2987	.2957	.2928	.2899	.2870
-36.0	.2842	.2814	.2786	.2758	.2730	.2703	.2676	.2649	.2623	.2597
-37.0	.2571	.2545	.2519	.2494	.2469	.2444	.2419	.2395	.2371	.2347
-38.0	.2323	.2299	.2276	.2253	.2230	.2207	.2185	.2163	.2141	.2119
-39.0	.2097	.2076	.2054	.2033	.2013	.1992	.1971	.1951	.1931	.1911
-40.0	.1891	.1872	.1853	.1833	.1814	.1796	.1777	.1758	.1740	.1722
-41.0	.1704	.1686	.1669	.1651	.1634	.1617	.1600	.1583	.1567	.1550
-42.0	.1534	.1518	.1502	.1486	.1470	.1455	.1439	.1424	.1409	.1394
-43.0	.1379	.1364	.1350	.1336	.1321	.1307	.1293	.1279	.1266	.1252
-44.0	.1239	.1225	.1212	.1199	.1186	.1174	.1161	.1148	.1136	.1124
-45.0	.1111	.1099	.1087	.1076	.1064	.1052	.1041	.1030	.1018	.1007
-46.0	.0998	.0985	.0974	.0963	.0953	.0942	.0932	.0922	.0911	.0901
-47.0	.0891	.0881	.0872	.0862	.0852	.0843	.0834	.0824	.0815	.0806
-48.0	.0797	.0788	.0779	.0771	.0762	.0753	.0745	.0737	.0728	.0720
-49.0	.0712	.0704	.0696	.0688	.0680	.0673	.0665	.0657	.0650	.0642
-50.0	.0636	.0628	.0621	.0614	.0607	.0600	.0593	.0586	.0579	.0573
-51.0	.0566	.0559	.0554	.0547	.0540	.0534	.0528	.0522	.0516	.0511
-52.0	.0504	.0498	.0492	.0486	.0481	.0475	.0469	.0464	.0459	.0453
-53.0	.0448	.0442	.0437	.0432	.0427	.0422	.0417	.0412	.0407	.0402
-54.0	.0398	.0393	.0388	.0383	.0379	.0374	.0369	.0365	.0361	.0357
-55.0	.0352	.0347	.0342	.0338	.0334	.0330	.0326	.0322	.0318	.0314
-56.0	.0312	.0308	.0305	.0301	.0297	.0294	.0290	.0286	.0283	.0279
-57.0	.0275	.0273	.0269	.0266	.0263	.0260	.0257	.0253	.0250	.0247
-58.0	.0244	.0242	.0239	.0236	.0233	.0230	.0227	.0223	.0220	.0217
-59.0	.0215	.0212	.0210	.0207	.0204	.0202	.0199	.0197	.0194	.0192

Table B-III

## DENSITY OF PURE WATER VAPOR AT SATURATION OVER ICE

TEMP(C)	.0	.1	.2	.3	.4	.5	.6	.7	.8	.9
UNIT	G/M 3	G/M 3	G/M 3	G/M 3	G/M 3	G/M 3	G/M 3	G/M 3	G/M 3	G/M 3
-0.0	4.847	4.809	4.771	4.734	4.696	4.659	4.623	4.586	4.550	4.514
-1.0	4.479	4.443	4.408	4.373	4.339	4.304	4.270	4.236	4.203	4.169
-2.0	4.136	4.103	4.070	4.038	4.006	3.974	3.942	3.910	3.879	3.848
-3.0	3.817	3.787	3.756	3.726	3.696	3.666	3.637	3.608	3.578	3.550
-4.0	3.521	3.492	3.464	3.436	3.408	3.381	3.353	3.326	3.299	3.272
-5.0	3.246	3.219	3.193	3.167	3.141	3.115	3.090	3.065	3.039	3.015
-6.0	2.990	2.965	2.941	2.917	2.893	2.869	2.845	2.822	2.799	2.775
-7.0	2.733	2.710	2.687	2.665	2.643	2.620	2.614	2.592	2.575	2.554
-8.0	2.532	2.510	2.489	2.470	2.449	2.428	2.408	2.388	2.368	2.348
-9.0	2.328	2.309	2.291	2.275	2.251	2.232	2.213	2.195	2.176	2.154
-10.0	2.189	2.171	2.153	2.137	2.121	2.105	2.086	2.115	2.198	2.181
-11.0	1.964	1.947	1.931	1.914	1.898	1.882	1.865	1.849	1.834	1.818
-12.0	1.802	1.787	1.771	1.756	1.741	1.726	1.711	1.696	1.682	1.667
-13.0	1.653	1.639	1.624	1.610	1.596	1.581	1.567	1.555	1.541	1.524
-14.0	1.514	1.501	1.488	1.475	1.462	1.449	1.437	1.424	1.411	1.399
-15.0	1.387	1.374	1.362	1.350	1.338	1.327	1.315	1.303	1.292	1.280
-16.0	1.269	1.258	1.246	1.235	1.224	1.214	1.203	1.192	1.181	1.171
-17.0	1.169	1.159	1.149	1.139	1.129	1.109	1.099	1.099	1.080	1.073
-18.0	1.0603	1.0507	1.0412	1.0318	1.0225	1.0132	1.0041	1.0041	1.0041	1.0041
-19.0	.8691	.8593	.8498	.8404	.8312	.8221	.8131	.8041	.8041	.8041
-20.0	.8833	.8736	.8641	.8548	.8456	.8364	.8273	.8183	.8093	.8003
-21.0	.8352	.8256	.8161	.8068	.7976	.7885	.7794	.7704	.7614	.7524
-22.0	.7336	.7246	.7156	.7066	.6976	.6886	.6796	.6706	.6616	.6526
-23.0	.6679	.6589	.6500	.6410	.6320	.6230	.6140	.6050	.5960	.5870
-24.0	.6375	.6285	.6195	.6105	.6015	.5925	.5835	.5745	.5655	.5565
-25.0	.5522	.5432	.5342	.5252	.5162	.5072	.4982	.4892	.4802	.4712
-26.0	.5015	.4925	.4835	.4745	.4655	.4565	.4475	.4385	.4295	.4205
-27.0	.4551	.4461	.4371	.4281	.4191	.4101	.4011	.3921	.3831	.3741
-28.0	.4127	.4037	.3947	.3857	.3767	.3677	.3587	.3497	.3407	.3317
-29.0	.3739	.3649	.3559	.3469	.3379	.3289	.3199	.3109	.3019	.2929
-30.0	.3385	.3295	.3205	.3115	.3025	.2935	.2845	.2755	.2665	.2575
-31.0	.3062	.2972	.2882	.2792	.2702	.2612	.2522	.2432	.2342	.2252
-32.0	.2767	.2677	.2587	.2497	.2407	.2317	.2227	.2137	.2047	.1957
-33.0	.2498	.2408	.2318	.2228	.2138	.2048	.1958	.1868	.1778	.1688
-34.0	.2254	.2164	.2074	.1984	.1894	.1804	.1714	.1624	.1534	.1444
-35.0	.2032	.1942	.1852	.1762	.1672	.1582	.1492	.1402	.1312	.1222
-36.0	.1830	.1740	.1650	.1560	.1470	.1380	.1290	.1200	.1110	.1020
-37.0	.1646	.1556	.1466	.1376	.1286	.1196	.1106	.1016	.0926	.0836
-38.0	.1480	.1390	.1300	.1210	.1120	.1030	.0940	.0850	.0760	.0670
-39.0	.1329	.1239	.1149	.1059	.0969	.0879	.0789	.0699	.0609	.0519
-40.0	.1193	.1103	.1013	.0923	.0833	.0743	.0653	.0563	.0473	.0383
-41.0	.10690	.10573	.10458	.10343	.10230	.10119	.10007	.09897	.09788	.09680
-42.0	.09574	.09464	.09356	.09260	.09158	.09057	.08956	.08857	.08759	.08662
-43.0	.08565	.08470	.08376	.08283	.08190	.08099	.08009	.07919	.07830	.07743
-44.0	.07656	.07570	.07485	.07401	.07318	.07235	.07154	.07073	.06993	.06914
-45.0	.06836	.06759	.06682	.06606	.06531	.06457	.06384	.06311	.06239	.06169
-46.0	.06098	.06028	.05959	.05891	.05824	.05757	.05691	.05625	.05561	.05497
-47.0	.05434	.05371	.05309	.05248	.05187	.05127	.05068	.05009	.04951	.04894
-48.0	.04837	.04781	.04725	.04670	.04615	.04562	.04508	.04456	.04404	.04352
-49.0	.04301	.04251	.04201	.04151	.04102	.04054	.04006	.03959	.03912	.03866
-50.0	.03820	.03775	.03731	.03686	.03643	.03599	.03557	.03514	.03472	.03431
-51.0	.03390	.03350	.03309	.03270	.03231	.03192	.03154	.03116	.03078	.03041
-52.0	.03005	.02969	.02933	.02897	.02862	.02824	.02793	.02760	.02726	.02693
-53.0	.02660	.02628	.02596	.02564	.02533	.02502	.02472	.02441	.02411	.02382
-54.0	.02353	.02324	.02295	.02267	.02239	.02212	.02184	.02157	.02131	.02104
-55.0	.02078	.02053	.02027	.02002	.01977	.01952	.01924	.01899	.01874	.01850
-56.0	.01834	.01811	.01788	.01766	.01744	.01722	.01700	.01679	.01658	.01637
-57.0	.01616	.01596	.01576	.01556	.01536	.01516	.01497	.01478	.01459	.01441
-58.0	.01423	.01404	.01387	.01369	.01351	.01334	.01317	.01300	.01283	.01267
-59.0	.01251	.01235	.01219	.01203	.01188	.01172	.01157	.01142	.01127	.01112



Table B-IV

## DENSITY OF PURE WATER VAPOR AT SATURATION OVER WATER

TEMP(C)	.0	.1	.2	.3	.4	.5	.6	.7	.8	.9
UNIT	G/M <sup>3</sup>	G/M <sup>3</sup>	G/M <sup>3</sup>	G/M <sup>3</sup>	G/M <sup>3</sup>	G/M <sup>3</sup>	G/M <sup>3</sup>	G/M <sup>3</sup>	G/M <sup>3</sup>	G/M <sup>3</sup>
-0.0	4.847	4.814	4.781	4.748	4.715	4.683	4.650	4.618	4.586	4.554
-1.0	4.523	4.491	4.460	4.429	4.398	4.368	4.337	4.307	4.277	4.247
-2.0	4.218	4.188	4.159	4.130	4.101	4.072	4.043	4.015	3.986	3.958
-3.0	3.930	3.903	3.875	3.848	3.821	3.793	3.767	3.740	3.713	3.687
-4.0	3.661	3.635	3.609	3.583	3.557	3.532	3.507	3.482	3.457	3.432
-5.0	3.407	3.383	3.359	3.334	3.310	3.287	3.263	3.239	3.216	3.193
-6.0	3.170	3.147	3.124	3.101	3.079	3.056	3.034	3.012	2.990	2.968
-7.0	2.947	2.925	2.904	2.882	2.861	2.840	2.820	2.799	2.778	2.758
-8.0	2.734	2.717	2.697	2.677	2.658	2.638	2.619	2.599	2.580	2.561
-9.0	2.542	2.523	2.504	2.485	2.467	2.448	2.430	2.412	2.394	2.376
-10.0	2.359	2.341	2.323	2.305	2.288	2.271	2.253	2.236	2.220	2.203
-11.0	2.186	2.170	2.153	2.137	2.121	2.105	2.089	2.073	2.057	2.041
-12.0	2.026	2.010	1.995	1.980	1.965	1.950	1.935	1.920	1.905	1.890
-13.0	1.876	1.861	1.847	1.833	1.819	1.805	1.791	1.777	1.763	1.749
-14.0	1.736	1.722	1.709	1.696	1.682	1.669	1.656	1.643	1.630	1.618
-15.0	1.605	1.593	1.580	1.568	1.555	1.543	1.531	1.519	1.507	1.495
-16.0	1.483	1.471	1.460	1.448	1.437	1.425	1.414	1.403	1.392	1.381
-17.0	1.370	1.359	1.348	1.337	1.326	1.316	1.305	1.295	1.284	1.274
-18.0	1.264	1.254	1.243	1.233	1.223	1.214	1.204	1.194	1.184	1.175
-19.0	1.165	1.156	1.146	1.137	1.128	1.119	1.109	1.101	1.091	1.082
-20.0	1.0736	1.0649	1.0559	1.0473	1.0387	1.0301	1.0216	1.0132	1.0049	.9966
-21.0	.9883	.9802	.9720	.9640	.9560	.9481	.9402	.9324	.9246	.9169
-22.0	.9092	.9017	.8941	.8866	.8792	.8719	.8646	.8573	.8501	.8429
-23.0	.8359	.8288	.8218	.8149	.8080	.8012	.7944	.7877	.7810	.7744
-24.0	.7677	.7613	.7544	.7484	.7420	.7356	.7294	.7231	.7169	.7109
-25.0	.7047	.6987	.6927	.6867	.6808	.6749	.6691	.6633	.6576	.6519
-26.0	.6463	.6407	.6351	.6296	.6242	.6187	.6134	.6080	.6027	.5975
-27.0	.5922	.5871	.5819	.5768	.5718	.5668	.5618	.5568	.5519	.5471
-28.0	.5423	.5375	.5327	.5280	.5233	.5187	.5141	.5096	.5050	.5005
-29.0	.4961	.4917	.4873	.4829	.4786	.4743	.4701	.4659	.4617	.4576
-30.0	.4535	.4494	.4453	.4413	.4373	.4334	.4295	.4256	.4217	.4179
-31.0	.4141	.4104	.4066	.4029	.3993	.3956	.3920	.3884	.3849	.3814
-32.0	.3770	.3744	.3710	.3676	.3642	.3609	.3575	.3542	.3510	.3477
-33.0	.3445	.3413	.3382	.3350	.3319	.3288	.3258	.3228	.3198	.3168
-34.0	.3138	.3109	.3080	.3051	.3022	.2994	.2966	.2938	.2910	.2883
-35.0	.2856	.2829	.2802	.2776	.2749	.2723	.2697	.2672	.2646	.2621
-36.0	.2596	.2572	.2547	.2523	.2499	.2475	.2451	.2428	.2404	.2381
-37.0	.2359	.2336	.2313	.2291	.2269	.2247	.2225	.2204	.2183	.2161
-38.0	.2140	.2120	.2099	.2079	.2058	.2037	.2018	.1999	.1979	.1960
-39.0	.1941	.1922	.1903	.1884	.1865	.1847	.1829	.1811	.1793	.1775
-40.0	.1750	.1740	.1723	.1706	.1689	.1672	.1656	.1639	.1623	.1607
-41.0	.1591	.1575	.1559	.1543	.1528	.1512	.1497	.1482	.1467	.1452
-42.0	.1434	.1423	.1409	.1395	.1380	.1366	.1353	.1339	.1325	.1312
-43.0	.1298	.1285	.1272	.1259	.1246	.1233	.1221	.1208	.1196	.1183
-44.0	.1171	.1159	.1147	.1135	.1124	.1112	.1101	.1089	.1078	.1067
-45.0	.10555	.10445	.10336	.10228	.10122	.10016	.9911	.9807	.9704	.9603
-46.0	.09502	.09402	.09303	.09205	.09108	.09011	.08915	.08822	.08728	.08636
-47.0	.08544	.08451	.08363	.08274	.08186	.08099	.08012	.07927	.07842	.07758
-48.0	.07655	.07592	.07511	.07430	.07350	.07271	.07192	.07115	.07038	.06961
-49.0	.06486	.06411	.06337	.06264	.06192	.06120	.06049	.05979	.05909	.05839
-50.0	.06171	.06104	.06037	.05970	.05905	.05840	.05775	.05712	.05649	.05586
-51.0	.05524	.05463	.05403	.05343	.05283	.05224	.05166	.05109	.05052	.04995
-52.0	.04939	.04884	.04829	.04775	.04722	.04669	.04616	.04564	.04513	.04462
-53.0	.04411	.04361	.04312	.04263	.04215	.04167	.04119	.04072	.04026	.03980
-54.0	.03935	.03890	.03845	.03801	.03757	.03714	.03672	.03629	.03588	.03546
-55.0	.03505	.03465	.03425	.03385	.03346	.03307	.03268	.03230	.03193	.03156
-56.0	.03119	.03092	.03064	.03031	.02997	.02964	.02930	.02897	.02864	.02831
-57.0	.02771	.02739	.02706	.02674	.02642	.02611	.02580	.02549	.02519	.02489
-58.0	.02459	.02430	.02401	.02372	.02344	.02316	.02288	.02261	.02233	.02206
-59.0	.02180	.02153	.02127	.02101	.02076	.02051	.02026	.02001	.01977	.01953

Table B-V

PERCENT S.S. W.R.T. ICE AT WHICH WATER SATURATION OCCURS

TEMP(C)	.0	.1	.2	.3	.4	.5	.6	.7	.8	.9
-0.0	.011	.108	.205	.303	.400	.497	.595	.692	.790	.888
-1.0	.09	1.09	1.184	1.279	1.374	1.468	1.562	1.657	1.751	1.845
-2.0	1.97	2.07	2.167	2.257	2.347	2.437	2.527	2.617	2.707	2.797
-3.0	2.86	3.07	3.17	3.267	3.357	3.447	3.537	3.627	3.717	3.807
-4.0	3.97	4.07	4.17	4.267	4.357	4.447	4.537	4.627	4.717	4.807
-5.0	4.99	5.09	5.19	5.289	5.379	5.468	5.558	5.648	5.738	5.828
-6.0	6.01	6.12	6.22	6.312	6.402	6.492	6.582	6.672	6.762	6.852
-7.0	7.05	7.16	7.26	7.356	7.446	7.536	7.626	7.716	7.806	7.896
-8.0	8.10	8.21	8.31	8.404	8.494	8.584	8.674	8.764	8.854	8.944
-9.0	9.16	9.27	9.37	9.468	9.558	9.648	9.738	9.828	9.918	10.008
-10.0	10.2	10.3	10.4	10.5	10.6	10.7	10.8	10.9	11.0	11.1
-11.0	11.1	11.2	11.3	11.4	11.5	11.6	11.7	11.8	11.9	12.0
-12.0	12.1	12.2	12.3	12.4	12.5	12.6	12.7	12.8	12.9	13.0
-13.0	13.1	13.2	13.3	13.4	13.5	13.6	13.7	13.8	13.9	14.0
-14.0	14.1	14.2	14.3	14.4	14.5	14.6	14.7	14.8	14.9	15.0
-15.0	15.1	15.2	15.3	15.4	15.5	15.6	15.7	15.8	15.9	16.0
-16.0	16.1	16.2	16.3	16.4	16.5	16.6	16.7	16.8	16.9	17.0
-17.0	17.1	17.2	17.3	17.4	17.5	17.6	17.7	17.8	17.9	18.0
-18.0	18.1	18.2	18.3	18.4	18.5	18.6	18.7	18.8	18.9	19.0
-19.0	19.1	19.2	19.3	19.4	19.5	19.6	19.7	19.8	19.9	20.0
-20.0	20.1	20.2	20.3	20.4	20.5	20.6	20.7	20.8	20.9	21.0
-21.0	21.1	21.2	21.3	21.4	21.5	21.6	21.7	21.8	21.9	22.0
-22.0	22.1	22.2	22.3	22.4	22.5	22.6	22.7	22.8	22.9	23.0
-23.0	23.1	23.2	23.3	23.4	23.5	23.6	23.7	23.8	23.9	24.0
-24.0	24.1	24.2	24.3	24.4	24.5	24.6	24.7	24.8	24.9	25.0
-25.0	25.1	25.2	25.3	25.4	25.5	25.6	25.7	25.8	25.9	26.0
-26.0	26.1	26.2	26.3	26.4	26.5	26.6	26.7	26.8	26.9	27.0
-27.0	27.1	27.2	27.3	27.4	27.5	27.6	27.7	27.8	27.9	28.0
-28.0	28.1	28.2	28.3	28.4	28.5	28.6	28.7	28.8	28.9	29.0
-29.0	29.1	29.2	29.3	29.4	29.5	29.6	29.7	29.8	29.9	30.0
-30.0	30.1	30.2	30.3	30.4	30.5	30.6	30.7	30.8	30.9	31.0
-31.0	31.1	31.2	31.3	31.4	31.5	31.6	31.7	31.8	31.9	32.0
-32.0	32.1	32.2	32.3	32.4	32.5	32.6	32.7	32.8	32.9	33.0
-33.0	33.1	33.2	33.3	33.4	33.5	33.6	33.7	33.8	33.9	34.0
-34.0	34.1	34.2	34.3	34.4	34.5	34.6	34.7	34.8	34.9	35.0
-35.0	35.1	35.2	35.3	35.4	35.5	35.6	35.7	35.8	35.9	36.0
-36.0	36.1	36.2	36.3	36.4	36.5	36.6	36.7	36.8	36.9	37.0
-37.0	37.1	37.2	37.3	37.4	37.5	37.6	37.7	37.8	37.9	38.0
-38.0	38.1	38.2	38.3	38.4	38.5	38.6	38.7	38.8	38.9	39.0
-39.0	39.1	39.2	39.3	39.4	39.5	39.6	39.7	39.8	39.9	40.0
-40.0	40.1	40.2	40.3	40.4	40.5	40.6	40.7	40.8	40.9	41.0
-41.0	41.1	41.2	41.3	41.4	41.5	41.6	41.7	41.8	41.9	42.0
-42.0	42.1	42.2	42.3	42.4	42.5	42.6	42.7	42.8	42.9	43.0
-43.0	43.1	43.2	43.3	43.4	43.5	43.6	43.7	43.8	43.9	44.0
-44.0	44.1	44.2	44.3	44.4	44.5	44.6	44.7	44.8	44.9	45.0
-45.0	45.1	45.2	45.3	45.4	45.5	45.6	45.7	45.8	45.9	46.0
-46.0	46.1	46.2	46.3	46.4	46.5	46.6	46.7	46.8	46.9	47.0
-47.0	47.1	47.2	47.3	47.4	47.5	47.6	47.7	47.8	47.9	48.0
-48.0	48.1	48.2	48.3	48.4	48.5	48.6	48.7	48.8	48.9	49.0
-49.0	49.1	49.2	49.3	49.4	49.5	49.6	49.7	49.8	49.9	50.0
-50.0	50.1	50.2	50.3	50.4	50.5	50.6	50.7	50.8	50.9	51.0
-51.0	51.1	51.2	51.3	51.4	51.5	51.6	51.7	51.8	51.9	52.0
-52.0	52.1	52.2	52.3	52.4	52.5	52.6	52.7	52.8	52.9	53.0
-53.0	53.1	53.2	53.3	53.4	53.5	53.6	53.7	53.8	53.9	54.0
-54.0	54.1	54.2	54.3	54.4	54.5	54.6	54.7	54.8	54.9	55.0
-55.0	55.1	55.2	55.3	55.4	55.5	55.6	55.7	55.8	55.9	56.0
-56.0	56.1	56.2	56.3	56.4	56.5	56.6	56.7	56.8	56.9	57.0
-57.0	57.1	57.2	57.3	57.4	57.5	57.6	57.7	57.8	57.9	58.0
-58.0	58.1	58.2	58.3	58.4	58.5	58.6	58.7	58.8	58.9	59.0
-59.0	59.1	59.2	59.3	59.4	59.5	59.6	59.7	59.8	59.9	60.0
-60.0	60.1	60.2	60.3	60.4	60.5	60.6	60.7	60.8	60.9	61.0
-61.0	61.1	61.2	61.3	61.4	61.5	61.6	61.7	61.8	61.9	62.0
-62.0	62.1	62.2	62.3	62.4	62.5	62.6	62.7	62.8	62.9	63.0
-63.0	63.1	63.2	63.3	63.4	63.5	63.6	63.7	63.8	63.9	64.0
-64.0	64.1	64.2	64.3	64.4	64.5	64.6	64.7	64.8	64.9	65.0
-65.0	65.1	65.2	65.3	65.4	65.5	65.6	65.7	65.8	65.9	66.0
-66.0	66.1	66.2	66.3	66.4	66.5	66.6	66.7	66.8	66.9	67.0
-67.0	67.1	67.2	67.3	67.4	67.5	67.6	67.7	67.8	67.9	68.0
-68.0	68.1	68.2	68.3	68.4	68.5	68.6	68.7	68.8	68.9	69.0
-69.0	69.1	69.2	69.3	69.4	69.5	69.6	69.7	69.8	69.9	70.0
-70.0	70.1	70.2	70.3	70.4	70.5	70.6	70.7	70.8	70.9	71.0
-71.0	71.1	71.2	71.3	71.4	71.5	71.6	71.7	71.8	71.9	72.0
-72.0	72.1	72.2	72.3	72.4	72.5	72.6	72.7	72.8	72.9	73.0
-73.0	73.1	73.2	73.3	73.4	73.5	73.6	73.7	73.8	73.9	74.0
-74.0	74.1	74.2	74.3	74.4	74.5	74.6	74.7	74.8	74.9	75.0

## APPENDIX C

### CALCULATION OF AMBIENT CONDITIONS

Table C-I gives specimen calculations of the specifications for the crystal growth environment for a chamber top plate temperature of  $-8.9^{\circ}\text{C}$  and a chamber bottom plate temperature of  $-22.1^{\circ}\text{C}$  using a linear vapor density profile between the plates. The column headings from left to right denote the following: TEMP (C) is the temperature in  $^{\circ}\text{C}$ , X (CM) is the height above the bottom plate in centimeters, TC (C) is the surface temperature in  $^{\circ}\text{C}$  of a growing ice crystal calculated from the conduction-diffusion equilibrium relationship for a static environment, DLT (C) is the difference in temperature in  $^{\circ}\text{C}$  between the ambient air and the calculated crystal surface temperature, TC (C), at a given height in the chamber, MVDX is the maximum vapor density excess in  $\text{g m}^{-3}$ , TVDXS is the 'true' vapor density excess over a growing crystal with a surface temperature, TC (C), VDICE and VDWAT are, respectively, the saturated vapor densities in  $\text{g m}^{-3}$  over a plane ice or water surface at the ambient temperature, SSICE and SSWAT are, respectively, the supersaturations in percent of the ambient environment with respect to a plane ice or water surface, WATSAT is the supersaturation with respect to ice at which water saturation occurs at that ambient temperature, and finally, XVDW is the vapor density difference in  $\text{g m}^{-3}$  between VDWAT and VDICE.

Figure C-1 is a diagram showing the calculated maximum vapor density excess,  $\Delta\rho_{\text{max}}$ , in  $\text{g m}^{-3}$  which occurs in the vertical middle of the chamber, i.e., at  $x = 1.25$  cm above the bottom plate, as a function of the top plate and midpoint of the chamber temperatures. The chamber

bottom plate temperature,  $T_{\text{bot}}$ , can be calculated from the equation

$$T_{\text{bot}} = 2 T_{\text{mid}} - T_{\text{top}}$$

where  $T_{\text{mid}}$  is the midpoint of the chamber temperature and  $T_{\text{top}}$  is the chamber top plate temperature. Thus, from Fig. C-1 the chamber top and bottom plate temperatures needed to produce any desired ambient conditions of temperature and vapor density excess at the vertical center of the chamber can be determined.

Table C-I Specimen Calculations of the Ambient Chamber Conditions.

TEMP(C)	X(ICM)	TC(C)	DLT(C)	MVDX	TVDXS	AMVDO	TRUVDG	VDICE	VDWAT	SSICE	SSWAT	WATSAI	AVDA
-8.90	2.51	-8.90	-0.00	0.00000	-0.00033	2.34810	2.34943	2.34910	2.56168	0.00	-8.30	9.05	.21294
-9.29	2.43	-9.24	.05	.02799	.01750	2.30041	2.28291	2.27242	2.49755	1.23	-7.52	9.47	.21513
-9.68	2.35	-9.57	.10	.05377	.03405	2.25273	2.21868	2.19196	2.41627	2.45	-6.77	9.83	.21731
-10.06	2.24	-9.91	.15	.07738	.04963	2.20504	2.15541	2.12766	2.34681	3.64	-6.04	10.30	.21914
-10.45	2.21	-10.26	.20	.09930	.06458	2.15736	2.09278	2.05906	2.27465	4.32	-5.32	10.72	.22059
-10.84	2.13	-10.61	.24	.11874	.07790	2.10967	2.03177	1.99993	2.21270	5.96	-4.66	11.14	.22177
-11.23	2.06	-10.96	.27	.13619	.09058	2.06198	1.97141	1.92579	2.14444	7.67	-4.02	11.56	.22254
-11.62	1.99	-11.31	.31	.15170	.10161	2.01430	1.91267	1.86260	2.08583	8.14	-3.43	11.99	.22323
-12.01	1.91	-11.67	.34	.16532	.11203	1.96661	1.85458	1.80130	2.02485	9.18	-2.88	12.41	.22395
-12.39	1.84	-12.03	.36	.17710	.12112	1.91893	1.79780	1.74183	1.96544	10.17	-2.37	12.84	.22361
-12.78	1.76	-12.39	.39	.18709	.12924	1.87124	1.74200	1.68416	1.90758	11.11	-1.91	13.27	.22343
-13.17	1.69	-12.76	.41	.19533	.13604	1.82356	1.68752	1.62822	1.85124	12.06	-1.50	13.70	.22312
-13.56	1.62	-13.13	.43	.20189	.14218	1.77587	1.63369	1.57394	1.79637	12.83	-1.14	14.13	.22239
-13.95	1.54	-13.51	.44	.20679	.14700	1.72819	1.58118	1.52139	1.74235	13.59	-.85	14.56	.22156
-14.34	1.47	-13.89	.45	.21009	.15050	1.68050	1.53000	1.47041	1.69094	14.29	-.62	15.00	.22054
-14.72	1.40	-14.27	.46	.21184	.15333	1.63281	1.47948	1.42098	1.64031	14.91	-.46	15.44	.21933
-15.11	1.32	-14.65	.46	.21206	.15484	1.58513	1.43029	1.37306	1.59103	15.44	-.37	15.87	.21797
-15.50	1.25	-15.04	.46	.21082	.15500	1.53744	1.38244	1.32663	1.54306	15.89	-.36	16.31	.21644
-15.89	1.18	-15.43	.46	.20813	.15450	1.48976	1.33526	1.28162	1.49639	16.24	-.44	16.76	.21476
-16.28	1.10	-15.82	.45	.20406	.15264	1.44207	1.28943	1.23801	1.45096	16.43	-.61	17.20	.21295
-16.66	1.03	-16.22	.45	.19963	.14979	1.39439	1.24460	1.19576	1.40677	16.61	-.88	17.65	.21131
-17.05	.96	-16.62	.43	.19188	.14590	1.34670	1.20080	1.15482	1.36377	16.62	-1.25	18.09	.20895
-17.44	.88	-17.02	.42	.18385	.14100	1.29901	1.15801	1.11516	1.32195	16.49	-1.73	18.54	.20678
-17.83	.81	-17.43	.40	.17458	.13475	1.25133	1.11658	1.07679	1.28126	16.21	-2.34	18.99	.20451
-18.22	.74	-17.84	.38	.16409	.12780	1.20364	1.07584	1.03955	1.24170	15.79	-3.06	19.45	.20215
-18.61	.66	-18.25	.35	.15244	.11949	1.15596	1.03647	1.00352	1.20322	15.19	-3.93	19.90	.19970
-18.99	.59	-18.67	.33	.13964	.11013	1.10827	.99814	.96463	1.16580	14.42	-4.93	20.36	.19717
-19.38	.51	-19.09	.30	.12573	.10008	1.06059	.96050	.93486	1.12982	13.45	-6.09	20.81	.19457
-19.77	.44	-19.51	.26	.11075	.08865	1.01290	.92425	.90215	1.09406	12.28	-7.42	21.27	.19190
-20.16	.37	-19.93	.22	.09471	.07617	.96521	.88904	.87050	1.05968	10.88	-8.91	21.73	.18918
-20.55	.29	-20.36	.19	.07779	.06298	.91753	.85454	.83974	1.02611	9.26	-10.58	22.19	.18638
-20.94	.22	-20.79	.14	.05975	.04874	.86984	.82110	.81009	.99365	7.38	-12.46	22.66	.18356
-21.32	.15	-21.23	.10	.04076	.03345	.82216	.78871	.78140	.96210	5.22	-14.55	23.12	.18070
-21.71	.07	-21.66	.05	.02083	.01708	.77447	.75739	.75364	.93144	2.76	-16.85	23.59	.17780
-22.10	0.00	-22.10	-.90	0.00000	-0.00034	.72679	.72713	.72679	.96166	0.60	-19.39	24.06	.17447

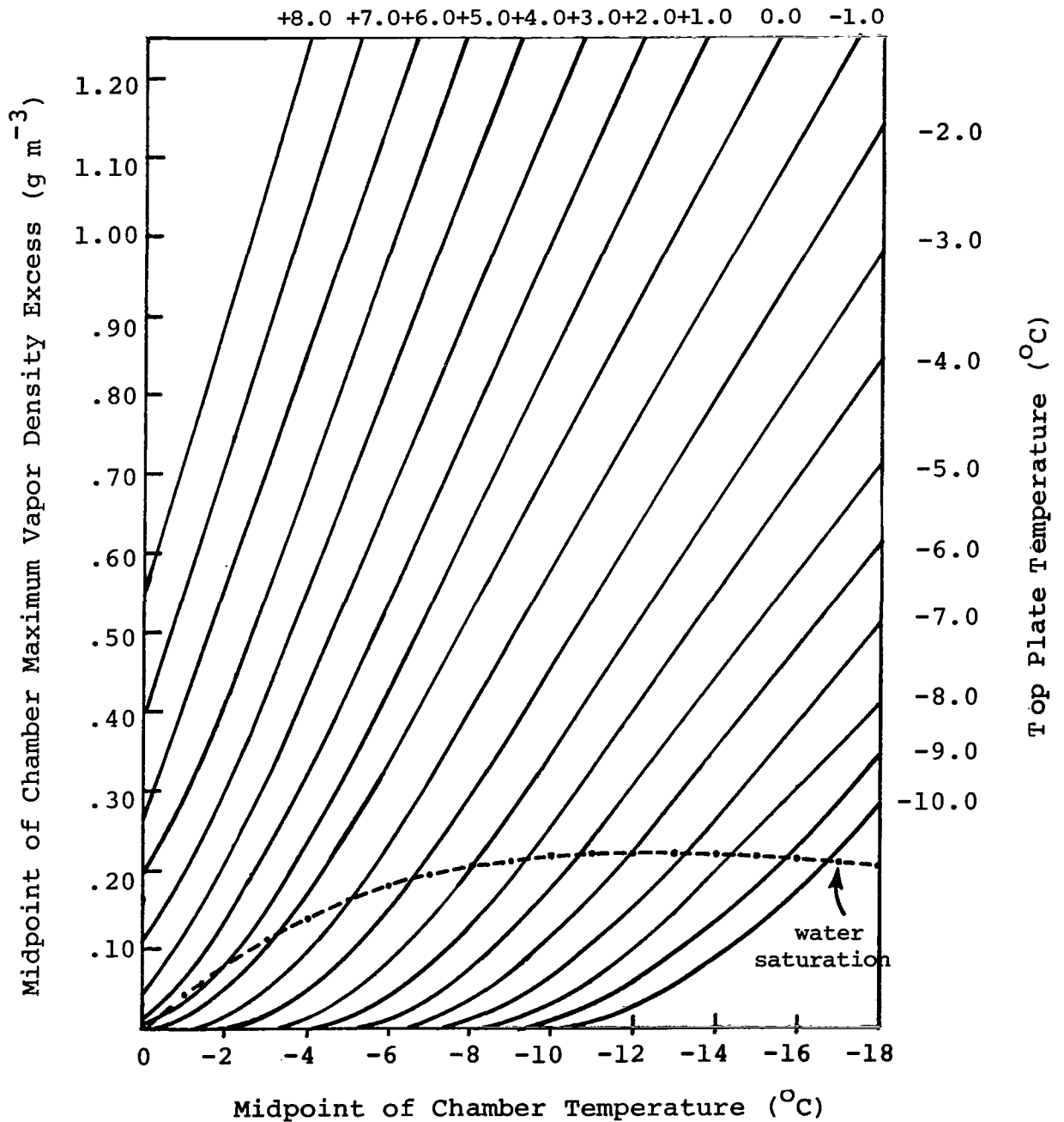


Fig. C-1 Calculated ambient crystal growth conditions at the chamber center can be determined for any pair of top and bottom plate temperatures.

## APPENDIX D

## RELATIVE MAGNITUDES OF HEAT TRANSFER

Heat transfer from a growing ice crystal surface takes place by conduction to the substrate, conduction to the air, convection to the air and radiation to the surroundings. The relative magnitudes of these terms were computed for this experiment.

I. Heat Transfer by Conduction

Heat transfer by conduction is calculated from the equation

$dQ/dt = -KA \, dT/dx$  where

$dQ/dt$  = Heat transferred per unit time

$K$  = Thermal conductivity of the heat transferring media

$A$  = Cross-sectional area through which heat transfer occurs

$dT/dx$  = Temperature gradient in the heat transferring media.

A. Heat Transfer by Conduction to the Substrate

The substrate in this case consisted of the vertical solid glass fiber from which the ice crystals grew. Thus, conduction to the substrate means conduction along the length of the ice crystal to the glass fiber. Since in this calculation the maximum heat transfer to the substrate is desired, the assumption is made that heat transferred to the fiber at the position of the base of the crystal is efficiently dissipated away. In actuality, the solid glass fiber was a poor heat conductor and was coated along its length with growing ice crystals, so the actual heat transfer by conduction to the substrate was probably somewhat less than that calculated.

The thermal conductivity of ice,  $K_{ice}$ , is given approximately by

$$K_{ice} \doteq 5 \times 10^{-3} \text{ cal cm}^{-1} \text{ s}^{-1} \text{ }^{\circ}\text{C}^{-1}.$$

For an ice crystal growing at an ambient supersaturation well above water saturation, the crystal tip may be a maximum of approximately  $1.0^{\circ}\text{C}$  warmer than either the ambient air or the glass fiber at that height in the chamber. Hence for an ice crystal 0.5 cm in length,  $dT/dx = 2^{\circ}\text{C cm}^{-1}$ . If the contact area of the crystal base is assumed to be as large as  $10^{-4} \text{ cm}^2$  then

$$dQ/dt = -1.0 \times 10^{-6} \text{ cal s}^{-1}.$$

#### B. Heat Transfer by Conduction to the Air

The thermal conductivity of air,  $K_{air}$ , is given approximately by

$$K_{air} \doteq 4.0 \times 10^{-5} \text{ cal cm}^{-1} \text{ s}^{-1} \text{ }^{\circ}\text{C}^{-1}.$$

If one assumes a temperature gradient near the crystal of  $dT/dx = \frac{1^{\circ}\text{C}}{0.1 \text{ cm}} = 10^{\circ}\text{C cm}^{-1}$  and assumes conduction takes place from both sides of a flat crystal of total surface area  $A = 2(1\text{mm})^2 = 2 \times 10^{-2} \text{ cm}^2$  then

$$dQ/dt = -8.0 \times 10^{-6} \text{ cal s}^{-1}.$$

## II. Heat Transfer by Convection

The equation employed in this study to calculate heat transfer by convection was the one used by Hall and Pruppacher (1976). That is,

$$dQ/dt = 4\pi CKF_{\alpha}(T_{\infty}-T_s)f_Q,$$

where



$$F_{\alpha} = \frac{r^*}{r^* + l_Q^*} \quad f_Q = \begin{cases} 1.00 + 0.14 (N_{Pr}^{1/3} N_{Re,L}^{1/2*})^2, & N_{Pr}^{1/3} N_{Re,L}^{1/2*} < 1.0 \\ 0.86 + 0.28 N_{Pr}^{1/3} N_{Re,L}^{1/2*}, & N_{Pr}^{1/3} N_{Re,L}^{1/2*} > 1.0 \end{cases}$$

$$l_Q^* = \frac{K f_Q}{\frac{1}{4} \rho_a \bar{v}_r \alpha C_p} \quad K = K_d [1 - (1.17 - 1.02 K_v K_d^{-1}) \rho_v \rho_a^{-1}]$$

$$r^* = S / (4\pi C) \quad K_d = (5.69 + 0.168T) \times 10^{-5} \text{ cal cm}^{-1} \text{ s}^{-1} \text{ } ^\circ\text{C}^{-1}$$

$$K_v = (3.73 + 0.020T) \times 10^{-5} \text{ cal cm}^{-1} \text{ s}^{-1} \text{ } ^\circ\text{C}^{-1}.$$

The individual parameters are defined in the following way:

$C \equiv$  capacitance =  $r$  for a spherical ice particle

$K \equiv$  thermal conductivity of moist air

$T_{\infty} \equiv$  environmental temperature

$T_s \equiv$  temperature at ice particles' surface

$f_Q \equiv$  heat ventilation factor

$S \equiv$  total surface area of ice particle

$\rho_a \equiv$  density of air

$\bar{v}_r \equiv$  average velocity of the air molecules striking the ice particles' surface =  $(8R_d T_s / \pi)^{1/2}$

$R_d \equiv$  specific gas constant for dry air

$\alpha \equiv$  thermal accommodation coefficient  $\doteq 1.0$

$C_p \equiv$  specific heat of moist air at constant pressure

$N_{Pr} \equiv$  Prandtl number  $[= \eta C_p / K] = 0.72$

$\eta \equiv$  dynamic viscosity of air  $[= 1.8325 \times 10^{-4} (T/296.16)^{1.5} (T+120)/(T+296.16)]$ , with  $T$  in  $^\circ\text{K}$

$N_{Re,L}^* \equiv$  Reynolds number based on  $L^* \left[ = \frac{v L^*}{\nu} \right]$

$\nu \equiv$  kinetic viscosity of air  $\doteq .2 \text{ cm}^2 \text{ s}^{-1}$

$L^* \equiv$  characteristic length defined as the total surface area divided by the perimeter normal to the flow for the ice particle

$\rho_v \equiv$  ambient water vapor density

For chamber plate temperatures of  $T_{\text{top}} = -1.8^\circ\text{C}$  and  $T_{\text{bot}} = -19.9^\circ\text{C}$  at an ambient pressure of  $p = 850$  mb, i.e., the average pressure at Reno, Nevada, the ambient temperature,  $T_\infty$ , at a height of  $x = 1.36$  cm above the bottom plate is  $T_\infty = -10.2^\circ\text{C}$ . Other values there are  $\rho_v = 2.664$  g  $\text{m}^{-3}$ ,  $T_s = -9.1^\circ\text{C}$ ,  $\Delta\rho_{\text{max}} = 0.563$  g  $\text{m}^{-3}$ ,  $\Delta\rho_{\text{static}} = 0.359$  g  $\text{m}^{-3}$ ,  $\rho_a \doteq 1.1$  kg  $\text{m}^{-3}$ ,

$$R_d = \frac{R}{m} = 2.871 \times 10^6 \text{ erg g}^{-1} \text{ } ^\circ\text{K}^{-1},$$

$$C_p = C_p(\text{dry air}) + wC_p'(\text{water vapor})$$

$$w = \text{mixing ratio} = \frac{\rho_v}{\rho_a} \doteq 10^{-2} \text{ to } 10^{-3} \text{ so } C_p \doteq 0.24 \text{ cal g}^{-1} \text{ } ^\circ\text{C}^{-1}, \text{ at}$$

$$T = -10^\circ\text{C}$$

$$K_d = 4.01 \times 10^{-5} \text{ cal cm}^{-1} \text{ s}^{-1} \text{ } ^\circ\text{C}^{-1}$$

$$K_v = 3.53 \times 10^{-5} \text{ cal cm}^{-1} \text{ s}^{-1} \text{ } ^\circ\text{C}^{-1}$$

$$K \doteq 4.01 \times 10^{-5} \text{ cal cm}^{-1} \text{ s}^{-1} \text{ } ^\circ\text{C}^{-1}$$

$$\bar{v}_r = \left( \frac{8R_d T_s}{\pi} \right)^{1/2} = 4.39 \times 10^4 \text{ cm s}^{-1}.$$

For a sphere of radius 1 mm

$$r^* = \frac{4\pi r^2}{4\pi C} = \frac{4\pi r^2}{4\pi r} = r = 0.1 \text{ cm and } L^* = \frac{4\pi r^2}{2\pi r} = 2r = 0.2 \text{ cm.}$$

$$N_{\text{Re},L}^* = \frac{vL^*}{\nu} = v \quad \text{for } v = 5.0 \text{ cm s}^{-1}, N_{\text{Re},L}^* = 5.0$$

$$\text{and } N_{\text{Pr}}^{1/3} N_{\text{Re},L}^{1/2} = 2.004 \text{ so } f_Q = 1.421, l_Q^* = 1.967 \times 10^{-5} \text{ cm}$$

$$\text{so } F_\alpha = 0.9998 \text{ and } dQ/dt = -7.87 \times 10^{-5} \text{ cal s}^{-1} \text{ for } v = 5.0 \text{ cm s}^{-1}.$$

### III. Heat Transfer by Radiation

The net radiative heat flux  $\Phi_R$  is equal to the difference between the amount of impinging radiation  $\Phi_I$  upon the ice particles' surface which is absorbed by the ice particle, and the radiation that is emitted by the particles' surface, i.e.,

$$\Phi_R = \Phi_I (1 - \overline{R(\lambda)}) \overline{A(\lambda)} - \epsilon \sigma T_s^4,$$

where  $\overline{R(\lambda)}$  is the reflectivity,  $\overline{A(\lambda)}$  the absorptivity and  $\epsilon$  the emissivity of ice.

$$\overline{R(\lambda)} = \frac{1}{\sigma T^4} \int_0^\infty B(T, \lambda) R(\lambda) d\lambda \doteq 0.034$$

$$\overline{A(\lambda)} = \frac{1}{\sigma T^4} \int_0^\infty B(T, \lambda) A(\lambda) d\lambda \doteq 1.0$$

where  $B(T, \lambda)$  is the Planck spectrum function.

$$\epsilon \doteq 0.95$$

$$\sigma = \text{Stefan constant} = 1.355 \times 10^{-12} \text{ cal cm}^{-2} \text{ } ^\circ\text{K}^{-4} \text{ s}^{-1}.$$

$$\Phi_R \doteq 0.966 \Phi_I - 0.95 \sigma T_s^4 \text{ but } \Phi_I \doteq 1/2 \sigma \left[ T_{\text{bot}}^4 + T_{\text{top}}^4 \right].$$

For  $T_{\text{top}} = -1.8^\circ\text{C} = 271.36^\circ\text{K}$  and  $T_{\text{bot}} = -19.9^\circ\text{C} = 253.26^\circ\text{K}$

$\Phi_I = 6.4609 \times 10^{-3} \text{ cal cm}^{-2} \text{ s}^{-1}$ . At a height,  $x$ , in the chamber of  $x = 1.36 \text{ cm}$  the ambient temperature was  $T_\infty = -10.2^\circ\text{C} = 262.96^\circ\text{K}$  and the ice crystal surface temperature was computed from conduction-diffusion equilibrium to be  $T_s = -9.1^\circ\text{C} = 264.06^\circ\text{K}$ . Thus,

$$\Phi_R \doteq [6.2412 \times 10^{-3} - 6.2585 \times 10^{-3}] \text{ cal cm}^{-2} \text{ s}^{-1}$$

or

$$\Phi_R \doteq -1.7 \times 10^{-5} \text{ cal cm}^{-2} \text{ s}^{-1}.$$

The term,  $\Phi_R$ , is very sensitive to the ice crystal surface temperature,  $T_s$ , being much larger or even positive for a surface temperature only  $0.2^\circ\text{C}$  colder.

The resultant heat transfer by radiation is given by  $dQ/dt = S \Phi_R$  where  $S$  is the radiating surface area of the crystal. For  $S = 2 \times 10^{-2} \text{ cm}^2$ , i.e., the same as assumed for conduction to the air,

$$dQ/dt = -3.4 \times 10^{-7} \text{ cal s}^{-1}.$$

## BIBLIOGRAPHY

- Anderson, B.J., Sutkoff, J.D. and J. Hallett, 1969: Influence of Methyl 2-Cyanoacrylate Monomer on the Habit of Ice Crystals Grown from the Vapor. J. Atmos. Sci., 26, 673-674.
- Anderson, B.J., 1974: Nucleation and Epitaxial Growth of Ice Crystals from the Vapor. Ph.D. Thesis, University of Nevada, Reno.
- Anderson, B.J., Keller, V.W., McKnight, C.V. and J. Hallett, 1976: Experimental Studies on the Influence of Crystal Defect and Surface Nucleation Mechanisms on the Growth Habit of Ice Crystals. IN: Proc. of Int. Conf. on Cloud Physics, Boulder, 97-102.
- Anderson, B.J. and J. Hallett, 1977: Influence of Strain and Electric Field on the Epitaxial Growth Rate of Ice Crystals from the Vapor. IN: Proc. of Int. Conf. on Cryst. Growth, Boston, 14.
- Aufm Kampe, H.J., Weickmann, H.K. and J.J. Kelley, 1951: The Influence of Temperature on the Shape of Ice Crystals Growing at Water Saturation. J. Met., 8, 168-174.
- Bartlett, J.R., Van den Heuvel, A.P. and B.J. Mason, 1963: The Growth of Ice Crystals in an Electric Field. Z. Angew. Math. Phys., 14, 599-610.
- Bentley, W.A. and W.J. Humphreys, 1931: Snow Crystals. McGraw-Hill, New York (paperback edition, Dover Press, 1963).
- Bernal, J.D., 1958: Comments on the Paper of Hallett and Mason. Proc. Roy. Soc., A, 247, 534-536.
- Bryant, G.W., Hallett, J. and B.J. Mason, 1959: The Epitaxial Growth of Ice on Single-Crystalline Substrates. J. Phys. Chem. Solids, 12, 189-195.
- Byers, H.R., 1965: Elements of Cloud Physics. The University of Chicago Press.
- Camp, P.R., 1965: The Formation of Ice at Water-Solid Interfaces. Trans. of the New York Acad. of Sci., 125, 317-343.
- Crowther, A.G., 1972: Preliminary Investigation into the Growth of Ice Crystals from the Vapour in an Electric Field in the Temperature Range  $-11^{\circ}\text{C}$  to  $-15^{\circ}\text{C}$ . J. Crys. Growth, 13/14, 241-243.
- Elliott, W.P., 1971: Dimensions of Thermal Diffusion Chambers. J. Atmos. Sci., 28, 810-811.
- Evans, L.F., 1973: The Growth and Fragmentation of Ice Crystals in an Electric Field. J. Atmos. Sci., 30, 1657-1664.

- Fernandez, R., 1967: The Growth of Ice in Flowing Water and NaCl Solutions. Ph.D. Thesis, Syracuse University, New York.
- Fernandez, R. and A.J. Barduhn, 1967: Growth Rate of Ice Crystals. Desalination, 3, 330-342.
- Fitzgerald, J.W., 1970: Non-Steady-State Supersaturations in Thermal Diffusion Chambers. J. Atmos. Sci., 27, 70-72.
- Fletcher, N.H., 1968: Surface Structure of Water and Ice. II. A Revised Model. Phil. Mag., 18, 1287-1300.
- Frank, F.C., 1949: The Influence of Dislocations on Crystal Growth. Disc. Faraday Soc., 5, 48-54.
- Frank, F.C., 1974: Japanese Work on Snow Crystals. J. Crys. Growth, 24/25, 3-5.
- Fukuta, N., 1969: Experimental Studies on the Growth of Small Ice Crystals. J. Atmos. Sci., 26, 522-531.
- Gamara, K.E., 1972: A Thermal Diffusion Wind Tunnel for the Study of Ice Crystal Growth. M.S. Thesis, University of Nevada, Reno.
- Gonda, T. and M. Komabayasi, 1970: Growth of Ice Crystals in the Atmospheres of Helium-Argon Mixture. J. Met. Soc. Japan, 48, 440-450.
- Gonda, T. and M. Komabayasi, 1971: Skeletal and Dendritic Structures of Ice Crystal as a Function of Thermal Conductivity and Vapor Diffusivity. J. Met. Soc. Japan, 49, 32-41.
- Gonda, T., 1976: The Growth of Small Ice Crystals in Gases of High and Low Pressures. J. Met. Soc. Japan, 54, 233-239.
- Gonda, T., 1977: The Growth of Small Ice Crystals in Gases of High and Low Pressures at -30°C and -44°C. J. Met. Soc. Japan, 55, 142-146.
- Hall, W.D. and H.R. Pruppacher, 1976: The Survival of Ice Particles Falling from Cirrus Clouds in Subsaturated Air. J. Atmos. Sci., 33, 1995-2006.
- Hallett, J. and B.J. Mason, 1958a: The Influence of Temperature and Supersaturation on the Habit of Ice Crystals Grown from the Vapour. Proc. Roy. Soc., A, 247, 440-453.
- Hallett, J. and B.J. Mason, 1958b: Influence of Organic Vapours on the Crystal Habit of Ice. Nature, 181, 467-469.
- Hallett, J., 1960: Crystal Growth and the Formation of Spikes in the Surface of Supercooled Water. J. of Glaciology, 3, No. 28, 698-704.

- Hallett, J., 1961: The Growth of Ice Crystals on Freshly Cleaved Covellite Surfaces. Phil. Mag., 6, 1073-1087.
- Hallett, J., 1964: Experimental Studies of the Crystallization of Supercooled Water. J. Atmos. Sci., 21, No. 6, 671-682.
- Hallett, J., 1965: Field and Laboratory Observations of Ice Crystal Growth from the Vapor. J. Atmos. Sci., 22, 64-69.
- Hallett, J., 1968: Nucleation and Growth of Ice Crystals in Water and Biological Systems. Low Temp. Biology of Foodstuffs, 23-52.
- Hellman, G., 1893: Schneekrystalle. J. Mückenberger, Berlin, p. 27.
- Hindman, E.E., 1968: Numerical Simulation of Supercooled Fog Dispersal. IN: Proceedings of the First Conf. on Weather Mod., Albany, 81-88.
- Hindman, E.E. and D.B. Johnson, 1972: Numerical Modeling of the Growth of Ice Crystals, Graupel, and Hail. IN: ENVPREDRSCHFAC Tech. Pap. No. 4-27, 48 pp. Also 1970: Numerical Simulation of Ice Hydrometer Development. IN: Preprints of the Conf. on Cloud Physics, Fort Collins, 63-64.
- Hobbs, P.V., 1974: Ice Physics. Clarendon Press, Oxford.
- Houghton, H.G., 1950: A Preliminary Quantitative Analysis of Precipitation Mechanisms. J. Met., 7, 363-369.
- Isono, K., Komabayasi, M., Yamanaka, Y. and H. Fujita, 1956: An Experimental Investigation in the Growth of Ice Crystals in a Supercooled Fog. J. Met. Soc. Japan, Ser. II, 34, 158-163.
- Isono, K., Komabayasi, M. and A. Ono, 1957: On the Habit of Ice Crystals Grown in the Atmosphere of Hydrogen and Carbon Dioxide. J. Met. Soc. Japan, 35, 327-338.
- Isono, K., 1958: Mode of Growth of Ice Crystals in Air and Other Gases. Nature, 182, 1221-1222.
- Jayaweera, K.O.L.F., 1971: Calculations of Ice Crystal Growth. J. Atmos. Sci., 28, 728-736.
- Kajikawa, M., 1972: Measurement of Falling Velocity of Individual Snow Crystals. J. Met. Soc. Japan, 50, No. 6, 577-583.
- Katz, J.L. and P. Mirabel, 1975: Calculation of Supersaturation Profiles in Thermal Diffusion Cloud Chambers. J. Atmos. Sci., 32, 646-652.
- Kay, J.M., 1963: Fluid Mechanics and Heat Transfer, Cambridge University Press, 2nd Edit., 66.

- Kikuchi, K., 1970: Peculiar Shapes of Solid Precipitation Observed at Syowa Station, Antarctica. J. Met. Soc. Japan, 48, No. 3, 243-249.
- Kikuchi, K., 1971: Peculiar Shapes of Snow Crystals of Antarctic Type Observed at Hokkaido. Geophys. Bull. Hokkaido Univ., 25, 167-180.
- Knight, C.A., 1962: Curved Growth of Ice Surfaces. J. of Applied Phys., 33, No. 5, 1808-1815.
- Knight, C.A., 1966: Grain Boundary Migration and Other Processes in the Formation of Ice Sheets on Water. J. of Applied Phys., 37, No. 2, 568-574.
- Kobayashi, T., 1957: Experimental Researches on the Snow Crystal Habit and Growth by Means of a Diffusion Cloud Chamber. J. Met. Soc. Japan, 75th Anniversary Vol., 38-47.
- Kobayashi, T., 1958: On the Habit of Snow Crystals Artificially Produced at Low Pressures. J. Met. Soc. Japan, 36, No. 5, 193-208.
- Kobayashi, T., 1961: The Growth of Snow Crystals at Low Supersaturations. Phil. Mag., 6, 1363-1370.
- Kobayashi, T., 1965: The Growth of Ice Crystals on Covellite and Lead Iodide Surfaces. Contrib. from the Inst. of Low Temp. Sci., Ser. A, No. 20, 1-22.
- Kobayashi, T., 1976: On Twinned Structures in Snow Crystals. J. Cryst. Growth, 32, 233-249.
- Koenig, L.R., 1971: Numerical Modeling of Ice Deposition. J. Atmos. Sci., 28, 226-237.
- Komabayasi, M., 1970: Shape Instability of Crystals of Ice, Carbon Dioxide and Ammonia Grown in a Cold Chamber. J. Met. Soc. Japan, 48, 270-286.
- Kumai, M. and K. Itagaki, 1953: Cinematographic Study of Ice Crystal Formation in Water. J. Fac. of Sci., Hokkaido Univ., Japan, Ser. II, 4, No. 4, 235-246.
- Kvlividze, V.I., Kiselev, V.F. and L.A. Ushakova, 1970: The Existence of Quasiliquid Films on the Surface of Ice. Dok. Phys. Chem. U.S.S.R., 191, 307-309.
- Kvlividze, V.I., Kiselev, V.F., Kurzaev, A.B. and L.A. Ushakova, 1974: The Mobile Water Phase on Ice Surfaces. Surf. Sci., 44, 60-68.
- Lacmann, R. and I.N. Stranski, 1972: The Growth of Snow Crystals. J. Cryst. Growth, 13/14, 236-240.



- Lamb, D., 1970: Growth Rates and Habits of Ice Crystals Grown from the Vapour Phase. Ph.D. Thesis, University of Washington, Seattle.
- Lamb, D. and P.V. Hobbs, 1971: Growth Rates and Habits of Ice Crystals Grown from the Vapor Phase. J. Atmos. Sci., 28, 1506-1509.
- Lindenmeyer, C.S., 1959: The Solidification of Supercooled Aqueous Solutions. Ph.D. Thesis, Harvard Univ., Cambridge.
- Lindenmeyer, C.S. and F. Chalmers, 1966: Growth Rate of Ice Dendrites in Aqueous Solutions. J. Chem. Phys., 45, 2807-2808.
- McDonald, J.E., 1963: Use of the Electrostatic Analogy in Studies of Ice Crystal Growth. Z. Angew. Math. Phys., 14, 610-619.
- McKnight, C.V., To Be Published: Dislocations in Vapor Grown Ice Crystals. Ph.D. Thesis, University of Nevada, Reno.
- Macklin, W.C. and B.F. Ryan, 1965: The Structure of Ice Grown in Bulk Supercooled Water. J. Atmos. Sci., 22, No. 4, 452-459.
- Magono, C. and C.W. Lee, 1966: Meteorological Classification of Natural Snow Crystals. J. Fac. of Sci., Hokkaido Univ., Japan, Ser. VII (Geophysics), 2, No. 4, 321-335.
- Marshall, J.S. and M.P. Langleben, 1954: A Theory of Snow-Crystal Habit and Growth. J. Met., 11, 104-120.
- Marshall, J.S. and K.L.S. Gunn, 1955: A First Experiment on Snow-Crystal Growth. IN: Proceedings of the First Conference on the Physics of Cloud and Precipitation Particles. Artificial Stimulation of Rain, 340-345.
- Mason, B.J., 1953: The Growth of Ice Crystals in a Supercooled Water Cloud. Quart. J. Roy. Met. Soc., 79, 104-111.
- Mason, B.J., Bryant, G.W. and A.P. Van den Heuvel, 1963: The Growth Habits and Surface Structure of Ice Crystals. Phil. Mag., 8, 505-526.
- Mason, B.J., 1963: Ice. IN: The Art and Science of Growing Crystals, Wiley, New York, 119-150.
- Mason, B.J., 1971: The Physics of Clouds. Oxford University Press.
- Maybank, J.E. and N.N. Barthakur, 1967: Growth and Destruction of Ice Filaments in an Electric Field. Nature, 216, 50-52.
- Miksch, E.S., 1969: Solidification of Ice Dendrites in Flowing Supercooled Water. Trans. of the Metallurgical Soc. of AIME, 245, 2069-2072.

- Nakaya, U. and T. Terada, Jr., 1935: Simultaneous Observations of the Mass, Falling Velocity and Form of Individual Snow Crystals. J. Fac. Sci., Hokkaido Univ., Japan, Ser. II, 1, No. 7, 191-203.
- Nakaya, U., 1954: Snow Crystals: Natural and Artificial. Harvard University Press.
- Poisot, J.M., 1968: The Linear Growth Rate of Ice Crystals in Flowing Sub-Cooled Water. M.S. Thesis, Syracuse University, New York.
- Pruppacher, H.R., 1967: Growth Modes of Ice Crystals in Supercooled Water and Aqueous Solutions. J. of Glaciology, 6, No. 47, 651-662.
- Reynolds, S.E., 1952: Ice-Crystal Growth. J. Met., 9, 36-40.
- Rottner, D., 1971: Snow Crystal Habit at Small Excesses of Vapor Density over Ice Saturation. IN: Report No. AR100, Dept. of Atmos. Resources, University of Wyoming, Laramie, 17 pp.
- Rottner, D. and G. Vali, 1974: Snow Crystal Habit at Small Excesses of Vapor Density over Ice Saturation. J. Atmos. Sci., 31, 560-569.
- Ryan, B.F. and W.C. Macklin, 1969: The Temperature Dependence of the Velocity of Steps Growing on the Basal Plane of Ice. J. Col. and Int. Sci., 31, 566-568.
- Ryan, B.F., Wishart, E.R. and D.E. Shaw, 1976: The Growth Rates and Densities of Ice Crystals Between  $-30^{\circ}\text{C}$  and  $-21^{\circ}\text{C}$ . J. Atmos. Sci., 33, 842-850.
- Schaefer, V.J., 1949: The Formation of Ice Crystals in the Laboratory and the Atmosphere. Chem. Rev., 44, 291-320.
- Scott, W.T., 1977: The Physics of Electricity and Magnetism. 2nd Edit. Reprint, R.E. Krieger Publishing Co., Huntington, N.Y., 65.
- Shaw, D. and B.J. Mason, 1955: The Growth of Ice Crystals from the Vapour. Phil. Mag., 46, 249-262.
- Thorpe, A.D. and B.J. Mason, 1966: The Evaporation of Ice Spheres and Ice Crystals. Brit. J. Appl. Phys., 17, 541-548.
- Todd, C.J., 1964: A System for Computing Ice Phase Hydrometeor Development. IN: Meteorology, Inc., Report No. ARG Pa-121, 30 pp.
- Twomey, S., 1963: Measurements of Natural Cloud Nuclei. J. Rech. Atmos., 1, 101-105.
- Van den Heuvel, A.P. and B.J. Mason, 1959: Habit of Ice Crystals Grown in Hydrogen, Carbon Dioxide, and Air at Reduced Pressure. Nature, 184, 519-520.

- Van den Heuvel, A.P., 1960: The Nucleation and Growth of Ice Crystals. Ph.D. Thesis, Imperial College, London.
- Vlahakis, J.G., 1972: The Anomalous Growth of Ice Crystals in Flowing NaCl Solutions. Ph.D. Thesis, Syracuse University, New York.
- Vlahakis, J.G. and A.J. Barduhn, 1974: Growth Rate of an Ice Crystal in Flowing Water and Salt Solutions. AIChE Jour., 20, No. 3, 581-591.
- Vonnegut, B., 1948: Influence of Butyl Alcohol on the Shape of Snow Crystals Formed in the Laboratory. Science, 107, 621-622.
- Wilcox, W.R., 1971: The Role of Mass Transfer in Crystallization Processes. IN: Preparation and Properties of Solid State Materials. Vol. 1, Aspects of Crystal Growth, Edited by R.A. Lefever, Marcel Dekker, Inc., New York, 100.
- Wolff, G.A., 1955: The Growth of Ice Crystals. IN: Conference on the Physics of Cloud and Precipitation Particles. Artificial Stimulation of Rain, Pergamon Press (1957), 332-339.
- Yamashita, A., 1971: Skeleton Ice Crystals of Non-Hexagonal Shape Grown in Free Fall. J. Met. Soc. Japan, 49, No. 4, 215-230.
- Yamashita, A., 1976: Growth Processes of Ice Crystals and a Law Which is Related to the Symmetric Growth of Plate-Like Snow Crystals. IN: Proceedings of the Intern. Conf. on Cloud Physics, Boulder, 136-141.

1. REPORT NO. NASA TP-1651		2. GOVERNMENT ACCESSION NO.		3. RECIPIENT'S CATALOG NO.	
4. TITLE AND SUBTITLE  Ice Crystal Growth in a Dynamic Thermal Diffusion Chamber		5. REPORT DATE May 1980		6. PERFORMING ORGANIZATION CODE	
7. AUTHOR(S) Vernon W. Keller		8. PERFORMING ORGANIZATION REPORT #		10. WORK UNIT NO. M-297	
9. PERFORMING ORGANIZATION NAME AND ADDRESS  George C. Marshall Space Flight Center Marshall Space Flight Center, Alabama 35812		11. CONTRACT OR GRANT NO.		13. TYPE OF REPORT & PERIOD COVERED  Technical Paper	
12. SPONSORING AGENCY NAME AND ADDRESS  National Aeronautics and Space Administration Washington, D. C. 20546		14. SPONSORING AGENCY CODE			
15. SUPPLEMENTARY NOTES  Prepared by Space Sciences Laboratory, Science and Engineering					
16. ABSTRACT <p>Ice crystals were grown in a supersaturated environment produced by a dynamic thermal diffusion chamber, which employed two horizontal plates separated by a distance of 2.5 cm. Air was circulated between and along the 1.2 m length of the plates past ice crystals which nucleated and grew from a fiber suspended vertically between the two plates. Using a zoom stereo microscope with a magnification which ranged from 3X to 80X and utilizing both 35 mm still photographs and 16 mm time lapse cine films taken through the microscope, the variation of the shape and linear growth rate of ice crystals was examined as a function of the ambient temperature, the ambient supersaturation and the forced ventilation velocity. The ambient growth conditions were varied over the range of temperature 0°C to -40°C, over the range of supersaturation 4% to 50% with respect to ice, i.e., over vapor density excesses ranging from 0.07 g m<sup>-3</sup> to 0.7 g m<sup>-3</sup>, and over the range of forced ventilation velocities 0 cm s<sup>-1</sup> to 20 cm s<sup>-1</sup>.</p> <p>It is shown that the introduction of a ventilation velocity is roughly equivalent to increasing the ambient supersaturation. For a fixed ambient temperature and ambient supersaturation, the linear 'a'-axis growth rate is directly proportional to the square root of the ventilation velocity, as theory predicts, provided the crystal shape does not change significantly. The transitions plate + dendrite and column + needle occur at a lower ambient supersaturation as the ventilation velocity increases. A definite time constant, which is a function of the ambient temperature, the ambient supersaturation and the magnitude of the change in the ventilation velocity, exists for the transition of both crystal shape and linear growth rate following a change in the ventilation velocity. For increasing ventilation velocities at a fixed ambient supersaturation the maximum in the linear growth rate near -15°C apparently occurs at successively colder temperatures. Over the temperature range -4°C to -6°C growth occurs along a direction up to 25° from the 'c'-axis as the local supersaturation is increased. Thus, under the proper temperature conditions a change in the local supersaturation can induce a change, not only in the absolute growth rates, but also in the relative growth rates along the 'a' and 'c'-axes.</p> <p>In the presence of 10 µm mean diameter droplets with concentrations of 10<sup>3</sup> to 10<sup>5</sup> cm<sup>-3</sup> droplet accretion accounted for over 90% of the growth of both ice crystal columns and dendrites at ventilation velocities of 15 cm s<sup>-1</sup>. However, even at higher velocities the most extensively rimed crystals still retained the original orientation of their crystalline axes. At velocities less than 1.0 cm s<sup>-1</sup> droplets of 10 µm diameter or smaller evaporated as they approached a growing ice crystal and crystal growth was entirely by vapor diffusion.</p> <p>The first vapor grown discoid ice crystals were observed. They grew in the temperature regime -5°C to -7°C at low local supersaturations, i.e., in the regime formerly believed to only support nearly equiaxed columns.</p> <p>Results from these experiments are interpreted in terms of diffusion through a local boundary layer whose thickness is a function of ventilation velocity, the diffusivity of water vapor and heat through air, and the crystal shape; and interaction with different nucleation and growth kinetics on different surfaces. Two-dimensional nucleation and layer growth from corners or edges is believed to occur at ambient supersaturations significantly lower than present theories would predict. At low supersaturation and temperature the crystal habit and growth may be controlled by the presence of defects sometimes giving rise to crystals of habit opposite to that normally observed.</p>					
17. KEY WORDS  Crystal Growth Ice Crystals Dynamic Thermal Diffusion			18. DISTRIBUTION STATEMENT  Unclassified - Unlimited    Subject Category 47		
19. SECURITY CLASSIF. (of this report)  Unclassified	20. SECURITY CLASSIF. (of this page)  Unclassified	21. NO. OF PAGES  215	22. PRICE  \$9.25		

For sale by National Technical Information Service, Springfield, Virginia 22161

National Aeronautics and  
Space Administration

Washington, D.C.  
20546

Official Business

Penalty for Private Use, \$300

SPECIAL FOURTH CLASS MAIL  
BOOK

Postage and Fees Paid  
National Aeronautics and  
Space Administration  
NASA-451



7 1 1U,E, 040180 S00903DS  
DEPT OF THE AIR FORCE  
AF WEAPONS LABORATORY  
ATTN: TECHNICAL LIBRARY (SUL)  
KIRTLAND AFB NM 87117

**NASA**

POSTMASTER: If Undeliverable (Section 158  
Postal Manual) Do Not Return

---